Optimal Air and Fuel-Path Control of a Diesel Engine

By

Zhijia Yang

Supervisor: Prof Richard Stobart

A Doctoral Thesis Submitted in partial fulfilment of the requirements

for the award of

Doctor of Philosophy

Department of Aeronautical and Automotive Engineering

Loughborough University

1st November 2014

Abstract

The work reported in this thesis explores innovative control structures and controller design for a heavy duty Caterpillar C6.6 diesel engine. The aim of the work is not only to demonstrate the optimisation of engine performance in terms of fuel consumption, NOx and soot emissions, but also to explore ways to reduce lengthy calibration time and its associated high costs. The test engine is equipped with high pressure exhaust gas recirculation (EGR) and a variable geometry turbocharger (VGT). Consequently, there are two principal inputs in the air-path: EGR valve position and VGT vane position. The fuel injection system is common rail, with injectors electrically actuated and includes a multi-pulse injection mode. With two-pulse injection mode, there are as many as five control variables in the fuel-path needing to be adjusted for different engine operating conditions.

The current techniques used to manage control inputs in both air-path and fuel-path are open-loop, based on look-up tables obtained during the calibration process. All the calibration efforts are directed at the optimisation of the combustion process under different engine operation conditions in terms of combustion noise, combustion efficiency, fuel economy and regulated emissions. However, by applying proper closed-loop control systems, these inputs can be adaptively controlled and automatically adjusted to meet the requirements placed on engine performance in a more accurate and robust way.

Several closed-loop control systems for air-path and fuel-path control have been investigated and demonstrated. A modern multi-variable control strategy: Model Predictive Control (MPC) has been demonstrated in the closed-loop control of both air-path and fuel-path. Control oriented dynamic models were obtained and studied by means of system identification methods. In the course of the investigation there were five avenues of exploration (with the associated research contributions):

- Estimation methods for EGR ratio and the effect of EGR ratio on NOx and soot emissions. (Real time estimation techniques.)
- Air Fuel Ratio (AFR) and EGR ratio based control of air-path. (Dynamic control oriented modelling in the air-path and the use of control oriented models.)
- The rail pressure wave inside the common fuel rail caused by the injection event. (The link between fuel rail conditions and subsequent combustion cycles and the characterisation of rail pressure variation as a control loop disturbance.)
- Investigation of combustion cyclic variation and cylinder inconsistency phenomena. (Proposal and demonstration of a combustion parameter based control system for reducing combustion cyclic variation and improving cylinder to cylinder consistency.)

- A closed-loop control system for online adjustment of Start Of Injection (SOI) and Rail Pressure (RP). (Demonstration of a novel type of combustion control and exploration of the control authority available for modifying combustion).

Generic conclusions include an understanding of the control authority available in both the air and fuel-path, and the particular requirements for control oriented models for application in this class of diesel engines. Proposals for further work include the development of a deeper understanding of sources of disturbance, and an understanding of the linkage between IMEP and other variables, notably maximum cylinder pressure.

Keywords: Diesel Engine, Air-Path and Fuel-Path Control, Emission Control, Combustion Control, Cylinder Pressure, Emission Model

Acknowledgements

I wish to thank so much my supervisor, Professor Richard Stobart. I still remember very clearly the first email I received from him about my enquiry of the possibility of PhD study at Loughborough University when I was in China five years ago. I could not come to UK to enjoy such wonderful research work without his trust and encouragement. He supported and guided me throughout this research and provided reassurance during difficult times. Every meeting with Professor Stobart proved a good chance for me to be inspired and encouraged. He is not only an excellent adviser but a creative and experienced experimentalist. All the engine tests and implementations of closed-loop control systems wouldn't have been done without his lead.

I would also like to thank Dr Jiamei Deng whom is now working in Kingston University. She provided me with much valuable help and guidance while I was doing the fuel path MPC control design and engine tests and soot neural network modelling during the first and second year of my PhD study. I wish to thank too the technicians of the Powertrain Laboratory at Loughborough University, namely: Adrian Broster, Steve Horner, Steve Taylor and Graham Smith. Without their valuable support and assistance, all the engine tests would not have been done properly, safely and on time. Thanks also go to Dr. Bastian Maass and Dr. Merenhya Wijewardane who were in my research group and have now completed their PhD degrees and have moved back in their own countries. Dr. Maass was so patient in teaching me how to use GT-Power, unfortunately I did not use it in my work. Dr. Wijewardane is so nice and wonderful. She helped me a lot with settling down in Loughborough and was always willing to help me with any problem.

I'm indebted so much both financially and spiritually to my dear friend Suyan Long back in China. Without her support, the lives of both I and my son in Loughborough could have been very hard in the past five years. I want to thank my brother Gelai Yang and his wife Hua Wang. They looked after our parents so well when I was not in China. They even looked after my son for me for few months when he was very poorly in 2010. Finally and most importantly to Edward Winward, without his excellent work on the development of an advanced engine controls prototyping system in the form of the C6.6 engine I used throughout my research and also his guidance and assistance; all the engine tests reported in this work would not have been possible. Without his support and encouragement, this thesis would not have been finished.

Zhijia Yang, November 2014

Author Publications

[1] Yang, Z., Stobart, R., Winward, E. and Steffen, T., Combustion Model Based Explanation of the Pmax and IMEP Coupling Phenomenon in Diesel Engine, SAE Paper 2014-01-1350.

[2] Yang, Z., Steffen, T., Stobart, R. and Winward, E., 'A Predictive Model Pmax and IMEP for Intra-Cycle Control, SAE Paper 2014-01-1344.

[3] Yang, Z., Steffen, T. and Stobart, R., Disturbance Sources in the Diesel Engine Combustion Process, SAE Paper 2013-01-0318.

[4] Yang, Z., Stobart, R. and Winward, E., 'Online Adjustment of Start of Injection and Fuel Rail Pressure Based on Combustion Process Parameters of Diesel Engine, SAE Paper 2013-01-0315.

[5] Steffen, T., Stobart, R. and Yang, Z., 'Challenges and Potential of Intra-Cycle Combustion Control for Direct Injection Diesel Engines', SAE Paper 2012-01-1158.

[6] Yang, Z. and Stobart, R., Predicting the Effect of Fuel Path Controllable Parameters on the Performance of Combustion Controlled Diesel Engine, Proceedings of the FISITA 2012 World Automotive Congress, Lecture Notes in Electrical Engineering Volume 189, pp 387-400.

[7] Deng, J., Maass, B., Stobart, R., Winward, E. and Yang, Z., 'Accurate and Contrinuous Fuel Flow Rate Measurement Prediction for Real Time Application', SAE Paper 2011-01-1303.

Table of Contents

List of Figures

Chapter 2

Chapter 3

Chapter 4

Chapter 5

*(Total of **141** Figures)*

List of Tables

Chapter 2

Chapter 3

Chapter 4

Chapter 5

*(Total of **8** Tables)*

Glossary

Nomenclature

AFR_s	Stoichiometric air fuel ratio for diesel fuel, 14.6
Alpha	Crank angle degree from SOI to CA50
A_{r_max}	Model constant set to 5.3 for the EGR valve in the C6.6 engine
A_r	Model parameter for EGR flow rate model
a_0, a_1, b_0, b_1	Constants
$[CO_2]_{ambient}$	Concentration of CO_2 in the ambient environment, [%]
$[CO_2]_{exhaust}$	Concentration of CO_2 in the exhaust, [%]
$[CO_2]_{intake}$	Concentration of CO_2 in the intake, [%]
$C_{p,air}$	Specific heat value of air, 1.007 [J/kg.K]
$C_{p,exh}$	Specific heat value of exhaust gas, 1.09 [J/kg.K]
d	Pipe inside diameter, [mm]
EGR_{ratio}	EGR ratio, [%]
H_p	Prediction horizon
$\mathrm{H_u}$	Control horizon
HR_{50}	Angular position of the engine at 50% of the total cycle heat release
K	Gain of one order transfer function
K_{exh}	Model constant for exhaust pipe pressure drop
l	Length of pipe, [m]
m_1	Main injection fuel quantity
m_2	Post injection fuel quantity
M_{gas}	Molecular weight of the gas mass into engine, [kg/kmol]
M_{air}	Molecular weight of fresh air, 28.97 [g/mol]
M_{exh}	Molecular weight of exhaust gas, 29 [g/mol]
M_{f}	Molecular weight of diesel fuel, 233 [kg/kmol]
N	Engine speed, [rpm]
n	Number of revolutions per power stroke (1 or 2)
η_v	Volumetric efficiency

η_c	Compressor efficiency
η_t	Turbine efficiency
N_{tc}	Turbo speed
p_c	Cylinder pressure, [kPa]
dp_c	Rate of change of cylinder pressure, [kPa/°]
$\frac{dp}{da}$	Rate of change of cylinder pressure with crank angle degree
P_{max}	Peak cylinder pressure
p_0	Average cylinder pressure just before start of combustion, [kPa]
p_1 , p_i	Intake manifold pressure or boost pressure [kPa]
p_2	Exhaust manifold pressure [kPa]
p_3	Exhaust pressure after turbine [kPa]
p_{amb}	Ambient pressure [kPa]
ρ_{exh}	Exhaust gas density, [g/m^3]
p_x	Exhaust manifold pressure, [kPa]
dp	Pressure drop along the exhaust pipe [kPa]
ρ	Inlet manifold density, [kg/m^3]
Q	Heat release, [J]
$\frac{dQ}{d\theta}$	Heat release rate with crank angle degree, [J/°]
Q_{LHV}	Lower heating value of diesel fuel, 43400 [kJ/kg]
R	Universal gas constant, 8.314462 [J/mol.K]
r_{CA50}	Reference or setpoint for CA50
r_{Alpha}	Reference or setpoint for Alpha
T_{amb}	Ambient temperature, [K]
T_s	System time of one order transfer function
T	Lag time
T_1	Intake manifold temperature, [K]
T_2	Exhaust manifold temperature, [K]
T_{egr}	Temperature before the EGR valve, [K]
T_{load}	Engine load, [Nm]
τ	Dead time
U(s)	Laplace transfer function of the input
V	Cylinder volume, [m^3]
V_d	Cylinder displacement volume, [m^3]

V_{swept}	Engine swept volume, [m^3]
W_C	Compressor air flow rate, [kg/s]
W_t	Turbine exhaust gas flow rate, [kg/s]
W_f	Fuel flow rate, [kg/s]
W_e	Gas flow rate into engine, [kg/min]
W_{egr}^{mes}	Measured EGR flow rate, [g/s]
W_{egr}^{est}	Estimated EGR flow rate, [g/s]
W_{egr}	EGR flow rate
$\mathrm{W_y}$	Prediction error weighting matrix
$\mathrm{W_u}$	Control gain weighting matrix
χ_{vgt}	VGT vane position
χ_{egr}	EGR valve position
$\hat{y}$	Model output
y	Measured variable
Y(s)	Laplace transfer function of the output
γ	Gamma (ratio of specific heats C_p/C_v)
γ_{air}	Specific heat value ratio of air, 1.35 at about 600°C
γ_{exh}	Specific heat value ratio of exhaust gas, 1.29 at about 600°C
θ	Crank angle degree, [°]
$\sigma(\mathrm{IMEP})$	Standard deviation of IMEP
$\mu(\mathrm{IMEP})$	Mean value of IMEP

Acronyms

ATDC	After Top-Dead-Centre
AFR	Air Fuel Ratio
AI	Analogue Input
ARX	Autoregressive Model with Exogenous Input
ARMAX	Autoregressive Moving Average Models with Exogenous Inputs
BP	Back Propagation
BTDC	Before Top-Dead-Centre
BDC	Bottom-Dead-Centre
BSFC	Break Specific Fuel Consumption
CA50	Angular position of the engine at 50% of the total cycle heat release
COV	Coefficient of Variation
CI	Compression Ignition
CAN	Controller Area Network
CT	Coolant Temperature
CAD	Crank Angle Degree
DOE	Design of Experiments
DPF	Diesel Particulate Filter
DW	Dwell Time
DMC	Dynamic Matric Control
ETA	Electric Turbo Assist
EOC	End of Combustion
EOI	End of Injection
ECM	Engine Control Module
EGR	Exhaust Gas Recirculation
ExP	Exhaust Pressure
ExT	Exhaust Temperature
EVC	Exhaust Valve Closing
EVO	Exhaust Valve Opening
EMPC	Explicit Model Predictive Control
FPGA	Field Programmable Gate Array

FR	Fuel Ratio
GTL	Gas to Liquid
GPC	Generalized Predictive Control
HRR	Heat Release Rate
HD	Heavy Duty
HSDI	High Speed Direct Injection
H∞	H-Infinity
HCCI	Homogenous Charge Compression Ignition
HC	Hydrocarbon
IMEP	Indicated Mean Effective Pressure
IC	Injection Current
IVC	Intake Valve Closing
IVO	Intake Valve Opening
IEM	Integrated Emission Management
LMI	Linear Matrix Inequalities
LPV	Linear Parameter Varying
LQ	Linear Quadratic
LQG	Linear-Quadratic-Gaussian
LTC	Low Temperature Combustion
MAP	Manifold Air Pressure
MAT	Manifold Air Temperature
MAF	Mass Air Flow
MVEM	Mean Value Engine Model
MD	Medium Duty
MPC	Model Predictive Control
MIMO	Multi-Input Multi-Output
mp-QP	Multi-Parametric Quadratic Program problem
NI	National Instruments
NL	Needle Lift
NN	Neural Network
NOx	Nitrogen Oxide
NARX	Nonlinear Autoregressive Model with Exogenous Input
NMPC	Nonlinear Model Predictive Control

NRTC	Non-Road Transient Cycle
OE	Output Error
PM	Particular Matter
PC	Personal Computer
PDW	Post Dwell Time
PDF	Probability Density Functions
PID	Proportional Integral Derivative
PRBS	Pseudo Random Binary Sequence
PWM	Pulse-Width Modulation
RP	Rail Pressure
SCR	Selective Catalytic Reduction
SetP	Setpoint for controller
SISO	Single-Input Single-Output
SI	Spark Ignition
SFC	Specific Fuel Consumption
SOC	Start of Combustion
SOI	Start of Injection
SIT	System Identification Toolbox
TEG	Thermoelectric Generator
3I3O	Three-Input-Three-Output
TDC	Top Dead Centre
TF	Transfer Function
2I2O	Two-Input-Two-Output
VGT	Variable Geometry Turbocharger
VNT	Variable Nozzle Turbocharger
VVA	Variable Valve Actuation
VVT	Variable Valve Timing
VI	Virtual Instrument

Chapter 1

1 Introduction

The diesel engine has come to dominate over the Spark Ignition (SI) engine in various applications such as: ships, trains, generators, agricultural, construction, mining, heavy road vehicles, military vehicles and submarines etc. due to a series of key advantages. Most significantly, the diesel engine has a higher fuel volumetric conversion efficiency compared to the SI engine even though diesel fuel has a slightly lower calorific value. A number of contributing factors are important in the greater thermal efficiency of the diesel engine and these include: the greater density of diesel fuel, the traditionally higher compression ratio of the diesel engine, lower frictional losses due to lower average operational engine speeds for the same power requirement and the avoidance of an intake throttle. The greater fuel conversion efficiency of the diesel engine leads directly to lower carbon dioxide (CO_2) emissions compared to an SI engine of equivalent power rating.

Many of the key advantages of the diesel engine derive from its foundation on the principle of Compression Ignition (CI) and the higher geometric compression ratio that this demands. By nature, CI is far simpler and more robust than SI, which requires a high voltage ignition system and precise management of both the fuel injection and fuel ignition systems. It also helps to avoid SI engine issues such as knock and misfire and is far less sensitive to fuel quality. Indeed, the diesel engine is far more flexible with regard to fuel as in addition to petro-diesel, which like gasoline is a fractional distillate of petroleum, the diesel engine can also use various biodiesel fuels and mineral-diesel/biodiesel fuel blends and also Gas to Liquid (GTL) fuels such as Fischer-Tropsch diesel. Such alternative fuels are obtained from sources other than petroleum such as vegetable oil, natural gas etc. [1] and therefore help diversity. Diesel fuel is also safer than gasoline because it has a much higher boiling temperature than that of gasoline and is also less volatile, characteristics which are requisite of the CI process. The higher compression ratio of the diesel engine combined with the lack of an intake throttle and the ability to operate at Air Fuel Ratio's (AFR) above stoichiometric, result in the diesel engine generally having greater torque output compared to an

equivalent sized gasoline engine. Taken together, all of these positive attributes of the diesel engine have traditionally given it a significant advantage in both Medium Duty (MD) and Heavy Duty (HD) applications where it dominates.

The diesel engine does however have several disadvantages relative to the SI engine which include: it is heavier (to withstand higher combustion pressures), noisier (downside of CI), slower to accelerate (greater inertia), has higher Nitrogen Oxide (NO_x) and Particular Matter (PM) emissions and is also more expensive. These have all been impediments to the widespread use of the diesel engine in passenger vehicles in history until relatively recently [2].

According to U.S. Department of Energy report, if light-duty diesel vehicles reach a 30 percent market share by 2020, it would reduce U.S. oil consumption by 350,000 barrels a day [3]. Since the CO_2 emissions from diesel are slightly lower than those from gasoline, then increase the portion of diesel vehicles would reduce total emissions of greenhouse gases.

During the last two decades, but especially the first decade of the 21st century, the popularity of the diesel engine has grown significantly in the light duty automotive market. This is because since the early 1990's a series of new technologies have been developed to reduce some of the disadvantages of the diesel engine, these technologies include: the introduction of pilot injection, high pressure common fuel rail injection system, Variable Geometry Turbocharger (VGT), Exhaust Gas Recirculation (EGR), Selective Catalytic Reduction (SCR), and Diesel Particulate Filter (DPF) etc. With these new technologies the modern diesel engine has greater power density, has become quieter, is faster in acceleration and has significantly reduced engine-out pollutant emissions – attributes especially important in automobiles.

Each of the technological improvements to the diesel engine have also invariably increased the complexity of the engine, especially in regard to the number of control inputs e.g. fuel injection pressure, multiple fuel injection pulses per cycle to manage, VGT actuator control (even multiple VGT actuators in compounded turbocharger systems), EGR actuator, intake restriction for the EGR system, post injections for aftertreatment management etc. Thus, the control task for diesel engines has grown significantly with the increased control freedom and control inputs requiring optimized control to optimize the diesel engine performance especially in fuel consumption and emissions over the whole engine operating range under both steady state and transient conditions.

The variety of diesel fuel type also demands such optimization control can adapt to the physical and chemical properties of fuel automatically. A review of literature shows that even though the research activities in this area are increasing rapidly, the control issues of modern diesel engine are still open. This study aims to explore this area both experimentally and theoretically.

1.1 Background and Motivation of the Study

From 1892 when the German inventor Rudolf Diesel first invented the diesel engine to now, about one-hundred-twenty years have elapsed. However, as stated earlier, only in the past two decades has the diesel engine been vastly improved with regard to engine performance, emissions and combustion noise. This is mainly because the introduction of several optimization-devices which include: common fuel rail injection, multi-pulse fuel injection, VGT, EGR and after-treatment systems These have been introduced alongside increasingly advanced electric microcontroller technology [4]; together these advances have proven very successful and universally adopted for the majority of diesel engines.

To summarise; a turbocharger enables the diesel engine to produce higher power outputs and lower emissions levels. A VGT fitted to a turbocharger turbine allows significant flexibility over the pressure ratio across the turbine and this flexibility can be used for improving low speed torque characteristics, reducing turbocharger lag and driving EGR flow [5]. EGR is an effective strategy to control NOx emissions from diesel engines through lowering the oxygen concentration in the combustion chamber, as well as through heat absorption. However, drawbacks of EGR include increased PM emissions and fuel consumption [6].

The aim of the control of vane position in a VGT device and the valve position in an EGR device is to adjust the boost pressure, fresh air flow rate and recirculated exhaust gas rate in the intake manifold. These parameters in turn affect the diesel combustion process through the initial gas conditions inside the combustion chamber just before the fuel injection [7]. The task of controlling the VGT vane position and EGR valve position is widely referred to as ***air-path control***.

A common rail fuel rail injection system provides the flexibility in controlling the fuel injection quantity, injection mode (i.e. number of injection pulses per engine cycle) and injection timing. Fuel pressure in common rail systems can also be controlled as a function of engine speed and load to optimize emissions and performance [8]. For a common rail system utilising a two-pulse injection

mode, there are at least five control variables which are: start of injection, dwell time, fuel ratio, total fuel injection quantity and fuel Rail Pressure (RP) [9]. The task of controlling of all these variables is widely referred to as ***fuel-path control***.

The conventional approach in managing both diesel engine air-path and fuel-path is an open loop control system developed using a normal or model based engine test calibration process. Such processes are very expensive and time consuming and it is also well known that open loop control has no ability to cope with disturbances such as the production tolerance, the variations of fuel type or fuel quality, environmental factors and engine ageing etc.

In the last decade there has been significant research effort invested in air-path feedback control with multiple examples found in literature [10-42]. The most common reported control structure is Two-Input-Two-Output (2I2O) closed-loop control and in most cases this is (VGT vane position, EGR valve position) to (Manifold Air Pressure (MAP), Mass Air Flow (MAF)), a few are (VGT vane position, EGR valve position) to (AFR or MAF, EGR ratio). Various controller design methods also have been applied such as decentralized Proportional Integral Derivative (PID) [38-43], decoupling PID [13, 14, 21], Linear Matrix Inequalities (LMI) [30, 33], Nonlinear Model Predictive Control (NMPC) [32; 35, 44], Linear-quadratic-Gaussian (LQG) [36], Model Predictive Control (MPC) [23, 26, 27, 37], Hinf and robust control [10, 12, 15, 16, 18, 31], internal model structure [10], Explicit Model Predictive Control (EMPC) [11, 28], loop shaping [45], Lyapunov Multi-Input Multi-Output (MIMO) control [17], nonlinear optimal control [19], nonlinear inverse model control [20], slide control [22, 46] and recursive model free control [29]. However, in many of these examples only simulation results are reported [14, 15, 18, 19, 23, 29-33, 35, 42]. Indeed, less than half of these publications report engine experimental results [12, 16, 17, 20, 21, 22, 24, 25, 27, 28, 40, 47]. When NOx and PM emissions are selected as controlled variables, normally, air-path and fuel-path coordinated control is considered [48-51].

It can be seen from this summary of published air-path control work that only a very limited number of studies have been carried out on the application of MPC to air-path control and which use AFR and EGR ratio as outputs, especially experimentally. Indeed, the accurate measurement or estimation of EGR ratio or EGR flow rate, which is very crucial in (AFR, EGR ratio) control, is rarely reported. Application of MPC control can be found in air-path and fuel-path coordinated control [49].

For fuel-path control, an electric speed governor is the first modern fuel-path closed-loop control system implemented in diesel engines [52-54]. Its advantage is that it vastly reduces the fluctuations in engine speed that is caused by load fluctuations. It also reduces the soot emissions, fuel consumption, engine vibrations, wear and tear of the engine which result in decreasing of engine life etc. [54]. However, these speed governors are all based on the speed feedback information alone with fast combustion process parameters such as Indicated Mean Effective Pressure (IMEP) not considered.

The injection mode involved in nearly all the diesel engine fuel-path closed-loop control systems is two-pulse injection mode with a pilot plus a main injection. Typical examples of fuel-path closed-loop control that can be found in literature use Start of Injection (SOI) as a control input to feedback control combustion phasing [55-59] and using injected fuel quantity to feedback control IMEP [55, 56, 60]. For piezoelectric injectors that have fast response dynamics, the cycle based heat release rate shape can be closed-loop controlled using estimators for Heat Release Rate (HRR) shape parameters [61]. Intra-cycle combustion control is also possible and in a pilot plus main injection mode, this utilizes the second injection fuel quantity to feedback control Heat Release (HR) with the aim to reduce the cycle-to-cycle combustion variations [62]. Fuel-path combustion phasing and IMEP closed loop control systems are usually found to be implemented using decentralized PID controllers because the fuel-path dynamics are fast and have less nonlinearity compared to air-path dynamics.

In summary, a review of diesel engine fuel-path control reveals that there are few works which discuss the application of multivariable control in fuel-path. Therefore, there remains much to investigate with innovative multivariable fuel-path closed loop control systems such as for fuel rail pressure, IMEP and or HR based speed governor, the closed-loop control of three-plus injection modes etc.

1.2 Research Questions

It is clear that there are multiple control inputs on a diesel engine that need to be adjusted according to changes in engine operating point or running state (i.e. steady-state/transient) in order to optimize its combustion process and satisfy the requirements of multi-objective performances such as fuel consumption and emissions etc. Additionally, all of these input variables couple strongly with each other via the combustion process. Therefore, a multi-variable control strategy is the best solution for optimal closed loop control performance.

Among all the multi-variable control strategies, MPC is widely accepted as a preferable control system because it is superior in cases of many manipulated variables where there is strong coupling. MPC is also an optimal control that can still perform in the event of actuator saturation and can also accommodate constraints on outputs and states. Its stability can always be achieved with a long horizon or a final step cost [63].

Given the background of the diesel engine air-path and fuel-path control, it is important to conduct an experimental study of the application of MPC on both air-path and fuel-path. More specifically, to explore new innovative closed loop control structures in fuel-path with the aim to optimize diesel engine performance. From this, there are two research questions posed to be investigated in this study:

1) How can multivariable control strategy MPC be applied in diesel engine control? What are the challenges and advantages to implement MPC in diesel engine control?
2) Are there new closed loop control structures that can either improve diesel engine performance or reduce engine control calibration effort?

1.3 Research Aims and Objectives

To answer the research questions proposed in the preceding section, the overall aim of this study is to improve the knowledge of application of MPC in diesel engines. More specifically, the aim is to improve the understanding of the diesel engine dynamics and the combustion process for the purposes of developing innovative and improved diesel engine feedback control systems.

The objectives for this study are outlined as follows:

- Demonstrate that identified dynamic models can form the basis for the design of the MPC controller for air-path and fuel-path control respectively.
- Design and test a controller for fuel injection that assists in the understanding of the degree of control authority that exists for the control of NO_x concentration in the exhaust flow.
- Compare two types of EGR flow rate model and explore the possibility of AFR and EGR ratio control structure.

- Discovery of new fuel-path closed loop control structures that enable the reduction of combustion variability, combustion inconsistency among cylinders and calibration effort.

1.4 Research Methods

Research methods used in this study include:

- Applying system identification technology using random perturbation of engine control inputs and collecting engine test data from which a model of the engine is derived for use in MPC control.
- Simulink® S-Function programing of an MPC controller and evaluation on an engine test bed to verify the controller design, controller calibration and controller performance.
- Applying a step response engine test to identify a low order transfer function model to investigate the general engine air-path and fuel-path dynamics.
- The use of engine sweep tests to determine relationships between inputs and outputs during the investigation of fuel-path control authorities and feedback control structures.
- Evaluation on the test engine of two EGR flow rate models to measure model reliability and accuracy.
- The use of LabVIEW software to develop and implement single loop PID controllers on the engine test bed based on identified dynamic models for innovative closed loop fuel-path control systems.

1.5 Research Contributions

This study makes several contributions to the body of knowledge in the field of diesel engine control. The major contributions are:

1) Reveals some basic features of the diesel test engine such as how the basic air-path and fuel-path dynamics vary with engine operating points; e.g. MAF-MAP relationships for both steady-state and transient conditions, disturbance sources, a standing wave type relationship between IMEP and injection dwell time attributed to a pressure wave inside the fuel rail and also significant combustion inconsistency among different cylinders.

2) Experimentally proves that MPC can be quickly implemented on a test engine and applied to both air-path (2I2O) and fuel-path (3I3O) and perform well in both steady-state and transient conditions.
3) Demonstration of a 2I2O SOI, RP online regulatory system which uses combustion diagnostics (CA50) and a pair of novel control set-points which relate CA50 to SOI and SOC and which requires minimal set-point calibration to achieve optimised diesel engine performance over a wide operating range.
4) Developed a novel two loop engine speed controller with an outer loop that controls IMEP set-point based on engine speed error and an inner loop which independently controls fuel quantity on each cylinder to match the IMEP demand of the outer control loop.
5) Reveals that for the test engine operating below 1400rpm with a three-pulse injection mode; the control of the split in fuel quantity between the second and third injections enables the separation of P_{max} and IMEP such that the second and the third injection fuel quantity can be used as control inputs respectively for P_{max} and IMEP.
6) Developed a closed-loop fuel-path controller which utilises the fuel rail pressure wave phenomenon to reduce combustion variation by adjustment of the dwell time between a split main injection.

1.6 Thesis Outline

This thesis comprises six chapters and each chapter is introduced as follows:

Chapter 1: **Introduction** describes the background and motivation of this study, proposes the research questions, states the research aims and objectives, briefs the research methods used in this study and contributions.

Chapter 2: **Literature review** focuses on the review of MPC technology and its applications in diesel engine control. The review also considers air-path and fuel-path controller design and controlled variable selection.

Chapter 3: **Understanding of engine dynamics** were gained in terms of low order air-path and fuel-path identified transfer function model, cycle-to-cycle variations, combustion inconsistency among cylinders, MAF and MAP relationships for different engine operating point.

Chapter 4: **Air-path control** presents the transient engine test of a developed 2I2O MPC system of MAF and MAP and the validation and choosing of a reliable EGR ratio model to be used in a 2I2O MAF and EGR rate PID control system.

Chapter 5: **Fuel-path control** presents an engine test of 3I3O fuel-path MPC control system, a two loop speed governor, a SOI and RP online adjustment closed loop control system and P_{max} and IMEP separated control system.

Chapter 6: **Conclusions** and contributions of this study.

Chapter 7: **Future Work** outlines the suggestions for future work in the research of diesel engine air-path and fuel-path control.

Chapter 2

2 Literature Review

2.1 Introduction

Literature reviews on MPC technology, diesel engine air-path and fuel-path control and their related topics such as control oriented model and EGR flow rate and volumetric efficiency model are presented in this chapter. These reviews help to narrow the research questions and find the proper research methodology used in this study.

The aims of the chapter are to:

1) Review of MPC technology and its application in diesel engine control to provide insights into the knowledge gaps in MPC technology and its strengths and weaknesses (Section 2.2).
2) Review of the control structures and control strategies used in air-path control to provide insights into air-path control problem formulation (Section 2.3.1 and Section 2.3.2).
3) Review of models used for EGR flow rate and volumetric efficiency estimation; identify candidate estimation approaches for EGR flow rate to implement in direct air-path EGR flow rate control (Section 2.3.3).
4) Review of fuel-path control to improve knowledge of the complexity and importance of the control fuel-path input variables (Section 2.4).
5) Review of diesel engine models to gain knowledge of the approaches utilised to develop control-oriented models for control (Section 2.5).

2.2 Review of MPC and its Application in Diesel Engine Control

This section reviews the literature concerning MPC technology and its application in diesel engine control and provides the foundation for the experimental study of MPC in both diesel air-path and fuel-path in this work.

2.2.1 MPC

The concept of MPC originates about thirty years ago [64, 65]. Nowadays, there are only two types of control strategy that have been successfully and

widely applied in industrial control tasks. One is PID control, the other is MPC. Compared to PID, MPC is a more advanced control technique since it belongs to model-based control design approach and can be used to control a wider variety of processes than PID control such as non-minimum phase and unstable processes [66]. Besides, MPC is the only generic control technology that can deal routinely with equipment and safety constraints [67]. When a state-space model is used as a predictive model, MPC is straightforward to apply to MIMO control problems and provides the best potential for decoupling control. Measureable disturbance and its disturbance model can also be included into MPC to develop a controlled system with the best disturbance rejection performance [66]. Compared to other advanced multivariable control designs such as Linear Quadratic (LQ) and H-Infinity (H_∞) control etc., MPC has the advantage of being easy-to-tune intuitively with online tuning parameters being closely related to control specifications [167] e.g.; adjustable weights, limits of rate of change of inputs/outputs and prediction and control horizons.

There are also several drawbacks to MPC design such as; the control problem formulation complexity, a high computation cost, the requirement for a high quality plant model and the complicated embedded optimization algorithm within the controller [66]. However, with the continuous rapid advances in microcontroller technology, MPC has become increasingly popular for fulfilling the control task of ‘fast systems’ such as engine control systems. Matured system identification technology also increases the possibility for the application of MPC to engine control, where the first principle model is very difficult to be obtained [68].

There are several different well-known ways to design a model predictive controller. They are: Dynamic Matric Control (DMC), Generalized Predictive Control (GPC), standard MPC, NMPC and EMPC. DMC uses step or pulse response models. GPC uses transfer function model or difference equation model. Standard MPC uses linear state-space model. NMPC uses nonlinear state-space model [69]. EMPC is equivalent to MPC in problem formation, but the optimal control is solved off-line as a Multi-Parametric Quadratic Program problem (mp-QP) and implemented as a piecewise optimal state feedback control law. This dramatically reduces the computation time of MPC but only practically applicable for low order systems [70].

Studies of the application of GPC, MPC, NMPC and EMPC methods in diesel engine control can be found in the literature from the last ten years. The following section provides a detailed review of these applications.

2.2.2 Application of MPC in Diesel Engine Control

In open literature only a limited number of research works consider the application of MPC in diesel engine control, especially works which discuss actual engine test results. In reference [71], two Single-Input Single-Output (SISO) and one MIMO standard MPC closed-loop control systems have been successfully developed and tested on a six-cylinder HD Homogenous Charge Compression Ignition (HCCI) engine on a cycle-to-cycle basis. The control structure of these two SISO MPC control systems are (Inlet valve close crank angle -> Angular position of the engine at 50% of the total cycle heat release (CA50)) and (Dual fuel ratio -> CA50). They both have very good tracking performance to CA50 set-point step change and very good disturbance rejection performance under step change of fuel energy per cycle. These two MPC SISO closed-loop systems are also implemented on a cylinder-to-cylinder basis.

The MIMO control structure is four-input and three-output. The inputs are 1) dual fuel ratio, 2) fuel energy per cycle, 3) inlet air temperature and 4) engine speed. The three outputs are 1) combustion phasing CA50, 2) Indicated Mean Effective Pressure (IMEP) and 3) cylinder pressure rate of change with crank angle degree. This MIMO MPC control system was only implemented on one cylinder. The good tracking performance of IMEP set-point and the good disturbance rejection performance under step change of inlet valve close angle are demonstrated by the engine test results. It can be seen that tracking performance was demonstrated on the other two outputs which are CA50 and cylinder pressure change rate, but the engine test results show that the required constraints on these two outputs were satisfied. The main function of this MIMO control system is closed loop IMEP control. The linear predictive state space models were obtained by using system identification technology. The exciting signals are Pseudo Random Binary Sequence (PRBS) signals.

A four-input five-output MPC control structure has been developed and tested on a six-cylinder turbo-charged HD diesel engine [49]. The four inputs are 1) crank angle degree of start of injection, 2) fuel injection duration in crank angle degrees, 3) position of the EGR valve, 4) position of the VGT vanes. The five outputs are 1) IMEP, 2) combustion phasing CA50, 3) maximum pressure derivative, 4) NOx emissions, 5) soot emissions. Predictive models were obtained using the same method as that in reference [71]. Engine test results show that this MIMO MPC control can track simultaneous IMEP and soot set-point changes meanwhile the combustion phasing was kept as constant and NOx emissions

and maximum pressure derivative were kept below the required maximum limits. The disturbance rejection performance to engine speed variation around the investigated operating point is also demonstrated. Since the inputs includes two air-path input variables and two fuel-path input variables, this MIMO MPC closed loop control system is an air-path and fuel-path coordinated control. This control structure is very promising, however, gain-scheduling work needed to be carried out to make this MPC controller work in a larger engine operating range.

A two-input-two-output air-path MPC control system was developed and tested on a diesel engine which equipped with EGR and Variable Nozzle Turbocharger (VNT) [27]. The two inputs are EGR valve position and nozzle open position and the two outputs are MAF and MAP. The tracking performance of this MPC control system was compared to PID control system on the same engine. Both MAF and MAP in the MPC control system had faster responses to set-point step change than with PID control and without overshoot. During a transient test, the PID control system produced a big overshoot on MAF and MAP while MPC control system did not. This test also confirms the potential for significant reductions in NOx emissions, but PM emissions are the same for these two control systems. The predictive model used in this MPC example is a system identified linear model plus Padé approximation of the dead time. However, this air-path MPC control is also requires extension to the whole engine operating range by model gain-scheduling.

An air-path EMPC control system has been developed and tested on a 2.2 litre diesel engine [11]. The control structure is two-input three-output and one measured disturbance. The two inputs are EGR valve position and VGT vane position. The three outputs are MAP, MAF and NOx emissions. The measured disturbance is fuel quantity. Very quick tracking performance of MAF and MAP to step set-point change has been obtained. No tracking performance is required on the third output NOx emissions. The third output only needs to be controlled under certain limit conditions. The predictive model is linear and is obtained using system identification technology. This research work is also lacking gain-scheduling.

Another example of air-path EMPC control can be found in reference [28]. The control structure consists of two inputs, two outputs and two measured disturbances. The two inputs are EGR valve position and VGT vane position. The two outputs are MAF and MAP. The two disturbances are engine speed and injected fuel amount. This control system was tested on a BMW diesel engine.

Good tracking performances on both MAF and MAP at fixed engine operating points were observed.

NMPC of air-path has been studied in reference [32, 44]. But this work only has simulation result on a virtual engine model.

The literature review in this section reveals that a system identified linear model is the most popular technique for practical MPC control in diesel engines. It also shows that the predictive model gain-scheduling method needs to be further investigated.

2.3 Review of Diesel Engine Air-Path Control

This section presents a review of control structure and controller design of air-path controls for a diesel engine that is equipped with both a VGT and high pressure EGR. Additionally, this section also presents a review of models of EGR flow rate and volumetric efficiency which are both going to be studied in this research for developing an air-path control system.

2.3.1 Controlled Variables Selection for Air-Path Control

Modern diesel engines are usually equipped with VGT together with high pressure EGR. The function of VGT is to use the energy of exhaust gas to compress air into the cylinder for combustion [72]. The VGT has a big impact on peak combustion pressure, AFR and pumping losses and the impact on each is in turn dependent upon the engine operating conditions. Therefore in a diesel engine equipped with VGT, both MAF and MAP need to be controlled to adapt to different engine operating points.

The function of EGR is to recirculate a portion of the exhaust gas back to engine cylinders to replace some of the excess oxygen, then lower combustion temperature and reduce the NOx emissions but with a penalty of increased PM emissions. The amount of EGR into the cylinder is closely related to the EGR gas flow rate and should be adjusted for different engine operating points. Since the EGR gas and the fresh intake air are mixed inside the intake manifold before entering into the cylinders, the EGR flow rate will change both MAF and MAP value. So most air-path closed-loop control system use MAF and MAP as controlled variables, because at a certain engine operating point, one pair of (MAF, MAP) values can uniquely reflect the amount of fresh air and EGR gas that enter the cylinders and these two variables are available in production engines equipped with MAF and MAP sensors [11-13, 15, 18-20, 22, 29-33, 40, 42].

There are other pairs of controlled variables selected to construct the air-path closed loop control which are: (MAF, EGR ratio) [17, 23, 27, 28], (AFR, EGR ratio) [16, 35], (EGR ratio, MAP) [14]. These control variables reflect the fact that the direct parameters that influence the combustion process are intake oxygen concentration or more precisely AFR inside the cylinder, the amount of intake EGR gas and intake manifold pressure. The intake manifold temperature normally does not change significantly due to the application of intake charge air and EGR gas cooling. Hence, AFR and EGR ratio are a good choice for air-path control variable selection for a diesel engine equipped with VGT and EGR as the design of set-point policy is more straightforward than that of (MAF, MAP) configuration. However, the measurement or estimation of EGR rate is the biggest challenge for this configuration.

2.3.2 Air-path Controller Design

The state-of-art closed loop control strategy in a production engine is decentralized PID control of MAF and MAP. The two SISO loops are normally: 1) VGT->MAP, 2) EGR->MAF [40]. However, the strong coupling between VGT and EGR implies that multivariable control will improve control performance especially during transients compared to decentralized PID control. It can be found in the literature that various multivariable control designs have been investigated in air-path control, for example LMI [30, 33], NMPC [32, 35], LQG [36], MPC [23, 26, 27, 37], H_∞ and robust control [10, 12, 15, 16, 18, 31], internal model structure [10], EMPC [11, 28], loop shaping [45], Lyapunov MIMO control [17], nonlinear optimal control [19], nonlinear inverse model control [20], slide control [22, 46], recursive model free control [29]. These advanced multivariable control strategies are complicated especially when air-path nonlinear dynamic model was used for controller design. The review of MPC in Section 2.2 also suggests that it is worth to further study the practical application of MPC in air-path.

2.3.3 EGR Flow Rate Model and Volumetric Efficiency

The following two sub-sections review the estimation methods of two important air-path variables which are EGR flow rate and volumetric efficiency respectively for the air-path in this study.

2.3.3.1 EGR Flow Rate Model

The commonly used first principle nonlinear air-path dynamic model in multivariable controller design requires the estimation of EGR flow rate. If one of the controlled variables of air-path control is selected as EGR ratio or EGR flow rate, the requirement on the accurate estimation of EGR flow rate is more noticeable. Practically, there are mainly two approaches to estimate EGR flow rate which are orifice equation model and total speed-density intake gas model. In the literature, the most used estimation method of EGR flow rate is the orifice flow equation [15-17, 21, 73, 74]. However, the validation results of an orifice EGR flow rate model over the whole engine operating range reported in [75] indicate that an orifice model alone is not accurate enough. A nonlinear correlation equation is also required but it is only valid for a particular engine setup.

2.3.3.2 Volumetric Efficiency Model

When the total speed-density intake gas model is used to estimate the EGR flow rate, a key part of this model is an accurate model of volumetric efficiency. Volumetric efficiency is affected by many factors such as compression ratio, engine speed, ratio of exhaust to inlet manifold pressure, intake and exhaust valve geometry, size, life and timing [5]. For a specific engine, the variables that have a big impact on volumetric efficiency are the gas flow speed and the residual gas amount and these are related to a further two variables which are engine speed and ratio of exhaust to inlet manifold pressure respectively [76].

The volumetric efficiency of a diesel engine is higher than that of an equivalent power SI engine and a turbocharged diesel engine can also have roughly 10% higher volumetric efficiency compared to naturally aspirated diesel engine. In the mid-speed range where an engine has high maximum torque, the volumetric efficiency of a turbocharged diesel engine can exceed 100% [77]. An example of a mathematical relationship between the volumetric efficiency and ratio of intake and exhaust pressure for a single cylinder SI engine is presented in [76]. An alternative to a physical model of volumetric efficiency is a correlation model obtained from engine test data for a particular engine.

2.4 Review of Diesel Engine Fuel-Path Control

First this section reviews the fuel injection modes used in diesel engines and the impact of different modes on engine performance. Then a review of rail

pressure wave phenomena is presented as this is going to be discussed later in this work. Finally, a review of fuel-path control literature is presented.

2.4.1 The Injection Mode and Rail Pressure Wave

The following two sub-sections focus on the reviews of fuel injection mode and common rail pressure wave to reveal the necessity in the study of control under multiple injection pulse mode and the investigation of the impact of rail pressure wave on combustion process.

2.4.1.1 Injection Mode

The fuel injection mode that is commonly used in modern diesel engine is two-pulse injection mode which is a pilot plus a main injection. Pilot injection is the injection of a small amount of diesel fuel before the main injection event. It was reported in literature [78] that the combustion noise was reduced by pilot injection, however, at high load and large EGR, the smoke has shown strong trade-off with combustion noise. Smoke emission has a relationship with the pilot flame when the main injection starts (dwell time); reducing the pilot flame can contribute to the control of smoke emission. Therefore more flexibility in pilot quantity and pilot-main interval time control can be a solution for breakthrough of the trade-off with combustion noise and smoke. The common rail fuel injection system has such flexibility by providing two controllable input variables which are fuel ratio and dwell time. The study in [4] reveals that when fuel ratio is decreased, that is the pilot injection fuel quantity increases whilst the main injection fuel quantity decreases to maintain the same total injected fuel quantity, both soot and NO_x emissions increase as premixed phase is reduced.

The effects of multiple injections where more than two-pulse injections are applied in a High Speed Direct Injection (HSDI) diesel engine equipped with common rail injection system were explored in [9]. It was found that pilot-injection reduced the ignition delay of main injection, and then contributed to the improvement of power output by controlling the premixed combustion. The post-injection was found to be very effective in completing the oxidation process and reducing the particulate emissions even when small fuel quantities were injected. It was also found that multiple injections could reduce particulate emissions by more than 40% in some cases. The results indicate that a significant improvement in the reduction of NO_x and smoke emissions can be achieved when multiple injections are used in combination with low pressure injection.

Multiple injections appear to be more effective at low pressure injection in reducing NO_x and PM than at high pressure injection.

2.4.1.2 Rail Pressure Wave

In [4] it was also found that the pressure wave caused by pilot injection event inside the common rail and injection pipes can change the characteristics of the main injection to a great extent when particular values of dwell time are selected. Figure 2.1 provides an example of the common rail pressure wave and the injection rate and is reproduced from [4]. Here, the SOI and End of Injection (EOI) are highlighted for the pilot injection and the corresponding disturbance of the fuel rail pressure is clear.

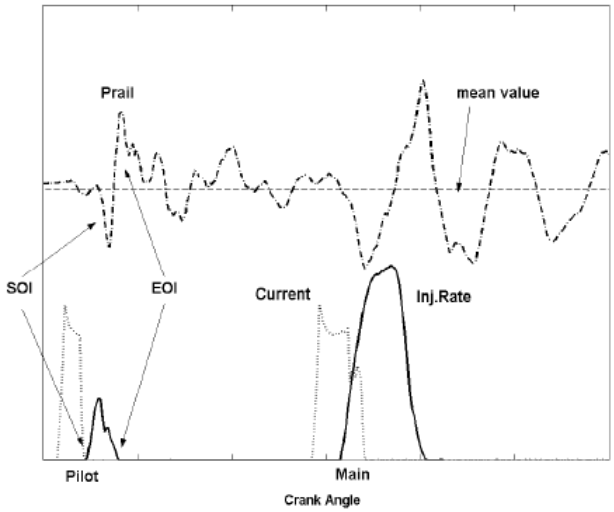

Figure 2.1: Comparison between the common rail pressure wave and the Injection rate (Reproduced from [4])

A similar pressure wave inside a common fuel rail was also found in [8]. This pressure wave was found to have an impact on the operation of the nozzle-needle and fuel delivery in the pilot-main-post 3-injection mode. The needle opening for post injection was affected by its timing relative to the main injection event (dwell time). The injection-to-injection variation for post injection caused by fuel rail pressure fluctuation is shown in Figure 2.2 for reference [8].

From Figure 2.2 it can be observed that a pressure wave developed after the main injection and it was found that this could cause the needle to fail to lift irrespective of the command signal period for the post injection and thus injection-to-injection variations were detected in the post injection. Although not shown in Figure 2.2, the pressure wave from the pilot injection, being relatively

small in amplitude compared to that induced by the main injection, was observed to have no effect on the main injection event.

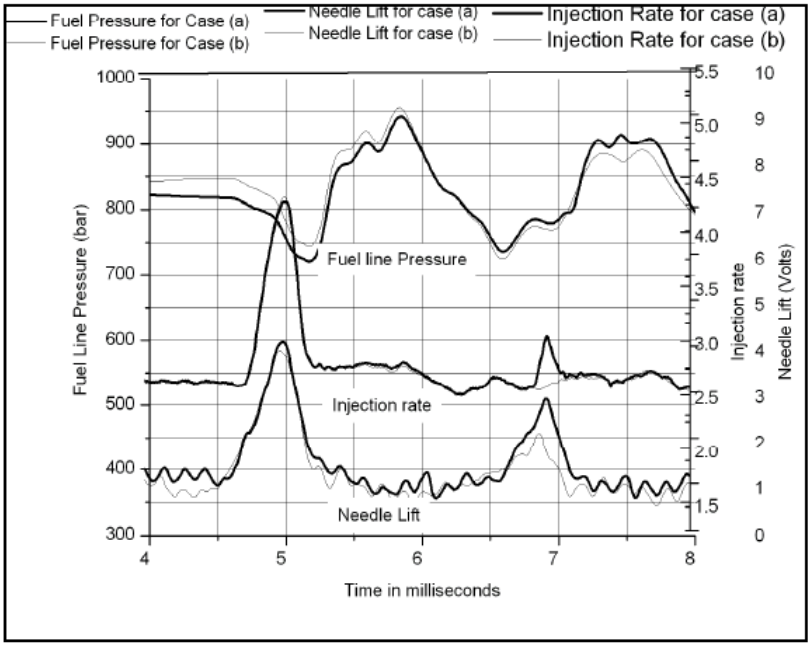

Figure 2.2: Injection-to-injection variation for post injection (Reproduced from [8])

The impact of such rail pressure wave on combustion process in terms of IMEP and P_{max} (peak cylinder pressure) has not been found in the literature.

2.4.2 Literature Related to Fuel-Path Control

The number of research works which discuss fuel-path control in literature is far less than the number concerned with air-path control. In regard to production diesel engines, a diesel engine speed governor that based on an engine speed sensor and engine speed demand is the only mature closed-loop fuel-path control system which is widely in use.

In literature, the most frequently studied fuel-path control systems are cylinder pressure sensor based combustion phasing control and IMEP control [55, 56, 60]. The control structure and control strategy are normally decentralized PID control with fuel quantity control of IMEP and SOI control of CA50. Figure 2.3 shows an example block diagram of single closed loop control of CA50 or IMEP using SOI that is reported in [56]. In this example, a PID controller uses the feedback from a cylinder pressure sensor (raw signal processed cycle CA50 or IMEP) to make next-cycle (inter-cycle) adjustment of fuel injection phasing (SOI, injection duration) to achieve a target CA50 or IMEP set-point. This form of control design therefore makes small changes in fuel injection phasing to adjust

for factors such as fuel quality or fuel type which cannot be wholly factored into a traditional diesel engine open loop engine calibration based control scheme.

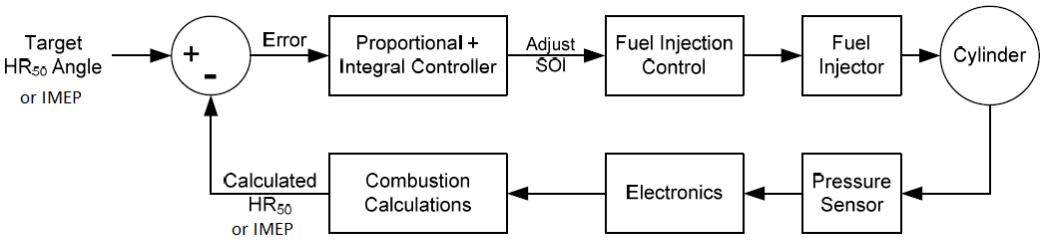

Figure 2.3: Block diagram of CA50 or IMEP closed loop control by using SOI as control input (Reproduced from [56])

Presented in Figure 2.4 is a block diagram of CA50 and IMEP closed loop control using SOI and fuel quantity as control inputs which is reproduced from [55]. As the controlled variables in such control systems are computed from measured combustion pressure, this form of control can be regarded as *combustion process control*. One application of combustion process control is to increase the combustion stability in engines that employ combustion concepts such as HCCI and Low Temperature Combustion (LTC) [71, 79, 80] and which have inherently greater cycle-to-cycle variability than a conventional CI cycle.

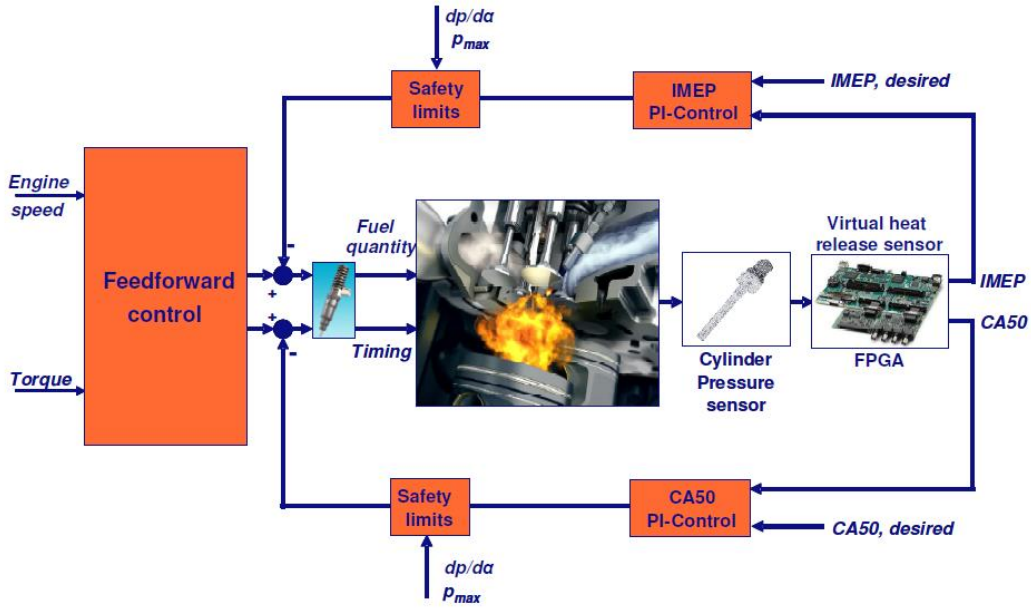

Figure 2.4: Block diagram of CA50 and IMEP closed loop control by using SOI and fuel quantity as control inputs (Reproduced from [55])

By controlling combustion phasing (CA50) and combustion power (IMEP) on the basis of in-cycle (intra-cycle), cycle-by-cycle (inter-cycle) and cylinder-by-cylinder; combustion variation at engine steady state will be reduced. This helps

to improve engine torque balance (refinement) and also has potential to slightly improve engine emission and fuel consumption performance [56, 57]. Engine test results show that combustion process control can have good tracking performance for set-point step change and disturbance rejection ability in respect to other inputs.

Summarising fuel-path control examples in literature: A feedback control system which utilises SOI to control the Start of Combustion (SOC) has been studied in reference [57]. The closed-loop control of predicted ignition delay using SOI is shown to be able to reduce NO_x emissions during engine transient [48]. Both air-path and fuel-path control were coordinated within a MPC control structure in [49]. An example of fuel-path control which utilises intra-cycle control to vastly minimize the cycle-to-cycle combustion variations is discussed in [62]. When fast response piezoelectric injectors are used as actuators, Heat Release Rate (HRR) shape control can be implemented [61]. However, this control work was only demonstrated on an injector test rig instead of a real engine. Combustion inconsistency among cylinders has been reported and was improved by individual fuel-path controller for each cylinder [55-57, 71].

This review indicates that there is strong potential in the study of the application of multi-variable control strategy in the form of MPC on the engine fuel-path. Highlighted topical areas include the closed-loop control of fuel rail pressure, closed-loop control with an IMEP based engine speed governor and the closed-loop control system of a three-plus injection mode etc.

2.5 Diesel Engine Models

A model is a set of mathematical equations, maps or digital representation from inputs to outputs or among states of the real physical object. There are different types of diesel engine models which have been developed for different purposes. Depending on the application, models may differ in model inputs, outputs, model states, model complexity and accuracy. For example, GT-POWER is the industry-standard engine simulation tool, it can be used to develop a "virtual diesel engine" in the computer for design validation, DOE/optimization, neural networks and control modelling. It has Direct Injection (DI) diesel multi-zone model (400 zones), 3-D CFD cylinder model, aftertreatment (catalyst) model, EGR and turbo charger model and acoustics model etc. It can be embedded in the MATLAB® Simulink® environment to simulate the controlled plant [7].

During the development of a diesel engine control system, not only is the virtual engine needed as the controlled object in control simulation, more importantly, a relatively accurate, simple, low order dynamic model for controller design is also required.

The dynamics of diesel air-path is well understood but the combustion process is not because the combustion is a highly complex chemical reaction process [5]. However, in literature there are many works which address combustion modelling [6, 81-121]. Such research is leading to a better understanding of the combustion process and also improved combustion control structure. The ultimate goal of diesel engine combustion control is to produce cleaner, more fuel efficient, more durable diesel engines by optimizing the engine combustion performance online.

A nonlinear physical dynamic model can be used in nonlinear controller design or it can be linearized into a linear dynamic model for linear controller design. Normally the order of those models should be as low as possible to get a lower order controller for implementation, otherwise the model order or controller order reduction should be considered [122]. If the physical dynamic model is difficult to develop, an alternative way is to get an identified model by perturbation of the control inputs on a test engine and then applying system identification techniques to the collected test data; models developed in this way are usually linear. Since such identified linear models are only valid within a limited engine speed and torque operating range, gain scheduling is unavoidable for a control system design that can work for the whole engine operating range [10, 11, 47, 52].

No doubt future engine control systems will greatly benefit from a model-based control approach for performance optimization and robustness enhancement [55]. Some of the commonly used control-oriented diesel engine models are reviewed in the following sections.

2.5.1 LPV Model

A Linear Parameter Varying (LPV) model defines a set of low order linear dynamic models in which the model parameters vary with engine operating point or other control inputs or measured engine variables. The typical application of LPV model in diesel engines is for air-path control [12, 13, 15, 30, 73]. Figure 2.5 shows the simplest type of LPV model which is a first order transfer model from exhaust pressure to intake manifold pressure which is reproduced from [12]. The

two model parameters a_1 and b_1 are not constant; they vary depending on the output value.

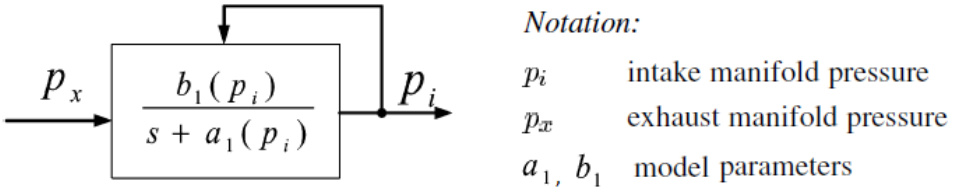

Figure 2.5: Intake manifold pressure LPV model (Reproduced from [12])

A complete air-path quasi-LPV model is shown in Figure 2.6 which is also reproduced from [12]. It can be seen that the nonlinearity of the air-path is modelled by using a static nonlinearity function or map.

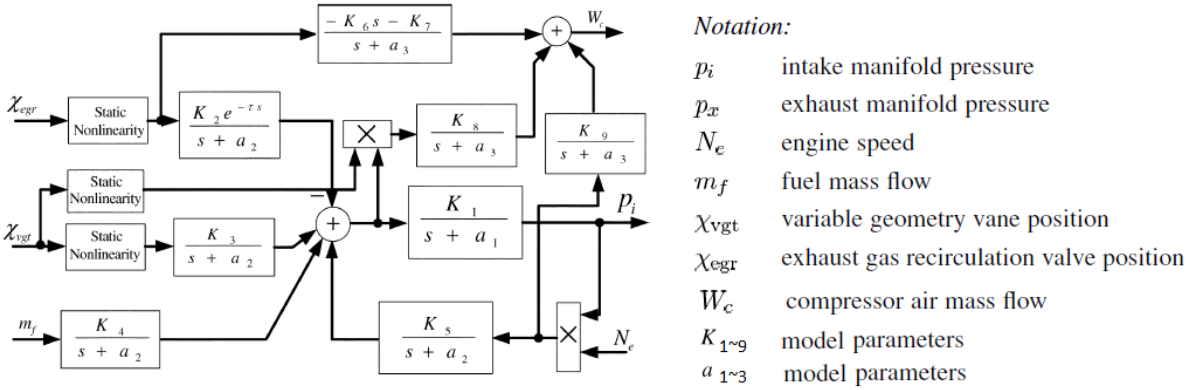

Figure 2.6: Complete quasi-LPV model for air-path dynamics (Reproduced from [12])

This transfer function LPV model set can be converted into a state space model (Equation 2.1) which is then used in the multi-variable H_∞ controller design in [12].

$$\begin{pmatrix}\dot{x}_1\\ \dot{x}_2\\ \dot{x}_3\end{pmatrix} = \begin{pmatrix}-12.6 & 8.2 & 0\\ 1.01+4.0\rho_1 & -2.08 & 0\\ 0.12+4.04\rho_1 & -0.37-0.44\rho_2 & -1.33\end{pmatrix} \times \begin{pmatrix}x_1\\ x_2\\ x_3\end{pmatrix} + \begin{pmatrix}0\\ 2.06\\ 0\end{pmatrix} d + \begin{pmatrix}0 & 0\\ -25.65 & 40.32\\ -18.27 & 0\end{pmatrix}\begin{pmatrix}u_1\\ u_2\end{pmatrix} \quad \textbf{(2.1)}$$

where, $x_1 := p_i$ $\quad d := m_f$ $\quad u_1 := \chi_{\text{egr}}$ $\quad \rho_1 = N_e/10\,000$

$x_2 := p_x$ $\quad u_2 := \chi_{\text{vgt}}$ $\quad \rho_2 = \chi_{\text{vgt}}/100.$

$x_3 := W_c$

However, the prediction of emissions by using LPV modelling method does not have as good accuracy compared with the application in engine air-path [123]. This is due to the underlying dynamics of the combustion process being much more complex and also a static nonlinearity map is unable to cover dynamic nonlinearities in the emission modelling, in particular for soot [68].

2.5.2 Mean Value Engine Model

A Mean Value Engine Model (MVEM) is a higher level modelling methodology compared to LPV model but lower level in comparison to a cyclic combustion event-based model. Like a LPV model, a MVEM model is usually used in air-path control system development. In this type of model, the combustion process is normally modelled as a static map which is established based on engine test experimental data [16-18]. A block diagram of MVEM of diesel engine for air-path AFR and EGR rate control is illustrated in Figure 2.7 and is based on the modelling work in [16].

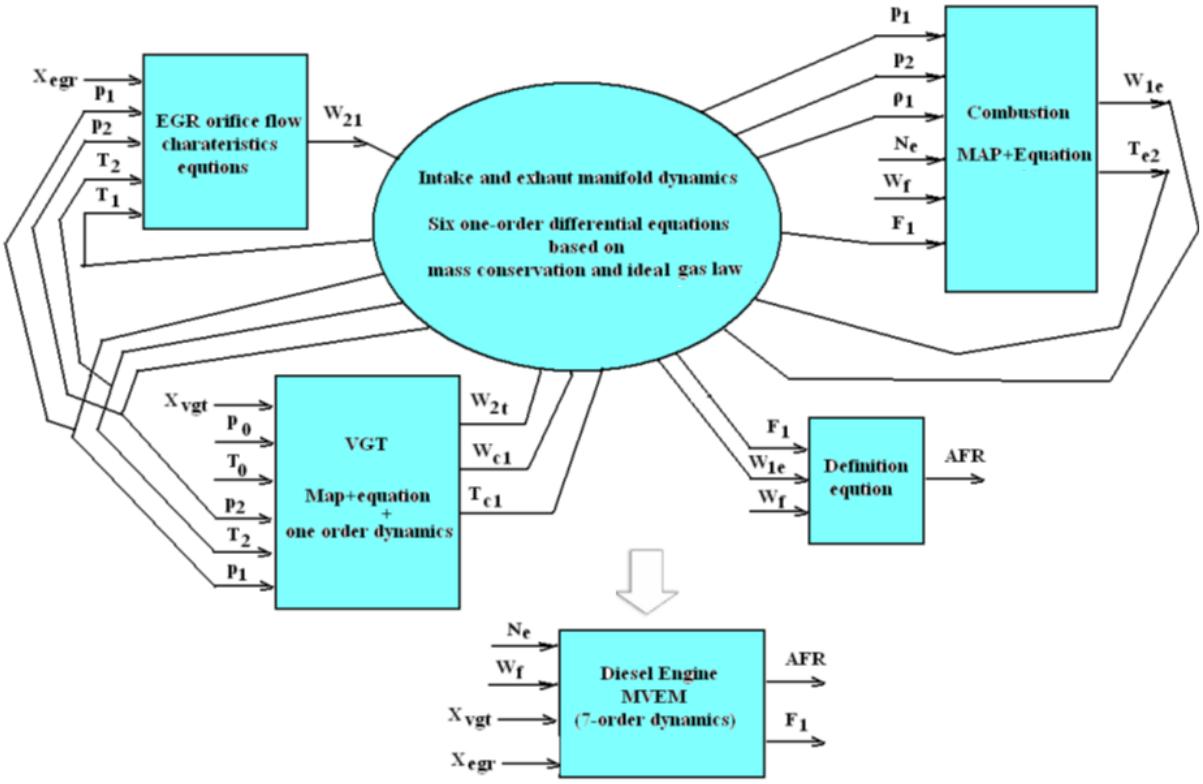

Figure 2.7: Block diagram of MVEM of diesel engine for air-path AFR and EGR rate control [16]

Notation in Figure 2.7:

X_{vgt}	VGT vane position	p_0	Atomsphere pressure	W_{c1}	Compressor mass flow rate
X_{egr}	EGR valve position	p_1	Intake manifold pressure	W_{1e}	Mass flow rate into engine
N_e	Engine speed	p_2	Exhaust manifold pressure	W_{21}	EGR mass flow rate
W_f	Fueling rate	T_0	Atomsphere temperature	W_{2t}	Turbine mass flow rate
AFR	Air fuel ratio	T_1	Intake manifold temperature	ρ_1	Intake air mass density
F_1	EGR ratio	T_2	Exhaust manifold pressure		
		T_{c1}	Compressor flow mass temperature		

For the block diagram presented in Figure 2.7, the main modelled dynamics are based on a six order scheme developed from gas mass conservation law and

ideal gas law. This scheme can be simplified into third order dynamics if the slow thermal dynamics are ignored. Combustion process dynamics are not included in MVEM except in the form of a nonlinear static map relationship. There are many examples in literature of research works which implement a MEVM in air-path control [19-23, 60, 124-129].

2.5.3 Phenomenological Combustion and Emission Model

A zero or quasi-dimensional phenomenological combustion and emission modelling methodology not only helps engine researchers to understand the dominant mechanisms involved in the combustion and emission formation process, but also provides a set of simple mathematical models that can be used in the design and implementation of an engine control system with the objective of engine performance optimization [120, 130].

Combustion and emission modelling are closely related. The emission model is usually a second modelling stage after combustion modelling. It uses the output of the combustion model as inputs. A combustion model is for prediction of combustion pressure and combustion temperature under different air-path and fuel-path input conditions and different engine operating conditions [130, 131].

Within the zero-dimensional combustion model, there are four main parts of sub-models which are: a spray model, a turbulence model, a fuel vaporization model and a combustion model. The block diagram of such a combustion model is shown in Figure 2.8 which is reproduced from [114].

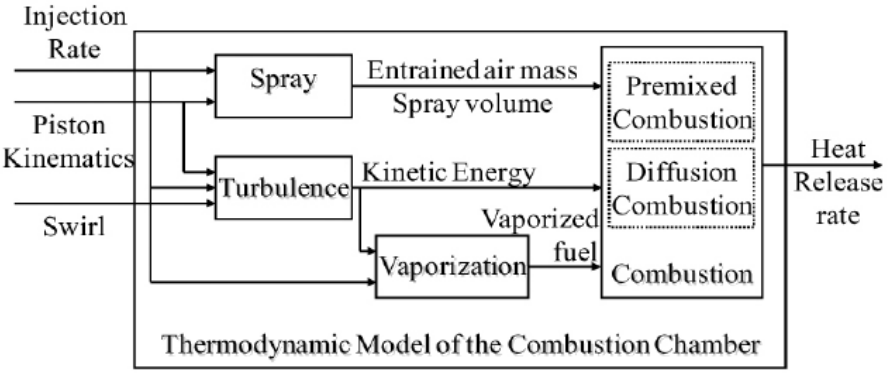

Figure 2.8: Block diagram of a phenomenological combustion model (Reproduced from [114])

Emission modelling is currently only for prediction of NO_x and soot emissions under various engine control inputs and operating conditions. NO_x modelling is usually based on the extended Zeldovich mechanism. The block diagram of an emission model for NO_x emission prediction developed in [132] is shown in

Figure 2.9. This model is based on cycle combustion information about burned rate, combustion flame temperature and the nitrogen and oxygen concentrations. A recent review about the state of NO_x modelling research can be found in [133] and further NO_x emission modelling methods are reported in [130, 134-143].

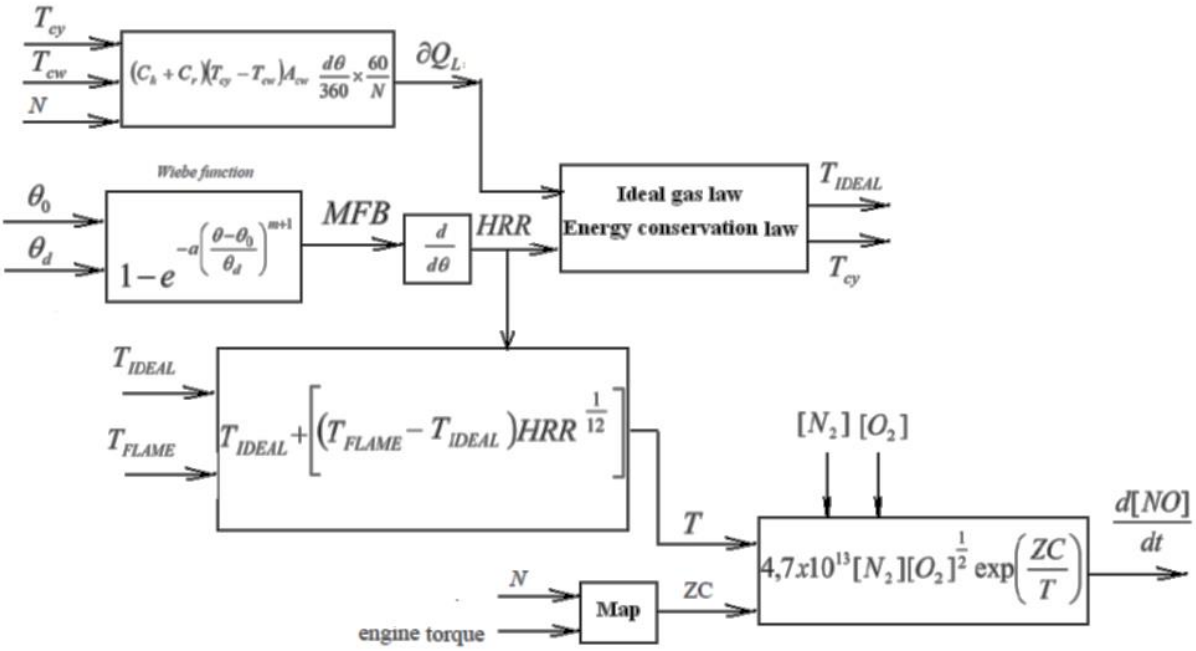

Figure 2.9: Block diagram of an emission model for NO_x emission prediction [132]

Notations in Figure 2.9:

MFB = mass fraction burned

HRR = heat release rate of main injection

A_{cw} = cylinder wall area,

C_h = convection heat transfer coefficient in W/m^{2}K,

C_r = radiation heat transfer coefficient in W/m^{2}K,

θ = instantaneous crank angle degree

θ_0 = ignition timing,

θ_d = burn duration

N = engine rotational speed,

T_{cy} = in cylinder temperature

T_{cw} = average wall temperature,

T = combined temperature used to determine the formation of NO_X,

T_{IDEAL} = average in cylinder temperature calculated from Ideal Gas Law

T_{FLAME} = adiabatic flame temperature,

ZC = A coefficient used to control the rate of NO formation with respect to temperature,

∂Q_L = heat transfer to cylinder walls,

a = coefficient relating to the combustion efficiency

m = coefficient which controls the Heat transfer during the closed cycle

Most soot modelling works found in the literature are based on the Hiroyasu model [6]. It was discovered that there are two opposite reactions undergoing the combustion process which are soot formation and soot oxidation. The net of soot formation rate equals the soot formation rate minus the soot oxidation rate. A block diagram of an example soot model developed in [144] is shown in Figure 2.10. There are four inputs used in this model. They are mass of unburned fuel vapour, cylinder pressure and temperature, and partial pressure of oxygen. Further soot modelling works are reported in [131, 145-151].

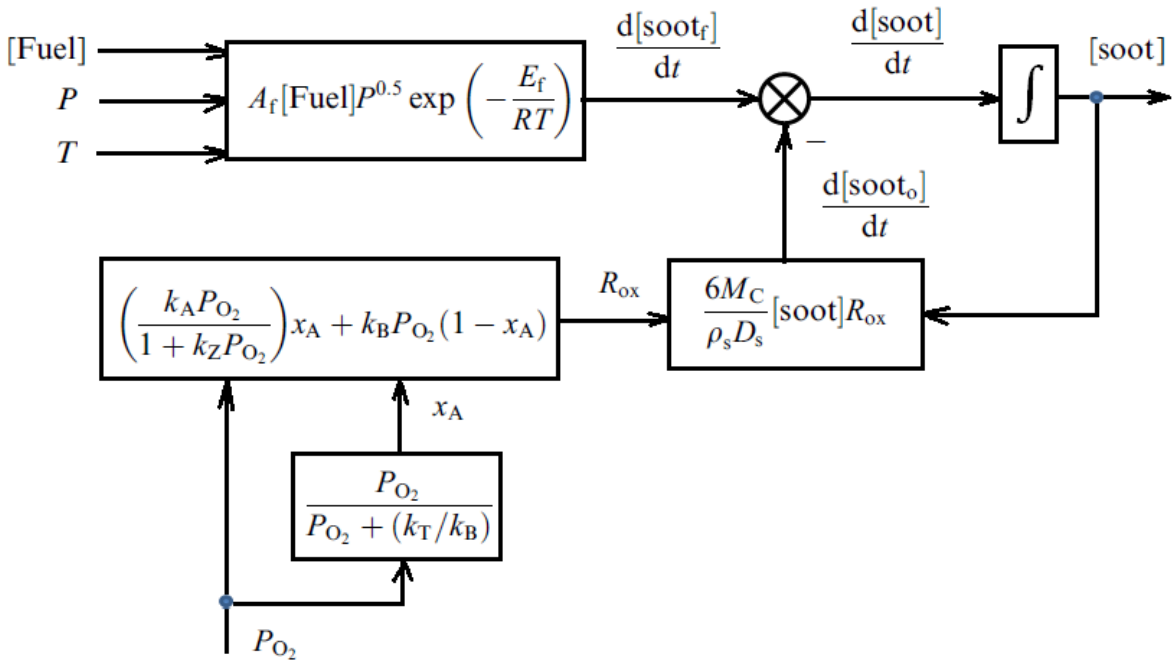

Figure 2.10: Block diagram of an emission model for soot emission prediction [144]

Notations in Figure 2.10:

$\frac{d[soot]}{dt}$ net soot formation rate

$\frac{d[soot_f]}{dt}$ rate of formation

$\frac{d[soot_o]}{dt}$ rate of oxidation

[soot] net soot mass

A_f empirical constant for formation

[Fuel] mass of unburned fuel vapor

P cylinder pressure

T cylinder temperature

E_f activation energy for the soot formation

M_c carbon molecular weight (12 g/mol)

ρ_s soot density (2000 kg/m^3)

D_s soot diameter (3×10^{-8} m^3)

R_{ox} sur- face oxidation rate.

P_{O_2} partial pressure of oxygen

x_A proportion of A sites

rate constants: $k_A = 20\exp\left(-\frac{15100}{T}\right)$

$k_B = 4.46 \times 10^{-3}\exp\left(-\frac{7640}{T}\right)$

$k_T = 1.51 \times 10^{5}\exp\left(-\frac{48\,800}{T}\right)$

$k_Z = 21.3\exp\left(\frac{2060}{T}\right)$

Prediction models for NO_x (e.g. Figure 2.9) and soot emission (e.g. Figure 2.10) were initially developed for the Integrated Emission Management (IEM) for the optimisation of the synergy between engine and after-treatment, of which the ultimate aim is to realize minimal fuel consumption within the limits by emission legislation. However, those models could be further developed into models for direct NO_x and soot emission control [51, 55].

2.5.4 Black Box Model

When no a priori system information is available and the experimental data are used throughout the modelling process, even in the early stages when the choosing model order, such modelling methods are named as *black box modelling* [152]. In the control field, such technology is referred to as *system identification* [153].

The utilisation of the System Identification Toolbox (SIT) in MATLAB® is a very convenient tool to develop either linear or nonlinear black box models from experimental data. For modelling a dynamic system between the inputs and outputs, the SIT candidates for linear black box models include: Autoregressive Model with Exogenous Input (ARX), Autoregressive Moving Average Models with Exogenous Inputs (ARMAX) and Output Error (OE) models.

Hammerstein, Wiener and Hammerstein-Wiener models are nonlinear black box models which can model a system with static nonlinear input output relationship connected in series with linear dynamics. Nonlinear ARX model (NLARX) is another nonlinear black box model which can model system nonlinear dynamics. The flexibility of setting the nonlinearity estimator in this model endows it with broad applicability in nonlinear dynamic system modelling. The nonlinearity estimator types could be wavelet network, sigmoid network, Neural Network (NN) and custom nonlinear network etc. [153].

In literature there are a number of examples of these forms of black box model which are derived from diesel engine test data that have been used for prediction of engine variables, especially emissions, and also control system implementation [152, 154-165]. In [152], the authors used a nonlinear Wiener model to model soot emission from heavy-duty diesel engines in transient operation. This is illustrated in Figure 2.11 in which 'NL' refers to a nonlinear Wiener function.

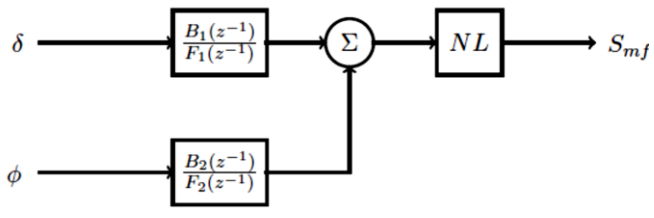

δ injected fuel mass per cycle
ϕ equivalence ratio
S_{mf} soot mass flow

Figure 2.11: Nonlinear black box model for soot emission estimation (Reproduced from [152])

In [155], a Back Propagation (BP) NN together with an improved training method by fuzzy if-then rules was used to develop a NO_x emission predictor, Figure 2.12, which was claimed to have very high accuracy with a validation coefficient of 0.96 for a diesel engine running a Non-Road Transient Cycle (NRTC). This model was developed for future NO_x emission control.

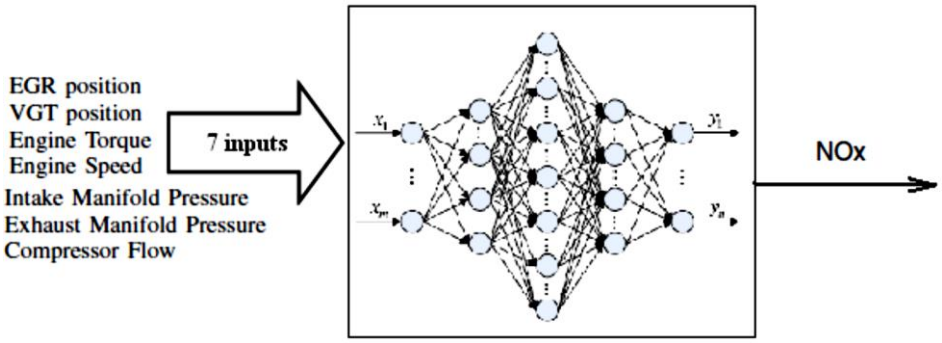

Figure 2.12: NN NO_x emission model (Reproduced from [155])

In [154], a NLARX model with recurrent NN as nonlinear estimator was used to estimate the Break Specific Fuel Consumption (BSFC) and intake MAP, the model structure is shown in Figure 2.13.

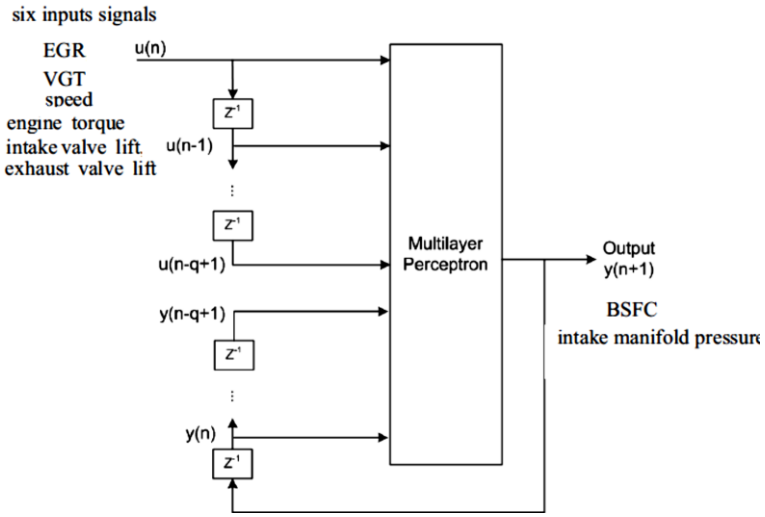

Figure 2.13: NLARX model for BSFC and intake manifold pressure estimation (Reproduced from [154])

The model depicted in Figure 2.13 was developed to be used in feedback air-path control and Variable Valve Actuation (VVA) control. The same group have also published a further three works which describe promising results about the application of NLARX modelling to NO_x emissions, in-cylinder pressure and fuel flow rate (fuel consumption). Compared to a NN model, a NLARX model structure uses not only the current inputs but the history of inputs and outputs as inputs to

a NN as well. Such a structure has potential to map or remember some certain dynamic patterns.

With system identification technology, it is also possible to get an identified transfer function and state space linear dynamic model based on perturbation test data. In [11], an identified two-input-two-output model was used in an air-path MPC control system and this model was developed from system identification based on engine data for PBRS excitation of the EGR and VGT positions. This excitation is illustrated on the left of Figure 2.14 along with the engine speed and fuel rate. As a single linear model is not able to approximate the engine over the whole operating range (different speed and fuel injection amount); at total of 12 regions were defined empirically for the speed and fuel rate operating range as illustrated on the right of Figure 2.14.

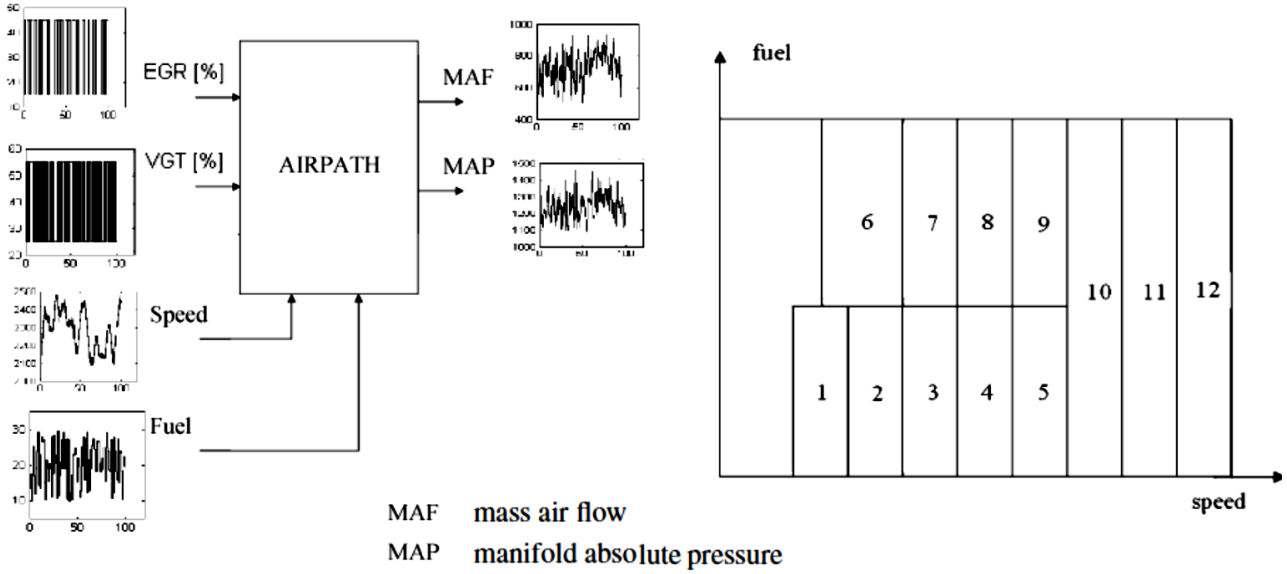

Figure 2.14: Perturbation test for air-path model identification (Reproduced from [11])

Model gain-scheduling was utilised in the air-path MPC control shown in Figure 2.14; this involves the model in use being selected based upon the region in which the engine is operating, defined in the right half of Figure 2.14. When the engine operating speed and fuel rate change such that the operating region also changes, the identified linear model applicable to the new region is then applied in the MPC controller. The same approach is also applied in the fuel-path control with three inputs and three outputs at 1550rpm and 250Nm engine operating point in [47]. The left half of Figure 2.15 illustrates the input-output configuration of the three-input-three-output fuel-path control structure detailed in [47] and the right half of Figure 2.15 illustrates the model gain-scheduling segments for MPC control over the whole engine operating range.

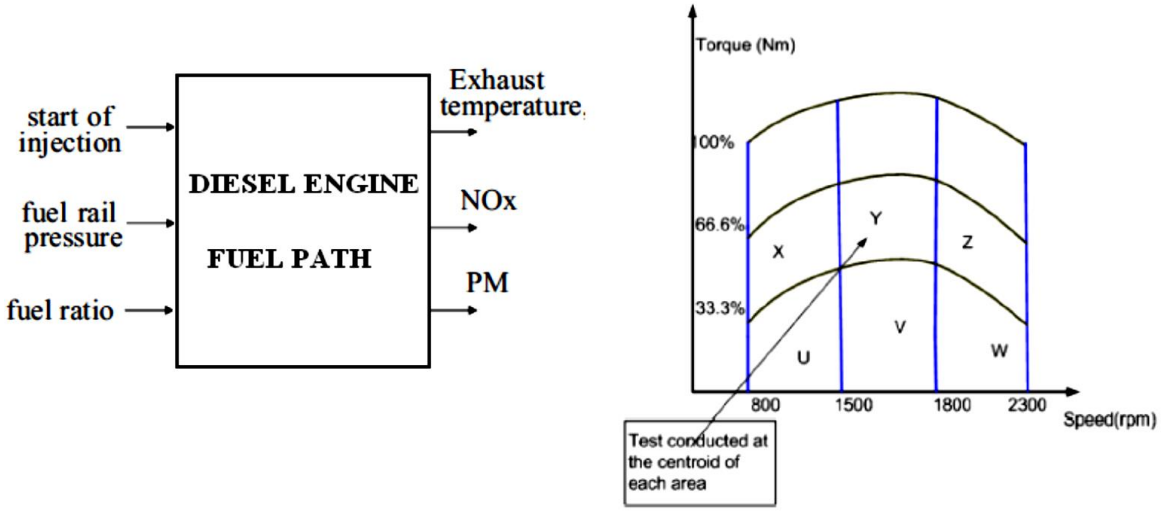

Figure 2.15: Three-input-three-output fuel-path control diesel engine for system identification modelling in (Reproduced from [47])

In [49], a four-input-five-output six order state-space model was identified at fixed engine speed 1200rpm while IMEP was allowed to vary from 6 to 8 bar. The controller used in this work was also a MPC controller which performed simultaneous control of the air-path and fuel-path. The outline of this controller is illustrated in Figure 2.16.

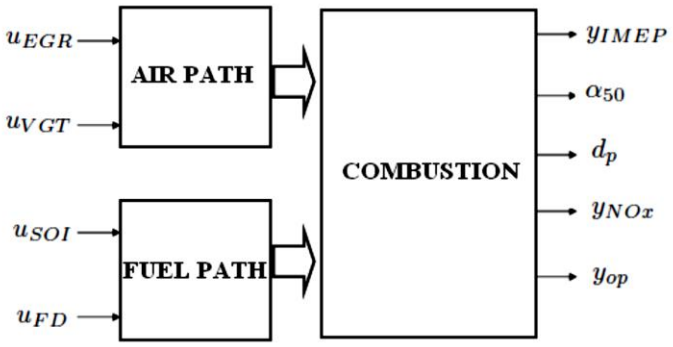

u_{EGR}	position of the EGR valve.
u_{VGT}	position of the VGT vanes.
u_{SOI}	crank angle degree of start of injection
u_{FD}	fuel injection duration
y_{IMEP}	indicated mean effective pressure
α_{50}	crank angle degree where 50 % of the heat has been released
d_p	maximum pressure derivative
y_{NOx}	Emissions of NO_x
y_{op}	Soot emissions

Figure 2.16: Four-input-five-output engine air-path and fuel-path simultaneous control layout for system identification (Reproduced from [49])

2.5.5 Summary of Diesel Engine Models

A summary of the four types of engine model discussed in the forgoing sections is presented in Table 2.1.

Table 2.1: Diesel engine modelling method

Model type	Modelling Method	Application
LPV	Model parameters identification	Controller design and control system simulation
MVEM	Physical law Empirical regression Data mapping	Engine simulation Static performance knowledge Air-path control
Phenomenological combustion and emission model	Thermal dynamics law Chemical kinetics law Spray model	Combustion and emissions control Engine performance optimization
Black box model	Transient experiment test Perturbation test MATLAB® SIT toolbox	Engine variables prediction Air-path control Fuel-path control Combustion and emission control

The review of diesel engine models in this section shows that the first principle models of the diesel engine, either for air-path or fuel-path, and which also include combustion processes, are complicated. For the purposes of control system design, a black box model is the quickest way to obtain a dynamic model for controls integration. This is however subject to the availability of appropriate engine data for model development.

2.6 Trade-off Phenomenon in the Diesel Engine

When a diesel engine operates at a steady-state condition, changes in either the air-path or fuel-path control inputs result in trade-off phenomenon for engine fuel consumption, NO_x and PM emissions. Consequently, when the air-path and fuel-path control inputs are automatically adjusted online via feedback closed-loop systems, the design of set-points of the controlled variables has to cope with this trade-off phenomenon. The trade-off phenomenon makes the optimization process of a diesel engine, in terms of fuel consumption and emissions for the

whole engine operating range, a difficult exercise due to the nonlinearity of engine behaviour and difficulty in developing an engine model for the optimization process.

Reports of such trade-off phenomenon in diesel engines can be found in the literature [166-170]. In general, when the EGR rate is increased, NO_x emissions decrease whilst the fuel consumption and PM emission increase. Figure 2.17 is copied from [166] and the left half provides an example of the trade-off between NO_x and PM emission for different fuel types when the EGR rate is increased. Injection timing is another input variable that has influence over the diesel engine trade-off between NO_x and PM emissions. The right half of Figure 2.17 illustrates that this trade-off relationship changes for different fuels, with biodiesel and GTL fuels producing generally less PM emissions at the same engine operating condition and that diesel fuel has a slightly greater sensitivity in PM emissions as injection timing is retarded (for the same AFR).

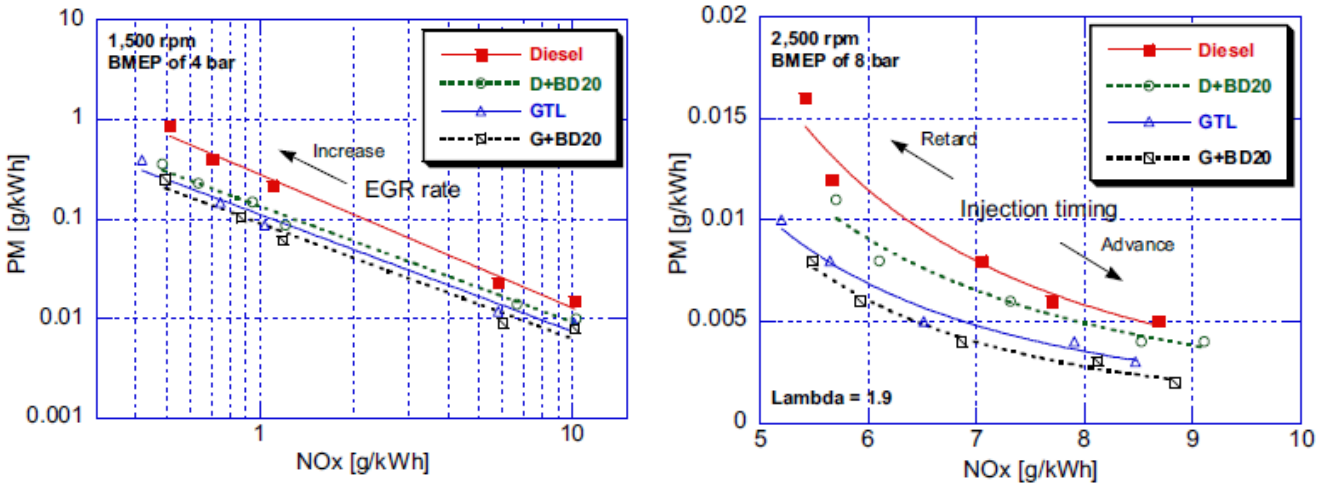

Figure 2.17: NO_x and PM trade-off for different fuels with EGR variation (left) and injection timing variation (right). D=diesel; BD=biodiesel, (Reproduced from [166])

The Specific Fuel Consumption (SFC) and NO_x emission trade-off, smoke emission and NO_x emission trade-off in response to injection timing variation under different engine operating conditions and fuel type are also reported in [167] and the findings are summarised in Figure 2.18. Figure 2.18 illustrates that both the SFC and PM emissions trade-off with NO_x emissions for the same engine load is engine speed dependent, especially in the case of PM emissions and emphasises the complex optimisation and control challenge of diesel engines.

The trade-off between NO_x emissions and Hydrocarbon (HC) emissions caused by EGR rate change under cold and hot conditions for different compression ratio engine configurations are shown in Figure 2.19 and are reproduced from [168].

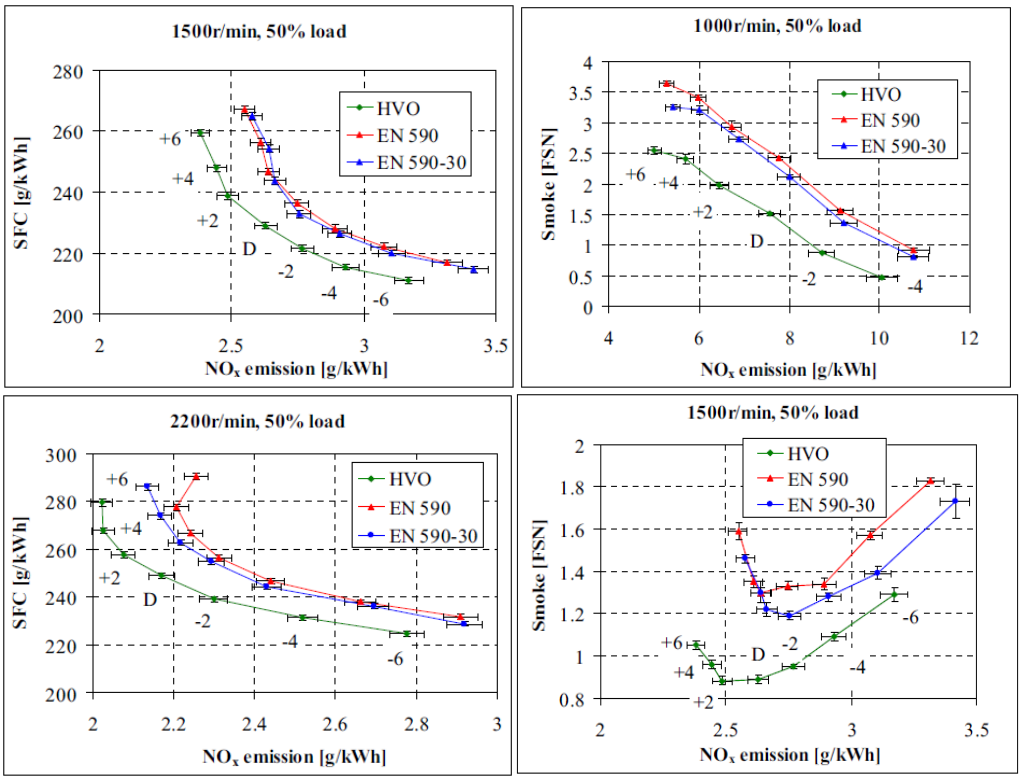

Figure 2.18: SFC and NO_x trade-off (left) and smoke-NO_x trade-off of different fuels with injection timing variation and at different engine operating point. HVO= hydrotreated vegetable oil; (Reproduced from [167])

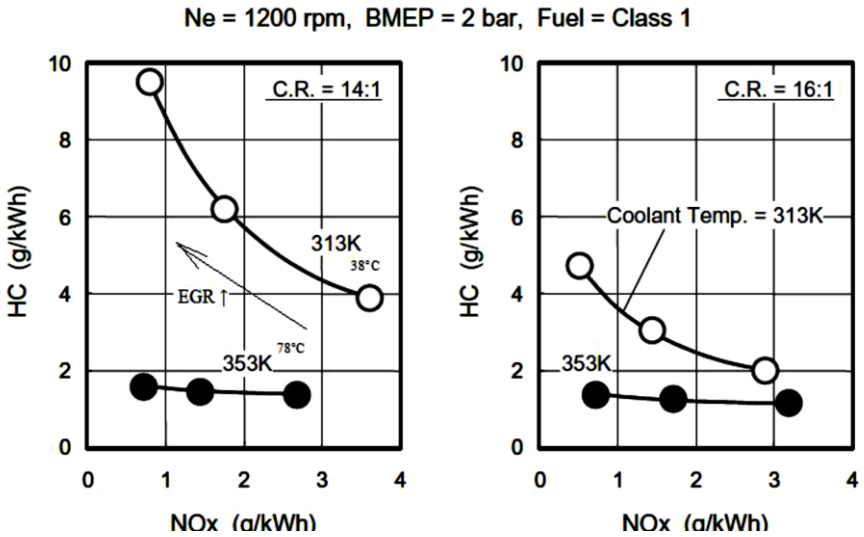

Figure 2.19: NO_x-HC trade-off in engine hot and cold condition (Reproduced from [168])

From Figure 2.19 it can be seen that a higher compression ratio results in a lower HC emission and NO_x emission trade-off curve which means both HC and NO_x emission are reduced but the trade-off phenomenon persists. It is also clear from Figure 2.19 that a cold engine has both higher HC and NO_x emissions than a warm engine and that the trade-off slope is somewhat different at cold engine conditions compared to that at warm engine conditions. Closed-loop combustion process control could be a good solution to reduce such variability in trade-off performance point selection by improving the system ability in regard to disturbance rejection [51].

In comparison to an SI engine, the optimum set-points for fuel and air-path control in a diesel engine are more complicated. For example, it was reported in [2] that for an SI engine, the best BSFC points appear centred about the empirically determined best location of 50% mass fraction burned timing of 9 degrees after Top Dead Centre (TDC) and best location of peak cylinder pressure at 13 to 15 crank angle degrees after TDC. For the diesel engine, the complexity of the trade-off phenomenon means that there are no equivalent governing principles that can be found broadly documented in literature. Therefore in final summary, multivariable model based control solutions have very good applicability to diesel engines due to the inherent requirements of the control problem.

2.7 Conclusions

The related issues concerning modern diesel engine control for both air-path and fuel-path such as control structure, the design of controlled variable set-points, the control strategy and the control-oriented model, remain open research topics.

A review of literature has found that MPC is the most successfully applied control solution after PID in industrial control problems. It is a multivariable control strategy which can deal with control constraints, can control non-minimum and unstable systems and is generally easy to tune. However, very little reported research work has been carried out on the application of MPC on air-path and fuel-path control for the diesel engine, especially in respect to the utilisation of linear MPC plus a predictive model gain-scheduling approach. Such an approach has been practically evaluated in this study both for air-path and fuel-path control and is presented in Section 4.3 and Section 5.2 respectively.

The literature review has revealed that there is minimal literature concerned with the estimation and validation of volumetric efficiency and EGR flow rate models that can be utilised in air-path control. In consideration of this, a regression model approach is presented in Section 4.2.4 for volumetric efficiency estimation and also in Section 4.2.5 a total flow rate based methodology is developed for EGR flow rate estimation and in both cases model performance is compared to measured engine test data.

The literature review has found that the control input variables typically used in fuel-path closed-loop control systems are mainly SOI and fuel quantity. Another very important fuel-path control input variable, fuel rail pressure, has not been found in literature to be used in a closed-loop control system. Importantly, in the context of this study and which is discussed in Section 5.4.1; evidence has been found in the literature that there is a fuel rail pressure wave that is caused by the previous injection event; however, the impact of this wave on the combustion processes has not been studied.

The use of multiple fuel injection events per engine cycle (such as a three-pulse injection mode) is reported in literature to both reduce combustion noise and emissions. However, the review of literature has found there are no studies of closed loop fuel-path control in which the fuel injection parameters of the three-injection mode are controlled using closed loop feedback. Such a control system has been practically evaluated in this study and is presented in Section 5.4.2.

The fuel-path literature review has also revealed that IMEP can be controlled by injection quantity cycle-by-cycle and also cylinder-by-cylinder to reduce cycle-to-cycle and cylinder-to-cylinder variability respectively. Interestingly, there have been no studies which use IMEP feedback based diesel engine speed control; such a novel engine speed control proposal has been demonstrated in this study and is discussed in Section 5.4.4.

A review of diesel engine models has revealed that there are multiple approaches to obtain a diesel engine model for control purposes. Since the diesel engine is a complex plant due to the combustion process involved, system identification is the quickest way to obtain a multi-input multi-output model suitable for rapid-prototyping MPC design and implementation. System identification has been practically tested in this study and is discussed in Section 4.3.2 for air-path control and Sections 5.2 and 5.3 for fuel-path control.

There is a trade-off phenomenon among fuel consumption, NOx and PM emissions which is widely reported in the literature. However, there is little discussion regarding the design of set-points for diesel engine closed loop control which specifically considers this trade-off phenomenon. Section 5.3 considers this topic and proposes a novel fuel-path 2I2O closed loop control system which practically demonstrates the capability to achieve an optimisation of fuel consumption, NOx and PM emissions. This uses cylinder pressure diagnostics with few set-points that cover a broad engine speed and load operating range and thus is far simpler to calibrate than an equivalent performing open loop control system.

This study therefore contributes to a series of identified gaps from this review of literature and also improves the understanding of how to develop diesel engine closed-loop control systems.

Chapter 3

3 Engine Dynamics and Experimental Setup

3.1 Introduction

The aim of this Chapter is to present the details of the test engine used in this study and its characteristics and to set the context for the experimental and analysis work that is presented in later Chapters. The Chapter covers the engine itself, the supporting experimental equipment and observations on the engine behaviour in regard to the design and implementation of control systems. The information is organised as follows. The hardware and control variables of the test engine used in this study are explained in Section 3.2. The engine experimental setup is summarised in Section 3.3. Engine dynamics which include cycle-to-cycle dynamics, cylinder inconsistency, air-path and fuel-path are discussed in Section 3.4.

3.2 Engine Hardware and Control Variables

The engine used in this study is a Caterpillar C6.6 HD engine designed for off-highway applications. It is a 6 cylinder, 4 stroke, 6.6 litre diesel engine equipped with a Caterpillar common rail fuel system which uses solenoid fuel injectors. Its maximum power and speed are 159kW and 2200rpm respectively. The peak torque is 920Nm occurring at 1400rpm. The engine calibration is for utility (power generation) applications. The engine specifications are shown in Table 3.1

Table 3.1: Engine Specifications

Bore	105.0mm
Stroke	127mm
Connect length	219.1mm
Crank radius	63.5mm
Compression ratio	16.5:1
Displacement	6.6 L
IVC	220° ATDC
EVO	485° ATDC

In its as-built condition, the engine meets Tier 3 emissions requirements, but for the purposes of experimental programmes, it has been modified with a high pressure loop EGR system and a VGT. Figure 3.1 shows a picture of the engine mounted on an engine test bed in the Powertrain Laboratory of the Aeronautical and Automotive Engineering Department of Loughborough University [171]. The engine is outfitted with a bespoke control and instrumentation system.

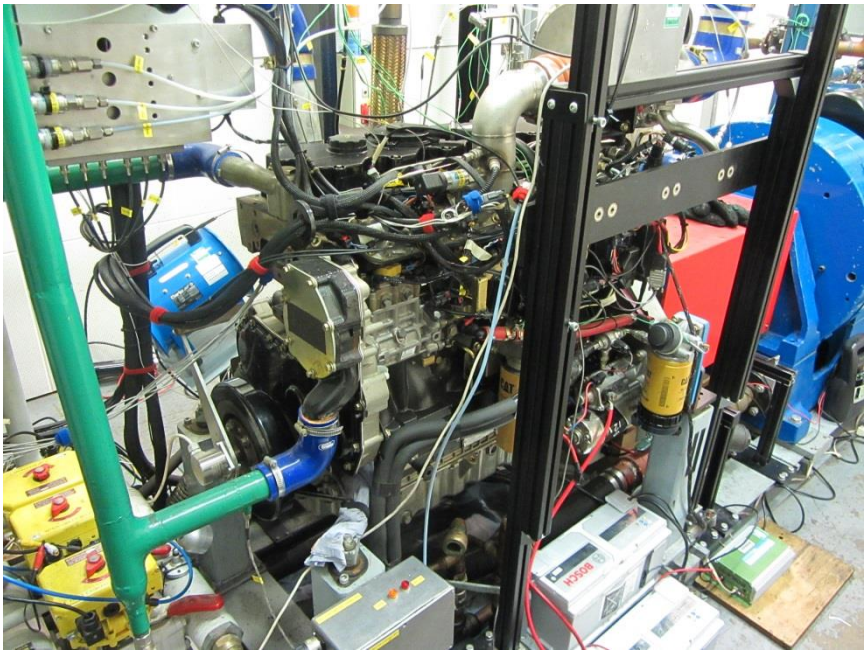

Figure 3.1: Engine in the Test Cell

3.2.1 C6.6 Engine Air-Path

A schematic of the C6.6 engine air-path is presented in Figure 3.2. The electric control system is not included in this diagram. It will be discussed in the next section. There is no aftertreatment system installed in this engine. The study of diesel engine optimal performance is limited in the configuration described in this chapter. However, the research methodology, the control strategy and the conclusions obtained in this work could be useful in the optimization research work of conventional combustion diesel engine which is equipped with new advanced devices, such as Variable Valve Timing (VVT), Electric Turbo Assist (ETA), Thermoelectric Generator (TEG), DPF and SCR aftertreatment system etc. The more devices, then the more constraints and objective items should be considered for the optimisation of the global engine performance. The knowledge or model of the new device is also needed in this optimization work. For such work, a physical phenomenon mathematic model is better than other types of model as it has clear physical meanings for the model variables and could be

easily coupled with engine mean value air-path model and phenomenological combustion and emission model.

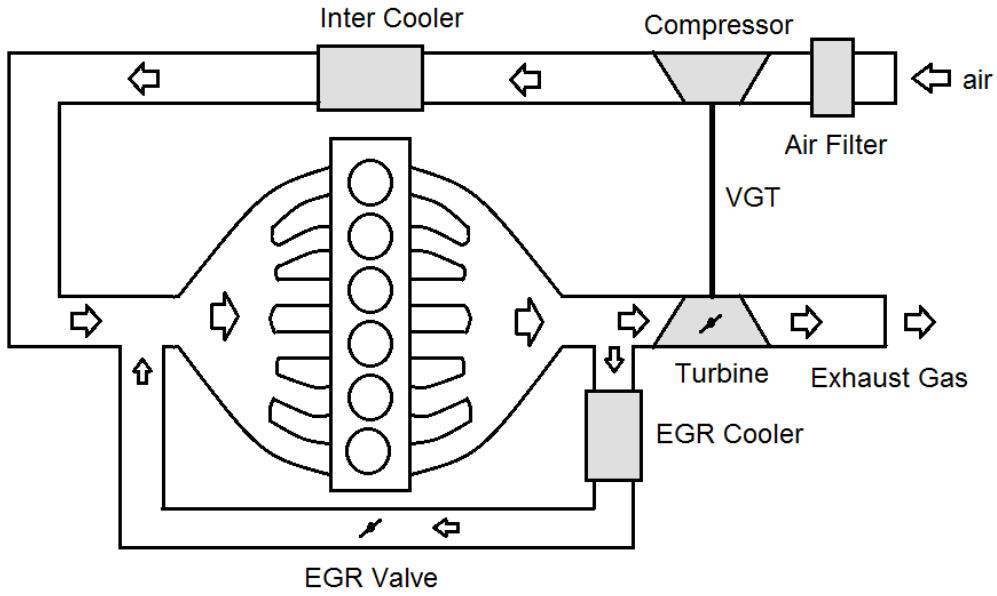

Figure 3.2: Engine Air-Path System

There are two control actuators located in the air-path system: one is an EGR valve, the other is a VGT vane position actuator. Each of them is controlled by a small permanent magnet direct current motor. The rotation speed of the motor is controlled via Pulse-Width Modulation (PWM) mode. These two actuators include a resistive position sensor. Consequently an inner closed-loop PID position controller of the EGR valve motor and an inner closed-loop PID position controller for the VGT vane position actuator motor are required before implementing the air-path outer loop control, see Figure 3.3.

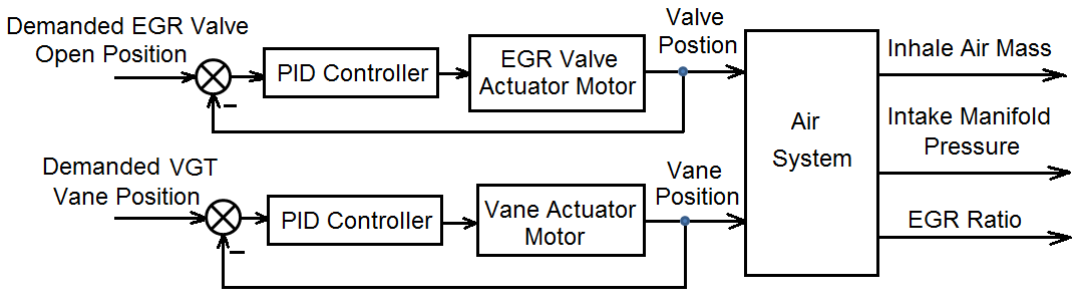

Figure 3.3: Diagram of EGR Valve and VGT Vane Position Control

These two PID controllers were implemented in an xPC machine via a MATLAB® SIMULINK® model. The EGR valve position and the VGT vane position together have coupling effects on engine air flow, EGR ratio and manifold pressure which in turn affect each engine cycle. Increased EGR ratio

results in reduced NO_x emissions but increased PM emissions. More detailed discussions of this EGR effect and the effects of air flow or AFR on combustion process are presented in Chapter 4.

3.2.2 C6.6 Engine Fuel-Path

The fuel-path system in a modern diesel engine consists of a fuel tank, low pressure fuel pump, high pressure fuel pump (or fuel injection pump), a common rail, rail pressure sensor, fuel pipe and injectors. There are also two types of control actuators in the fuel-path which are the high pressure pump valve and the injectors. The high pressure part of the fuel-path system is shown in Figure 3.4.

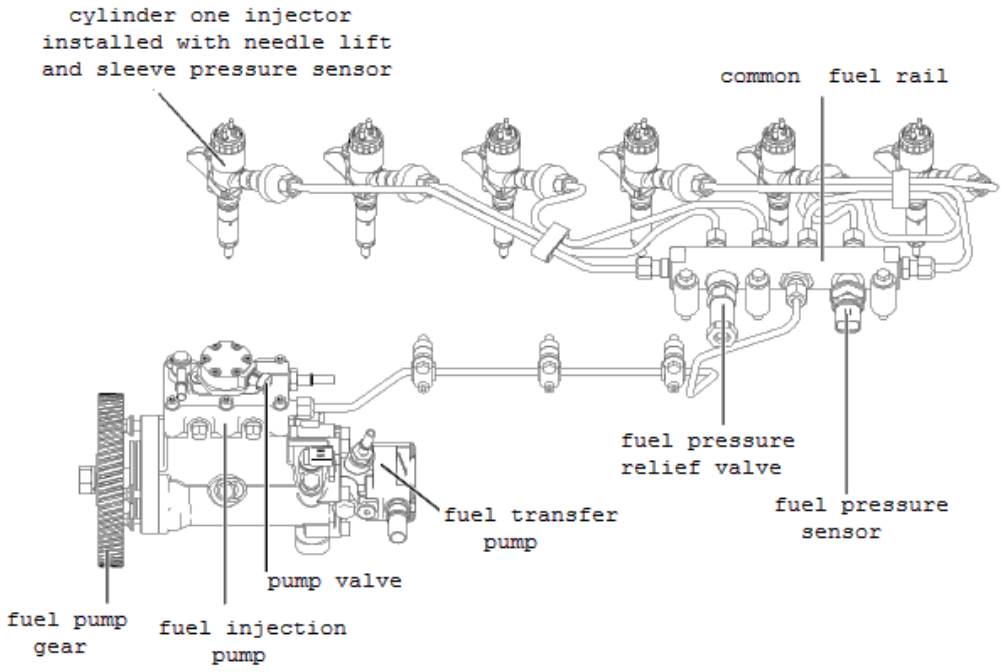

Figure 3.4: C6.6 Engine Fuel-Path System (High Pressure Part) (Reproduced from [172])

The C6.6 engine high pressure fuel pump is a mechanical pump which is driven by the camshaft continuously once the engine is started and its rotational speed is proportional to the engine speed. The pump valve is a two position (closed or open) valve that enables or blocks the pumped high pressure fuel flow into the common fuel rail. This valve is controlled to open once for each cycle for each cylinder. The opening timing and duration of this pump valve is controlled by a common fuel rail pressure controller. It is a combined feed-forward and feedback PID controller. Figure 3.5 shows the diagram of the rail pressure control structure.

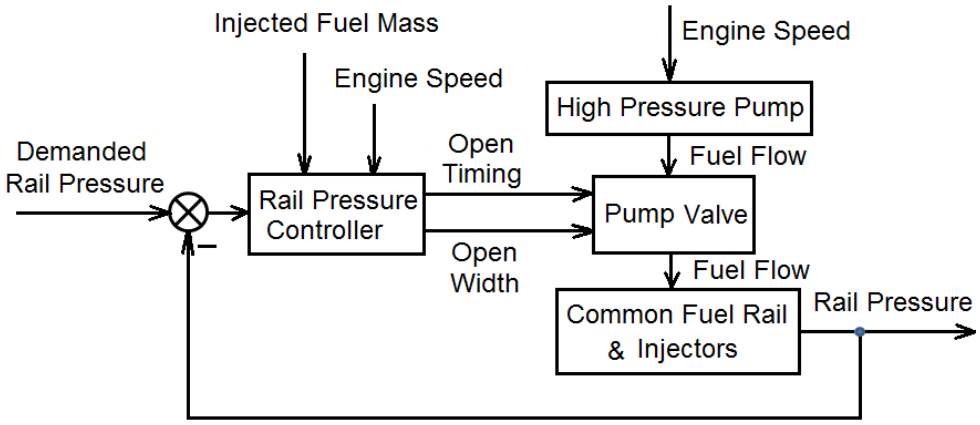

Figure 3.5: Diagram of High Pressure Pump Valve Control

For fixed load and speed, higher rail pressure results in faster fuel injection velocity (and reduced droplet size) or fuel injection rate, hence higher combustion temperature. With higher combustion temperature, NO_x emissions will increase and PM emissions will decrease. Higher rail pressure also results in better combustion efficiency, hence less fuel consumption. The range of rail pressure in C6.6 engine common rail system is from 45MPa to 120MPa.

The other important actuator in the fuel-path system is the fuel injector with each cylinder having a single injector. High pressure fuel is directly injected into the cylinder at the required crank angle position by the injector in response to a short duration solenoid control signal from an injector driver circuit. This opens a valve inside the injector enabling fuel to enter from the common rail and as the fuel pressure inside the injector rises, the pressure of the fuel (measured as the sleeve pressure) pushes another small valve (the needle valve) against a spring. When the force of the sleeve pressure is greater than the force of the spring, the needle valve will lift and high pressure fuel is injected into the cylinder chamber. Leakage of fuel from each injector passes into a channel running inside of the cylinder head. A pipe connected to the cylinder head returns the leaked fuel back to the low pressure side of the high pressure fuel pump [172].

At low engine load, if the rail pressure is set high, a lot of surplus fuel will flow from the injector to the cylinder head and then back to the fuel tank. Excessive leakage tends to lead to high fuel temperatures through repeated compressions. The number of adjustable control variables for the injector increases with the number of injection pulses. For one pulse injection mode, there are only two control variables namely injection timing or SOI and injection width or injection duration. SOI is the crank angle relative to TDC. However, injection duration is a

variable with units of time usually expressed in milliseconds. Two or three pulse multi-injection modes were used in this study. The control variables for these three types of injection mode are defined in Figure 3.6.

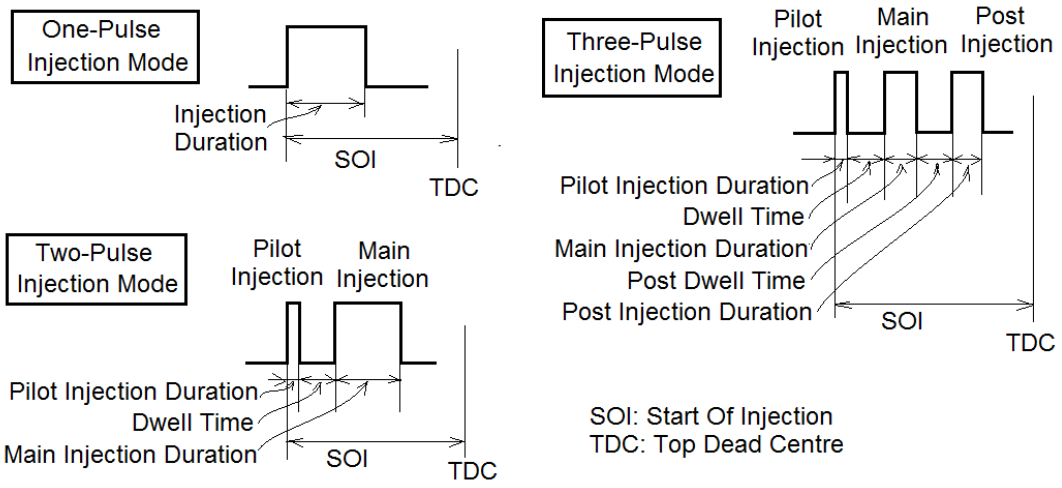

Figure 3.6: Control Variables for Different Injection Modes

In the *two-pulse injection mode*, there are four control variables: SOI, pilot injection duration, Dwell Time (DW) and main injection. Alternatively, these three control variables can be total injection duration, fuel ratio and dwell time. The relationships of total injection duration and fuel ratio to pilot injection duration and main injection duration are shown in Equation (3.1) and (3.2):

$$total\ injection\ duration = pilot\ injection\ duration + main\ injection\ duration \quad (\mathbf{3.1})$$

$$fuel\ ratio = \frac{main\ injection\ duration}{total\ injection\ duration} \quad (\mathbf{3.2})$$

In the *three-pulse injection mode*, the number of controllable variables is six. They are SOI, pilot injection duration, dwell time, main injection duration, post dwell time, post injection duration. Similar to two injection pulse mode, these six control variables could alternatively be SOI, total injection duration, fuel ratio, dwell time, post-split ratio and post dwell time. The definitions of total injection duration, fuel ratio, and post-split ratio in three injection pulse mode are shown in Equation (3.3) to (3.5).

$$total\ injection\ duration$$

$$= pilot\ injection\ duration + main\ injection\ duration$$

$$+ post\ injection\ duration \quad (\mathbf{3.3})$$

$$fuel\ ratio = \frac{main\ injection\ duration + post\ injection\ duration}{total\ injection\ duration} \qquad (3.4)$$

$$post\ split\ ratio = \frac{post\ injection\ duration}{main\ injection\ duration + post\ injection\ duration}$$

$$= \frac{post\ injection\ duration}{fuel\ ratio \times total\ injection\ duration} \qquad (3.5)$$

All these injection related control variables affect engine combustion performance such as combustion noise, emissions and fuel consumption. Proper engine operation also requires proper control of coolant temperature and EGR cooler and intercooler. The optimization of these additional control systems lies outside the scope of this study.

Pilot plus main injection mode vastly reduces combustion noise with a slight penalty on fuel economy. This is the major injection mode applied in this study. Three-injection-pulse mode was also used in exploring the possibility of intra-cycle control and implementing P_{max} and IMEP combustion control.

When two-pulse injection mode is used, the total number of control input variables from both air-path system and fuel-path system is as many as seven as illustrated in Figure 3.7.

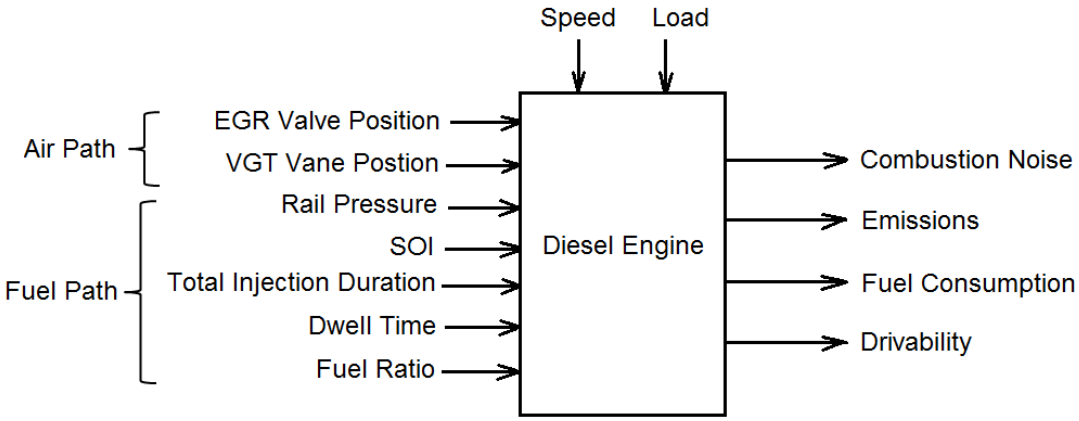

Figure 3.7: Inputs and Outputs in Optimal Control Design of Diesel Engine for Two-Pulse Injection Mode

Under different engine speed and load conditions, these seven control inputs have different nonlinear coupled effects on the engine outputs. These outputs can be categorized mainly as combustion noise, emissions, fuel consumption and drivability. The requirement placed on the engine performance outputs varies according to the application of the diesel engine. For example, when the diesel

engine is used for propulsion in transport applications, there is a requirement on drivability performance. Within the fixed engine hardware frame, the optimal design of the engine control system can be viewed as an optimization task to find the solution of these seven control inputs to minimize a performance related cost function under some performance related constraints. However, currently, this kind of control approach is challenged by the lack of a sufficiently accurate control-oriented model suitable for this optimization requirement. This study focusses on research of a low level innovative control structure for the combustion process that can be further developed into a global optimal control for the complete engine, energy recovery and after-treatment processes.

3.3 Experimental Engine Test System

The test bed control system, Cadet V12 (supplied by CP Engineering) managed both the engine and the eddy current dynamometer (Froude AG400-HS) to follow a speed and torque profile as a series of steady-state points or a transient test cycle. The Cadet system was also programmed to control the engine coolant temperature and control the water flow of the EGR cooler and intercooler.

The engine is fully instrumented and the sensors and measurement devices installed and utilised in this study are listed in Table 3.2.

Table 3.2: Installed Sensors and Measurement Devices

No.	Sensor and Device Name	Type
1	Needle Lift sensor	Kaman KD-2300-.5SU position sensor
2	Sleeve pressure sensor	Strain gauge
3	Cylinder pressure sensor	Kistler 6125B ThermoCOMP® Quartz Pressure+ Kistler 2854A Signal Conditioning Platform (SCP)
4	NO_x sensor	NGK 20Hz CAN sensor
5	EGR flow rate meter	Coriolis mass flow meter
6	Opacity meter	AVL 439 opacity meter
7	Engine crank position sensor	Hengstler optical encoder
8	Fuel flow meter	AVL 735S
9	Emission measure	Horiba 9100 exhaust gas analyzer
10	Temperature sensor	All k-series thermocouples
11	Intake and Exhaust pressure sensor	Piezoelectric

The original Engine Control Module (ECM) was removed and the engine control functions in the original ECM were implemented in two computer control systems: (i) xPC system for managing the air-path system (using a MATLAB®

SIMULINK® model), and (ii) National Instrument (NI) PXI real time system (using a series of LabVIEW Virtual Instrument (VI) programs) for managing the fuel-path system [171]. This change makes the air-path and fuel-path control of engine open to advanced and innovative control research work.

These two engine control systems exchange data via Controller Area Network (CAN) bus. The LabVIEW software running in the PXI real time system was programmed on and deployed from a host Personal Computer (PC) named '*PC1*'. In total there are three LabVIEW VIs running in the PXI real time system. The first, named *Main RT* VI conducts fuel-path control. The second, named *Low Speed* VI conducts measurement of most of the sensor values and measurements from devices such as fuel flow meter and opacity meter etc. The third which is named *Crank Angle degree for 50% heat release* VI is a code to compute the key combustion parameters for each combustion cycle from cylinder pressure data.

The control values for rail pressure and injectors in RT VI are updated at a fixed 30Hz frequency. This control frequency was inherited from the original ECM control algorithms when adapted versions of these were implemented in the LabVIEW real time PXI engine control system [171]. Alternative fixed frequencies could have been implemented for these Vis but this would have required extensive tuning of the control system gains and such work was outside the scope of this study. Therefore the LabVIEW real time PXI control system as used in this study is a good approximation of the original C6.6 ECM control basic system performance in regard to fuel-path control.

For saving the computer resources, the sampling frequency within the Low Speed VI is set as low as 10Hz. The update frequency of combustion parameters within CA50 VI depends on engine speed as they were computed once for each cycle. Using the NI SIT, a SIMULINK® model based controller which is running on the host PC *PC1* can communicate to the NI PXI real time control system. Meanwhile, a *Host* VI is also running on the host PC *PC1* as a human-machine interface for monitoring and setting parameters both for the engine and controllers. A NI 16 channel Analogue Input (AI) module USB-6259 is connected to a second host PC, named 'PC2' to monitor and record all six cylinder pressure traces and other interesting engine variables like injector currents, cylinder one needle lift etc. in one crank angle degree resolution. The LabVIEW VI running in this machine is able to log 16 channels data in one crank angle degree resolution for up to 1000 continuous consecutive cycles.

3.4 Engine Dynamics

The Diesel engine is a complicated machine that converts chemical energy stored in diesel fuel or other alternative fuel into mechanical energy by means of combustion. Dynamics refers to the phenomenon that a system‘s variables vary with time due to either a change of control inputs or an internal disturbance. There are three principal types of dynamics involved in the diesel engine system: combustion dynamics, thermodynamics and mechanical rotational dynamics. Combustion dynamics are the result of the combustion chemical reaction kinetics. The compression ignition process of diesel fuel combustion is sensitive to many factors, such as compressed intake gas states, fuel injection pressure, swirl kinetics, piston movement, coolant temperature etc. So that there is cycle-to-cycle variation dynamics even when all control variables are kept constant. The thermodynamics related to heat transfer during combustion affects the work done by the combustion process. Mechanical rotational dynamics reflects the engine acceleration and deceleration performance. These three classes of dynamic behaviour inside the engine are closely coupled with each other. However, each cycle event is the key component among all dynamics.

When six cylinders work together, the firing order and the relationship of each cylinder’s stroke is fundamental to the engine’s operation. Figure 3.8 shows the C6.6 test engine firing order and the connection between the DRIVVEN power circuit drive modules and injectors [171]. C1 to C6 refers to cylinder one to cylinder six respectively.

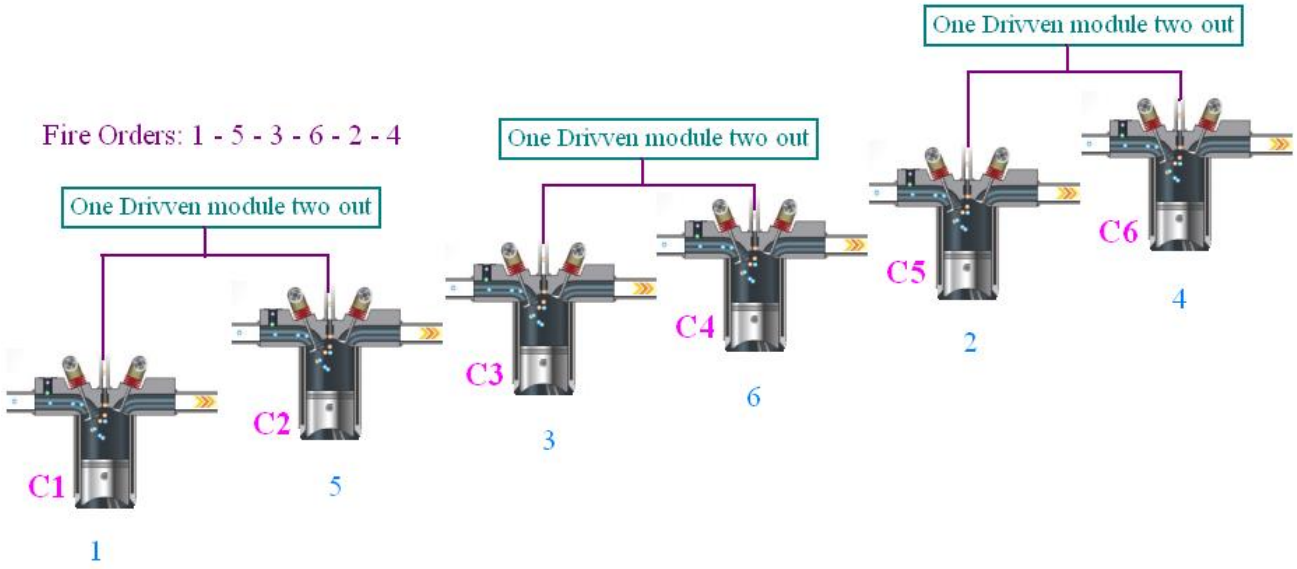

Figure 3.8: Drivven Module Connection and Fire Order for C6.6 Diesel Engine

Figure 3.9 presents schematically the evolution of the whole cycle process in relation to crank angle degree. The number 1 to 5 refers to five specific sub-processes of the combustion process. Ideally, Number 1 is the process of compressing the cylinder charge. Number 2 is the combustion process. Number 3 is the process of expanding the burned gas. Number 4 corresponds to when the exhaust valve opens connecting the cylinder to the outside exhaust manifold while the piston is moving up. Number 5 corresponds to the intake valve opening so that the cylinder chamber is connected to the outside intake manifold while the piston is moving down. There is a small overlap when intake and exhaust valve both open and piston is moving up and down close to TDC.

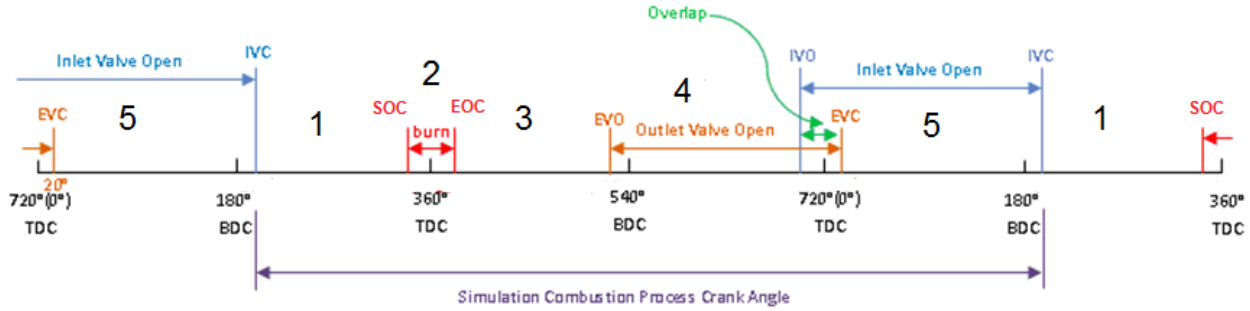

TDC: Top Dead Centre BDC: Bottom Dead Centre

SOC: Start of Combustion in Crank Angle Degree EOC: End of Combustion in Crank Angle Degree

EVC: Exhaust Valve Closing Timing in Crank Angle Degree

EVO: Exhaust Valve Opening Timing in Crank Angle Degree

IVC: Intake Valve Closing Timing in Crank Angle Degree

IVO: Intake Valve Opening Timing in Crank Angle Degree

Figure 3.9: One Complete Combustion Cycle for One Cylinder

When considering six cylinders working together, the firing sequence of each cylinder and their relationship can be seen clearly from Figure 3.10. For simplicity, the combustion is marked at TDC during power stroke.

Conventional diesel combustion starts with auto-ignition (or CI as it is often referred to) when the fresh air ingested into the cylinders is mixed with the high pressure injected fuel to produce auto ignition when the local equivalence ratio and the local temperature and pressure combine to produce a self-ignitable mixture. To avoid the so-called diesel knock characteristic of this type of combustion in modern direct injection diesel engines, a small initial pilot fuel injection occurs which is equivalent to only a few mm^3 of fuel to initiate this premixed or *diffusion controlled* combustion phase prior to the main injection which proceeds after auto-ignition in what is called the *mixing controlled phase*.

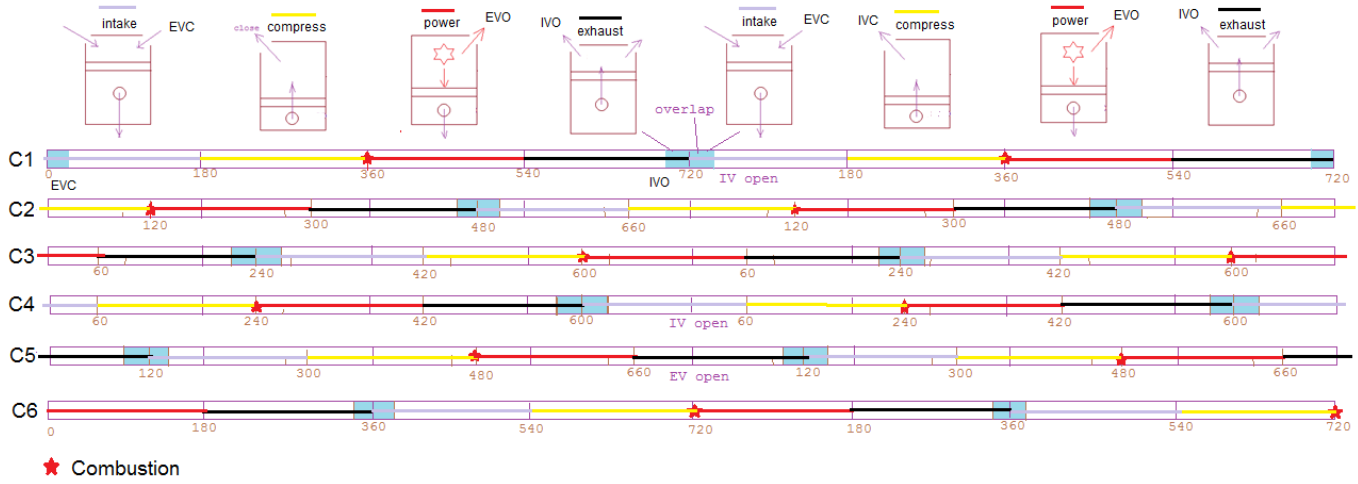

Figure 3.10: Six Cylinders Four Stroke Sequence

As one complete cycle for each cylinder needs two crankshaft rotations, in each rotation, there are three combustion power strokes and these are illustrated in Figure 3.11. In the first rotation, combustion takes place in cylinder 1, cylinder 5 and cylinder 3 and does work on the crankshaft with an interval of 120 crank angle degrees. In the second rotation, the three cylinders that do work on the crankshaft are cylinder 2, cylinder 4 and cylinder 6. Similarly, there are also three intake events for three individual cylinders during one crankshaft rotation.

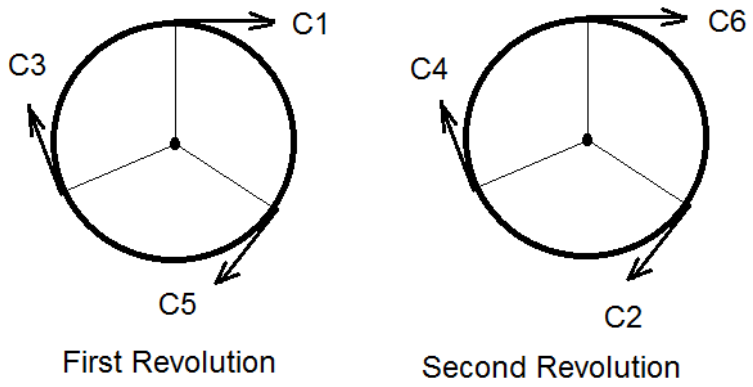

Figure 3.11: Six Cylinder Combustion Work Force Relative to Revolution

3.4.1 Cycle-to-Cycle Variation

When the engine is running at steady-state with both air-path and fuel-path control inputs fixed at constant values by open-loop controllers; the engine speed and load are controlled at constant value by the engine speed governor and the dynamometer controller respectively. However, the combustion process within each cylinder still exhibits some level of cycle-to-cycle variation. These dynamics could be observed by the combustion cylinder pressure trace or combustion

parameters such as IMEP, P_{max} etc. that are computed from the cylinder pressure trace. The plots of cylinder 1 combustion pressure, injector current, needle lift, sleeve pressure, rail pressure during injection and MAP near IVC for 300 consecutive cycles are shown in Figure 3.12.

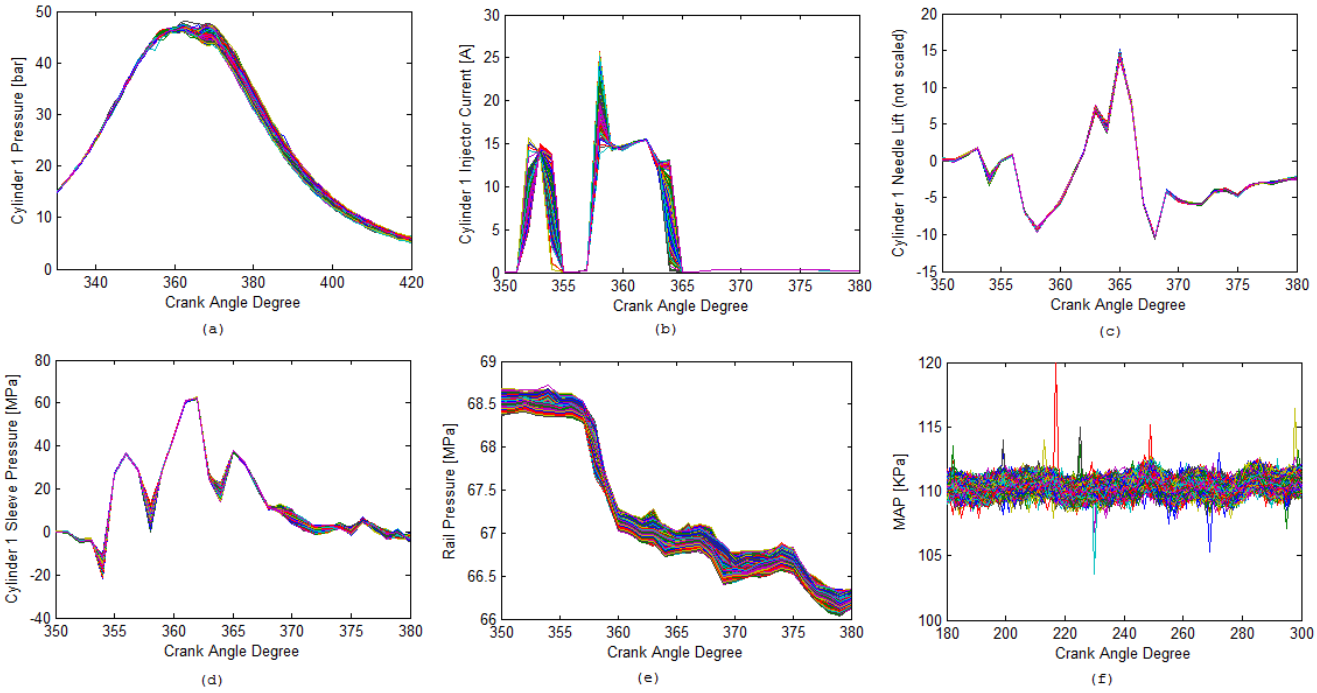

Figure 3.12: Cylinder one: (a) Combustion Pressure; (b)Injector Current; (c) Needle Lift; (d) Sleeve Pressure; (e) Rail Pressure and (f) MAP near IVC of 300 continues cycles when engine running at 1400rpm, 100Nm

The engine was warmed up and the coolant temperature was kept constant at 90°C. Injection mode was pilot plus main (i.e. two-pulse injection). Engine speed was controlled in closed-loop at 1400rpm by a speed governor programmed using LabVIEW real time and which executed on the NI real time PXI chassis which in turn controlled the DRIVVEN injector driver modules via a Field Programmable Gate Array (FPGA) module [171]. This LabVIEW based speed governor reproduced the features of the original speed governor algorithm implemented in the original engine ECM [171]. This speed governor has a setpoint input which is a speed demand signal generated originally as a fixed frequency PWM signal by the Cadet V12 test bed automation system, with the duty cycle of the PWM being proportional to the speed demand. The speed governor then compares this demand speed (1400rpm) with the present engine speed and then makes adjustments to the fuel injection quantity to either increase or reduce the engine speed as required to achieve the demand speed.

Engine load was controlled in closed-loop by the Cadet V12 System at 100Nm using a dynamometer-torque control mode.

The cycle-to-cycle combustion variation for this system can be seen by the cylinder pressure trace overlay in Figure 3.12 (a). The plots of other engine parameters in Figure 3.12 show they also have variations. The variation of MAP implies the variation of the cylinder charge and therefore the combustion and from Figure 3.12 (f) there is an overall wave like pattern observed in the MAP signal against crank angle which is not obscured by the signal background noise. Injector current, rail pressure, needle lift, sleeve pressure are fuel injection system parameters also show subtle variations cycle-to-cycle. Such variation would affect the fuel spray dynamics, and hence be another significant source of combustion process variation.

The ensemble variance of the cylinder one combustion pressure is shown in Figure 3.13 (a). There are two big variation peaks observed in the cylinder combustion pressure trace. They are all located during the fuel combustion process:

(i) 368 Crank Angle Degree (CAD)

(ii) 378 CAD

The Probability Density Functions (PDF) of cylinder pressure value at 368 CAD and at 378 CAD for 300 consecutive cycles are plotted in Figure 3.13 (b) and (c) respectively.

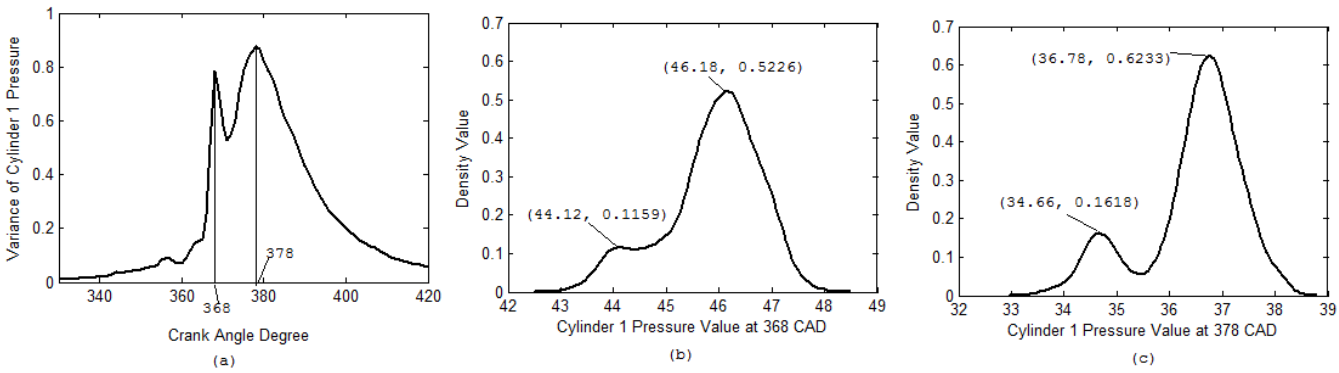

Figure 3.13: (a) Variance of cylinder one combustion pressure; (b) Density distribution of cylinder one pressure at 368 crank angle degree; (c) Density distribution of cylinder one pressure at 378 crank angle degree. Engine running at 1400rpm, 100Nm

The variance and density distribution were computed using MATLAB functions *var* and *ksdensity*. It can be seen that the cylinder pressure cycle-to-cycle variation has two noise sources with a Gaussian distribution. One is large

whilst the other is relatively smaller. The cross-correlation value of cylinder one combustion pressure at 378 CAD with the other engine variables: injector current, needle lift, sleeve pressure, rail pressure and MAP during the crank angle range of interest are shown in Figure 3.14. The cross-correlation value was computed using MATLAB function *corrcoef*.

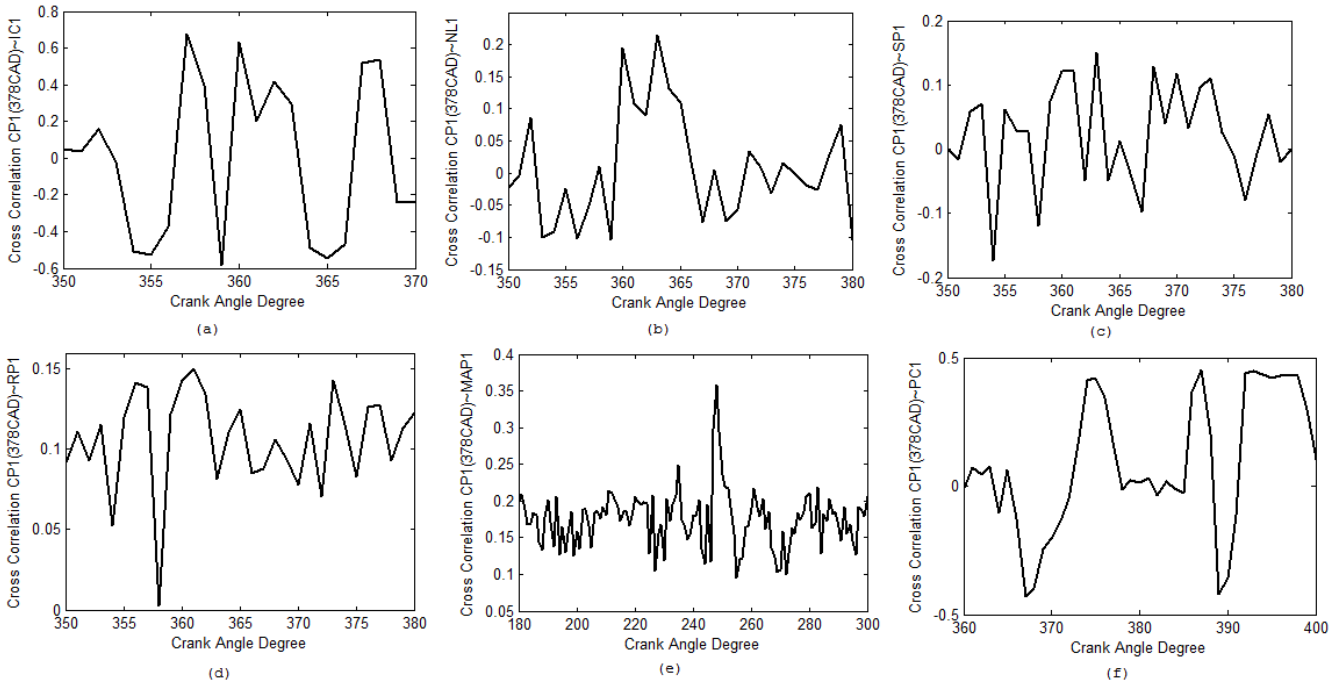

Figure 3.14: Cross-Correlation between cylinder one combustion pressure data at 378 CAD between: (a) cylinder one injector current; (b) cylinder one needle lift; (c) cylinder one sleeve pressure; (d) cylinder one rail pressure during injection process; (e) cylinder one MAP near IVC; (f) fuel pump valve drive current during cylinder injection process

It can be seen that both injector current and fuel pump valve drive current have high correlation value (over 0.4) to the cylinder combustion pressure value at 378 CAD which has the biggest cylinder pressure variance. This implies that the variation of electrical control signals could be a big source of engine combustion process cycle-to-cycle variation during engine steady-state. The variation of the fuel pump valve drive current is a result of common rail fuel pressure feedback control. Improving this closed-loop control system performance will lead to less variation that would help to reduce combustion process variation. However, the possible cause of variation of injector current may not only be the electrical circuit drive pulse control pattern and performance but also could be the variation of injector performance caused by engine vibration etc.

Interestingly, Figure 3.14 (e) shows that the MAP at 248 CAD has a high 0.3587 cross-correlation with cylinder pressure data at 378 CAD. This indicates that the fluctuation in air-path also has contribution to cycle-to-cycle combustion variation.

Reducing cycle-to-cycle combustion variation will lead to a decrease in engine combustion noise, improved fuel economy and reduced engine exhaust gas emissions. Besides the improvement of electrical drive control circuit and rail pressure feedback control performance, intra-cycle control could be a good candidate to reduce engine cycle-to-cycle combustion variation.

3.4.2 Cylinder-to-Cylinder Inconsistency

In addition to cycle-to-cycle combustion variation discussed in the previous section, there was also inconsistency observed cylinder-to-cylinder of the C6.6 test engine. This can be quantified through cylinder pressure based combustion analysis, combustion temperature and emissions etc. From the cylinder pressure data, the variation between cylinders can be first evaluated by the difference in IMEP and P_{max}. The P_{max}, IMEP and exhaust port temperature data of the C6.6 test engine whilst running steady-state at 1400rpm and 100Nm are shown in Figure 3.15. As the cylinder 6 pressure sensor had failed, only the data of cylinder 1 to 5 are shown in the figure; the absence of cylinder 6 pressure data is applicable to the whole of this study for this reason.

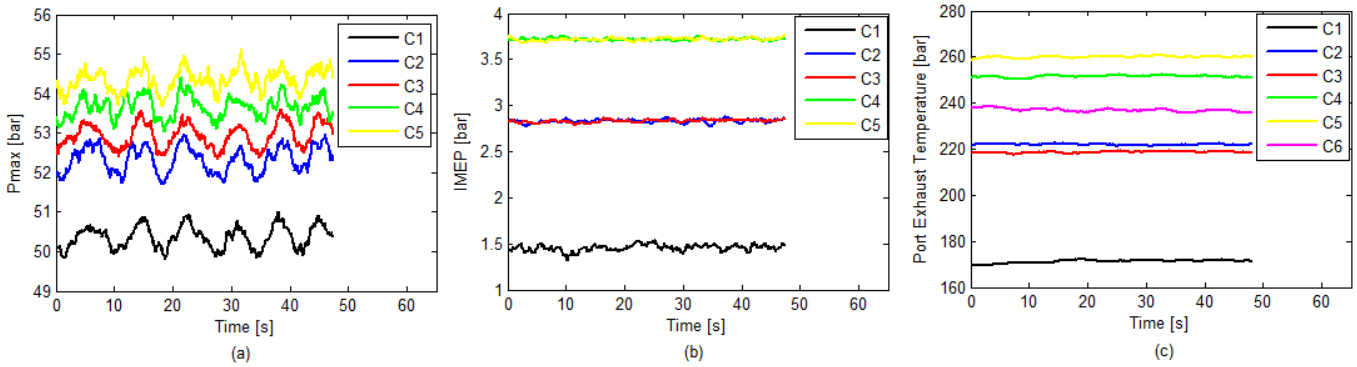

Figure 3.15: (a) P_{max} of five cylinders; (b) IMEP of five cylinders; (c) exhaust port temperature of all six cylinders. Engine at steady-state operating point: 1400rpm, 100Nm; C refers to cylinder

The plots in Figure 3.15 show that the three parameters (P_{max}, IMEP and exhaust port temperature) all indicate that for the C6.6 test engine used in this study there was somewhat significant differentiation between the cylinders. It can be seen that cylinder 1 has by far the smallest P_{max}, IMEP and port exhaust temperature (ExT) and was distinct from the grouping of the other cylinders.

Comparing P_{max} values in Figure 3.15 (a) to the port exhaust temperature in Figure 3.15 (c), it can be seen that generally higher P_{max} correlates to higher port exhaust temperature except for cylinder 3. For cylinder 3 the P_{max} was higher than that of cylinder 2 whilst the IMEP was slightly lower. This relationship between P_{max} and exhaust port temperature appeared however to be a factor of engine load with related data from 1400rpm and 400Nm presented in Figure 3.16 (a) and (c) showing reduced association between P_{max} and IMEP. From Figure 3.16 (a) and (c), the P_{max} of cylinder 2 and 3 are very close, but the exhaust port temperature of cylinder 3 is much lower than the exhaust port temperature of cylinder 2.

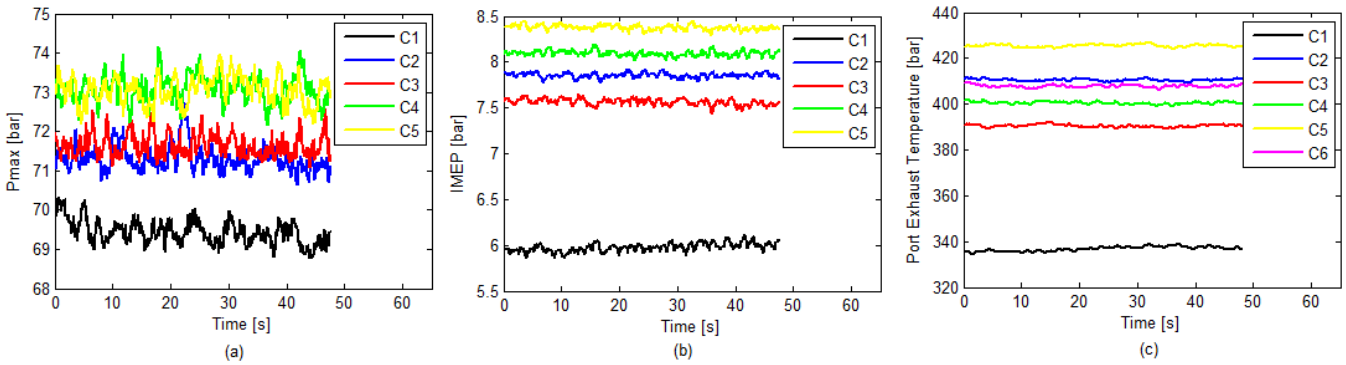

Figure 3.16: (a) P_{max} of five cylinders; (b) IMEP of fixe cylinders; (c) port exhaust temperature of six cylinders. Engine was running at steady-state operating point: 1400rpm, 400Nm; C refers to cylinder

Figure 3.15 (b) shows that at low-load, the IMEP of cylinders 2 and 3 was nearly the same and also that cylinders 4 and 5 also had the same IMEP. The IMEP of these two pairs of cylinders were also quite different. However, at higher load, Figure 3.16 (b) shows that the IMEP of all five cylinders were quite different and also shows that the IMEP of cylinder 1 remained significantly lower.

Clearly, from Figure 3.15 and Figure 3.16 the variation cylinder-to-cylinder for the C6.6 test engine was significant and was sensitive to engine operating condition. The explanation for this cylinder inconsistency resides in several key factors that are attributable to firstly the replacement of the original ECM with the LabVIEW real time PXI control system and secondly the specially instrumented injector fitted to cylinder 1.

With the replacement of the original ECM with the LabVIEW real time PXI control system, there are *three key attributes* of the latter system that meant that it could not fully reproduce all the characteristics of the ECM. *Firstly*, the injector

current signal generated by the original ECM driver circuitry had a three-tier current hold shape with a high initial peak current used to open the injector solenoid which was then followed by two longer duration lower current hold events to maintain the injector solenoid opening. The LabVIEW real time PXI control system with the DRIVVEN injector driver modules [171] could produce only a two-tier current hold shape and thus the injector current of this system was best approximated to that of the original ECM. The peak current of the first current hold phase was matched and then the average hold current of the two subsequent ECM current hold phases was used as the hold current for the LabVIEW system second phase. Furthermore, the duration of the first ECM phase could not be matched precisely. Consequently, the response characteristics of the injectors to the ECM and the LabVIEW real time PXI control system were different. It is believed that the effect of these differences would be to amplify any differentiation between injectors in regard to response time and fuel quantity delivered for a specific energising current to the solenoid.

Secondly, the ECM also directly drives a solenoid on the high pressure fuel pump using an electrical signal analogous to that which drives the injectors. To replicate this in the LabVIEW real time PXI control system, a single DRIVVEN injector driver module was used and again the current shape of the output electrical signal was matched as close as possible to that of the original ECM using an oscilloscope. The fundamentals of the original ECM rail pressure control algorithms were also developed in the LabVIEW real time software. However, since the electrical signal to the high pressure fuel pump was an approximation of that of the original ECM signal, it is possible that the rail pressure control characteristics of the LabVIEW real time PXI control system were not an exact match to the original C6.6 engine ECM - especially during fuel injection events. Any discrepancies in the rail pressure control, particularly during injection, are believed to potentially contribute to cylinder-to-cylinder variation but the effect is believed to be somewhat lower than that caused by the individual injector drive current discrepancies between the ECM and the LabVIEW real time PXI control system as described above.

Thirdly, the ECM incorporates compensation for injector variation in the form of individual ‘trim’ adjustments to the duration of the electrical signal sent to an injector. This compensation acts to balance out differences in fuel injection quantity vs. injection signal across different injectors based on a calibration done

prior to fitting an injector to the engine. This compensation mechanism was not implemented in the LabVIEW real time PXI control system and thus the variation in cylinder IMEP as illustrated in Figure 3.15 (b) and Figure 3.16 (b) is highly likely to be largely attributable to this lack of individual injector compensation.

The effect of there being a lack of compensation for variation between injectors was amplified it is believed by the heavily instrumented injector that was used in cylinder 1. This injector was instrumented for needle lift and also the fuel pressure in the area of the sac volume (sleeve pressure). Figure 3.15 and Figure 3.16 show that cylinder 1 consistently had a somewhat lower P_{max}, IMEP and exhaust port temperature compared to the other cylinders and it is therefore believed that this was a consequence of the remedial work performed on the cylinder 1 injector to install the two sensors (this work was done by Caterpillar Fuel Systems). This remedial work is believed to have resulted in the fuel quantity delivered by this injector being somewhat smaller compared to the other injectors for the same electrical control signal.

Consequently, the mitigation of cylinder-to-cylinder inconsistency through closed loop control would be a valuable enhancement to the C6.6 test engine coupled with the LabVIEW real time PXI control system utilised in this study. Indeed, Section 5.4.4 of this work describes a closed IMEP based control system which compensates for the cylinder-to-cylinder inconsistency caused by the factors discussed in this section.

3.4.3 Air-Path Dynamics

Understanding and modelling air-path dynamics is a critical step in the development of an optimal air-path control system. The air-path of the C6.6 engine in this study has two control inputs. The sub-dynamics in the air-path system are shown in Figure 3.17 and are defined as: VGT vane position and EGR valve position feedback closed-loop control dynamics, VGT mechanical dynamics, intake air and EGR gas flow dynamics, combustion dynamics and engine speed closed-loop control dynamics. Combustion dynamics is cycle event based, so that the response time of combustion process strongly depends on engine speed, e.g. at higher engine speed there are greater flow rates. In addition, pumping effects in the cylinder have a strong effect on gas dynamics. Therefore, gas flow rate which is proportional to engine load when engine speed is fixed is another factor that would affect the response time of intake air and

EGR gas flow dynamics. As a consequence, the response time of the air-path system strongly depends on engine speed and load.

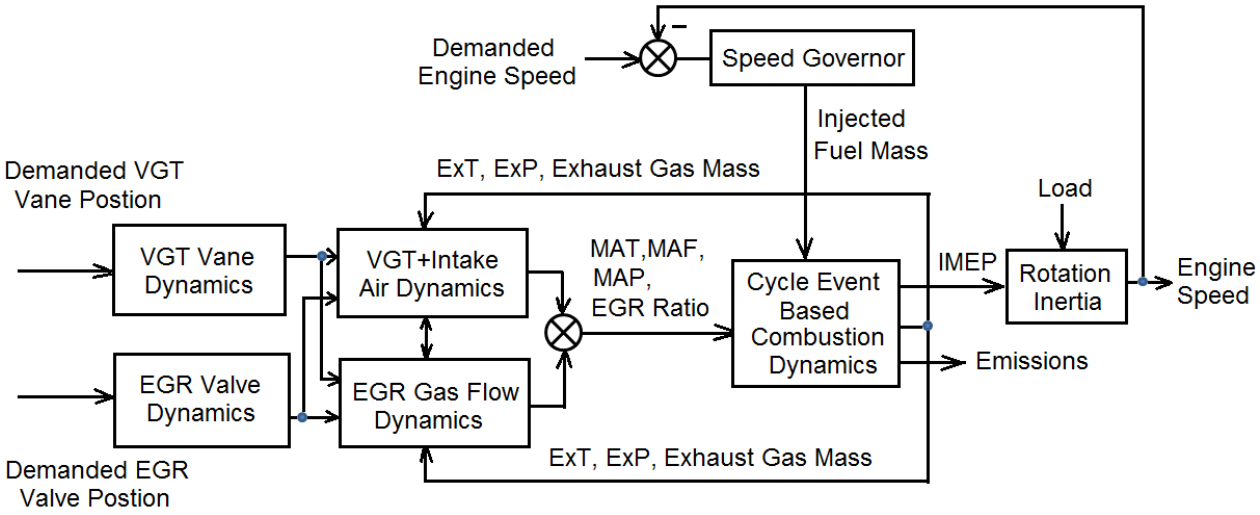

NB: ExT: Exhaust Temperature; ExP: Exhaust Pressure;
MAT: Manifold Air Temperature; MAF:Manifold Air Flow; MAP: Manifold Air Pressure

Figure 3.17: Air-Path Dynamics Diagram

Change in the engine speed caused by changes in the air-path control inputs is expected to be small when the engine is running steady-state. This can be reasoned on the basis of a change of VGT vane position or EGR valve position resulting in only a small variation of combustion power which is quickly compensated for by the engine speed governor through the adjustment of the injected fuel mass.

3.4.3.1 VGT Vane Position Step Change

The responses of six key air-path engine variables to a step change in VGT vane position when the EGR valve was completely closed are plotted in Figure 3.18. The engine was running at 1300rpm, 400Nm and the engine speed was controlled in closed-loop by the engine speed governor implemented in the LabVIEW real time PXI control system and which was a reproduction of the algorithm in the original engine ECM [171]. This speed governor was the primary speed and load control system of the original engine and functioned according to the minimisation of the difference in demand speed (set via an electronic throttle signal of type PWM) and actual engine speed (determined from the engine crank and cam position sensors) by adjustment of fuel injection quantity. Since the engine was speed governed, the dynamometer control of the Cadet V12 system was configured to torque-control so that the system torque could be precisely controlled in steady-state.

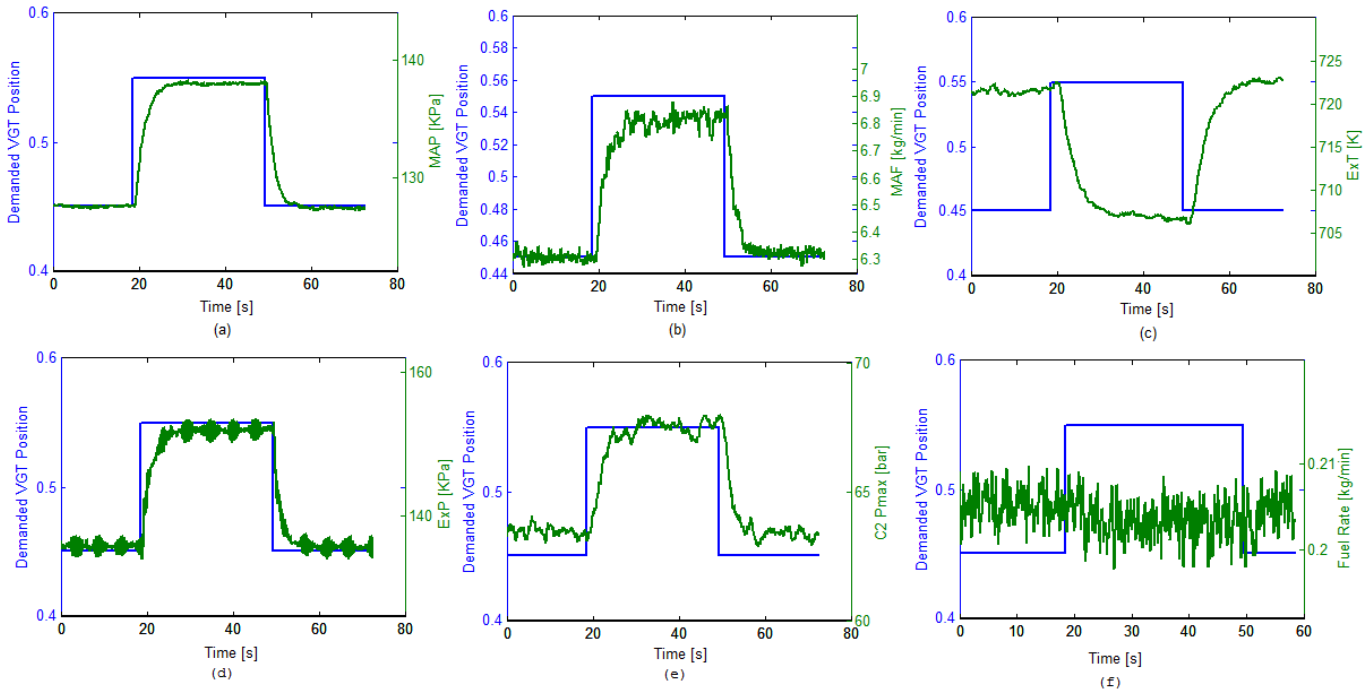

Figure 3.18: (a) MAP and VGT vane position demand step change signal; (b) MAF and VGT vane position demand step change signal; (c) ExT and VGT vane position demand step change signal; (d) ExP and VGT vane position demand step change signal; (e) Cylinder 2 P_{max} and VGT vane position demand step change signal; (f) Measured fuel flow rate and VGT vane position demand step change signal; Engine operating at 1300rpm, 400Nm. Engine Speed was closed-loop controlled by a speed governor. Engine load was controlled in closed-loop by the Cadet V12 System

It can be seen from Figure 3.18 that when the VGT vanes are closed down (i.e. closer to 1), MAP, MAF, Exhaust Pressure (ExP) and also P_{max} increase; however, the Exhaust Temperature and measured fuel flow rate reduce. The increase in MAP and MAF is because of the more closed vane position acting to increase the exhaust gas energy imparted to the turbine which in turn results in a higher compressor speed. Figure 3.19 (a) illustrates the increased turbocharger speed with the more closed vane position.

The higher MAP results in a higher cylinder pressure, higher P_{max} and hence higher exhaust pressure. Exhaust pressure is also coupled to the vane position however with a more closed vane position acting to increase the back-pressure at the exhaust manifold (ExP) due to the turbocharger. The lower exhaust temperature (ExT) indicates that the combustion temperature is lower at a more closed VGT vane position. This is explained by the larger intake charge mass at higher in-cylinder pressure resulting in a shorter ignition delay, faster diffusion combustion rate and reduced consumed fuel, i.e. more advanced combustion

phasing. This is supported by the CA50 data presented in Figure 3.19 (b) which shows a reduction in the angle of CA50 After Top Dead Centre (ATDC) with the more closed vane position.

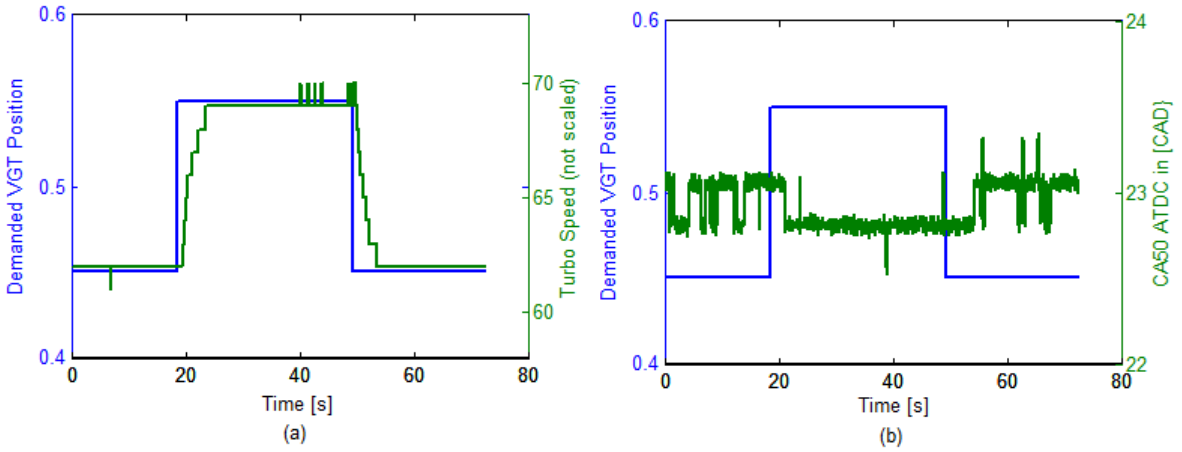

Figure 3.19: (a) Turbo speed and VGT vane position demand step change signal; (b) Average CA50 and VGT vane position demand step change signal; Engine operating at 1300rpm, 400Nm. Engine Speed was controlled in closed-loop by a speed governor. Engine load was controlled in closed-loop by Cadet V12 System

Other variables: Manifold Air Temperature (MAT), engine speed and engine load are plotted together with VGT vane position step change demand signal in Figure 3.20. These three variables remained constant as result of an air charge cooler, engine speed closed-loop control and Cadet V12 engine load closed-loop control respectively. Figure 3.20 (b) therefore confirms what was stated earlier in Section 3.4.3 that a change in VGT at engine steady state conditions results in very little disturbance in engine speed due to the closed loop speed governor control.

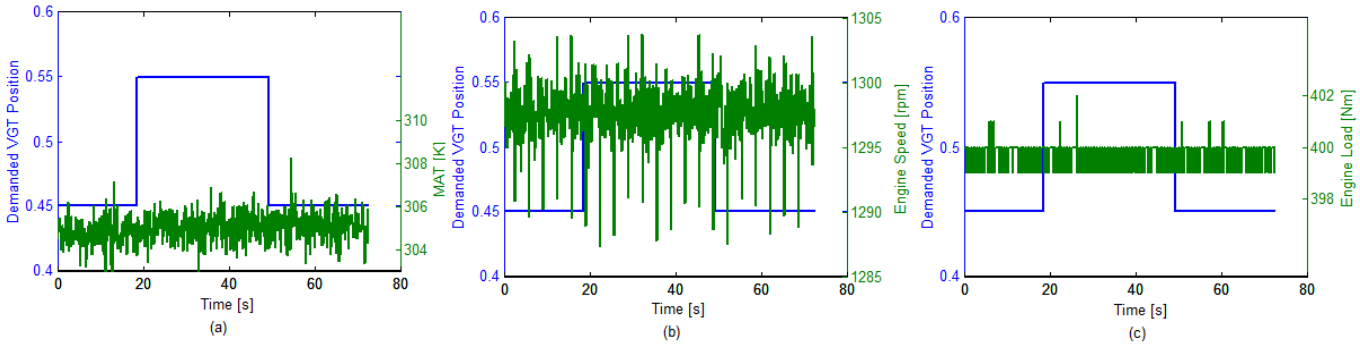

Figure 3.20: (a) MAT and VGT vane position demand step change signal; (b) Engine speed and VGT vane position demand step change signal; (c) Engine load and VGT vane position demand step change signal; Engine was running at 1300rpm, 400Nm

The step response pattern of MAP, MAF etc. to VGT vane position step change in Figure 3.18 indicates that the air-path dynamics could be modelled as a one order lag system with response dead time. See the following Transfer Function (TF) form:

$$\frac{Y(s)}{U(s)} = \frac{K}{Ts+1} e^{-\tau s} \qquad (\mathbf{3.6})$$

Where, $Y(s)$ and $U(s)$ are the Laplace transfer of the output and input variables respectively, K is the gain, T is the lag time, τ is the dead time.

Using MATLAB® system identification function *pem* with the step response data set, the TF with one gain, one system log time and a dead response time of VGT vane position demand to MAP were obtained at combinations of different engine speeds (800rpm to 1300rpm with 100rpm step change) and different engine loads (100Nm to 400Nm with 100Nm step change), a total of 24 engine operating points which are defined in Table 3.3.

Table 3.3: Twenty-four engine steady-state operating points used in the study of air-path and fuel-path dynamics

Load / Speed	100Nm	200Nm	300Nm	400Nm
800rpm	(1) RP=45; FR=85	(2) RP=55; FR=90	(3) RP=73; FR=91	(4) RP=90; FR=91
900rpm	(5) RP=50; FR=85	(6) RP=60; FR=90	(7) RP=70; FR=91	(8) RP=87; FR=91
1000rpm	(9) RP=55; FR=87	(10) RP=65; FR=90	(11) RP=75; FR=91	(12) RP=86; FR=91
1100rpm	(13) RP=60; FR=86	(14) RP=68; FR=89	(15) RP=83; FR=89	(16) RP=85; FR=91
1200rpm	(17) RP=68; FR=84	(18) RP=78; FR=87	(19) RP=86; FR=88	(20) RP=80; FR=92
1300rpm	(21) RP=66; FR=84	(22) RP=81; FR=86	(23) RP=88; FR=88	(24) RP=77; FR=93

NB: 1) The number inside the brackets is the No. of the engine test point; 2) (RP) refers to Rail Pressure, (FR) refers to Fuel Ratio ; they are determined from the engine ECM look up tables; 3) For all 24 engine operating points, the initial setting of VGT vane position=0.5; EGR valve position=0; SOI=3; Dwell Time (DW)=0.4ms; 3) DW is the time between the end of pilot injection and the start of the main injection.

The gain and system time for the solutions found for Equation 3.6 using the *pem* function (lag time plus dead time) for the 24 operating points are plotted against engine speed and load in Figure 3.21.

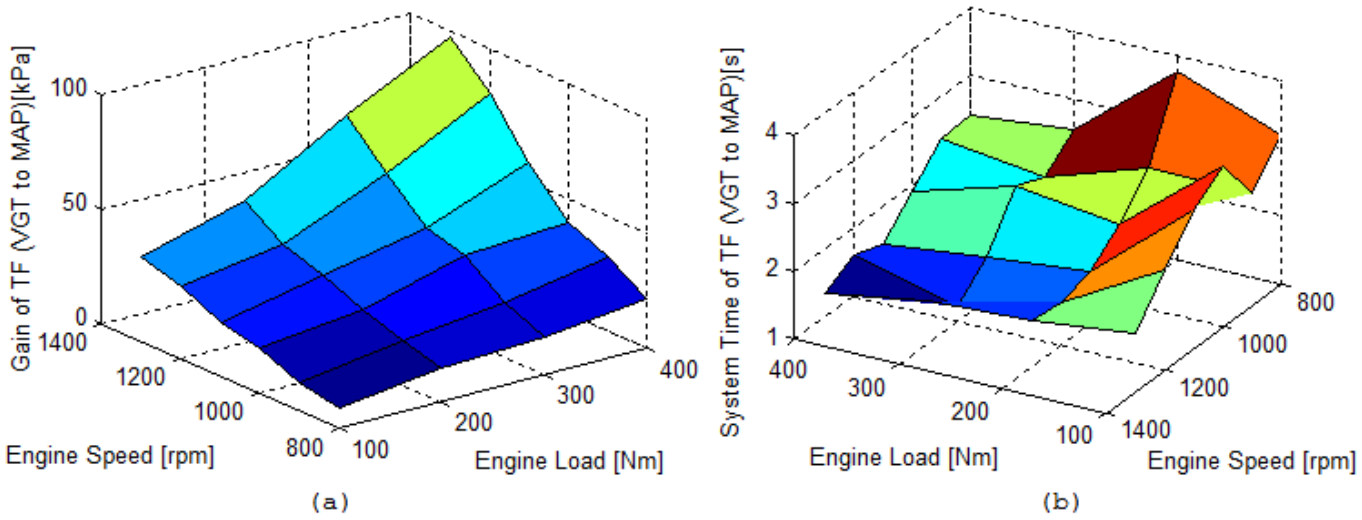

Figure 3.21: (a) Gain and (b) system time of the transfer functions describing VGT vane position demand input to MAP at 24 steady-state C6.6 engine operating points

It can be seen that at higher engine speed and higher load, the gain is larger but the system time is smaller. The slowest air-path dynamics, with a system time close to 4 seconds Figure 3.21 (b), occurs at the lowest engine speed together with the lowest load.

At the model identification and validation stage, fit number was used to evaluate the accuracy of the TF models derived using the *pem* function. Equation (3.7) is the algorithm used in MATLAB® to compute the fit number of a model:

$$Fit\_number = 1 - \frac{\|\hat{y} - y\|}{\|y - mean(y)\|} \times 100\% \qquad (\mathbf{3.7})$$

Where, $\hat{y}$ is the model output, y is measured variable. Using this methodology the fit numbers of all 24 TF models were greater than 80%.

The trends illustrated in Figure 3.21 for TF model gain and system time suggest that these two parameters could be a modelled using linear regression based on engine speed and engine load as the inputs. The application of this model to air-path control is discussed in detail in Chapter 4.

3.4.3.2 EGR Valve Position Step Change

The responses of the same six key air-path engine variables to a step change in EGR valve position when the VGT vane position was unchanged are shown in Figure 3.22 with the EGR valve going from completely closed to 10% open.

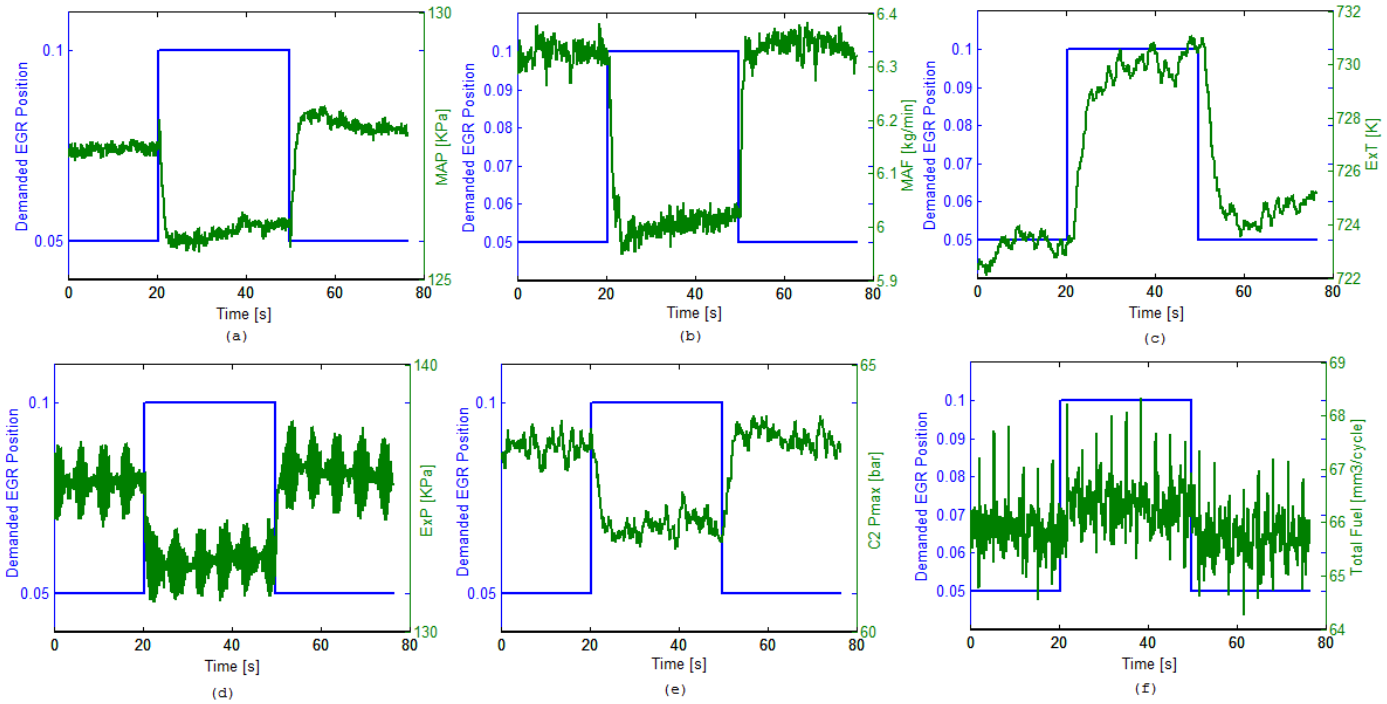

Figure 3.22: (a) MAP and EGR valve position demand step change signal; (b) MAF and EGR valve position demand step change signal; (c) ExT and EGR valve position demand step change signal; (d) ExP and EGR valve position demand step change signal; (e) Cylinder 2 P_{max} and EGR valve position demand step change signal; (f) Measured fuel flow rate and EGR valve position demand step change signal; Engine was running at 1300rpm, 400Nm. Engine Speed was controlled in closed-loop by a speed governor. Engine load was controlled in closed-loop by Cadet V12 System

For the data presented in Figure 3.22, the engine was running at the same operating point (1300rpm, 400Nm) with the same speed governor and Cadet V12 system configuration as described earlier in Section 3.4.3.1. Compared to the same variables for the VGT vane position step change presented earlier in Figure 3.19; each of these variables changed in the opposite direction in response to the EGR opening. When the EGR valve opened, the exhaust manifold pressure (ExP) dropped quickly as the exhaust gas bypassed the turbine by feeding into the EGR system, this reduction in turbine mass flow coupled with the lower ExP resulted in a reduction in the energy absorbed from the exhaust gas by the turbine.

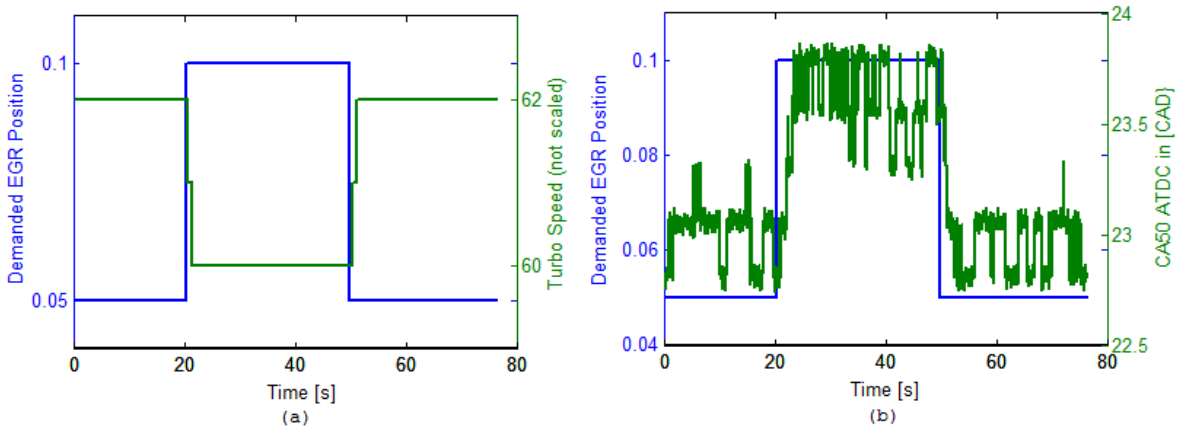

Figure 3.23: (a) Turbo speed and EGR valve position demand step change signal; (b) Average CA50 and EGR valve position demand step change signal; Engine was running at 1300rpm, 400Nm. Engine Speed was controlled in closed-loop by a speed governor. Engine load was controlled in closed-loop by Cadet V12 System

This resulted in a reduction in the turbo speed, as shown in Figure 3.23 (a), and thus without any compensation with the VGT vanes both the MAP and the MAF reduced which resulted in a lower P_{max}, Figure 3.22 (e).The increase in exhaust temperature (ExT) Figure 3.22 (c), results from both the increase in CA50 Figure 3.23 (b) (more retarded combustion) and the increase in injected fuel mass Figure 3.22 (f). The fuel mass increases as the engine speed governor increases fuel injection quantity to maintain engine speed and thus the combustion efficiency has reduced with the EGR valve opening due to the retardation of combustion as shown in Figure 3.23 (b). Since the exhaust back pressure (ExP) Figure 3.22 (d) was lower, this would have reduced the pumping work and thus the reduction in combustion efficiency due to the retardation was on balance more significant.

Figure 3.24 (a) shows that the intake manifold temperature (MAT) was largely unchanged by the air system changes that resulted from the EGR valve opening and this was because the EGR cooler and intercooler which maintained the manifold temperature.

Similar to the VGT vane position step change case discussed earlier in Section 3.4.3.1, the EGR valve step opening did not cause a notable disturbance to the engine speed and load due to the LabVIEW real time PXI control system speed governor and the Cadet V12 closed-loop load control respectively, see Figure 3.24 (b) and (c).

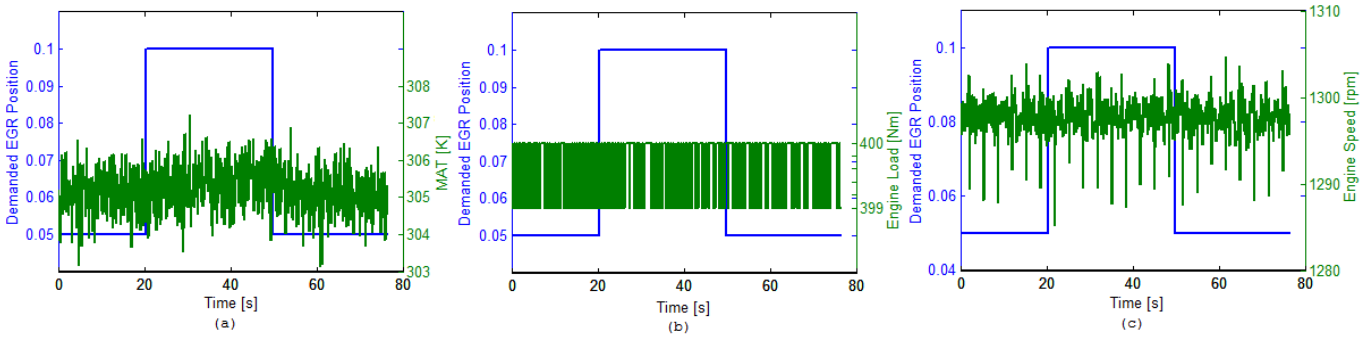

Figure 3.24: (a) MAT and EGR valve position demand step change signal; (b) Engine speed and EGR valve position demand step change signal; (c) Engine load and EGR valve position demand step change signal; Engine was running at 1300rpm, 400Nm

A repeat of the approach used for modelling air-path dynamics caused by the step change in VGT vane position (Section 3.4.3.1) has been used to model the air-path dynamics caused by EGR valve position step change. The engine operating points were also the same to those used in the previous section, Table 3.3. The gain and system time of the dynamics from EGR valve opening to MAP variable are plotted against engine speed and load in Figure 3.25 for the 24 operating points.

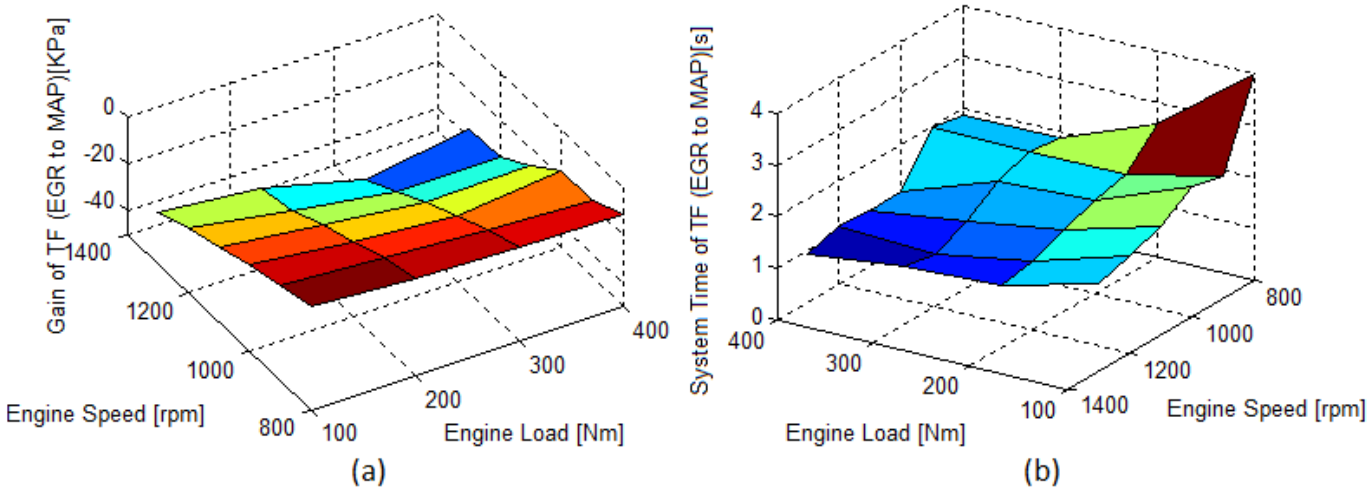

Figure 3.25: (a) Gain and (b) system time of transfer function from EGR valve position demand input to MAP with combination of engine different speed (800rpm to 1300rpm with 100rpm step change) and engine different load (100Nm to 400Nm with 100Nm step change)

The general shape of the surface plots for both the gain and system time model parameters are similar to that of the TF model for VGT dynamics, Figure 3.21 vs. Figure 3.25. However, the gains for the EGR dynamics are opposite to the VGT dynamics in that the highest gain for the EGR dynamics was at low

engine speed and load, Figure 3.25 (a), whereas the highest gain was high engine speed and load for the VGT dynamics, Figure 3.21 (a). Furthermore, the VGT gains were all positive whereas the EGR gains were all negative, therefore reflecting the preceding discussion of the effects of VGT closing and EGR valve opening. The slowest system time for both the VGT and EGR dynamics was roughly 4 seconds and occurred at the lowest engine speed and lowest engine load, 800rpm, 100Nm.

The MATLAB® *pem* function Equation (3.7) was again used to compute the fit number of the EGR TF models and the fit numbers were greater than 80% for each of the 24 engine operating points. Thus, like the VGT TF model parameters, the EGR TF model parameters could be modelled using linear regression based on engine speed and load as the inputs. The application of this model to air-path control is discussed in detail in Chapter 4.

3.4.3.3 Nonlinear Coupling Effect of VGT and EGR

Even though the direction of change of engine variables such as MAP, MAF, P_{max}, CA50, fuel rate, turbo speed, exhaust temperature, exhaust pressure etc. are opposite for the opening of the EGR valve and VGT vane closing, the purpose of applying VGT and EGR in regard to combustion are not in conflict. This reasoning is supported by Figure 3.26 which presents both the response of the two main regulated emissions (NO_x and opacity) to step closing of VGT vane position (Figure 3.26 (a) and (b)) and also the response to a step opening of the EGR valve (Figure 3.26 (c) and (d)) at engine speed 1300rpm and engine load 400Nm.

Figure 3.26 (a) and (b) show small decreases in NO_x emissions and opacity caused by the VGT vane closing (fully closed position is VGT position = 1). In contrast, the decrease in NO_x (Figure 3.26 (c)) caused by the opening of the EGR valve is relatively large (~100ppm). The prime reason for using EGR in diesel engines is to reduce NO_x emission by reducing P_{max} and combustion temperature. However, there is penalty with using EGR which is the increase in smoke emissions and fuel consumption. Consequently the VGT is used to provide a broader air-path system operating envelope at a given engine condition in respect to EGR, MAP and MAF to help offset the penalties caused through the use of EGR alone. VGT therefore contributes not only the reduction in emissions but also to reduction in pumping losses and the increase engine power output especially at low speed.

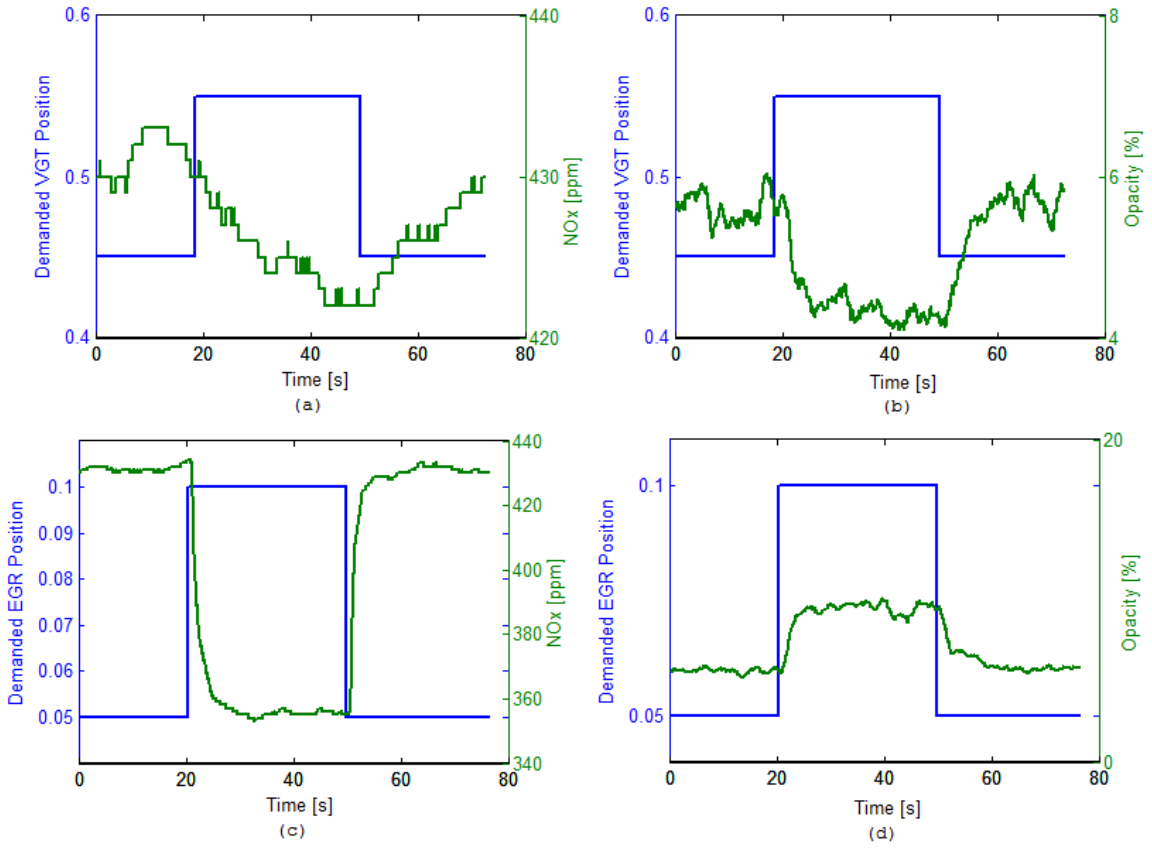

Figure 3.26: (a) NO_x and VGT vane position demand step change signal; (b) Opacity and VGT vane position demand step change signal; (c) NO_x and EGR valve position demand step change signal; (d) Opacity and EGR valve position demand step change signal; Engine operating at 1300rpm, 400Nm

The plots in Figure 3.27 show there is nonlinear coupling effect between VGT and EGR in respect to NO_x emissions and opacity.

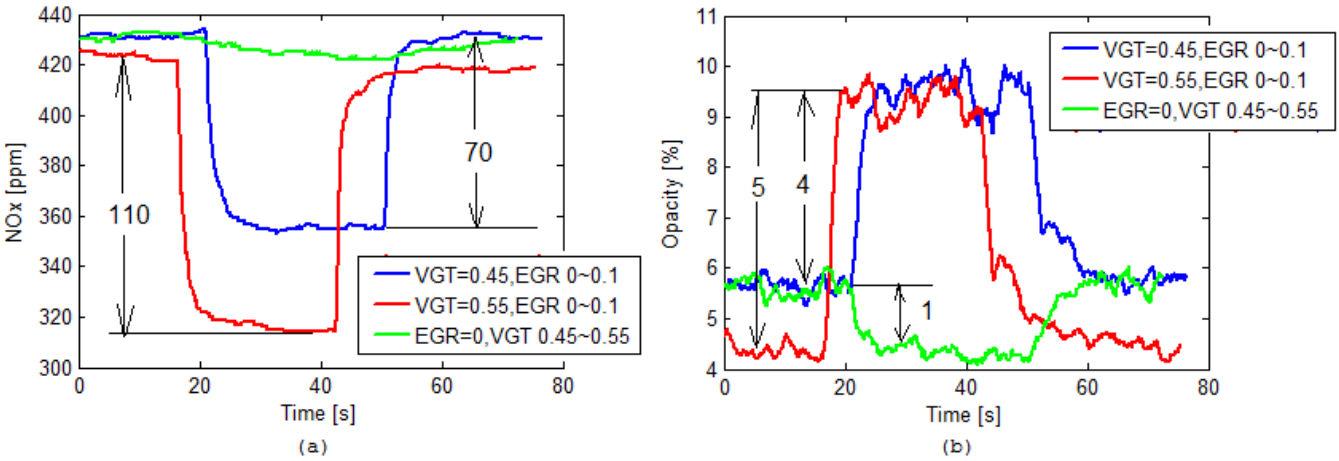

Figure 3.27: (a) NO_x during VGT vane or EGR valve position change; (b) Opacity with VGT vane or EGR valve position step change; Engine operating at 1300rpm, 400Nm

Description of the results in Figure 3.27 (a):

(i) when the VGT vanes were fixed at 0.45 closed, the EGR valve was changed from completely closed to 0.1 open position, NO_x emissions reduced ~70ppm.

(ii) when the VGT vanes were fixed at 0.55 closed, the EGR valve was changed from completely closed to 0.1 open position, NO_x emissions reduced ~110ppm.

This indicates that at this engine operating point for the same EGR valve position change, the more closed the VGT vanes, the greater the NO_x reduction. The drop in NO_x when the VGT vane position was changed from 0.45 to 0.55 with the EGR valve closed was as small as 10ppm. Therefore the nonlinear coupling effect between VGT and EGR means that based on the three examples in Figure 3.27 (a), the reduction in NOx with EGR closed and a VGT position change from 0.45 to 0.55 is just 10ppm (green); however, with the EGR valve at 0.1 open, the reduction in NOx caused by the same VGT 0.45 to 0.55 change is a somewhat larger 110 – 70 = 40ppm.

Figure 3.27 (b) shows the nonlinear coupling effect of VGT and EGR on smoke (opacity) emissions. If the coupling effect of VGT and EGR on smoke emissions is linear, the increase in the smoke emissions with EGR valve step change from 0 to 0.1 and with VGT vanes at 0.55 position should be 4 -1 = 3 %. However the measured increase in opacity is actually 5% and therefore at the same EGR valve position of 0.1, the opacity at VGT = 0.45 (blue) and VGT = 0.55 (red) is close. This nonlinear coupling effect is due to the high order combustion process dynamics. It may be explained and understood by physical modelling of engine combustion process and emissions formation.

There is also nonlinear coupling effect found in other variables like MAP. For example in Figure 3.28, if the coupling effect is linear, the increase in MAP (green) caused by a more closed VGT (from 0.45 to 0.55) when EGR valve is closed, minus the reduction in value of MAP (blue) caused by EGR valve open from 0 to 0.1 s when VGT vane position is 0.45 should be equal to the drop in value of MAP (red) caused by EGR valve opening from 0 to 0.1 (with the VGT vane position at 0.55). From the plot, it can be seen that this is not the case and it can be concluded that there is significant coupling.

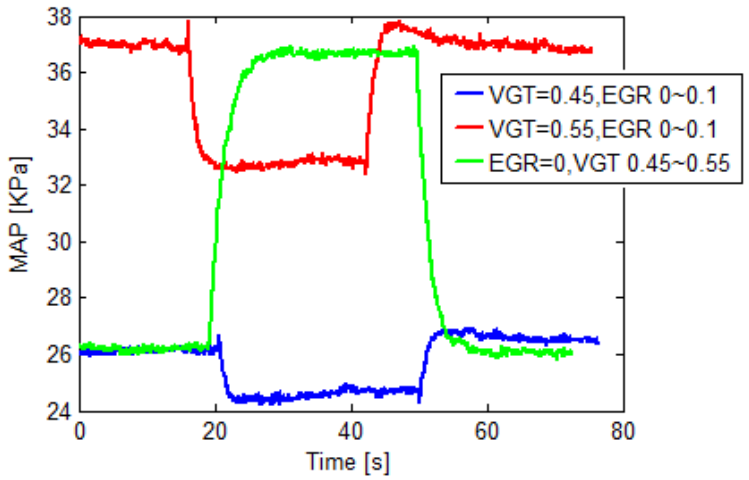

Figure 3.28: MAP during VGT vane or EGR valve position change; Engine was running at 1300rpm, 400Nm

Figure 3.29 (a) shows that the gain from EGR valve position input to MAP is negative and becomes more negative with increasing engine speed. This means that at higher engine speed, the same position change in the EGR valve results in a larger reduction in MAP. At the same speed, with higher engine load, the gain is also more negative. The closing of the VGT vanes also acts to make the gain more negative and this tendency increases with both increases in the engine speed and load.

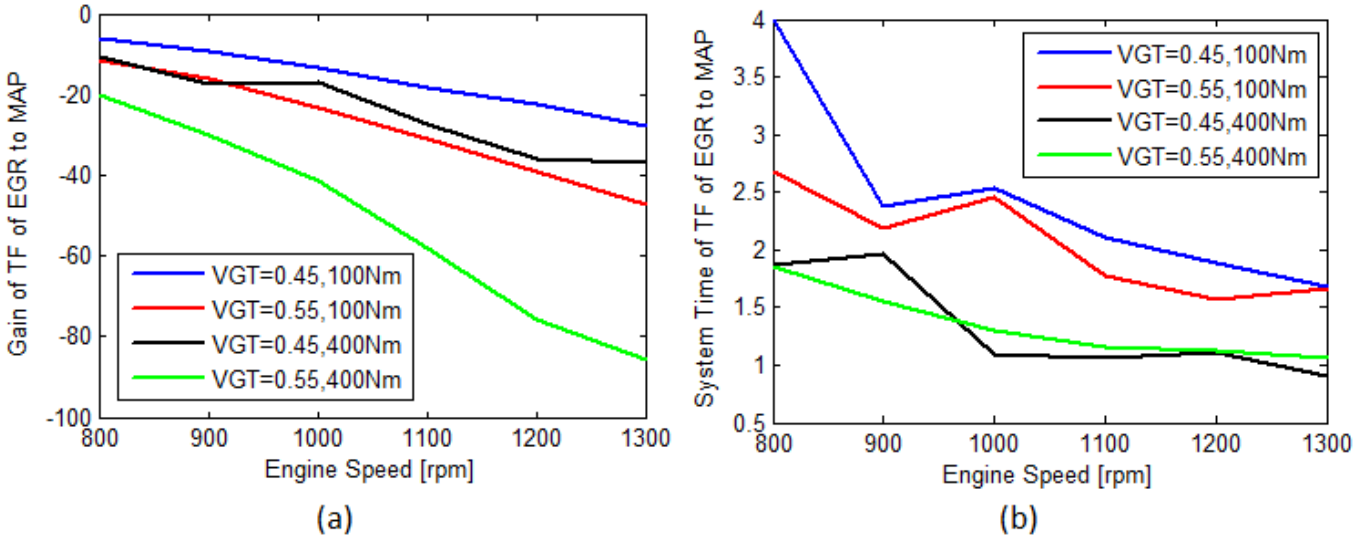

Figure 3.29: (a) Gain of TF of EGR valve position input to MAP output; (b) System Time of TF of EGR valve position input to MAP output

Figure 3.29 (b) shows that the system time reduces with engine speed and also engine load. However, the change in VGT from 0.45 to 0.55 does not produce a consistent change in the system time; comparing the blue to red and

the black to green traces, there is a general reduction in system time at 100Nm with a large reduction at low engine speeds which then narrows with increasing engine speed. However, at 400Nm there is no consistent change in the system time for the two VGT positions. This behaviour emphasises the nonlinear coupling effect between EGR and VGT.

A nonlinear regression has been used to model the gain of the TF models presented in Figure 3.29 (a). The model uses four inputs: engine speed, engine load, speed times load and VGT vane position. Figure 3.30 presents the identified TF model gains from the test data and the comparison nonlinear regression model prediction for both VGT vane position 0.45 (Figure 3.30 (a)) and 0.55 (Figure 3.30 (b)). The agreement is good for all for most speed and load cases. Therefore this demonstrates that one model can be used to predict dynamic model parameters and therefore nonlinear regression combined with TF models can be used to form an overall model of key air-system dynamics.

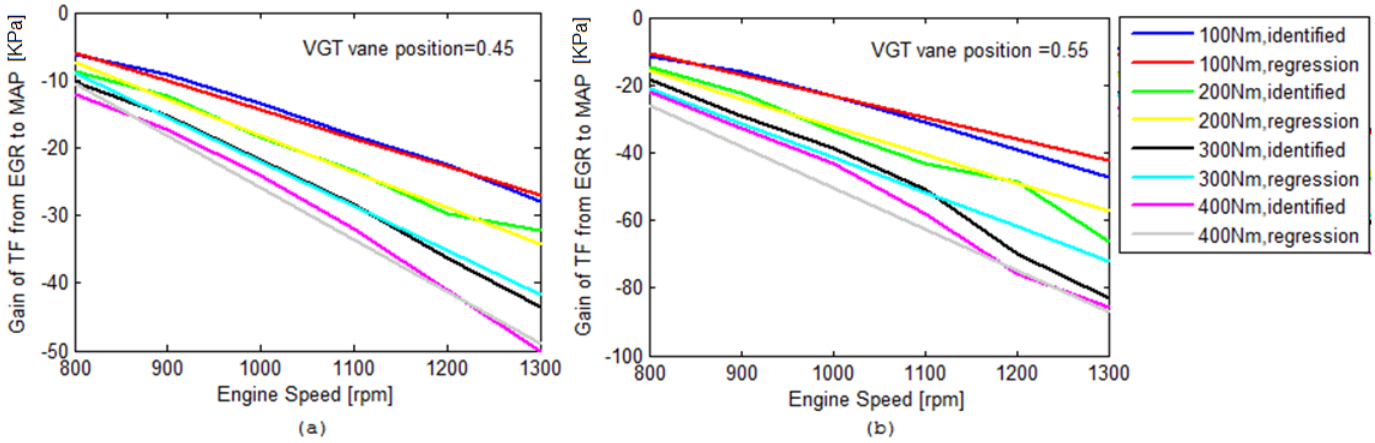

Figure 3.30: Comparison of identified gain and gain predicted from regression mode for: (a) when VGT vane position is 0.45; (b) when VGT vane position is 0.55

3.4.4 Fuel-Path Dynamics

The fuel-path of a diesel engine equipped with common rail injection system has several adjustable variables such as: injected fuel amount, start of injection, rail pressure, dwell time and fuel ratio for two-pulse injection mode. The injected fuel amount for the C6.6 engine used in this study is controlled by a speed governor but the other variables need to be set properly for different engine operating points to give the engine the required performance in respect of: combustion noise, fuel economy and gas emissions etc. Compared to start of injection and rail pressure, dwell time and fuel ratio have relatively small range of adjustment for different engine operating conditions. It will be shown in Chapter 5

that it is possible to adjust or control the start of injection and rail pressure online based on the feedback of combustion parameters. Engine dynamics caused by the fuel-path inputs, respectively start of injection and rail pressure, are discussed in the following sections.

3.4.4.1 Start of Injection Step Change

SOI is a variable used mainly for controlling the combustion phasing and it is adjusted according to different engine speed and load to give the best combustion efficiency and hence optimal fuel economy. It also has big influence on both NO_x and PM emissions. There exist trade-off phenomena between fuel economy and emissions, especially NO_x emissions, according to different timing for SOI. Consequently, the start of injection can be used as a control variable to select the trade-off point between fuel economy and emissions.

The dynamic responses of MAP, MAF, exhaust temperature, exhaust pressure, combustion peak pressure and fuel rate to a step retardation of SOI from 3 degrees Before Top Dead Centre (BTDC) to TDC are plotted in Figure 3.31.

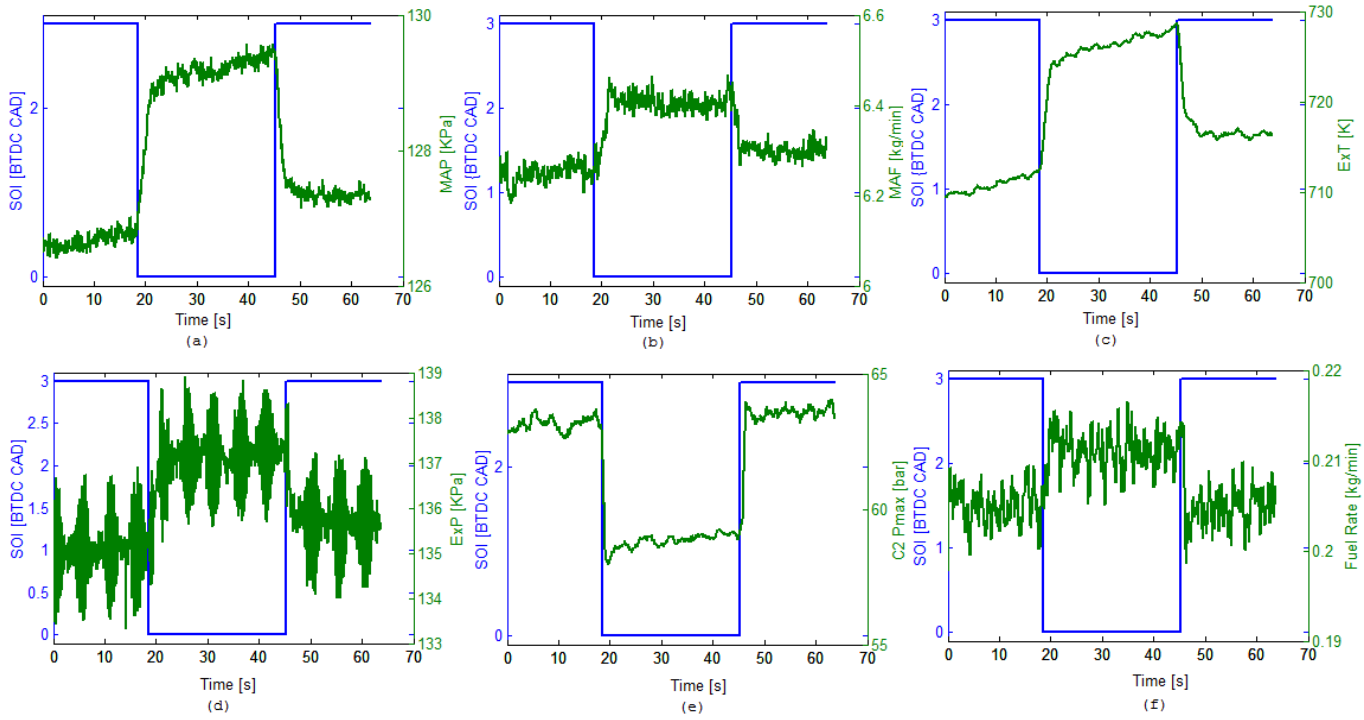

Figure 3.31: (a) MAP and SOI demand step change signal; (b) MAF and SOI demand step change signal; (c) ExT and SOI demand step change signal; (d) ExP and SOI demand step change signal; (e) Cylinder 2 P_{max} and SOI demand step change signal; (f) Measured fuel flow rate and SOI demand step change signal; Engine was operating at 1300rpm, 400Nm. Engine Speed was controlled in closed-loop by a speed governor. Dynamometer load was controlled in closed-loop by Cadet V12

The slow time trend of the all the variables shown in Figure 3.31 (before, during and after the SOI step) is because the engine load had been increased from 300 to 400Nm only a few minutes prior to this data being recorded and temperature equilibrium had not been achieved in the C6.6 engine intake and exhaust systems. For the C6.6 test engine used in this study, a steady-state period of up to 10 minutes was required to achieve system temperature equilibrium when transitioning between operating points. The focus in this section is the step response characteristics, so these longer time-history thermal equilibrium effects are only mentioned to aid clarity.

From Figure 3.31 the retardation of SOI with VGT and EGR unchanged is observed to result in retarded combustion that leads directly to reduced P_{max} and increased exhaust pressures and temperatures as the End of Combustion (EOC) occurs later in the cycle. This also has the effect of reducing the combustion efficiency on the basis of the increase in fuel rate. Since the exhaust manifold pressure and temperature increases and the VGT and EGR remain unchanged, the available energy that can be absorbed by the turbine also increased and this resulted in an increase in turbocharger speed, Figure 3.32 (a).

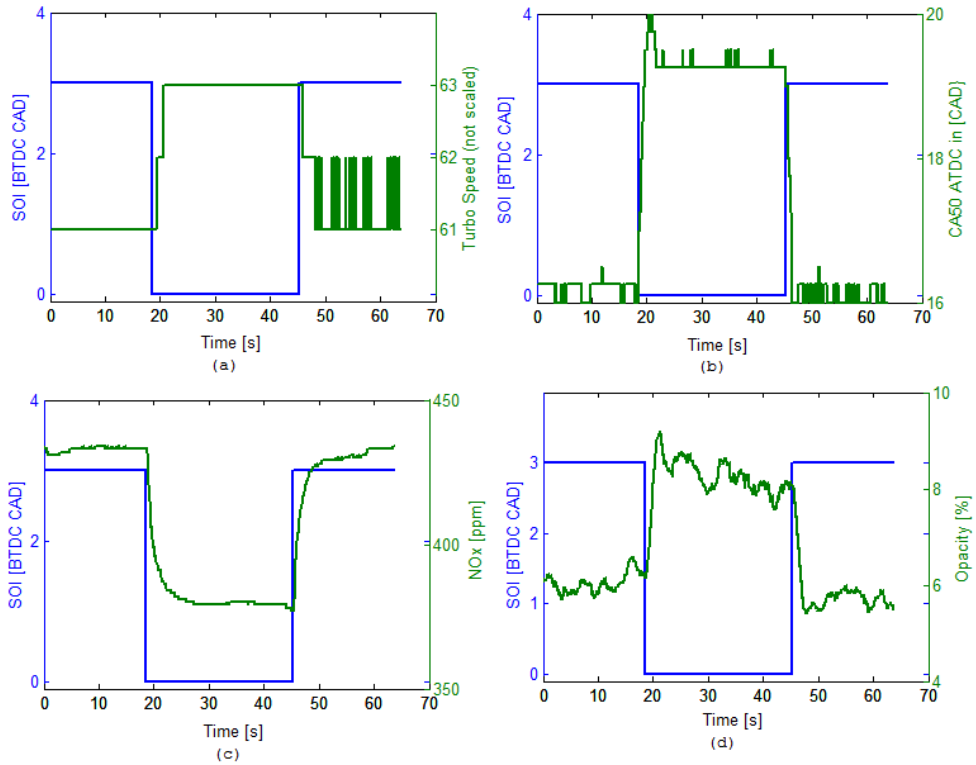

Figure 3.32: (a) Turbo speed and SOI demand step change signal; (b) CA50 and SOI demand step change signal; (c) NO_x emissions and SOI demand step change signal; (d) Opacity and SOI demand step change signal; Engine was operating at 1300rpm, 400Nm

This increase in turbocharger speed results in the higher MAP and MAF shown in Figure 3.31. This is therefore an example of fuel and air-path coupling. The retardation of combustion is shown in Figure 3.32 (b) where the CA590 is observed to retard about 3 degrees, thus mirroring the retardation of the SOI. Figure 3.32 (c) shows that the NO_x emissions decreased and this is explained by the reduction in combustion temperature which would have occurred in parallel with the reduction in P_{max}, Figure 3.31 (e). Smoke emissions increased due to the reduction in the cylinder temperatures and the retarded combustion which would have resulted in reduced soot oxidation.

The control performances of the intercooler controller, engine speed governor and Cadet V12 engine load controller during this SOI step change are shown in Figure 3.33. The intake air temperature remained fairly constant even though the MAP and MAF increased due to SOI retardation, Figure 3.31. The engine speed had two short duration spikes which coincided with the step change in SOI and thus it is clear that such sudden change in SOI will cause a disturbance to the engine speed governor, Figure 3.33 (b). This therefore illustrates the particular sensitivity of the work done by a cylinder to the combustion phasing; SOI is therefore a critical parameter in this regard and closed loop control of SOI needs to take this phenomenon into account.

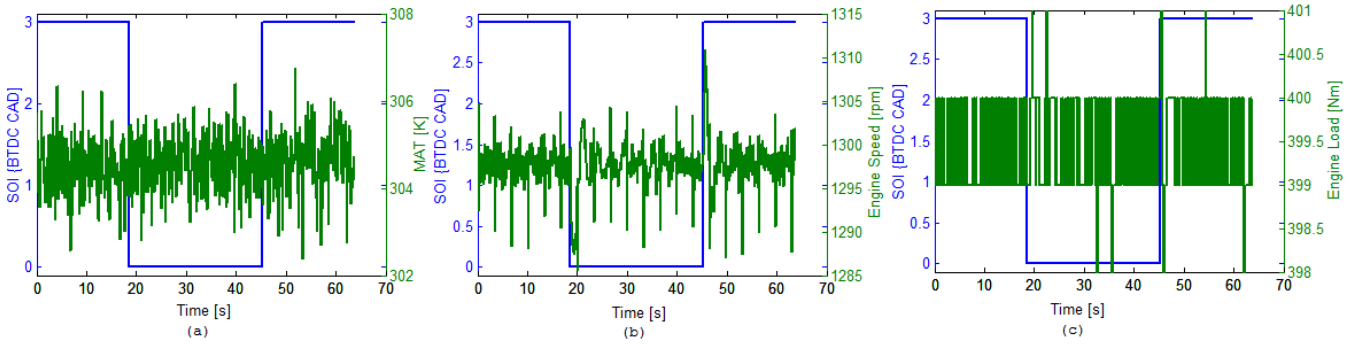

Figure 3.33: (a) MAT and SOI demand step change signal; (b) Engine speed and SOI demand step change signal; (c) Engine load and SOI demand step change signal; Engine was running at 1300rpm, 400Nm

The influence of SOI on air-path variables such as MAF and MAP varies with speed and load. At higher speed and load, the influence is stronger. Figure 3.34 (a) shows MAP changes when the SOI step change from 3BTDC to 0BTDC for four engine operating points: speed is at constant 800rpm, engine load is 100Nm, 200Nm, 300Nm and 400Nm respectively. Figure 3.34 (b) is the plot of MAP changes with SOI step change for the same four engine load conditions but

engine speed is at 1300rpm. This reveals that at high engine speed (above 1200rpm) and high-load condition (above 300Nm), the coupling effect between air-path dynamics and fuel-path dynamics is more significant.

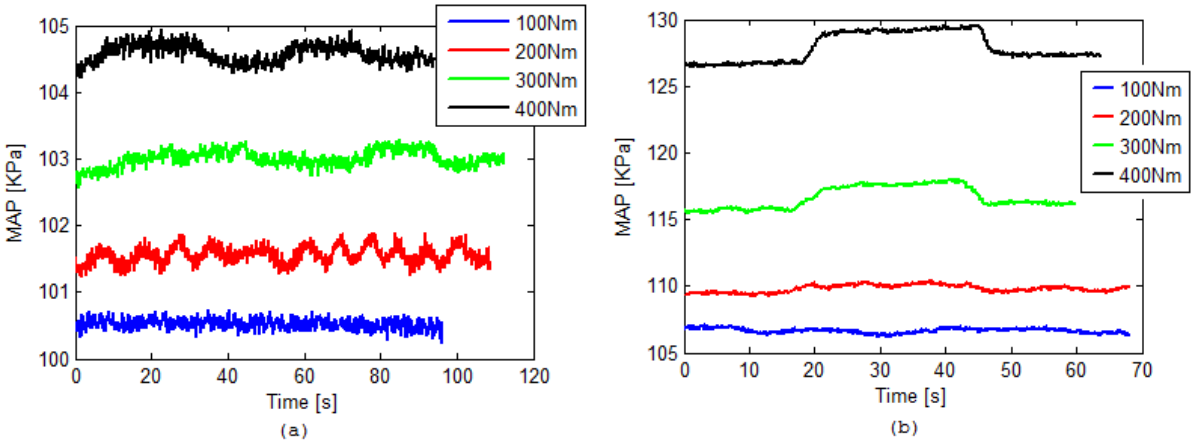

Figure 3.34: MAP during SOI step change for (a) engine speed is 800rpm; (b) engine speed is 1300rpm

The plot of MAF against MAP corresponding to step changes in SOI for all 24 engine operating points described in Table 3.3 is presented in Figure 3.35 (a) and this shows that at only three operating points: (1200rpm, 400Nm); (1300rpm, 300Nm); (1300rpm, 400Nm), the effect of the step change in SOI on MAF and MAP is significant (the three elongated data groups in the upper right corner of Figure 3.35 (a)).

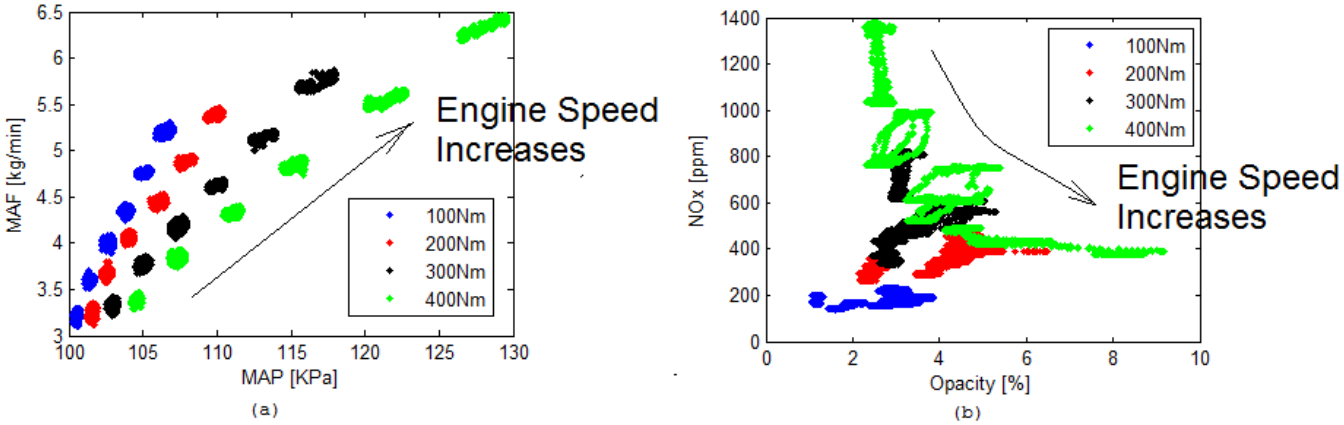

Figure 3.35: (a) MAF against MAP (b) NO_x emission against Opacity during SOI step change for the 24 engine operating points detailed in Table 3.3

Figure 3.35(b) shows the NO_x emissions against opacity for the 24 engine operating points when SOI was subject to a step change from 3BTDC to 0TDC. For clarity, this relationship is plotted again in Figure 3.36 by separating the different engine load cases. From Figure 3.35 (b) and the individual plots of

Figure 3.36; it can be seen that SOI has a big effect on NO_x emissions for almost all 24 engine operating points. However, the effect of SOI step change on particulate emissions is not always significant, an example being at the lowest engine speed 800rpm, where there is sufficient time for soot oxidation. In contrast, at higher load (400Nm) and higher engine speed (1300rpm), the effect of SOI on particulate emissions becomes especially significant, Figure 3.36 (d).

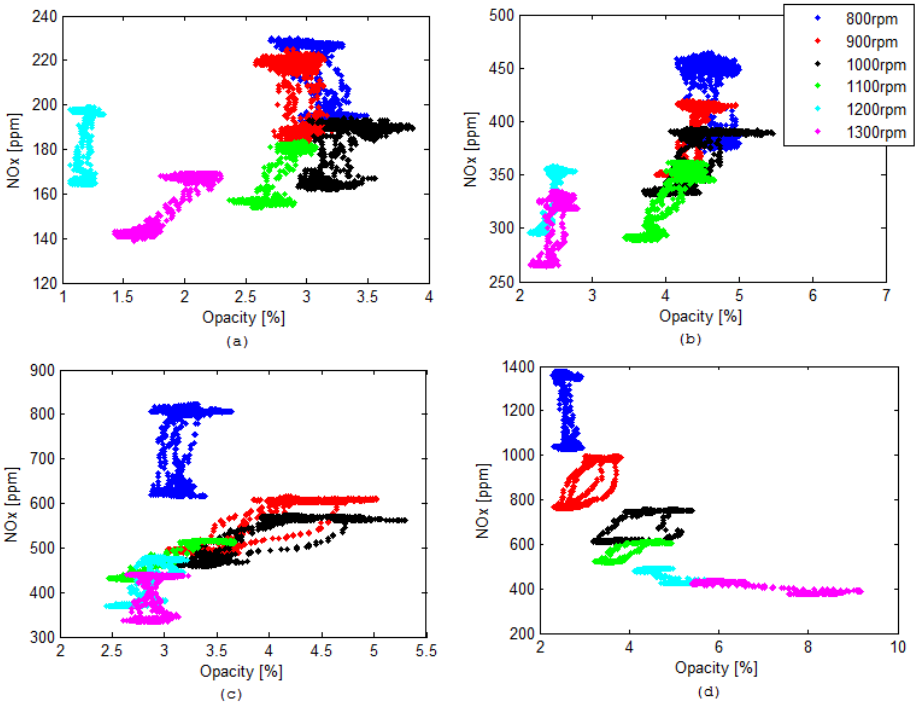

Figure 3.36: NO_x emission against Opacity during SOI step change for six different engine speeds from 800rpm to 1300rpm (a) engine load is 100Nm; (b) engine load is 200Nm; (c) engine load is 300Nm; (d) engine load is 400Nm

A very informative comparison is fuel rate against NO_x emissions when SOI is subject to a step change and this is shown in Figure 3.37. This shows a clear trade-off phenomenon between fuel rate and NO_x. This trade-off occurs due to the phasing of combustion, with a more advanced SOI resulting in higher cylinder pressure and temperature and hence greater NO_x emissions but with the benefit of a reduction in fuel consumption as more useful work is extracted from the combustion process due to the more optimal distribution of the cylinder pressure over the combustion and exhaust phases of the cycle. This therefore illustrates that SOI can be used to regulate the trade-off between fuel consumption and NO_x emissions for different engine operating conditions.

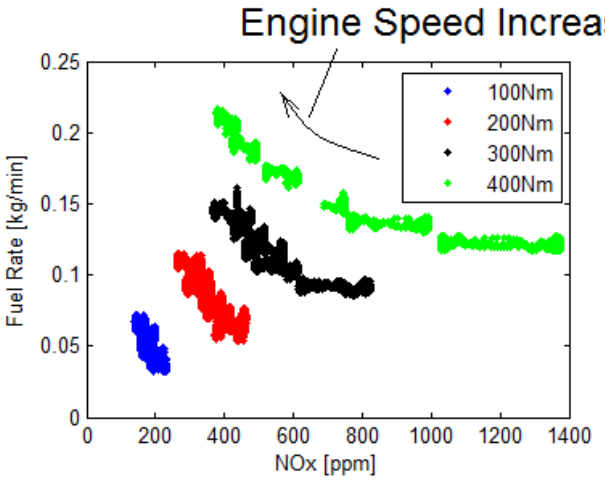

Figure 3.37: Fuel rate plotted against NO_x emission for 24 engine operating points in Table 3.3

In order to investigate an SOI closed-loop control system, the dynamic model from SOI to CA50 has been studied. Using the MATLAB function, *pem* and the collected SOI step change engine test data set; 24 transfer functions of the form of Equation (3.6) have been developed to describe the relationship of SOI to CA50 for all 24 engine operating points detailed in Table 3.3. The gain and system time for these 24 models are shown in Figure 3.38 (a) and (b) respectively.

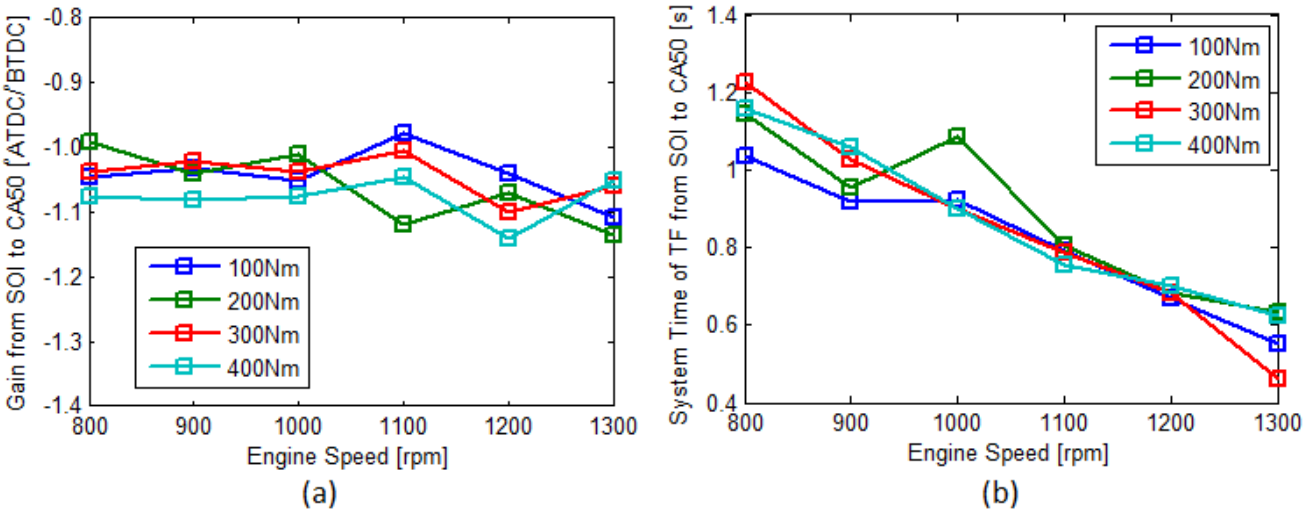

Figure 3.38: (a) Gain and (b) system time of the transfer function from SOI to CA50

Interestingly, the gain for all 24 operating points was found to be very close, ranging from -0.98 to -1.15, Figure 3.38 (a). This means that under different engine operating conditions, the change of SOI always results in a roughly similar change in CA50, with a slight overall greater retardation of combustion in

response to SOI retardation at higher engine speeds for the loads investigated. Figure 3.38 (b) shows the time constant of the dynamic model from SOI to CA50 and it is clear that the system time increases with engine speed but there is very little sensitivity to engine load. The reduction in system time with increasing engine speed is intuitive due to the shorter cycle time.

3.4.4.2 Rail Pressure Step Change

The same analysis procedure as above has been applied to the step change in rail pressure. Figure 3.39 and Figure 3.40 show that when rail pressure was subject to a step change from 78 MPa to 88 MPa at engine speed 1300rpm and engine load 400Nm, only P_{max} and NO_x emission increase while all other engine variables fall in value. The higher rail pressure shortens the combustion period giving lower exhaust pressure, exhaust temperature, etc.

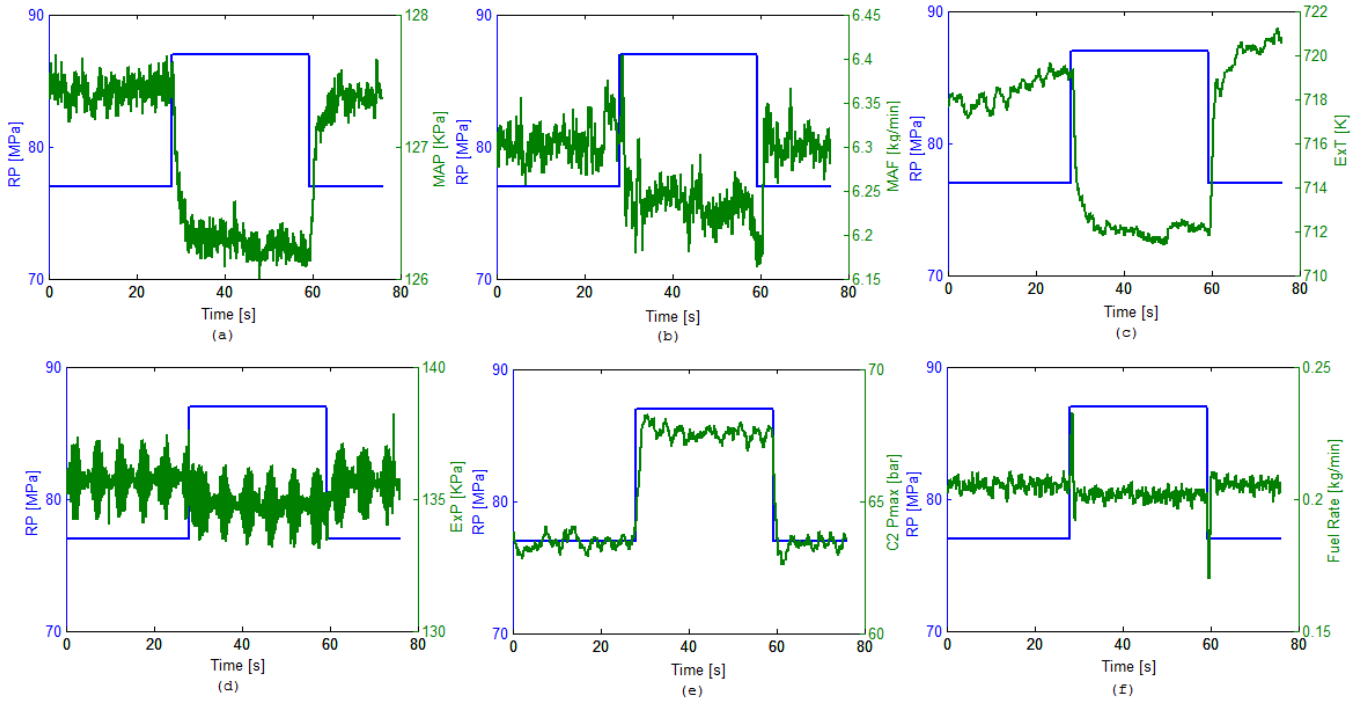

Figure 3.39: (a) MAP and rail pressure demand step change signal; (b) MAF and rail pressure demand step change signal; (c) ExT and rail pressure demand step change signal; (d) ExP and rail pressure demand step change signal; (e) Cylinder 2 P_{max} and rail pressure demand step change signal; (f) Measured fuel flow rate and rail pressure demand step change signal; Engine operating at 1300rpm, 400Nm. Engine Speed was controlled in closed-loop by the speed governor. Engine load was controlled in closed-loop by the Cadet V12

The combustion duration is shorter because the rate of fuel mass delivery into the cylinder is higher at higher rail pressure; this in turn increases the fuel

atomisation due to the higher energy of the injected fuel mass. Since the combustion duration is shorter, it occurs closer to TDC leading to higher combustion zone temperatures and thus higher P_{max} and NO_x emissions. The shorter combustion duration in response to the increase in fuel rail pressure is shown in Figure 3.40 (b).

Since the increase in rail pressure resulted in an earlier EOC, the exhaust gas pressure at blow down was lower, Figure 3.39 (d), and this had a similar cascade effect as was observed for SOI advance in Section 3.4.4.1 in that the slightly lower exhaust pressure and temperature caused the energy absorbed from the exhaust gas by the turbine to be reduced; this in turn reduced the turbocharger speed, Figure 3.40 (a), and therefore reduced the MAP and MAF, Figure 3.39 (a) and (b) respectively.

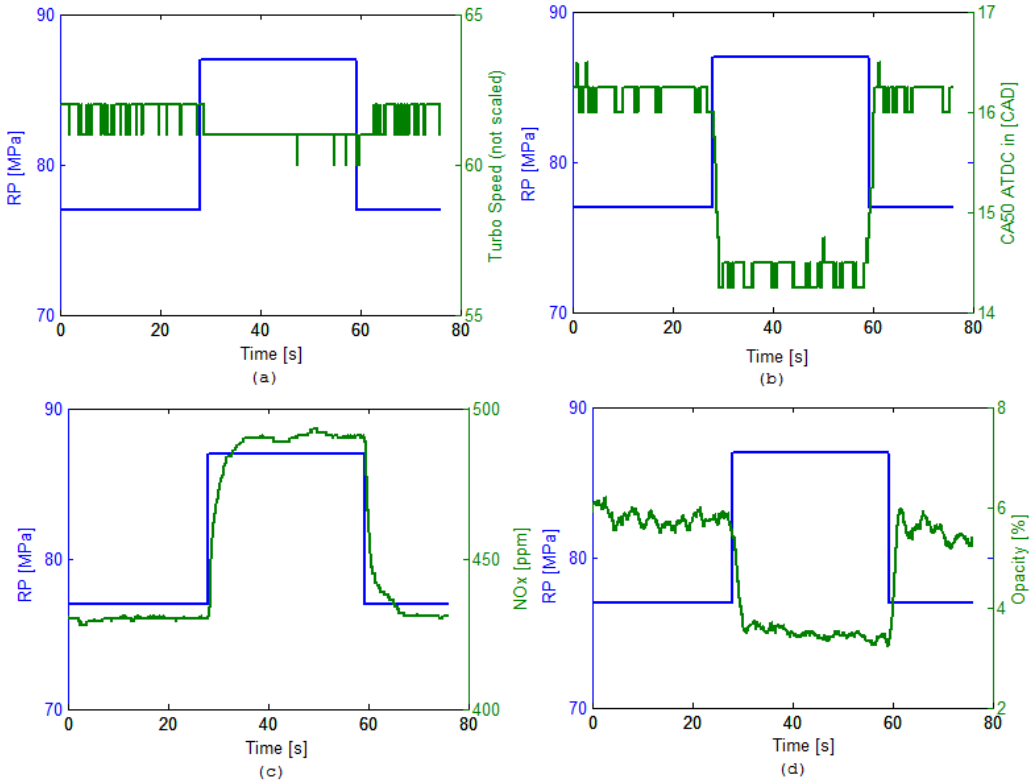

Figure 3.40: (a) Turbo speed and rail pressure demand step change signal; (b) CA50 and rail pressure demand step change signal; (c) NO_x emissions and rail pressure demand step change signal; (d) Opacity and rail pressure demand step change signal; Engine was operating at 1300rpm, 400Nm

Figure 3.41 shows that intake temperature, engine speed and engine load were regulated well during rail pressure step change. Like with the SOI step change, the rail pressure step change was observed to cause small spikes in engine speed as the speed governor adjusted the fuel quantity to account for the

change in the work output of the cylinders as the combustion phasing was changed with rail pressure. Therefore similar to SOI, this rail pressure – engine speed control phenomena is also an important consideration in any closed loop fuel path control that involves engine speed control and closed loop rail pressure control.

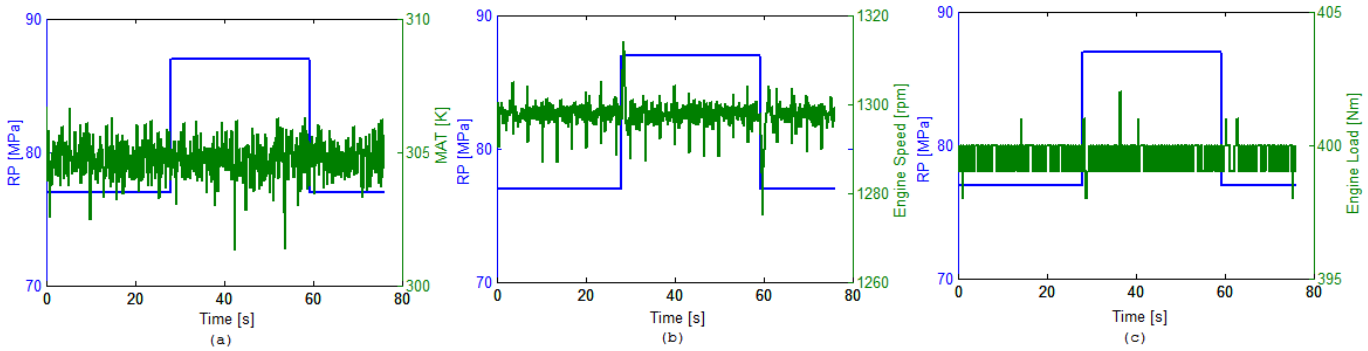

Figure 3.41: (a) MAT and rail pressure demand step change signal; (b) Engine speed and rail pressure demand step change signal; (c) Engine load and rail pressure demand step change signal; Engine was running at 1300rpm, 400Nm

The MAP variable is plotted for step changes in rail pressure at engine speeds of respectively 800rpm and 1300rpm, in Figure 3.42 (a) and (b) respectively. MAF against MAP for all 24 engine operating points is shown in Figure 3.43 (a).

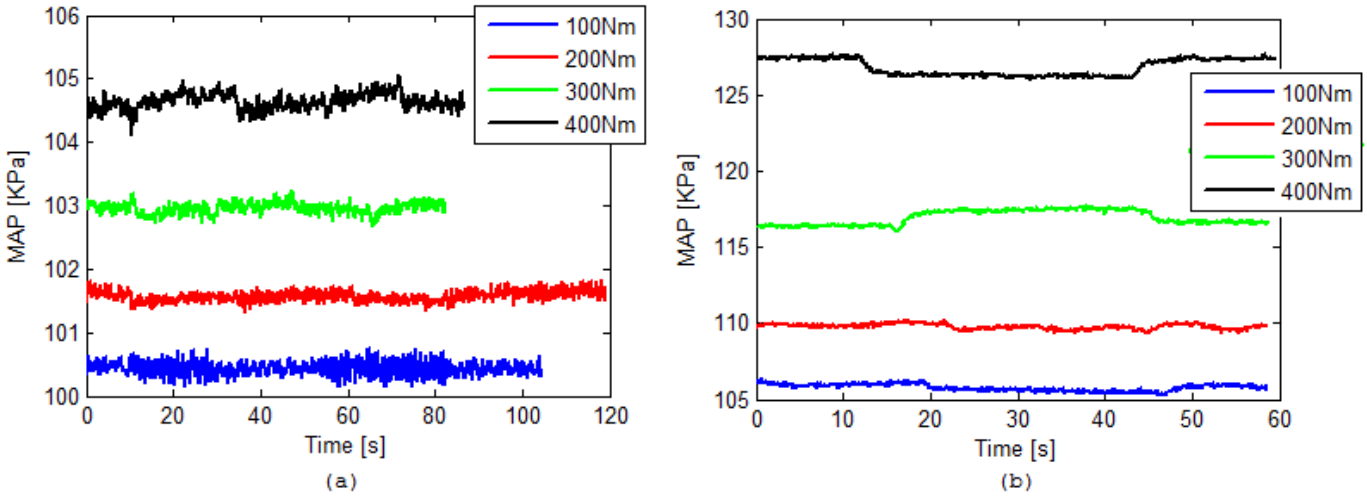

Figure 3.42: MAP during rail pressure step change for (a) engine speed is 800rpm; (b) engine speed is 1300rpm

From Figure 3.42 it is clear that in a similar way to the SOI step change, the influence of rail pressure on air-path variables such as MAP, is only significant at high engine speed together with high engine load.

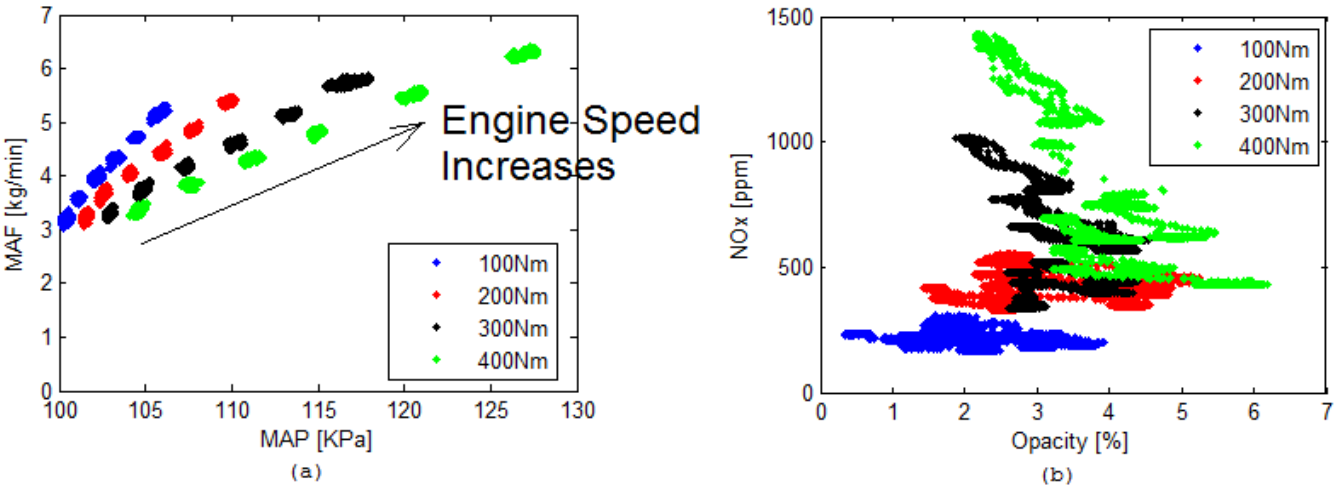

Figure 3.43: (a) MAF against MAP and (b) NO_x emission against Opacity emission during rail pressure step change for 24 engine operating point in Table 3.3

In Figure 3.43 (b) NO_x emissions are plotted against particulate emissions (using opacity as measure) during the rail pressure step change for all 24 engine operating points. These data are drawn again in Figure 3.44 with the data segregated into 4 different engine loads and for six engine speeds at each load.

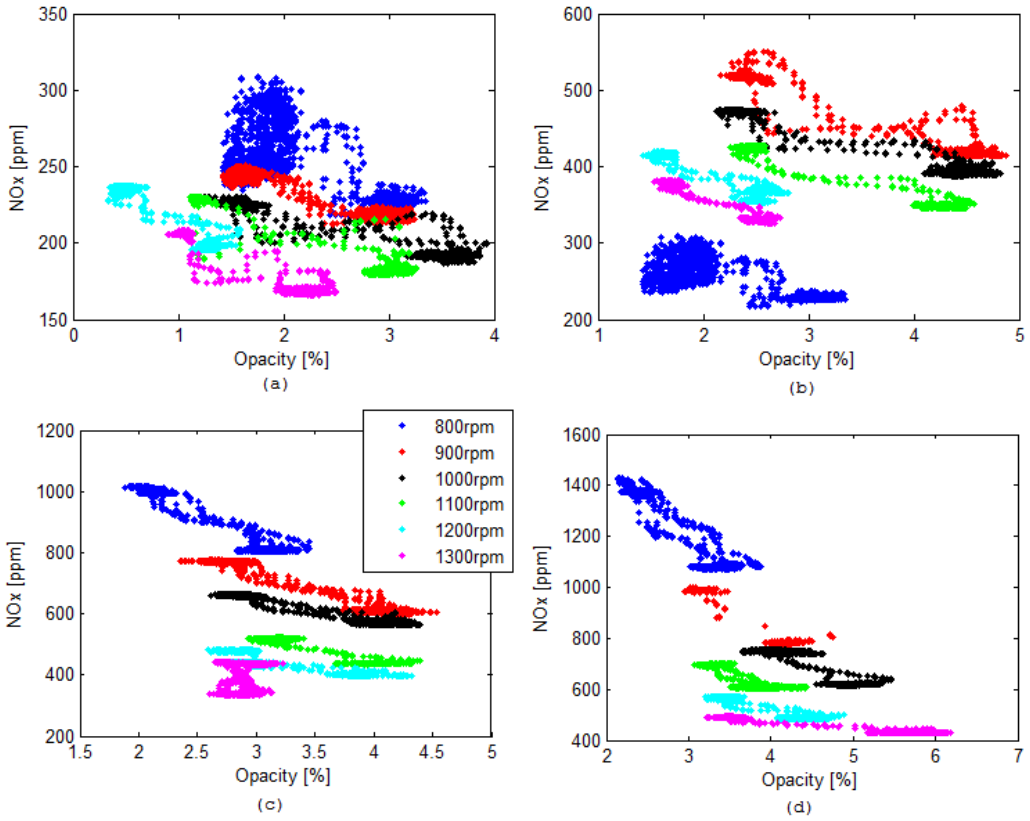

Figure 3.44: NO_x emission against Opacity during rail pressure step change for six different engine speeds from 800rpm to 1300rpm (a) engine load is 100Nm; (b) engine load is 200Nm; (c) engine load is 300Nm; (d) engine load is 400Nm

From Figure 3.44 it can be seen that rail pressure has big effect on both NO_x and PM emissions. NO_x emission and PM emission have an obvious trade-off relationship when rail pressure changes for the majority of the engine operating conditions investigated. This useful attribute therefore makes rail pressure a good candidate for selecting the trade-off point between NO_x emission and PM emission.

A good feedback variable for rail pressure closed loop control is CA50 due to the direct relationship between rail pressure and combustion duration described earlier and evidenced in Figure 3.40 (b). Using the same system identification technique as described in earlier sections; the gain and time constant of the TF dynamic model, Equation (3.6), have been determined for rail pressure to CA50 for all 24 engine operating points (Table 3.3) and these model parameters are shown in Figure 3.45.

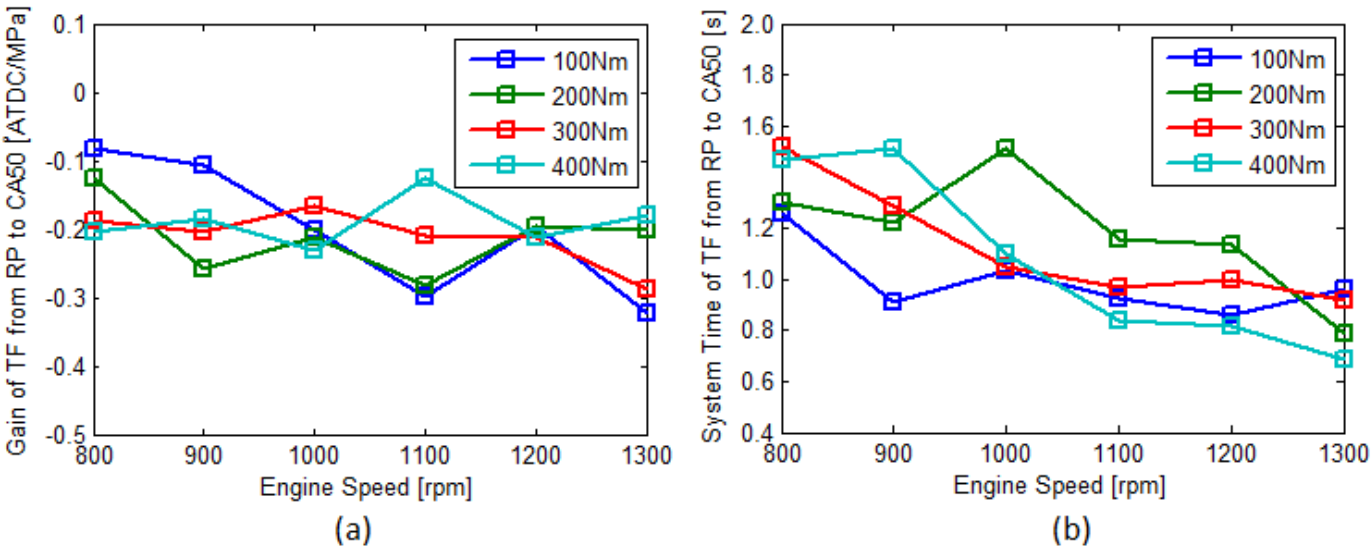

Figure 3.45: (a) Gain and (b) system time of transfer function from SOI to CA50

Similar to the SOI case (Figure 3.38 (a)), the gain can be treated as a constant value of -0.2° After Top Dead Centre (ATDC)/MPA for all 24 engine operating points. The negative gains are because at higher rail pressure, the combustion process is shortened leading to more advanced CA50. Again, similar to the SOI findings shown in Figure 3.38 (b), the time constant decreases linearly as engine speed increases, Figure 3.45 (b), and again the effect of load is not clear and significant. The reduction with engine speed again follows intuitively the shorter cycle time at higher engine rpm. The quite similar behaviour of the TF model parameters for SOI (Figure 3.38) and fuel rail pressure (Figure 3.45) to

CA50 show how similar these two control parameters influence combustion dynamics and how both may be feasibly used to close loop control CA50.

3.4.5 Coupling Between Air-path and Fuel-Path Dynamics

The discussion in the preceding two sections showed evidence of the coupling that exists between air-path and fuel-path dynamics. The change of EGR valve position or VGT vane position has an influence on combustion parameters such as P_{max}, CA50 and IMEP. All of these three combustion parameters are also coupled to fuel-path control variables. In the opposite way, fuel-path inputs like SOI and rail pressure also have an effect on air-path variables such as exhaust pressure and temperature, intake pressure and temperature etc.as was outlined previously in Section 3.4.4.1 and Section 3.4.4.2. This influence is universal but only becomes obvious at high engine speeds and loads as is illustrated by Figure 3.34 and Figure 3.42 which show the SOI and fuel rail pressure effect on MAP. A schematic outlining the connection between air-path and fuel-path dynamics is shown in Figure 3.46.

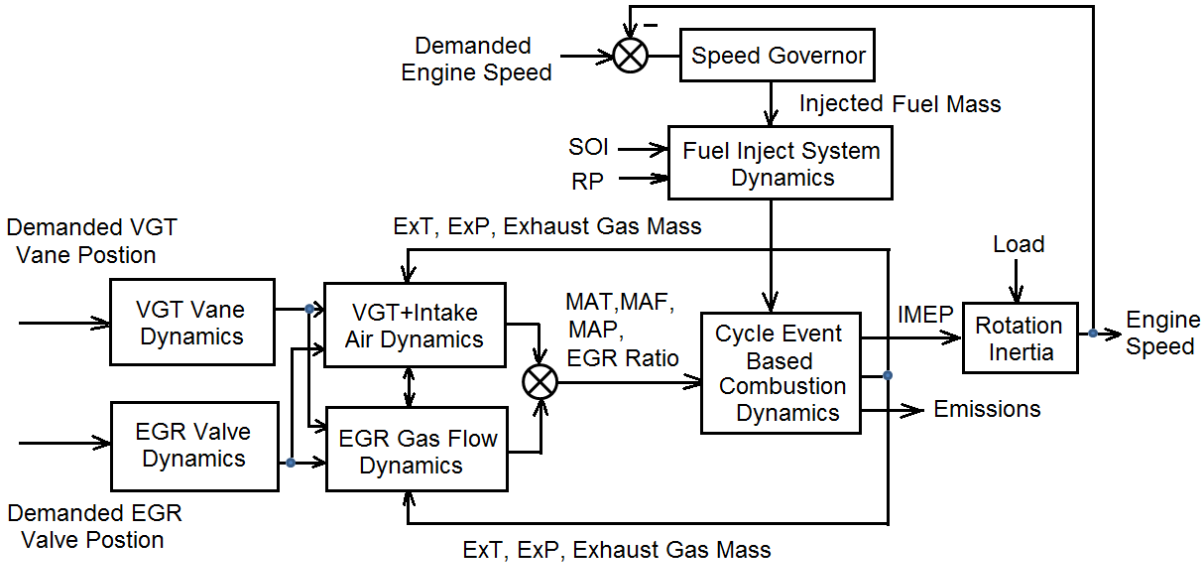

NB: ExT: Exhaust Temperature; ExP: Exhaust Pressure;
MAT: Manifold Air Temperature; MAF:Manifold Air Flow; MAP: Manifold Air Pressure
SOI: Start of Injection; RP: Rail Pressure

Figure 3.46: Schematic diagram of air-path together with fuel-path

On the lower left of Figure 3.46 the VGT and EGR dynamics are grouped together and show that there is coupling between VGT and EGR in respect to the air system dynamics such that for example the EGR gas flow dynamics are dependent upon both VGT and EGR valve inputs. The resulting MAT, MAF, MAP and EGR ratio air-path parameters then contribute to the cycle event based

combustion dynamics. Separately, the fuel injection system dynamics also contribute to the combustion dynamics. Therefore the IMEP, exhaust pressure, exhaust temperature, emissions etc. resulting from combustion then feedback into the system such that the dynamics of the air-path and fuel-path are fundamentally coupled and made complex by the use of EGR.

The schematic of Figure 3.46 therefore captures in overview the behaviour that was described in the preceding analysis of the C6.6 engine air-path and fuel-path dynamics in this chapter. For an integrated air-path and fuel-path control system to perform, the knowledge and understanding of the coupling between these systems as shown in Figure 3.46 is critical. This knowledge and understanding has been applied to develop novel air-path and fuel-path control practical demonstrations on the C6.6 test engine used in this study and these practical demonstrations are discussed in Chapter 4 and Chapter 5 respectively.

3.5 Conclusions

The details of the Caterpillar C6.6 experimental diesel engine and the unique LabVIEW real time PXI control system that controls the engine air-path and fuel-path have been introduced in this chapter.

Investigation of cycle-to-cycle combustion variation of the C6.6 engine was carried out using 300 continuously measured cycle cylinder pressure signals. Utilising a cross-correlation methodology, the measured variables which included combustion pressure, injector current, needle lift, sleeve pressure, pump drive current and rail pressure were investigated to understand the cause of observed cycle-to-cycle variation. It was concluded that the cause of the variation was attributable to the hardware utilised for driving the fuel injectors and high pressure pump in the LabVIEW real time PXI control system.

Specifically, the DRIVVEN injector driver modules used to drive the six injectors and the high pressure pump solenoid control valve could not reproduce all the fine details of the original drive signals produced by the ECM. Additionally, the compensation for differences in injector fuel quantity delivery in the original ECM were not implemented in the LabVIEW real time PXI control system and this resulted in cylinder-to-cylinder inconsistency which was exacerbated for the cylinder 1 injector as this injector had undergone remedial work to install a needle lift sensor and a sac volume pressure sensor. The cycle-to-cycle variation and the cylinder-to-cylinder variation detailed in this chapter both require a closed

loop control methodology to reduce both types of variation and demonstrations of approaches for this are discussed in Section 5.4.

The air-path dynamics in regard to VGT vane position or EGR valve position to MAP and also the fuel-path dynamics in regard to SOI and RP to CA50 of the C6.6 engine were studied using a step response test combined with system identification techniques for 24 steady-state operating points. A transfer function model was then parameterised for each of these input-output pairings for all engine operating points and the gain and system time of these models were discussed. The results revealed that fuel-path dynamics were less sensitive to the change of engine operating point compared to the air-path dynamics. The results also revealed it is practical to use a form of regression model to predict the gain and system time of the transfer model with greater than 80% accuracy and thus demonstrates the applicability of model based control to both air-path and fuel-path, such techniques are demonstrated practically in Chapter 4 and Chapter 5 respectively. Critically, a complex coupling between the engine air-path and fuel-path systems was demonstrated and a scheme was proposed to encapsulate the mechanisms of this coupling.

Chapter 4

4 Air-Path Control

4.1 Introduction

For a diesel engine that is equipped with VGT and EGR systems, there are two control inputs that need to be controlled to optimize engine performance for load acceptance, fuel consumption and regulated emissions. In this chapter, the function of VGT and EGR has been experimentally studied. The picture of the effect of VGT and EGR variations with engine operating point has been drawn. Models for estimating the gas flow rate into the engine and also the EGR flow rate have been validated against engine test data respectively. Models for describing the deterministic relationship from the exhaust system to the intake system via the turbocharger for the engine running at steady-state has been developed and validated. Dynamic models for air-path control were studied using system identification methods. Two air-path closed-loop control systems have been developed and tested on the C6.6 test engine.

4.2 Air-Path System

4.2.1 VGT Function

Nowadays, a VGT is widely installed in diesel engines with the aim of increasing engine performance in terms of both maximum power and transient capability. It also has another advantage in that some of the otherwise wasted exhaust energy in the exhaust pipe is reused. Consequently, the VGT is able to both increase the fuel economy of the diesel engine and also form the basis for engine downsizing. The vane position of the VGT can be used as the basis for optimization of diesel engine performance in regard to both fuel consumption and drivability. The effect of vane position on engine variables such as MAF, MAP, CA50, P_{max}, IMEP, NO_x and soot emission etc. is shown in Figure 4.1; the engine schematic in this figure is reproduced from [25].

The individual data plots of engine variables are from a VGT sweep test on the C6.6 test engine used in this study. In this sweep test the VGT vane position was increased from 0.45 to 0.65 whilst the EGR valve was closed. Speed was kept constant at 1400rpm by the engine speed governor implemented into the

LabVIEW real-time PXI control system that controlled the engine fuel-path [171] and the engine torque was kept constant at 400Nm by the dynamometer control system (Cadet V12) which was in torque control mode. The injection mode was set to 2 pulse injections, a pilot and a main. Fuel-path control variables other than total injection quantity, such as SOI, RP, DW and fuel ratio were kept constant.

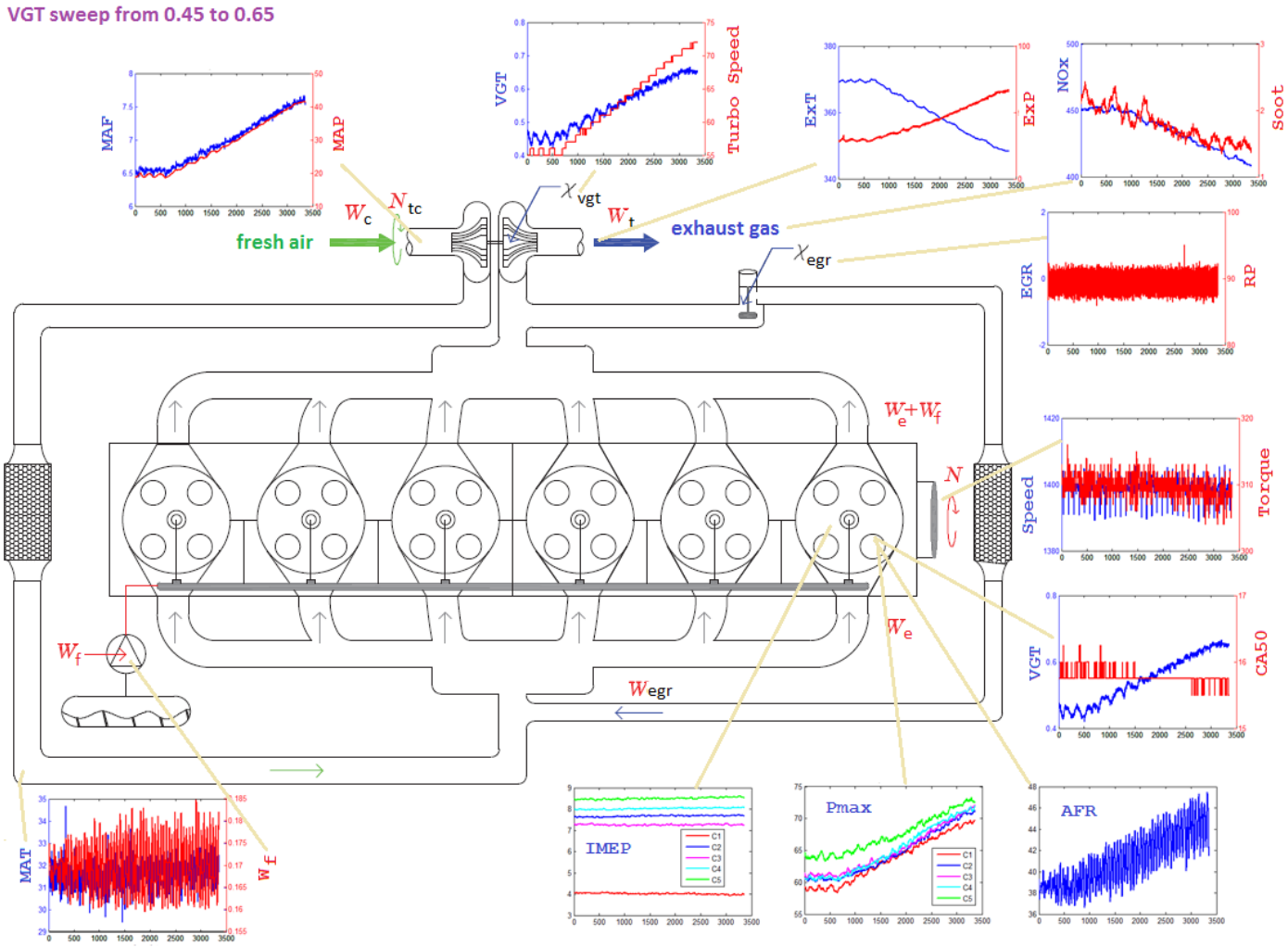

Figure 4.1: Effect of VGT on engine variables (Engine schematic is reproduced from [25])

The variables in Figure 4.1 are: W_c - intake fresh mass flow rate (compressor flow rate); W_t - exhaust gas flow rate (turbine flow rate); W_f - fuel flow rate (consumed fuel); W_{egr} – EGR flow rate, W_e - gas flow rate into engine cylinders (=W_{egr}+W_c), χ_{vgt} - VGT vane position; χ_{egr} - EGR valve position;N_{tc} - turbo speed; N - engine speed, ExT - Exhaust Temperature, ExP - Exhaust Pressure, MAT - Manifold Air Temperature.

It can be seen that when the VGT vane is closed, the turbo speed is increased. The increased turbo speed then results in increased boost pressure

(MAP) and increased MAF due to the increase in exhaust energy captured by the turbine and transferred to the compressor. With the engine torque kept constant, the increased MAF leads to increased AFR; increased AFR means that the proportion of oxygen mass involved in the combustion process is increased. This change of combustion gas condition causes a higher peak combustion pressure P_{max}, hence the higher exhaust pressure but lower exhaust temperature. NO_x and soot emissions are both decreased. There are no obvious changes observed with other engine variables: MAT, fuel rate and CA50.

The reason for the application of a VGT in a diesel engine is to take advantage of its enabling of greater flexibility in AFR and MAP control. For example, a higher MAP and more oxygen for a specific engine speed means a greater fuel quantity can be injected to give a higher output power and minimised soot emissions. When the VGT vanes are closed, this acts to increase the energy transfer from the exhaust gas passing through the turbine to the turbine and then the compressor via the common connecting shaft. Additionally, the closing of the VGT vanes also acts to increase the exhaust back pressure and thus the pumping work of the engine and the fuel consumption. This higher back pressure can however also assist with increasing the delta pressure between the exhaust and intake manifolds which can help to increase the external EGR rate. When the VGT vanes are opened, the opposite is true. Depending on the engine turbocharger configuration; generally at higher load conditions the VGT vane position will be decreased in response to the increased energy in the exhaust system to control boost pressure, P_{max} and turbocharger speeds. Whilst at lower loads, a more closed VGT position is used to generate boost pressure and drive higher rates of EGR. VGT is also used in transients in combination with the EGR valve to improve the engine responsiveness to sudden load changes, particularly for fast load application.

Due to the interplay between the exhaust and intake systems which is mediated by the VGT and the EGR valve and also the effect that both of these then have on the external EGR rate; there exists a strong coupling between the VGT and EGR and significant complexity in the control of both during engine steady-state and transient operation.

4.2.2 EGR Function

A similar picture to Figure 4.1 concerning the effect of EGR on engine variables is shown in Figure 4.2. The engine was running at the same steady-state operating point: 1400rpm and 400Nm. The VGT vane position was kept constant at 0.5. The EGR valve position was increased from 0 to 0.2.

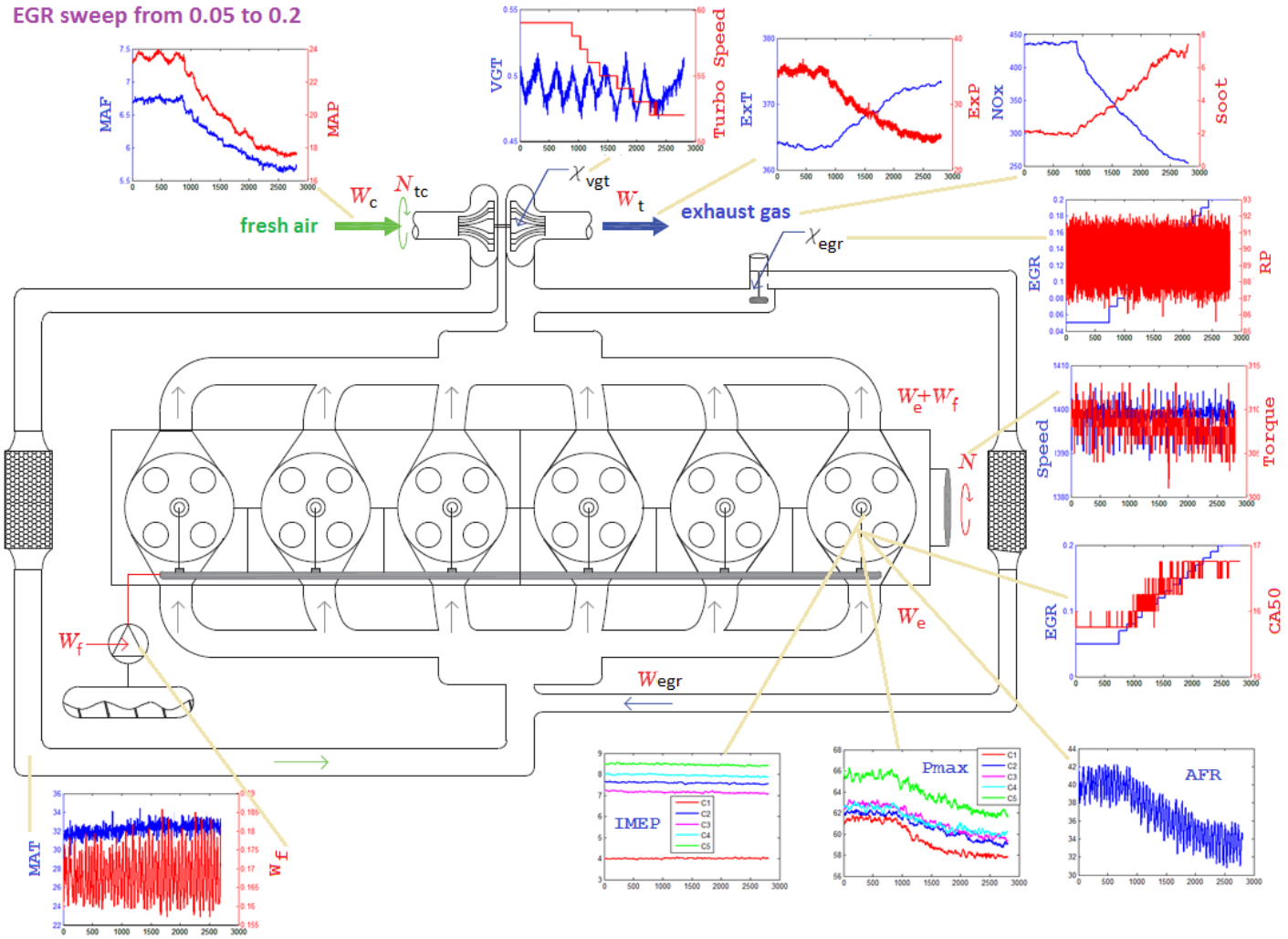

Figure 4.2: Effect of EGR on engine variables (Engine schematic is reproduced from [25])

It can be seen that when the EGR valve is opened, the turbo speed decreases because part of the exhaust gas is diverted before entering the turbine i.e. the turbine mass flow is reduced. Consequently, both the MAP and MAF decrease as turbine and therefore the compressor output power is decreased. This leads to a decrease in AFR and thus less oxygen is available to for combustion. Hence, the value of P_{max} and exhaust pressure both decrease. Since the SOI was fixed, the increase in CA50 denotes a later EOC as a consequence of the high EGR rates which changed the intake air composition. Even though the

combustion is retarded, exhaust temperature still decreases which implies a decrease in combustion temperature. A slightly higher rate of fuel supply was observed with higher EGR with the engine speed and load unchanged from the lower EGR condition. This can be explained by the deterioration in the combustion efficiency associated with a more prolonged ignition delay and incomplete combustion caused by increased CO2 and decreased O2 in the engine intake [173] and also the retarded combustion being less well matched to the piston position.

Importantly, the NO_x emissions are significantly decreased whilst the soot emissions are increased. The only reason for using EGR in diesel engines is to decrease NOx emissions. However, there are two main penalties, one is an increase in soot emissions and the other is fuel economy. Due to the implications for combustion, the design of control of the EGR valve position can be considered as more complicated than that of VGT vane position. The control of the EGR can be described as the search for the optimal conditions that balance NOx and soot emissions and fuel consumption at a given engine operating condition.

4.2.3 VGT and EGR Effects and Engine Operating Point

In order to study experimentally how the influence of VGT and EGR on engine variables varies with engine operating point, a series of EGR value position and VGT vane position step response tests were carried out at 24 different engine operating points. These 24 engine operating conditions are combinations of six engine speeds that are: 800rpm, 900rpm, 1000rpm, 1100rpm, 1200rpm and 1300rpm with four engine loads which are: 100Nm, 200Nm, 300Nm and 400Nm, Table 3.3. At each engine operating point, a step change of 0 to 0.1 in the EGR valve was made and a separate step change in the VGT vane position was made from 0.5 to 0.6. When doing the individual step response tests with the EGR and VGT, the other engine inputs were kept at constant values; these inputs include SOI, DW, RP. Two variables from the intake system, MAF and MAP, are plotted together in Figure 4.3 and Figure 4.4 to show the influence of VGT vane position and EGR valve position respectively on the engine air-path. The step response tests at each engine operating point are denoted by the constant bands of colour in Figure 4.3 and Figure 4.4 so as to highlight both the MAF-MAP relationship at each engine condition and also how these relationships change with engine speed and load.

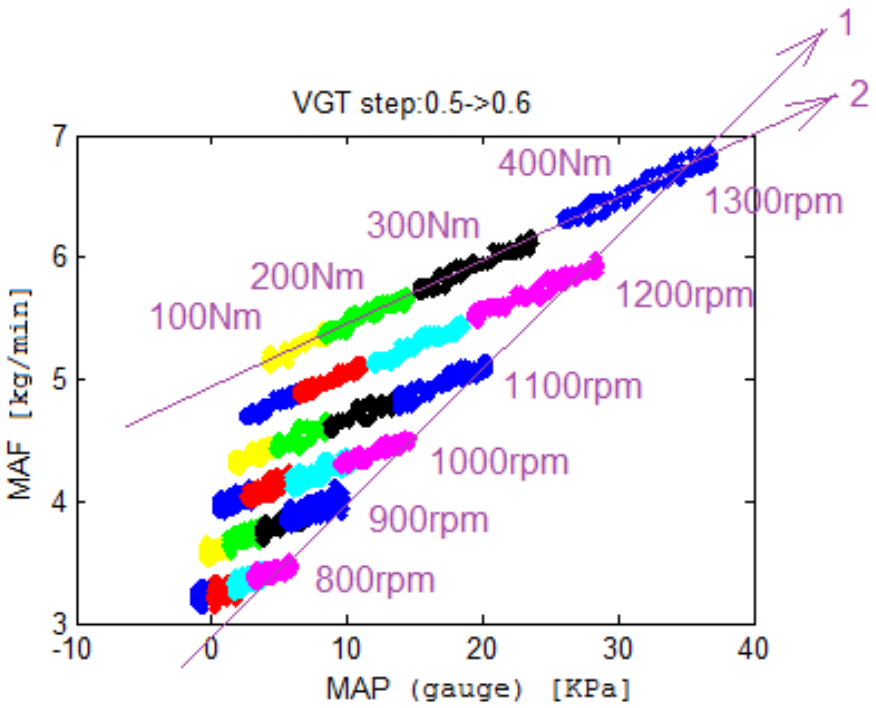

Figure 4.3: MAF against MAP from VGT step change at 24 different engine operating points with EGR closed

Figure 4.3 is a plot of MAF against MAP for the VGT step response tests at 24 different engine operating points. In Figure 4.3, the arrow marked as 1 denotes test points where the engine speed increases (different colours) at the same load with the same single point VGT vane position. The arrow marked 2 denotes test points which are at the same engine speed and different loads (different colours) with a VGT vane position step change.

It can be seen from Figure 4.3 that engine speed has a big impact on MAF and MAP. When engine speed is low, both MAF and MAP are small and the increase of both MAF and MAP caused by the increase of engine load is also small. However as engine speed is increased, both MAF and MAP increase and importantly the influence of engine load on MAF and MAP becomes more significant, with a greater range of both MAF and MAP change in response to VGT position change as both the engine speed and the load increase.

It can also be seen from the steeper slope of arrow 1, that engine speed has the bigger impact on MAF compared to the impact of engine load and conversely that engine load has a bigger impact on MAP than engine speed. Interestingly, the effect of VGT vane position on MAF and MAP follows arrow 2, i.e. the effect of changing VGT position has a similar effect on the MAF-MAP relationship as

the change in engine load at constant engine speed. This is made clear by the number of coloured points which intersect either arrow 1 (different speeds) or arrow 2 (different loads), with the number of points intersecting arrow 2 being much greater. This implies that at the same engine speed, opening the VGT vanes is equivalent to decreasing engine load for MAF and MAP.

Figure 4.4 shows the plot of MAF against MAP for the EGR valve position step response tests at 24 different engine operating points. In Figure 4.4, the arrow marked as 1 denotes test points where the engine speed increases (different colours) at the same load with a step change in EGR. The arrow marked 2 denotes test points which are at 1300rpm and different loads (different colours) with the same EGR valve position. The arrow marked 3 denotes the same as arrow 2 but with the lower engine speed of 800rpm.

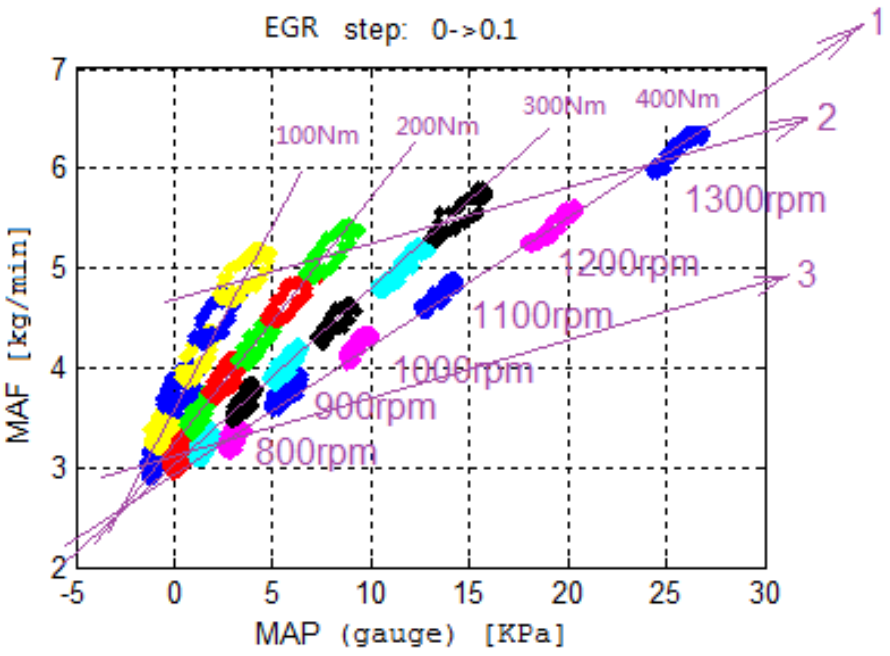

Figure 4.4: MAF against MAP from EGR valve step change at different engine operating points with VGT fixed at 50% open

In Figure 4.4 the engine speed effect and load effect lines are presented in the same way as those in Figure 4.3. However, the effect of EGR valve position on MAF and MAP follows the engine speed effect line not the engine load effect line as is observed for VGT in Figure 4.3. The impact of EGR valve position on MAF and MAP only varies slightly across the range of engine speed and load conditions, contrasting with VGT. The straight line patterns of variation of MAF and MAP with engine speed and torque can be used to develop an MVEM to replace look-up tables for engine operating conditions.

It can also be seen from Figure 4.3 that MAP is more sensitive to VGT vane position than MAF. Therefore, it is better to use MAP rather than MAF as the feedback variable in developing a VGT closed-loop control system. By default, MAF is therefore the only choice for the feedback variable in an EGR closed-loop control system - if the feedback variables are limited to MAF and MAP. This feedback control selection is only necessary in developing decentralized an air-path control system within which the VGT and EGR closed-loop control systems are two single control loops. In a multi-variable control structure, such as MPC demonstrated later in this chapter, no such distinction is needed.

4.2.4 Volumetric Efficiency

The compressor fresh air mass flow rate (MAF) is measured using a MAF sensor. If the EGR valve is closed, the compressor mass flow rate equals to the gas mass flow rate into the engine. However, when the EGR valve is open, the measured MAF is no longer the gas flow rate into the engine. Using an ideal gas assumption, the gas mass flow rate into the engine can be estimated from measured MAP and MAT. Equation (4.1) is the estimation algorithm for gas flow rate into a six cylinder four-stroke engine used in this study:

$$W_e = \frac{3\eta_v \times N \times MAP \times M_{gas}}{R \times MAT} \qquad (\mathbf{4.1})$$

Where W_e is the estimated gas flow rate into the engine in unit [kg/min]; n_v is volumetric efficiency; N is engine speed in unit [rpm] and M_{gas} is molecular weight of the gas mass into the engine. When the EGR valve is closed, all gas into the engine is fresh air which will correspond to the measured MAF. In this case the molecular weight of air with value 28.97 [kg/kmol] is applicable.

Volumetric efficiency measures the pumping performance of the engine intake system. Ideally, if there is no residual gas inside the cylinder, no wall friction in the intake manifold and no intake valve to restrict the air amount into cylinder; the volumetric efficiency should be 1. However, in real world, volumetric efficiency is always less than 1. It varies with engine speed and load and it also varies with EGR rate because EGR rate changes the back pressure which will affect the amount of residual gas. Roughly speaking, at high engine speed, there is more significant friction to air flow, hence smaller volumetric efficiency. At wider EGR valve open position, there is smaller back pressure, so that there is less residual gas which results in higher volumetric efficiency. The computation of volumetric efficiency is shown in Equation (4.2):

$$\eta_v = 100 \times \frac{\frac{W_c + W_{egr}}{\rho}}{N \times 60 \times V_{swept} \times \frac{2}{n}} \qquad (\mathbf{4.2})$$

Where: η_v is the volumetric efficiency; $W_c + W_{egr}$ is the total manifold mass flow (air mass flow plus EGR mass flow) [kg/h]; ρ is the inlet manifold density [kg/m^3]; N is the engine speed [rpm]; V_{swept} is the engine swept volume [m^3] and n is the number of revolutions per power stroke (1 or 2). Clearly, for precise volumetric efficiency estimation, it is very important that the EGR mass flow is accurately known in addition to MAF.

For the C6.6 engine speed sweep test data with no EGR applied, the volumetric efficiency was calculated according to Equation (4.2). Figure 4.5 (a) shows that the volumetric efficiency decreases as the engine speed increases. At higher engine load, volumetric efficiency is higher. Volumetric efficiency is also slightly higher during an engine speed decrease transient than during an engine speed increase transient. Figure 4.5 (b) shows that volumetric efficiency only slightly changes with the two VGT positions investigated and also the Coolant Temperature (CT) which varied between 80°C and 90°C.

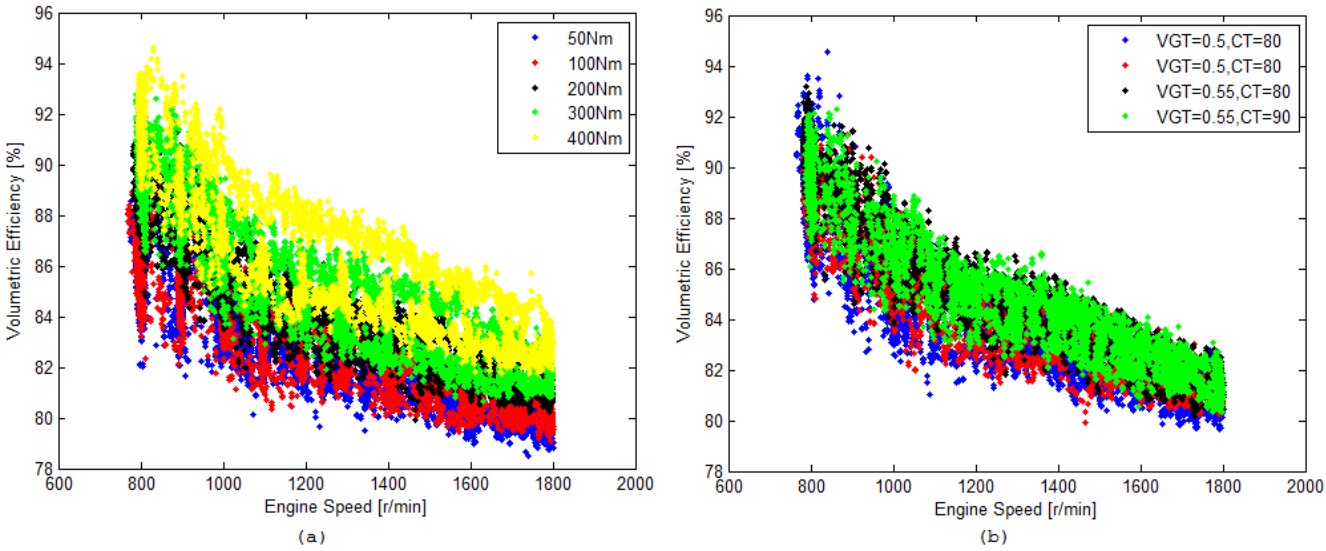

Figure 4.5: Volumetric efficiency of C6.6 engine; (a) at different engine load; (b) at different VGT vane open position and engine coolant temperature. (CT refers to coolant temperature)

Ignoring the effect of other engine control variables, a linear regression model for volumetric efficiency was developed by least square method using the engine speed sweep test data of Figure 4.5, this model is shown in Equation (4.3).

$$\eta_v = 93.2 + 0.0016 \times T_{load} - 0.0084 \times N \qquad (\mathbf{4.3})$$

Where, T_{load} is engine load in unit [Nm], N is engine speed in unit [rpm]. The validation result for this regression model is shown in Figure 4.6. The R square value for this model is 0.8667.

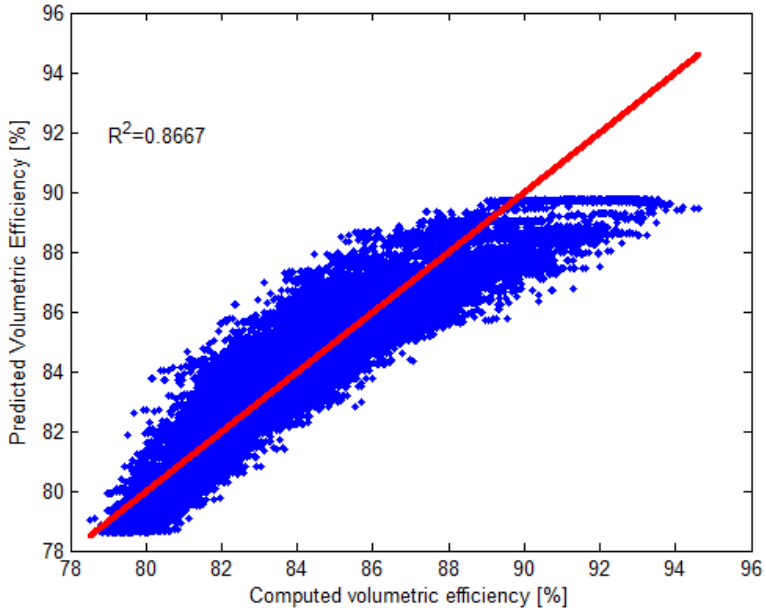

Figure 4.6: Validation result of volumetric efficiency regression model

Horizontal lines of computed η_v against the stable value predicted by the model are clear in Figure 4.6. Investigations indicate that these horizontal lines were caused by the variations in computed η_v caused by signal noise on the measured MAF, MAP and MAT at engine steady-state conditions (these parameters are not part of the model, Equation 4.3).

Additionally, the red line in Figure 4.6 denotes a 1:1 measured and predicted η_v agreement and when the actual prediction results are compared to this line it can be seen that there is a slight overall residual curvature amongst the computed volumetric efficiency 'noise'. It is believed that this is partially explained by the model not accounting for VGT position. Therefore, a more accurate volumetric efficiency model could be obtained by using a higher order model and adding extra inputs to also account for the effect of VGT. However, such changes will increase the model complexity and to implement would require considerable improvement in the measurement of MAF, MAP and MAT on the C6.6 test bed to remove the inherent signal noise.

Figure 4.7 shows the mean value of the measured η_v at engine steady-state conditions (1400rpm 400Nm) for each EGR valve opening position and was computed using Equation 4.2; the blue line in Figure 4.7.

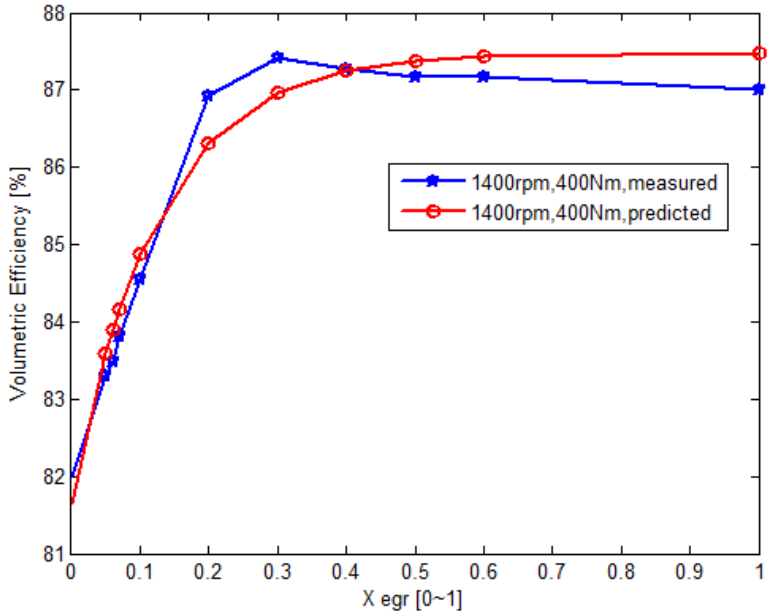

Figure 4.7: Volumetric efficiency varies with EGR valve position. Engine operating condition is 1400rpm, 400Nm

The mean value of η_v was observed to increase with EGR valve position up to an EGR valve position of 0.3. When the EGR valve position was set above 0.3, the η_v stopped increasing and instead η_v slightly reduced. The EGR flow rate W_{egr} in Equation (4.2) was estimated by synchronising the EGR ratio which was measured by an Horiba 9100 Emissions Analyser (time delayed due to sample line lengths) with measured intake air flow rate W_c. An exponential function was then developed to model this measured η_v variation with EGR valve position and this is shown in Equation (4.4). The output of this model is shown as the red line in Figure 4.7 and can be observed to achieve a reasonable approximation to measured η_v. A nonlinear regression model was used in this case as a physical model would require significant information regarding the parameters of the full engine air system including but not limited to: pipe diameters, surface roughness, EGR valve area, residual gas estimation etc.

$$\eta_v = 93.2 + 0.0016 \times T_{load} - 0.0084 \times N + 5.4 \times (1 - e^{-8.1\chi_{egr}+0.076}) \quad (\mathbf{4.4})$$

Where, χ_{egr} is the EGR valve position from 0 (closed) to 1 (wide open). The validation of this mode is shown in next section.

4.2.5 Model for EGR Flow Rate

4.2.5.1 Orifice Flow Model

The estimation of EGR flow rate (W_{egr}) is very important in model based air-path control. The majority of air-path control research uses the orifice valve flow rate model similar to that in reference [5]. The simplest version is shown in Equation (4.5) [33]. There is no significant difference between this equation and an alternative form which also includes the specific heat ratio in the index of term $\frac{p_i}{p_x}$.

$$W_{egr} = A_r \frac{p_x}{\sqrt{RT_{egr}}} \sqrt{2\frac{p_i}{p_x}(1-\frac{p_i}{p_x})} \qquad (\mathbf{4.5})$$

Where, A_r is the effective EGR valve open area, p_x is the exhaust manifold pressure [KPa], p_x is the exhaust manifold pressure [KPa] (assuming no pressure drop in the EGR cooler); T_{egr} is the temperature before the EGR valve [K], p_i is the intake manifold pressure [KPa], R is the universal gas constant with value 8.314462 [J/mol.K]. Equation (4.5) is only applicable when $0.5 \leq \frac{p_i}{p_x} < 1$ is met; for an engine equipped with a turbocharger this condition is always true. This pressure ratio has been checked for all sensible operating points of the C6.6 engine used in this study and has been found to be within these limits at all conditions. A_r is the effective area of the EGR valve opening and is defined by Equation (4.6).

$$A_r = A_{r\_max} \times \left(1 - \cos^2(\chi_{egr} \times \frac{\pi}{2})\right) \qquad (\mathbf{4.6})$$

Where, A_{r_max} is a model constant with a tuned value of 5.3 for the EGR valve in the C6.6 engine used in this study. The validation results of this model using the C6.6 engine EGR valve sweep test data are shown in Figure 4.8. The measured EGR flow rate was computed from EGR ratio using Equation (4.7).

$$W_{egr}^{meas} = \frac{MAF \times EGR_{ratio}}{100 - EGR_{ratio}} \qquad (\mathbf{4.7})$$

Where, MAF is the measured air flow rate [kg/min], EGR_{ratio} is the EGR ratio [%] computed using Equation (4.8), W_{egr}^{meas} is the EGR flow rate [kg/min].

$$EGR_{ratio} = \frac{[CO_2]_{intake} - [CO_2]_{ambient}}{[CO_2]_{exhaust} - [CO_2]_{ambient}} \times 100 \qquad (\mathbf{4.8})$$

$[CO_2]_{intake}$ and $[CO_2]_{exhaust}$ are the [%] concentrations of CO_2 in the intake and exhaust manifoldrespectively. The intake and exhaust CO2 concentrations were measured by a Horiba 9100 exhaust gas analyser. The $[CO_2]_{ambient}$ is the concentration of CO_2 in ambient environment.

Figure 4.8 shows the validation results of the EGR flow rate model in Equation (4.5) for three engine operating points which are (1400rpm, 45Nm), (1400rpm, 400Nm) and (2000rpm, 400Nm). The EGR valve position range is 0 to 0.6 (effectively fully open) for these three engine operating points. It can be seen from Figure 4.8 (a) and (c) that the estimation of EGR flow rate is too conservative when the EGR valve opening position is small. This may be compensated by adding a nonlinear compensation factor in Equation (4.5).

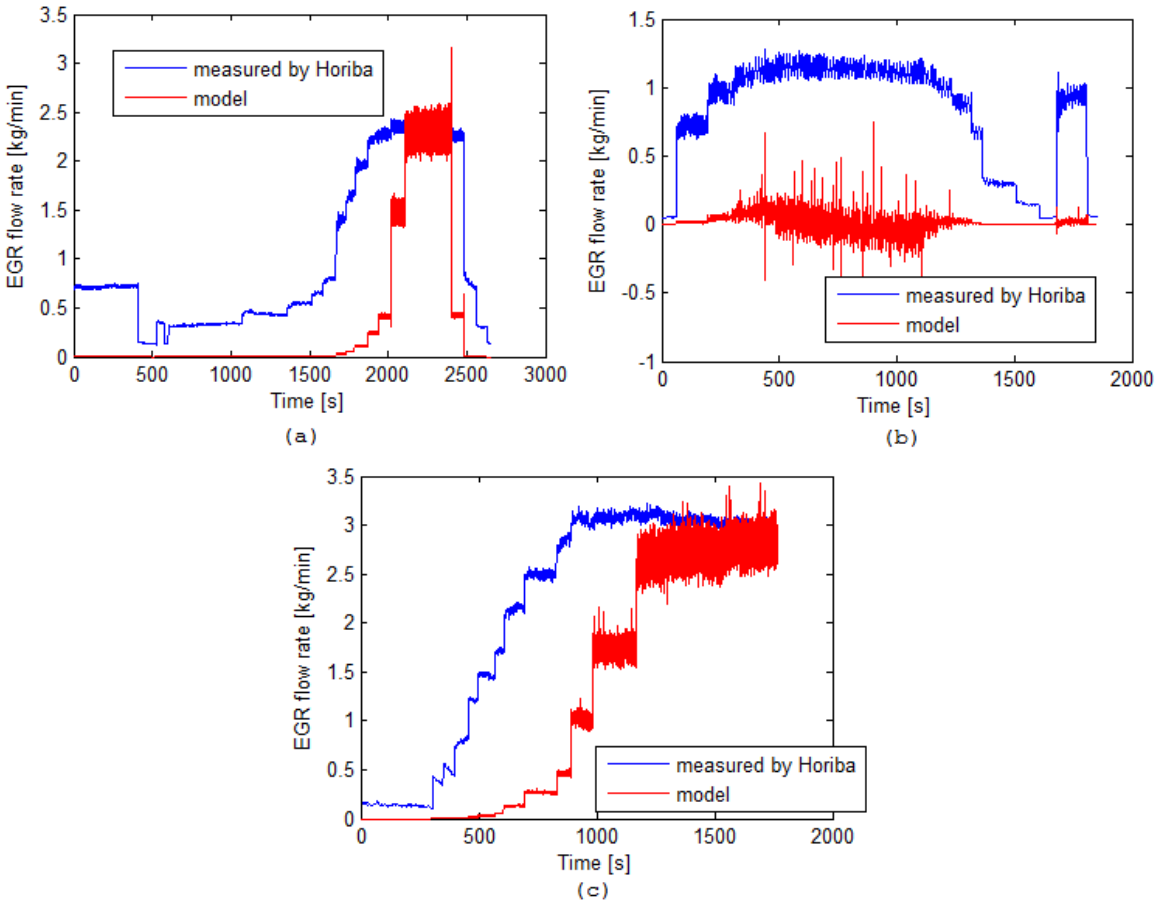

Figure 4.8: Validation of EGR flow rate model for different engine operating points: (a) 1400rpm, 45Nm; (b) 1400rpm, 400Nm; (c) 2000rpm, 400Nm

There is a big disadvantage of using an orifice flow model to predict EGR flow rate. Figure 4.8 (b) shows that at engine operating point (1400rpm, 400Nm) the EGR flow rate model fails to predict the small EGR flow rate. The reason is that with this case, the boost pressure is very close to exhaust pressure so that item

$\frac{p_i}{p_x}$ is close to 1. Hence the estimated EGR flow rate using Equation (4.5) is close to zero. The values of the ratio $\frac{p_i}{p_x}$ for these three engine operating points are shown in Figure 4.9. Figure 4.9 (b) shows that the pressure ratio $\frac{p_i}{p_x}$ is between 0.96 to 1 when the engine is running at 1400rpm, 400Nm. However, the measured EGR flow rate is not zero at this case as illustrated in Figure 4.8 (b). This can be explained by the engine pumping work which acts to create the EGR gas flow with negligible exhaust to intake manifold pressure difference.

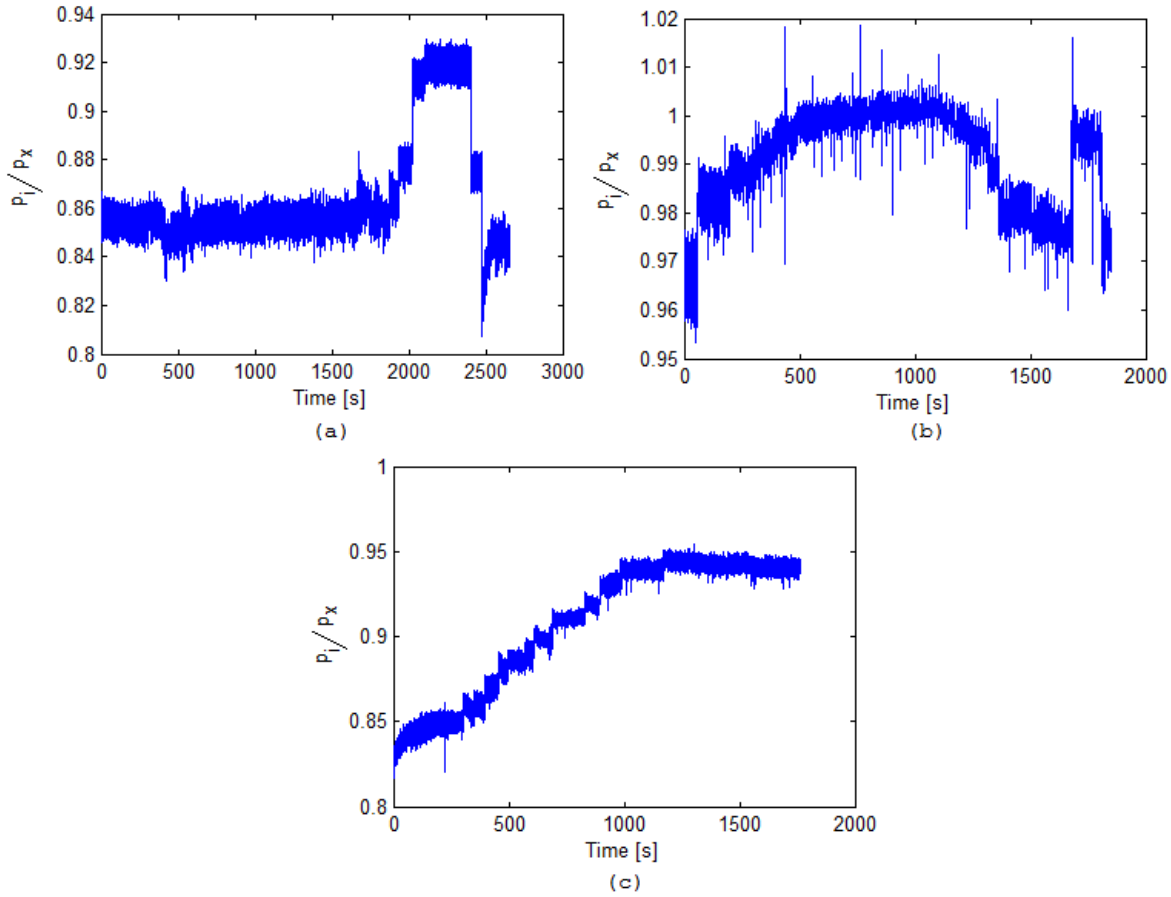

Figure 4.9: Values of $\frac{p_i}{p_x}$ for different engine operating points; (a) 1400rpm, 45Nm; (b) 1400rpm, 400Nm; (c) 2000rpm, 400Nm

The two pressure values p_i and p_x used in Equation (4.5) were sampled from two absolute pressure sensors with a range of 0-500kPa. If a differential pressure sensor with a smaller range was used, then an improved ratio of p_i to p_x would have been possible. As a result of these constraints, an alternative approach has been utilised in this study to estimate the EGR flow rate. This uses the total flow rate minus the measured air flow rate when EGR valve is opened and this is discussed in the following section.

4.2.5.2 Total Flow Rate Method

The total flow rate method for the estimation of EGR flow rate is based on the EGR flow rate being the difference between the gas flow rate into engine cylinders and the measured fresh air flow rate as shown in Equation (4.9).

$$W_{egr} = W_e - MAF \qquad (\mathbf{4.9})$$

The gas flow rate into engine W_e cannot be measured directly but can be estimated using Equation (4.1). The key for achieving high estimation accuracy of EGR flow rate is the accuracy of volumetric efficiency η_v. Using the linear regression model for volumetric efficiency in Equation (4.4), together with the estimation model for total gas flow rate into engine in Equation (4.1) and model for EGR flow rate in Equation (4.9), the predicted EGR flow rate for three engine operating points: (1400rpm, 45Nm), (1400rpm, 400Nm) and (2000rpm, 400Nm) are plotted together with the measured EGR flow rate in Figure 4.10.

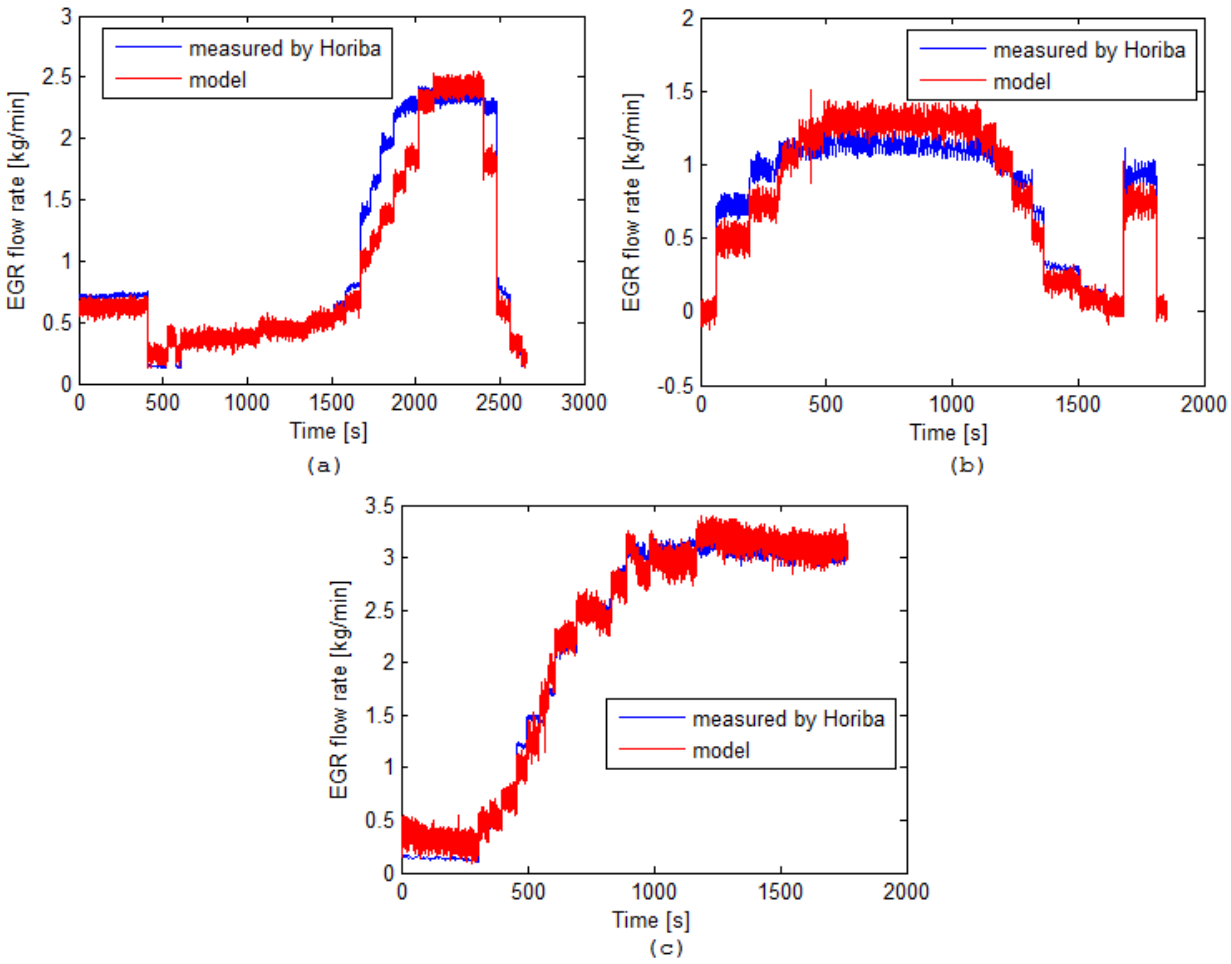

Figure 4.10: Validation of EGR flow rate model for different engine operating points; (a) 1400rpm, 45Nm; (b) 1400rpm, 400Nm; (c) 2000rpm, 400Nm

This model performance can also be seen in Figure 4.11 which is a plot of the predicted EGR flow rate against computed EGR flow rate from the measured EGR ratio - i.e. the exhaust and intake CO2 concentrations measured by a Horiba 9100 exhaust gas analyser and Equation (4.8).

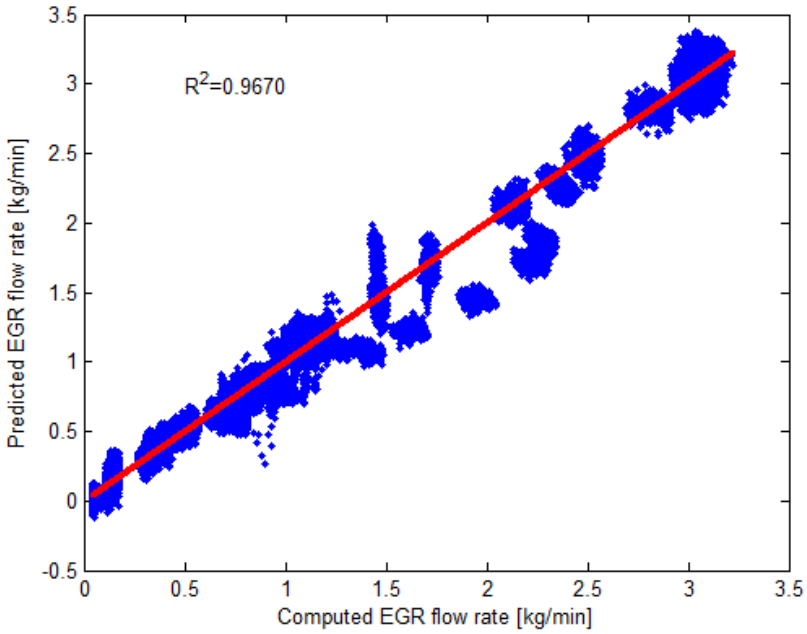

Figure 4.11: Predicted EGR flow rate against measured EGR flow rate for three engine operating points: (1400rpm, 45Nm); (1400rpm, 400Nm) and (2000rpm, 400Nm)

In Figure 4.11 there are two vertical lines in the data points which were caused by variations in measured intake manifold temperature during the engine steady-state tests. There are also some points which deviate from red line (1:1 match of predicted and computed EGR flow rate) which indicate the accuracy of this EGR flow rate model is lower at some conditions due to the lower accuracy of volumetric efficiency model at these conditions. The R square value of this model for total validation data set is 0.9670. If the volumetric efficiency can be predicted more precisely as was discussed previously in Section 4.2.4, then this EGR flow rate model could be further improved.

4.2.5.3 EGR Ratio and Engine Emissions

For the C6.6 engine used in this study, there was found to be nonlinearity between the EGR valve position and EGR ratio, see Figure 4.12.

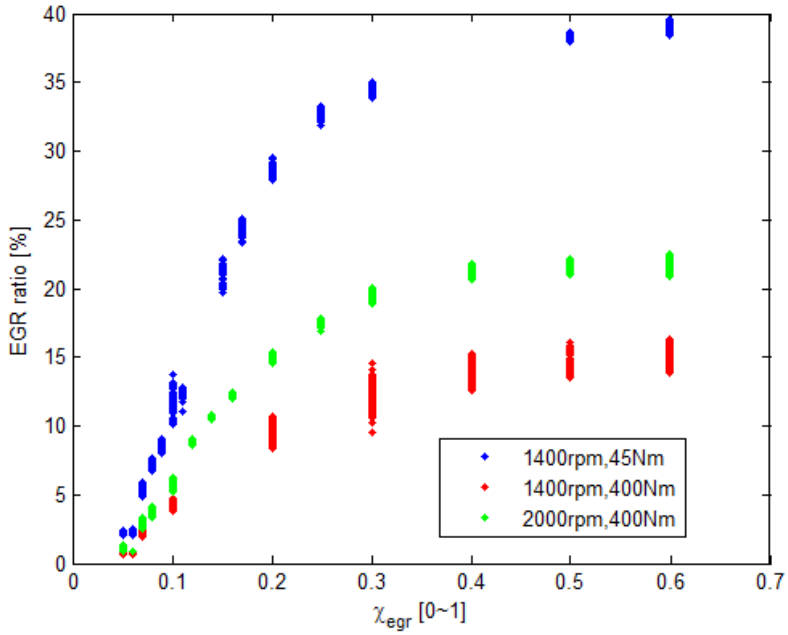

Figure 4.12: EGR flow rate against EGR valve position

When the EGR valve position was over 0.3, the EGR ratio had a saturation phenomenon. Even so, linear relationships between the EGR ratio and engine emissions, especially NO_x emission, existed and these are illustrated in Figure 4.13. Such linearity therefore makes EGR ratio a good candidate as a controlled variable in a closed-loop air-path control system that is focused on NOx emissions control.

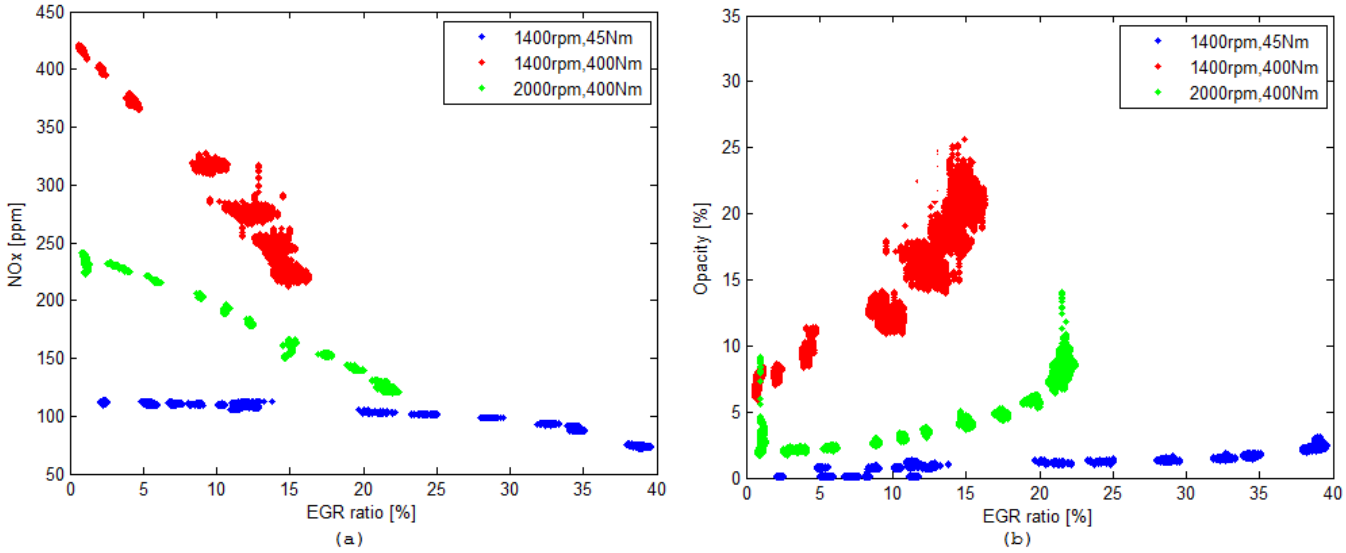

Figure 4.13: Variation of engine emissions with EGR ratio: (a) NOx emission; (b) opacity

Figure 4.13 (b) shows a rapid increase in opacity can be seen when the EGR ratio saturates. Therefore, EGR ratio should be controlled to be below its saturation value at a given operating condition. Figure 4.13 (a) shows that the

controllable EGR ratio range is different for different engine operating points. The maximum EGR ratio is 40%, 22% and 15% for the three engine operating points (1400rpm, 45Nm), (2000rpm, 400Nm) and (1400rpm, 400Nm). Consequently, the setpoint for EGR rate will change depending upon the engine operating conditions and must be determined based on the trade-off between NOx and smoke emissions.

The trade-off phenomenon between opacity and NO_x emissions for three engine operating points is shown in Figure 4.14. Figure 4.14 (a) is the absolute value of NO_x emissions and opacity for EGR variation. Figure 4.14 (b) is the relative change in NO_x emissions and opacity to condition of no EGR. It can be seen from Figure 4.14 (a) that high NO_x and soot emissions appear at high engine load and low engine speed. Figure 4.14 (b) shows that the reduced NOx emission and increased soot emission relative to their values when there is no EGR for three engine operating points locate on the same trade-off curve. This phenomen could be very helpful in the design of EGR ratio setpoint according to engine emissions requriements.

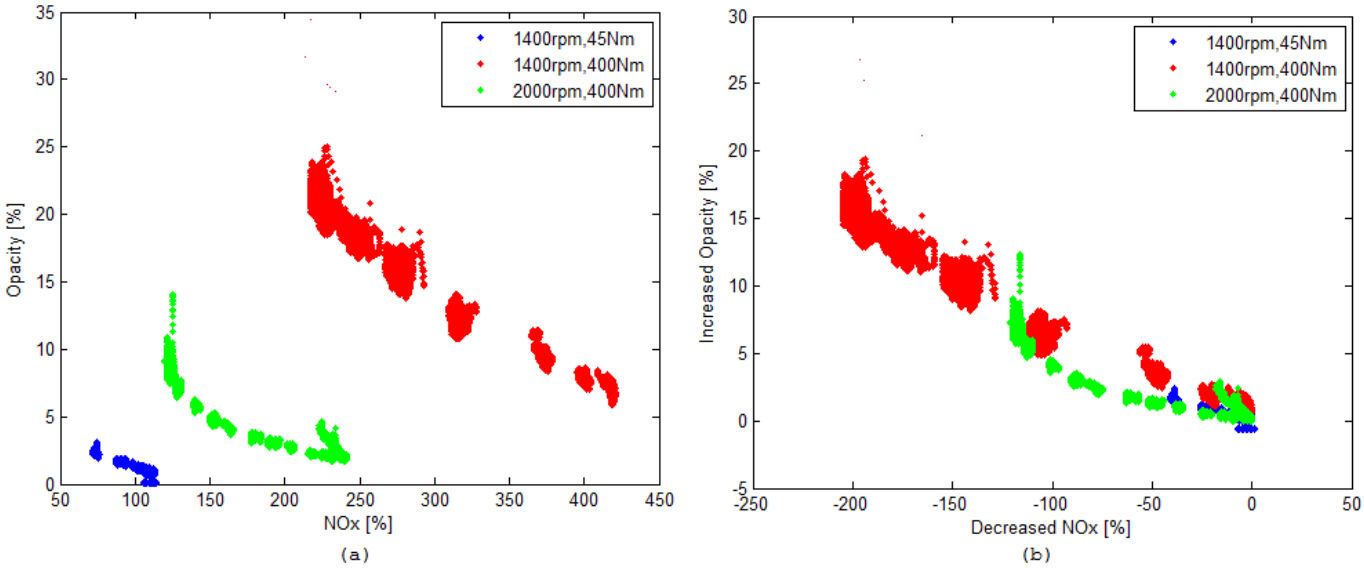

Figure 4.14: Measured opacity against NO_x for EGR variation: (a) absolute value; (b) relative value compared to no EGR

4.2.6 Relationship Between Intake and Exhaust System

If there is neither a turbocharger nor EGR, the intake air flow rate only varies with engine speed. When there is turbocharger but no EGR, both the exhaust gas properties of pressure and temperature and engine speed affect the intake air flow rate. Such relationship can be described mathematically by Equations (4.9), (4.10) and (4.11):

$$C_{p,air} \times \frac{W_C}{\eta_c} \times T_{amb} \times \left(\left(\frac{p_1}{p_{amb}} \right)^{\frac{\gamma_{air}-1}{\gamma_{air}}} - 1 \right) = C_{p,exh} \times \eta_t \times W_t \times T_2 \times \left(1 - \left(\frac{p_2}{p_3} \right)^{\frac{1-\gamma_{exh}}{\gamma_{exh}}} \right) \quad (\mathbf{4.9})$$

$$W_c = \frac{3 \times \eta_v \times N \times p_1 \times M_{air}}{R \times T_1} \quad (\mathbf{4.10})$$

$$W_t = W_c + W_f \quad (\mathbf{4.11})$$

The constants and variables in Equation (4.9) are defined in Table 4.1.

Table 4.1: Constants and variables for air-path model

Constants and Variables	Description
$C_{p,air}$	Specific heat value of air, 1.007 [J/kg.K]
$C_{p,exh}$	Specific heat value of exhaust gas, 1.09 [J/kg.K]
γ_{air}	Specific heat value ratio of air, 1.4
γ_{exh}	Specific heat value ratio of exhaust gas, 1.34
W_C	Compressor air flow rate, [kg/s]
W_t	Turbine exhaust gas flow rate, [kg/s]
W_e	Gas flow rate into engine, [kg/s]
W_f	Fuel flow rate, [kg/s]
T_{amb}	Ambient temperature, [K]
p_{amb}	Ambient pressure, [kPa]
p_1	Intake manifold pressure, [kPa]
p_2	Exhaust manifold pressure, [kPa]
p_3	Exhaust pressure after turbine, [kPa]
T_1	Intake manifold temperature, [K]
T_2	Exhaust manifold temperature, [K]
M_{air}	Molecular weight of fresh air, 28.97 [g/mol]
M_{exh}	Molecular weight of exhaust gas, 29 [g/mol]
η_c	Compressor efficiency, [%]
η_t	Turbine efficiency, [%]
η_v	Volumetric efficiency, [%]
R	Ideal gas constant, 8.134 [J/mol.K]
N	Engine speed, [rpm]
K_{exh}	Model Coefficient, [m^{-2}]
ρ_{exh}	Exhaust gas density, [g/m^3]
l	Length of pipe, [m]
d	Pipe inside diameter, [mm]
dp	Pressure drop along the exhaust pipe, [kPa]

Assuming the intake temperature T_1 is known, the intake air flow rate W_c and pressure p_1 are uniquely determined by the exhaust gas flow rate states in temperature T_2 and pressure p_2 . The reference pressure p_3 in Equation (4.9) is computed using Equation (4.12) considering the pressure drop in the exhaust pipe.

$$p_3 = p_{amb} + dp \tag{4.12}$$

The pressure drop in the exhaust pipe can be estimated using the ideal steam pipe pressure drop model shown in Equation (4.13) and (4.15) [174].

$$dp = K_{exh}\frac{W_t^2}{\rho_{exh}} \tag{4.13}$$

$$K_{exh} = \frac{0.6753 \times 10^6 \times l \times (1 + \frac{91.4}{d})}{d^5} \tag{4.14}$$

$$\rho_{exh} = \frac{p_2 \times M_{exh}}{R \times T_2} \tag{4.15}$$

Even though the model constant K_{exh} in Equation (4.13) is determined by the exhaust pipe physical parameters in length and diameter, it can be identified using engine test data. The estimated K_{exh} for the test engine is 0.088 [m^{-2}].

Using engine steady-state test data at 400Nm with five different speeds, the measured MAF and MAP and their estimated values W_c and p_1 using the above model were plotted together in Figure 4.15.

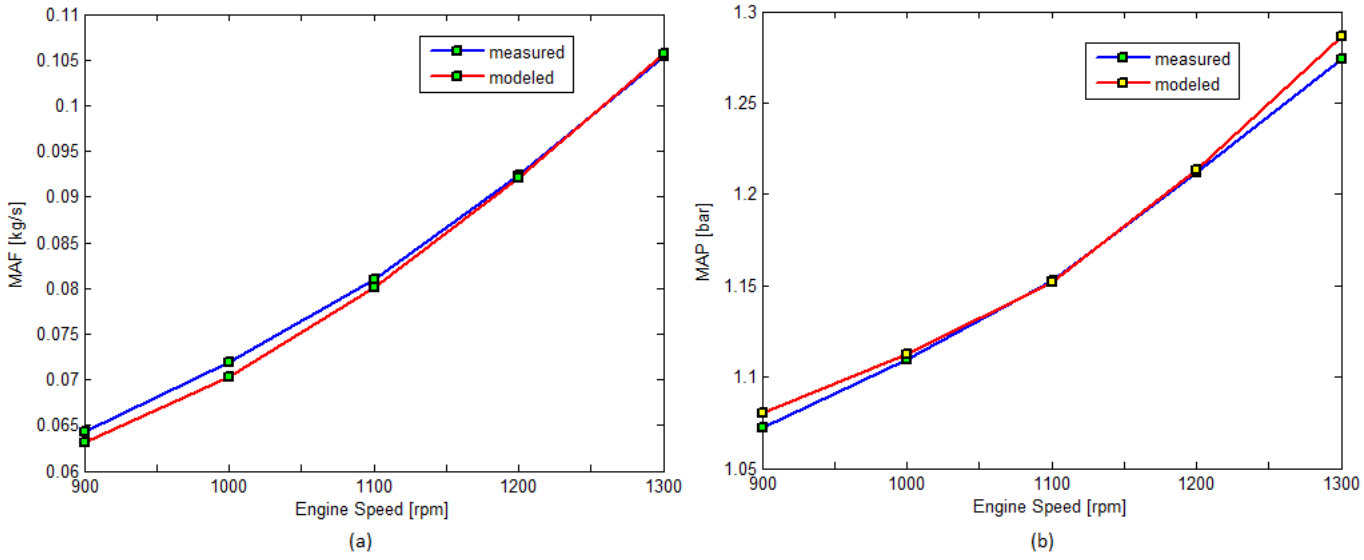

Figure 4.15: (a) Measured and estimated MAF; (b) Measured and estimated MAP. Engine load is 400Nm. No EGR, VGT = 0.5

For the data presented in Figure 4.15, the VGT vane position was kept at 0.5 for all speed conditions. Both estimated W_c and p_1 matches the measured MAF and MAP well. This indicates that exhaust gas pressure and temperature are the principal variables that determine compressor flow rate and temperature. So that any change of combustion process that results in variation of exhaust pressure or exhaust temperature will affect the intake flow rate and temperature which in turn will influence the combustion process. The model discussed meets the requirements in regard to accuracy and algorithmic processing demand for model based engine steady-state control.

4.3 Air-Path Control

Normally, in a production diesel engine, the air-path is controlled using open-loop control that relies on look-up tables to control VGT vane and EGR valve positions. The look-up tables can be a set of setpoints for VGT vane and EGR valve position with reference to different engine speed and injected fuel quantity or alternatively boost pressure demand and EGR mass flow rate. However, the closed-loop air-path control system with combustion processes included in the loop would not only increase the system disturbance rejection capability but also would more precisely control the desired engine variables. The question is which kind of control structure is better and how to design the setpoint for the controlled engine variables. A well designed controller could improve the control system's transient performance which in turn will improve the engine performance during transient operation. A relatively accurate air-path dynamic model is crucial in the effective design of an air-path controller.

4.3.1 Open-loop Control Setpoint for VGT and EGR

The open-loop look-up tables for VGT vane and EGR valve position used by the LabVIEW real time PCI control system [171] are shown in Figure 4.16. The VGT vane position is fully closed at low engine speed and high-load, but almost fully open at high speed and high-load. As the EGR system was added later as a later update to the engine, the EGR valve look-up table was developed by a member of the Loughborough research team. The EGR valve is only fully open in a very small range around low speed low-load. When a closed-loop control strategy is applied, no matter what kind of control structure is used, the steady-state control solution of VGT vane and EGR valve position should approximate the solutions shown in Figure 4.16.

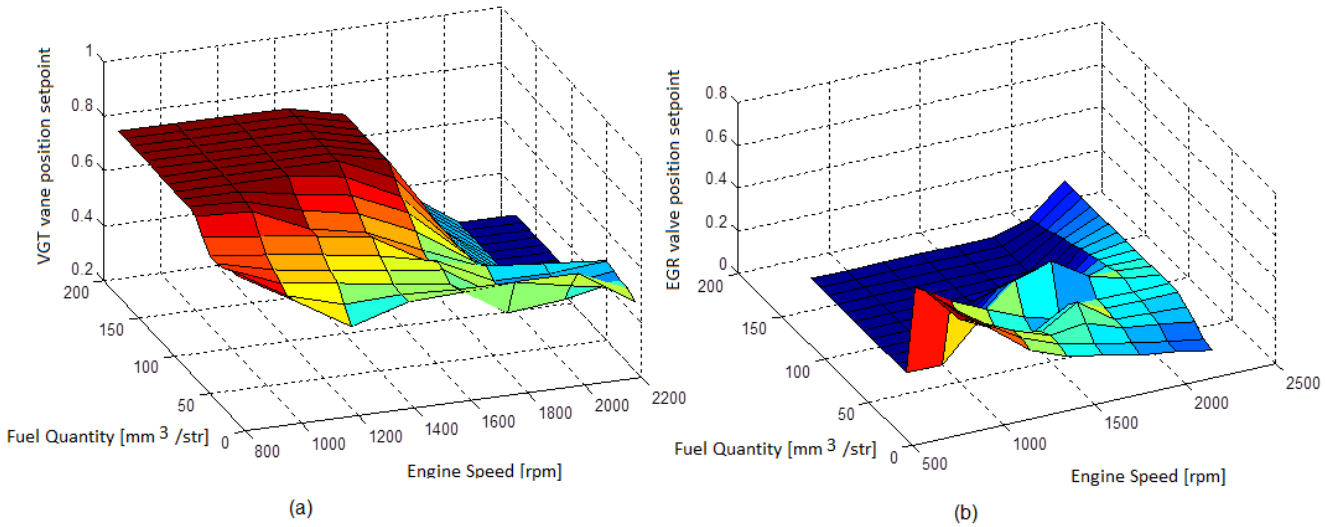

Figure 4.16: Look-up table for (a) VGT vane position setpoint; (b) EGR valve position setpoint LabVIEW real time PCI control system [171]

4.3.2 Air-path Dynamic Model

The dynamic model is very important in controller design. Rather than develop a complex full nonlinear physical air-path dynamic model, an alternative modelling method based upon system identification was proposed and used in this study. This study therefore focusses on the system identification methodology for creating models for air-path model based control.

4.3.2.1 State-Space Model for Air-path MPC Control

The application of a MPC approach to the air-path needs a dynamic model in the implementation of the controller. The control structure is 2I2O using VGT vane position χ_{vgt} and EGR valve position χ_{egr} to control the intake manifold pressure p_1 and compressor flow rate $\mathrm{W_c}$. Using a system identification methodology, the first step is to collect a perturbation test data set. The perturbation test method developed in this study is illustrated in Figure 4.17.

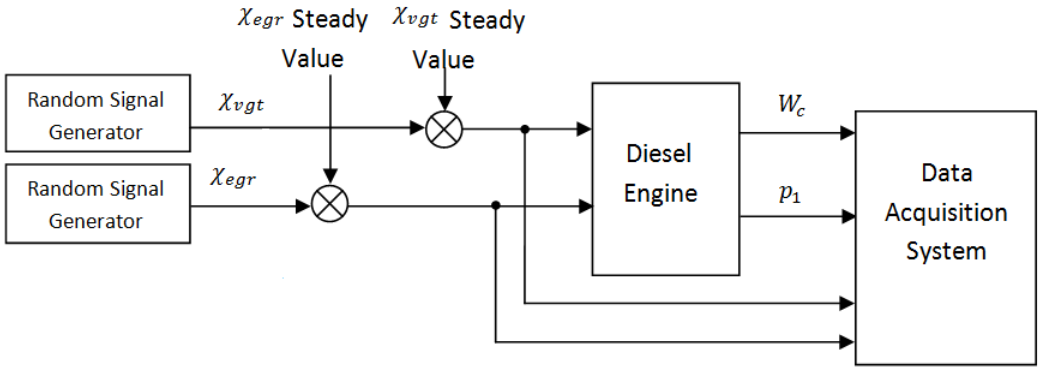

Figure 4.17: Perturbation test for obtaining data for system identification

The random signal generator is a random signal block in MATLAB® Simulink® for identification purpose. This block implements a random walk in discrete time with random switching probability. It was reported in [175] that random Gaussian signal perturbation is more capable and informative to exhibit the nonlinearity behaviour of system dynamic than PRBS. Even though linear models were identified here, it still can be expected that random excitation signals will help achieve better models than using pseudorandom inputs. When doing the perturbation test, the engine is run at steady-state conditions.

The function *pem* in the MATLAB® system identification toolbox was used to obtain the dynamic model. A fifth order state-space model was found to have sufficient model accuracy for MPC control. This discrete state-space model has the form shown in Equation (4.16) and (4.17).

$$\boldsymbol{x}(k+1) = A\boldsymbol{x}(k) + B\boldsymbol{u}(k) \tag{4.16}$$

$$\boldsymbol{y}(k) = C\boldsymbol{x}(k) \tag{4.17}$$

Where, $(k) = \begin{pmatrix} \chi_{vgt}(k) \\ \chi_{egr}(k) \end{pmatrix}$, $\boldsymbol{y}(k) = \begin{pmatrix} p_1(k) \\ W_c(k) \end{pmatrix}$, $\boldsymbol{x}(k) = \begin{pmatrix} x_1(k) \\ \vdots \\ x_5(k) \end{pmatrix}$

The measured and predicted value from the state-space model of ΔW_c and Δp_1 for engine operating point 1400rpm 400Nm are shown in Figure 4.18.

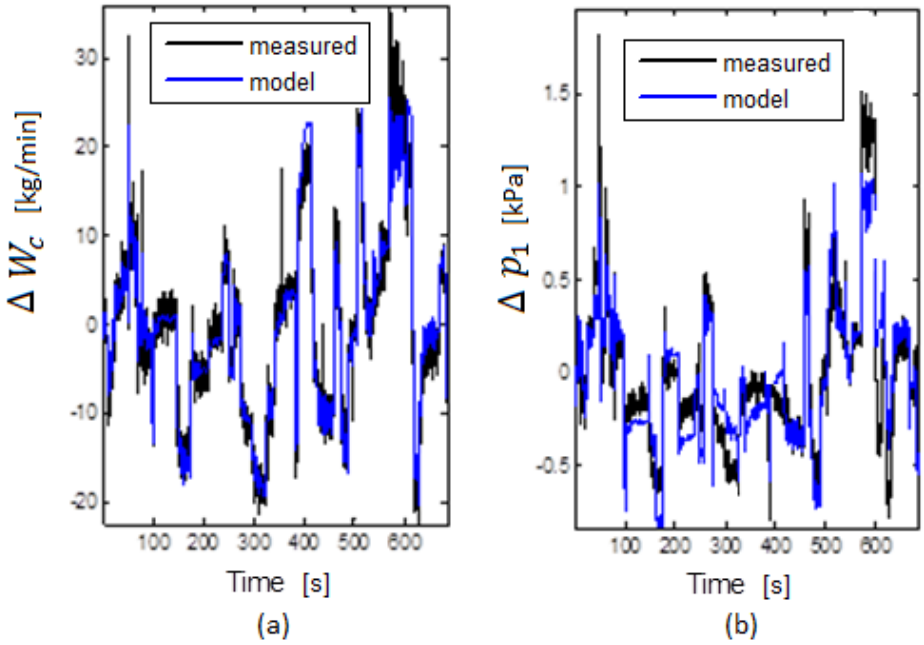

Figure 4.18: Measured and predicted (a) ΔW_c and (b) Δp_1; Engine operating point is 1400rpm 400Nm

ΔW_c and Δp_1 values were compared instead of absolute W_c and p_1 because the identified model is a dynamic model with the steady value removed. The fit numbers (See Section 3.4.3.1, Equation (3.7)) for ΔW_c and Δp_1 in Figure 4.18 were 80% and 60% respectively. The higher the fit number, the more accurate is the predictive model and will therefore result in better control performance in response time and tracking error.

The step response from inputs to outputs of the identified state-space model for the engine operating point 1400rpm and 400Nm is shown in Figure 4.19.

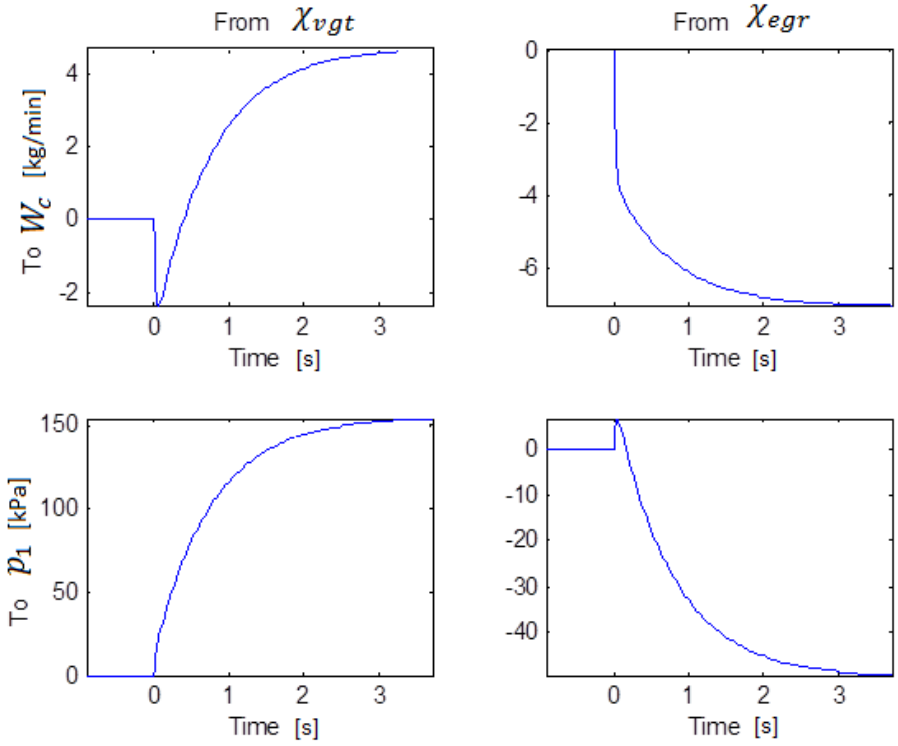

Figure 4.19: Step response of 2I2O dynamic model from [χ_{vgt}, χ_{egr}] to [p_1, W_c] obtained by system identification for the engine operating point 1400rpm 400Nm

The initial reduction of W_c to the VGT vane position step change before the subsequent positive W_c response was caused by the initial increase in back pressure as the VGT vanes closed and then the slower mechanical dynamics of the turbocharger became prominent as the turbocharger accelerated due to the increased energy absorbed by the turbine at the more closed vane position thereby increasing the compressor power and the compressor mass flow W_c. Similarly, the initial positive increase of p_1 in response to the EGR valve step change prior to the more dominant reduction in p_1, was caused by the initial opening of the EGR valve which enabled the high initial exhaust pressure to increase p_1 due to the pipe connections. p_1 then reduced due to the effects of the

slower dynamics of the turbocharger with the EGR valve opening causing an exhaust manifold pressure drop and thus reduced pressure ratio across the turbine and therefore less compressor power and reduced boost pressure. If these two short duration events are ignored then each individual channel in this 2I2O control structure could be roughly modelled as a first order transfer function.

4.3.2.2 Transfer Function Model

If the identified dynamic model form is chosen as the first order transfer function shown in Equation (4.18), then two parameters K and T_s would give straightforward information about the physical dynamics of the channel:

$$G(s) = \frac{K}{T_s s + 1} \qquad (\mathbf{4.18})$$

For example, when the channel is from VGT vane position χ_{vgt} to boost pressure p_1, K represents the influence of the turbine geometry (expressed as χ_{vgt}) on p_1. The time constant, T_s represents the system response speed to the change of VGT vane position. Using the system identification method, the picture of the relationship between K and T_s and the engine operating point can be determined and the findings are presented in Figure 4.20.

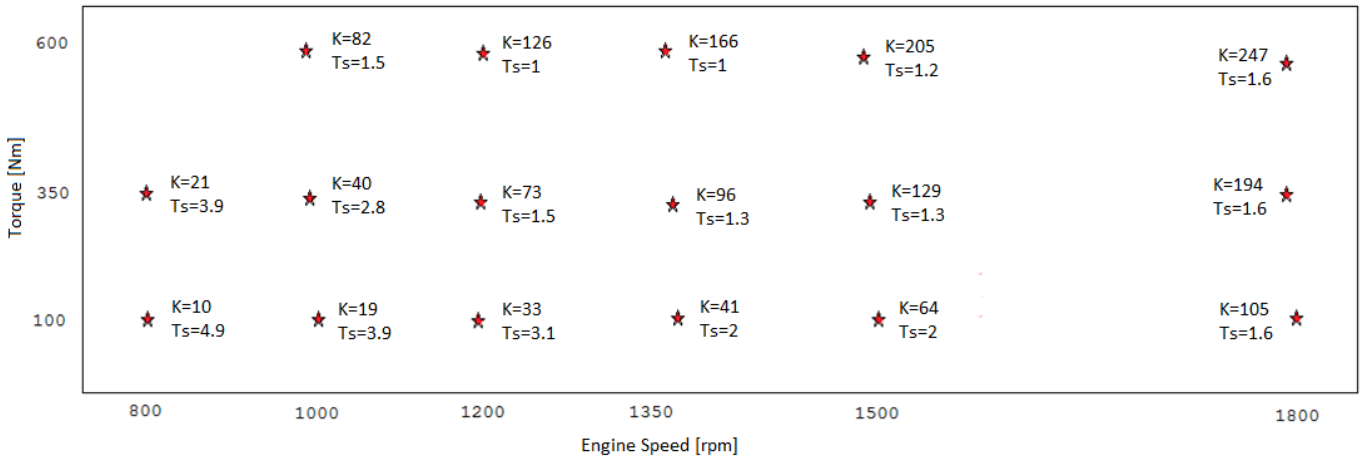

Figure 4.20: Transfer function model parameters varying with engine speed and torque from χ_{vgt} to p_1

The gain K shows a large change from 10 to 247 which is from low-speed low-load operating point (800rpm, 100Nm) to high-speed and high-load operating point (1800rpm, 600Nm). At the same speed, the operating point with higher load always has higher K value. The same is true with speed change. At the same load, the operating point with the higher speed has the higher K value.

The relationship of system time T_s with engine operating point is not as consistent as that of gain K. But at the low speed and low-load range, T_s is bigger than that of engine operating point with higher speed and load. Therefore, for such system dynamics, gain-scheduling techniques should be applied in linear controller design to obtain the required closed-loop control performance for the whole engine operating range.

A transfer function network was obtained using system identification for another 2I2O control structure which is of the from [χ_{vgt}, χ_{egr}] to [W_c, W_{egr}]. Figure 4.21 shows this as a transfer function net for the engine operating point 1300rpm 300Nm.

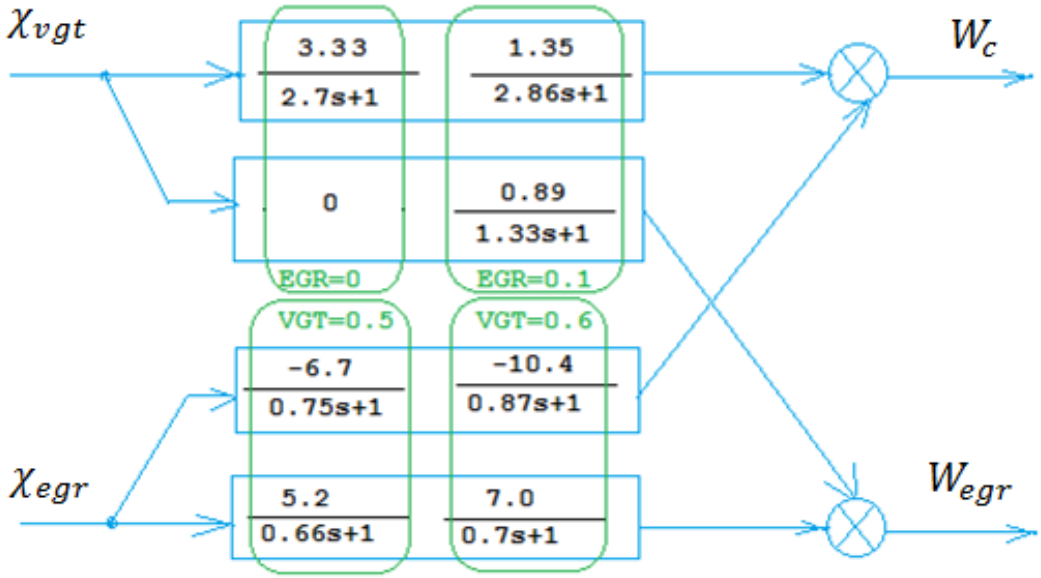

Figure 4.21: Transfer function net for [χ_{vgt}, χ_{egr}] to [W_c, W_{egr}]. Engine operating point: 1300rpm, 300Nm

In Figure 4.21 the green elements outline the group transfer functions for different EGR valve open conditions and VGT vane positions. The dynamic relationship between [χ_{vgt}, χ_{egr}] and [W_c, W_{egr}] means that χ_{vgt} not only affects W_c but also W_{egr} when the EGR valve is open. χ_{egr} always influences the two output variables: W_c and W_{egr}. The change of VGT vane position changes the strength of such influence. A more closed (i.e. closer to 1) VGT vane position increases the absolute gain from χ_{vgt} to both outputs: W_c and W_{egr}. For a linear PID controller design, the transfer functions with average gain and system time among the different EGR valve position and VGT vane position conditions were used.

4.3.3 2I2O MPC Control Engine Test Results

A 2I2O MPC control system for the air-path of the from [χ_{vgt}, χ_{egr}] to [p_1, W_c] was developed and tested. The block diagram of the control system is shown in Figure 4.22.

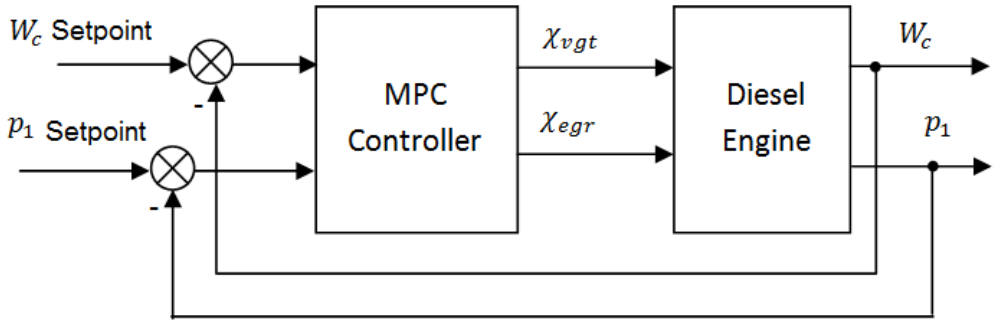

Figure 4.22: Air-path MPC control for 2I2O system: [χ_{vgt}, χ_{egr}] to [p_1, W_c]

The linear MPC controller depicted in Figure 4.22 is a quadratic programming problem solver. The optimal quadratic programming problem is finding a control input set with control horizon H_u:

$$\boldsymbol{u}(i),\ \ i = k, k+1, \dots, k+H_u \qquad (\mathbf{4.19})$$

that minimizes the cost function:

$$J = E'W_yE + U'W_uU \qquad (\mathbf{4.20})$$

Where, $E = \begin{pmatrix} \boldsymbol{r}_y(k+1) - \boldsymbol{y}(k+1|k) \\ \vdots \\ \boldsymbol{r}_y(k+1+H_p) - \boldsymbol{y}(k+1+H_p|k) \end{pmatrix}$, $U = \begin{pmatrix} \boldsymbol{u}(k) \\ \vdots \\ \boldsymbol{u}(k+H_u) \end{pmatrix}$, H_p is the prediction horizon, W_y and W_u are weighting matrices on prediction error and control strength respectively.

Subject to system model equation constraints Equations (4.16), (4.17) and control inequality constraints:

$$\boldsymbol{u}_{min} \le \boldsymbol{u}(i) \le \boldsymbol{u}_{max} \qquad j = k, k+1, \dots k+H_u \qquad (\mathbf{4.21})$$

Here the actuator constraints are:

$$\begin{pmatrix} 0.45 \\ 0 \end{pmatrix} \le \begin{pmatrix} \chi_{vgt}(k) \\ \chi_{egr}(k) \end{pmatrix} \le \begin{pmatrix} 0.75 \\ 0.3 \end{pmatrix} \qquad j = k, k+1, \dots k+H_u \qquad \mathbf{4.22})$$

The control solution at the current time, $\mathrm{u(k)} = \begin{pmatrix} \chi_{\mathrm{vgt}}(\mathrm{k}) \\ \chi_{\mathrm{egr}}(\mathrm{k}) \end{pmatrix}$ is sent to the controller output to update the actuators.

The fifth order state-space model identified from perturbation test data was used to implement the MPC controller. The control result of this 2I2O air-path MPC controller from tests on the C6.6 engine used in this study are shown in Figure 4.23.

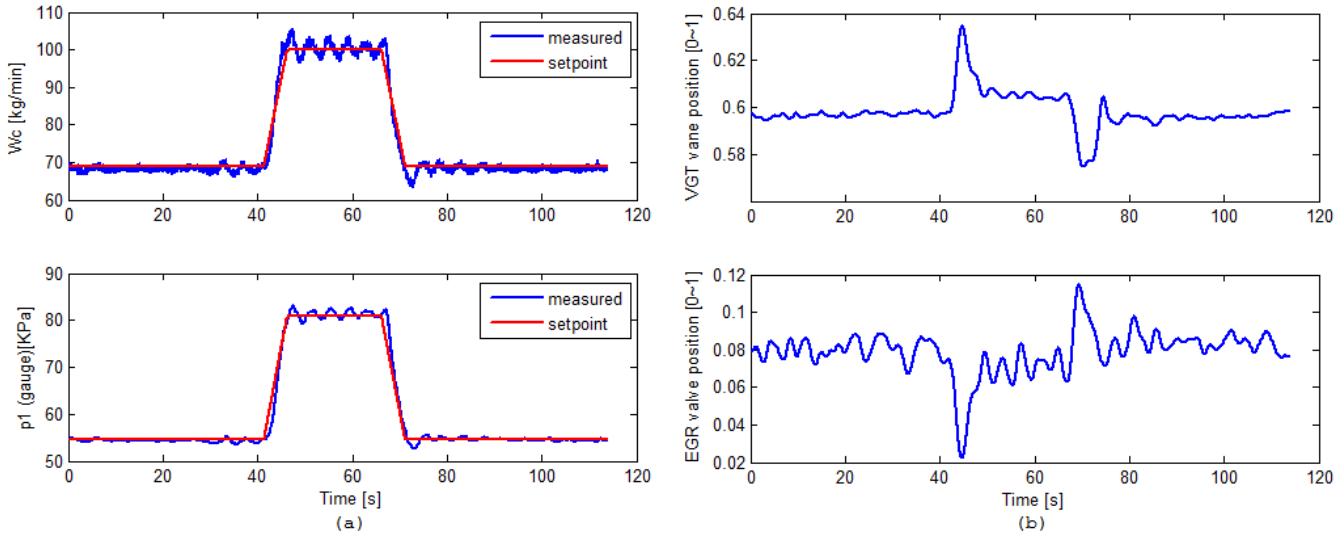

Figure 4.23: MPC control result for $[\chi_{vgt}, \chi_{egr}]$ to $[p_1, W_c]$ 2I2O control system; (a) setpoint tracking performance; (b) VGT vane and EGT valve position

The engine was running at a fixed speed of 1550rpm, the engine torque was ramped over 5 seconds from 370Nm to 470Nm and then back, see Figure 4.24. The tracking performance for either W_c or p_1 was good by observation. This indicates that the system identified model is valid and can be used to build MPC controllers. However, to develop the MPC controller for the whole engine operating range, model gain-scheduling has to be carried out. This work has not been done in this study due to time constraints.

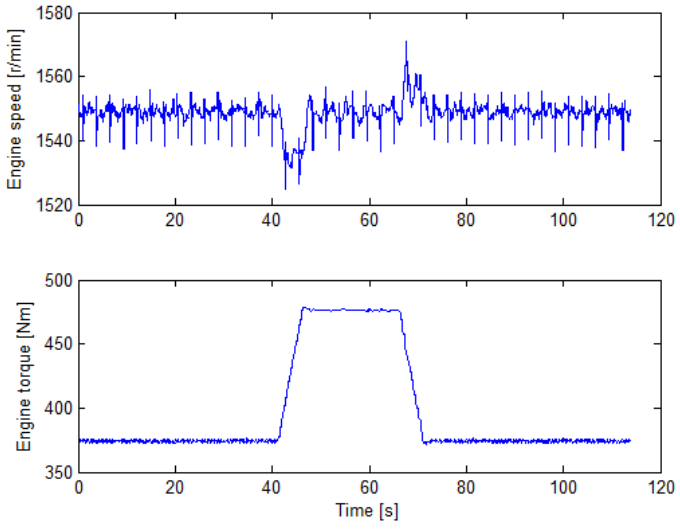

Figure 4.24: Engine speed and torque during the MPC control test

4.3.4 2I2O MAF and EGR Flow Rate Control Engine Test Results

Based on the estimation of EGR flow rate W_{egr}, a 2I2O decentralized PID control system was developed and this is shown in Figure 4.25. The two inputs are the same as those used in the above MPC control system, namely χ_{vgt} and χ_{egr} and the two outputs are W_c and W_{egr}. EGR flow rate W_{egr} replaced the boost pressure p_1 as one of the feedback variables. Consequently this control structure has a clearer physical significance ($[\chi_{vgt}, \chi_{egr}]$ to $[W_c, W_{egr}]$) over the previous 2I2O control structure. It can be described as using VGT to control fresh air mass flow and EGR to control EGR flow rate, this design therefore matches up the input and outputs based on physical significance.

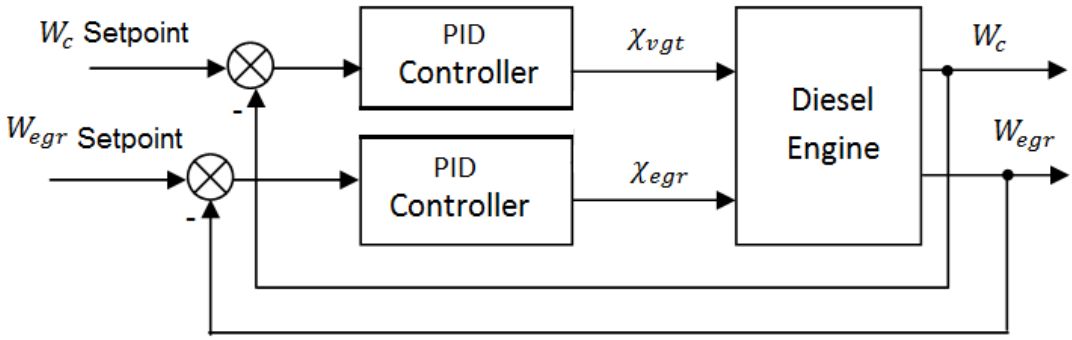

Figure 4.25: Air-path decentralized PID control for 2I2O system: $[\chi_{vgt}, \chi_{egr}]$ to $[W_c, W_{egr}]$

Only decentralized PID control strategy was implemented to demonstrate the feasibility of this control structure due to time constraints. The two PID controllers in Figure 4.25 were designed based on the identified transfer function models shown in Figure 4.21. These were then adjusted slightly during engine testing. Test results with the C6.6 engine used in this study based on this 2I2O control system are shown in Figure 4.26. During the tests, the engine was running steady-state with a speed of 1300rpm and a load of 300Nm.

Figure 4.26 (a) and (b) show that the setpoint step change and estimated EGR flow rate W_{egr} (Section 4.2.5.2) and measured compressor flow rate W_c respectively. It can be seen that both estimated W_{egr} and measured W_c follow the corresponding setpoint step change with a reasonable step change response that is not heavily damped and avoids excessive over or undershoot. Compared to the 2I2O MPC control result shown in Figure 4.23, the MPC controller is observed to have improved setpoint tracking compared to the decentralised 2I2O PID control. The response to the step change cannot be quantifiably compared

for these two controllers as the setpoint was ramped for the MPC test but was immediately changed for the PID test.

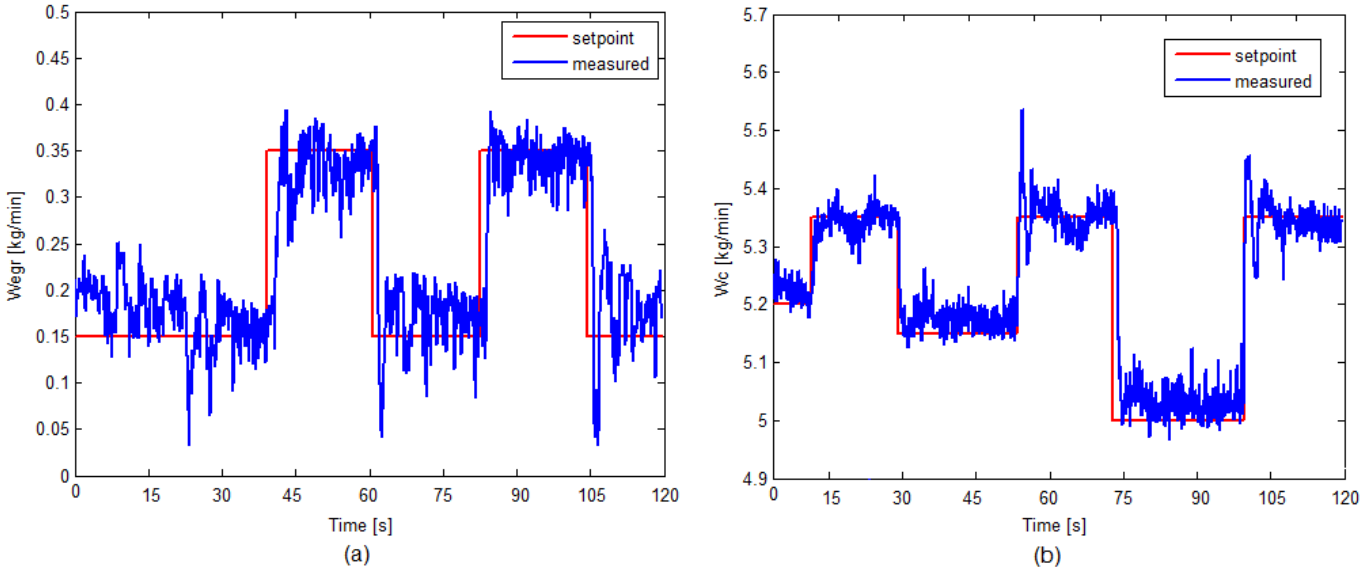

Figure 4.26: Setpoint and measured value of (a) W_{egr} and (b) W_c from the 2I2O [χ_{vgt}, χ_{egr}] to [W_c, W_{egr}] air-path PID control system. Engine was running at 1300rpm 300Nm operating point

Based on the result in Figure 4.26, there are two clear possibilities for future work into diesel engine air-path control:

- The decentralised 2I2O PID control system can be easily adapted into a direct AFR and EGR ratio control system. AFR can be computed by dividing intake fresh air quantity by injected fuel quantity. Injected fuel quantity for each cycle is available within the engine control system. EGR ratio can be computed from estimated EGR flow rate and measured intake air flow rate using Equation (4.23):

$$EGR_{ratio} = \frac{W_{egr}}{MAF + W_{egr}} \qquad (\mathbf{4.23})$$

  However, the direct control of EGR rate is limited by the fact that the EGR gas composition is a function of engine operating point and AFR. Thus for a given EGR rate the actual gas composition concentration in the engine intake can vary with the operating condition. It is therefore more appropriate to consider the more fundamental intake CO2/O2 fraction and also the fuel/O2 ratio which fundamentally describe the intake mixture composition. Working backwards, from these fundamental ratios, the required EGR mass flow and fresh air flow and hence EGR rate and also boost pressure can then be determined. Thus, through measurement and

control of intake O2 concentration, a more precise and fundamental control of the intake composition and hence combustion can be achieved than through the less fundamental EGR ratio.

- The comparison of the results in Figure 4.23 and Figure 4.26 suggest that control performance of engine air-path can be improved by applying MPC as an alternative to decentralised PID.

4.4 Conclusions

Investigation of the air-path relationship of MAF and MAP in respect to step changes in VGT and EGR, revealed that there exists a series of linear MAF to MAP relationships that scale with engine speed and load when the EGR and VGT respectively are fixed. The details of these relationships demonstrated that MAP is more sensitive to VGT position than MAF (VGT should therefore be used to close-loop control MAP) and that at constant engine speed, closing the VGT vane position is equivalent to increasing the engine load in regard to the effects on MAF and MAP. Conversely, the opening of the EGR valve at fixed engine load has the same effect on the MAF to MAP relationship as decreasing the engine speed. These clear linear relationships demonstrate the feasibly to use an MVEM to model the MAF and MAP for different engine operating conditions. These findings confirm the viability of closed-loop model based control as a replacement for open-loop look-up table air-path control methods.

For the C6.6 engine used in this study, nonlinearity was identified between the EGR valve position and the EGR ratio which can be attributed to the variation in EGR gas composition as a function of engine operating point and AFR (i.e. intake manifold CO_2 concentration being dependent also on the concentration in the exhaust manifold). For a linear model based closed–loop control system this would be difficult to manage. However, evaluation of the NOx emissions in respect to the EGR ratio revealed clear linear relationships and thus EGR ratio is a far better candidate for closed-loop control of engine out NOx emissions than closed-loop control of EGR valve position directly. EGR ratio estimation requires either direct EGR mass flow measurement or alternatively it can be estimated using an EGR mass flow model.

Therefore accurate knowledge of the EGR mass flow is very important in the proper control of diesel engine air-path, especially for model based control. In the majority of air-path control research an orifice valve flow rate model is use to estimate EGR mass flow but in this study the performance of this form of model

was shown to be poor on a practical engine due to sensor noise. An alternative model based on the total flow rate minus the measured air flow rate (MAF) when the EGR valve is open was used. This model fundamentally requires accurate estimation of volumetric efficiency and a nonlinear regression model of the C6.6 engine volumetric efficiency was developed from experimental data. The combination of the total flow rate model with this nonlinear volumetric efficiency model proved to be far more successful for predicting the EGR mass flow than the orifice flow model.

A 2I2O linear air-path MPC control system was developed on the C6.6 diesel engine to control MAP and MAF with VGT and EGR respectively. An accurate air-path dynamic model was found to be crucial in the effective design of this air-path controller and in this study a system identification methodology was employed using the *pem* function in the MATLAB® system identification toolbox. It was found that a fifth order identified state-space model was sufficient for achieving good steady state and transient control performance. This study therefore confirms that system identification derived linear MPC of the diesel engine air-path MAP and MAF is feasible and practical. However, model gain-scheduling is required for this controller to perform over the full engine operating range.

To provide a point of comparison, a 2I2O PID decentralized intake air flow rate (MAF) and EGR mas flow rate (model estimated) control was also implemented and tested on the C6.6 engine. This controller was based on identified transfer function models. Decentralised PID was found to deliver good steady-state air-path control performance following local tuning but for good control performance at multiple engine operating points, gain scheduling is essential due to the complex air-path dynamics as discussed in Section 3.4.3. Consequently, when transiting engine operating points, it was found that MPC control generally performed better in regard to set-point tracking compared to decentralised PID. At the engine operating points examined, the MPC controller was also observed to have improved setpoint tracking compared to the decentralised 2I2O PID control. This comparison is however subject to the success achieved in the tuning of the decentralised PID controller gains at each operating point.

These comparisons of controller performance are intuitive due to the strong and complex coupling described in this study between VGT and EGR and also the engine fuel path, Section 3.4.5. For such a system, the performance of a

properly configured MIMO MPC controller should exceed that of a decentralised controller due to its ability to deal with strong coupling, actuator constrains, disturbance rejection and forward prediction capability.

More research is required to develop a fast and low cost way of obtaining accurate dynamic models for MPC and to explore the feasible setpoints' space as well as the setpoint determination policy. Furthermore, a combined air-path and fuel-path model based control system would have increased system disturbance rejection capability and also potentially achieve more precise control the desired engine variables. This is because the system would manage the mutual disturbances of the coupling between the air-path and fuel-path systems where currently in traditional open loop diesel engine control, such mutual disturbances are managed using time consuming and costly engine calibration.

Chapter 5

5 Fuel-Path Control

5.1 Introduction

Three types of MIMO fuel-path control system have been developed and tested on a C6.6 test engine. The first system is a Three-Input-Three-Output (3I3O) MPC multi-variable feedback control system that uses SOI, fuel RP and FR as manipulated input variables to control three engine output variables: NO_x, soot emissions and exhaust temperature. The second system is a SOI and RP online adjustment system in the form of a 2I2O feedback control system that uses estimated combustion parameters (CA50 and pseudo-combustion width based on cylinder pressure data as feedback variables) to automatically adjust fuel-path control inputs SOI and RP under different engine operating points and conditions, including transient operation. The third system is a P_{max} and IMEP control system based again on a 2I2O form that uses the second and third injection pulse in the three-injection mode to control combustion P_{max} and IMEP independently. A two loop IMEP based engine speed closed-loop control (speed governor) system has also been developed and tested.

5.2 3I3O MPC Control

5.2.1 3I3O MPC Control at Engine Steady-State

Model predictive control is an advanced multi-variable control strategy that has been widely and successful applied in industry control applications [67]. However, it is well known that the main drawback of MPC is its heavy computational burden due to the solving online of the optimization problem. EMPC has been developed to remove this drawback by computing the optimal control action off line as an ‘explicit’ function of the state and reference vectors [176]. However, EMPC usually gives a suboptimal solution and the complexity of the partition grows in the worst case exponentially due to the combinatorial nature of the problem [177]. Additionally, the number of controller regions also grows exponentially with the prediction horizon and the states [178]. Since the control system of the test engine used in this study was implemented in a National Instruments PXI computer [171] which has very high performance (2.16

GHz dual core processor) and the MPC controller was implemented in an another even higher performance PC (8 processor cores), it is possible to implement a MIMO linear online MPC algorithm and to test it experimentally. In this study the online MIMO linear MPC was implemented in an *S-Function* in the MATLAB® Simulink® environment.

It was used here to control engine exhaust temperature, NO_x and soot emissions directly via fuel-path control inputs: SOI, rail pressure and FR. FR is defined in Chapter 3 as the ratio of main injection fuel pulse width (or main injection fuel quantity) over the total injection width (or total injection quantity). The diagram of this 3I3O diesel engine fuel-path MPC system is shown in Figure 5.1.

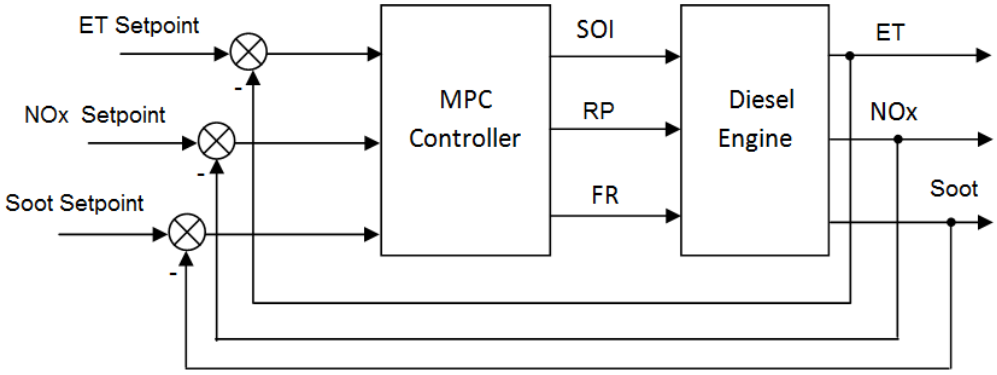

Figure 5.1: Diagram of 3I3O fuel-path MPC control system

The MPC controller is actually a quadratic programming problem solver. Assuming that the discrete system state space model from the three inputs: SOI, RP and FR to the three outputs: ET, NO_x and soot is

$$\boldsymbol{x}(k+1) = A\boldsymbol{x}(k) + B\boldsymbol{u}(k) \qquad (\mathbf{5.1})$$

$$\boldsymbol{y}(k) = C\boldsymbol{x}(k) \qquad (\mathbf{5.2})$$

Where, $\boldsymbol{u}(k) = \begin{pmatrix} u_{SOI}(k) \\ u_{RP}(k) \\ u_{FR}(k) \end{pmatrix}$ and $\boldsymbol{y}(k) = \begin{pmatrix} y_{ET}(k) \\ y_{NOx}(k) \\ y_{Soot}(k) \end{pmatrix}$

The optimal quadratic programming problem is to find a control input set with control horizon $\mathrm{H_u}$

$$\boldsymbol{u}(i), \;\; i = k, k+1, \ldots, k+H_u \qquad (\mathbf{5.3})$$

that will minimize the following cost function:

$$J = E'W_yE + U'W_uU \qquad (\mathbf{5.4})$$

Where, $E = \begin{pmatrix} \boldsymbol{r}_y(k+1) - \boldsymbol{y}(k+1|k) \\ \vdots \\ \boldsymbol{r}_y(k+1+H_p) - \boldsymbol{y}(k+1+H_p|k) \end{pmatrix}$, $U = \begin{pmatrix} \boldsymbol{u}(k) \\ \vdots \\ \boldsymbol{u}(k+H_u) \end{pmatrix}$

H_p is the prediction horizon, W_y and W_u are weighting matrices on prediction error and control effort respectively. They are used as tuning parameters for the controller. They will affect the distribution of control effort among the three control inputs: SOI, rail pressure and FR. Subject to control constraints:

$$\boldsymbol{u}_{min} \leq \boldsymbol{u}(i) \leq \boldsymbol{u}_{max} \qquad j = k, k+1, \ldots k+H_u \qquad (\mathbf{5.5})$$

The linear system state space model was obtained by system identification technique using the *pem* function in MATLAB®. The input-output data set used in *pem* function was obtained from a perturbation test. The perturbation test was carried out when the engine was running at steady-state with speed and load (torque) constant and controlled by the engine speed governor and the dyno control system respectively. Air-path and fuel-path control variables other than SOI, RP and FR were kept constant during the test. The block diagram of the perturbation test is displayed in Figure 5.2. Each perturbation test lasted for 20 minutes with 30Hz fixed sampling frequency chosen to be the same as the engine control frequency. The data collected at each load and speed operating point was split into two parts: half for training and half for validation purposes.

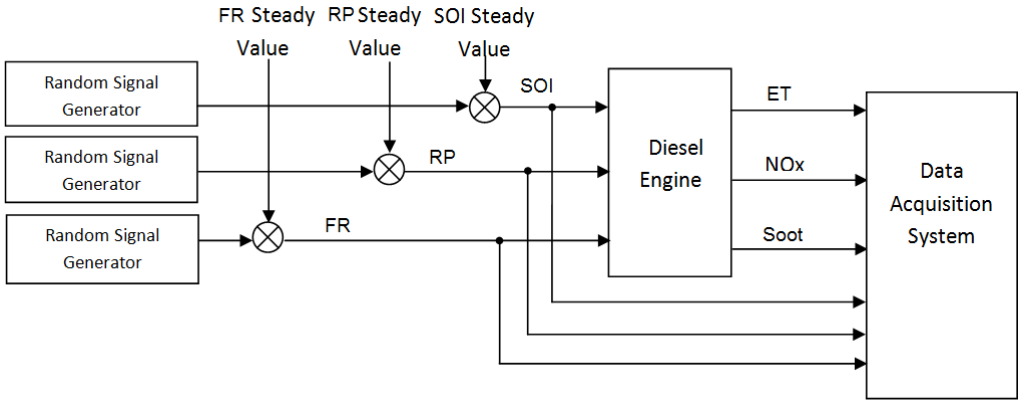

Figure 5.2: Block diagram of engine perturbation test for system identification

This 3I3O MPC controller was implemented in Simulink®, see Figure 5.3. The MPC algorithm was programmed as a Simulink® S-Function. The controller was run in the host PC [171] which had 8 processor cores. The link of input/output variables between the engine real time injection control software and the Simulink® MPC controller was implemented via National Instruments Simulation Integration Toolkit using Local Internet TCP protocol [171]. This arrangement

enabled the execution frequency of the MPC control system to be the same as that of real time engine control system (30Hz).

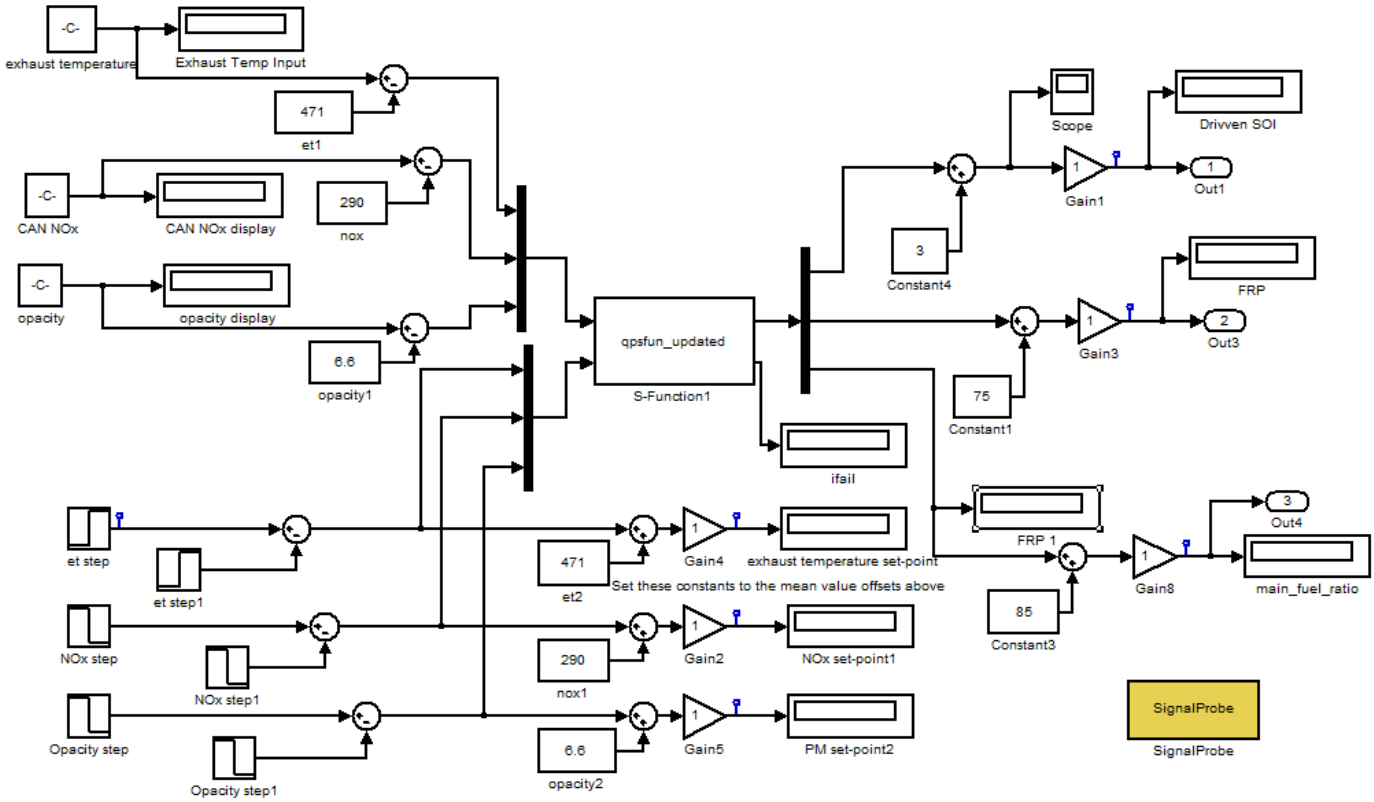

Figure 5.3: MPC controller implemented in MATLAB® Simulink® model

The results for a setpoint step change test are shown in Figure 5.4. The engine was running at steady conditions of 1550 rpm and 475 Nm.

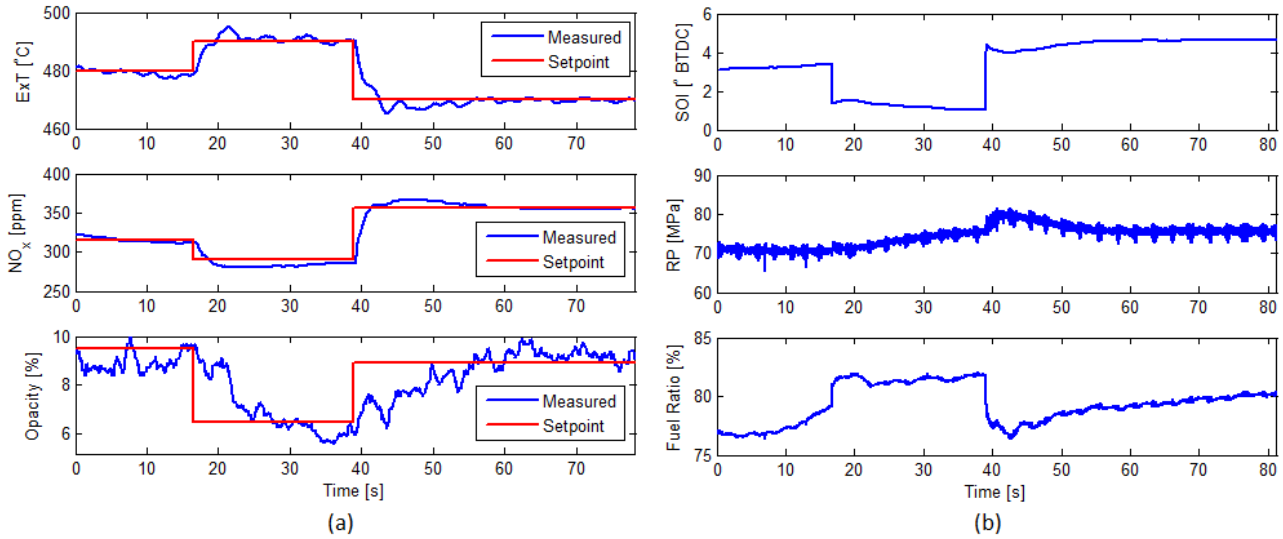

Figure 5.4: Step change response of 3I3O MPC control system at engine steady-state: speed=1550rpm, torque=475Nm

There are three different setpoint combinations of the three controlled variables: Exhaust Temperature, NO_x emission and soot emission (measured by AVL 439 Opacity Meter). These three designs of setpoints and corresponding control inputs at steady-state are listed in Table 5.1.

Table 5.1: Steady-state value of control inputs and outputs of 3I3O fuel-path MPC control system at engine steady-state: speed=1550rpm, torque=475Nm

No.	Setpoints for Controlled Variables			Control Inputs		
	ExT [°C]	NO_x [ppm]	Opacity [%]	SOI [°BTDC]	RP [MPa]	FR [%]
1	480	315	9.5	3.27	70.6	77
2	490	290	6.5	1.06	76	81
3	470	358	8.9	4.6	76.8	76.86

NB: ExT refers to exhaust temperature; SOI refers to start of injection; RP refers to rail pressure; FR refers to fuel ratio

The three-dimensional plots of the three setpoints and the steady-state control solutions are shown in Figure 5.5 (a) and (b) respectively.

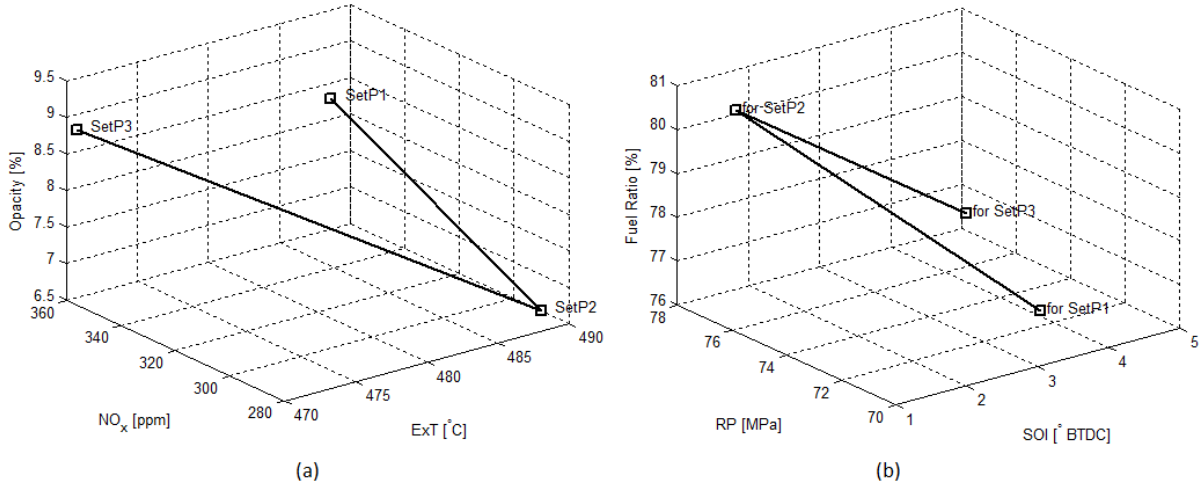

Figure 5.5: Steady-state value of control inputs and outputs of 3I3O fuel-path MPC control system at engine steady-state: speed=1550rpm, torque=475Nm: (a) three setpoints; (b) three control inputs; (SetP refers to setpoint)

It can be seen from Figure 5.4 that the exhaust temperature follows the step change demand from 480 °C to 490 °C and then 490 °C to 470°C. NO_x emission follows the step change demand from 315 ppm to 290 ppm and from 290 ppm to 358 ppm. Meanwhile, soot emissions follow the step change in opacity demand from 9.5% to 6.5 % and 6.5% to 8.9%. The maximum response time for all three controlled variables is 20 s. This engine test result shows that the 3I3O MPC

controller has ability to control in closed-loop the three engine output variables: exhaust temperature, NO_x emissions and soot emissions using the three fuel-path input variables: SOI, rail pressure and fuel ratio. For the operation of such a control system, the combination of these three setpoints should be within the achievable engine output space.

5.2.2 3I3O MPC Control During Engine Transient

In order to apply this 3I3O MPC function to a wider engine operating range, gain-scheduling is required. The design for gain-scheduling begins with the segmentation of the engine operating range. The segmentation of the engine operating range for the C6.6 engine used in this study for MPC gain-scheduling is shown in Figure 5.6 and shows that a total of nine zones based on divisions in thirds of both the speed and engine torque range.

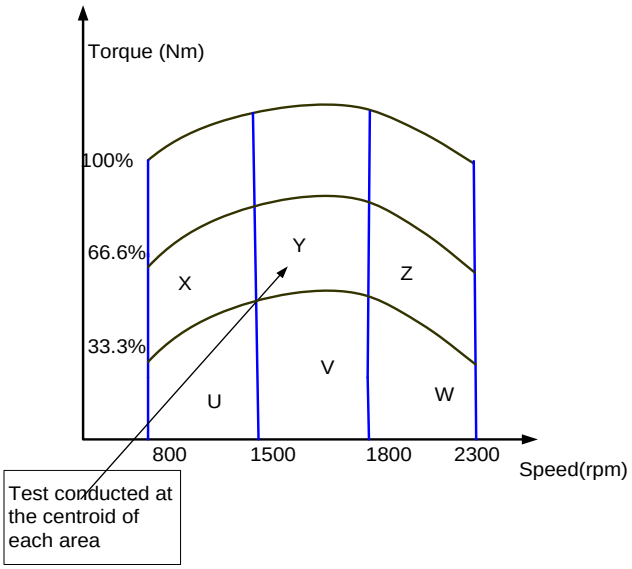

Figure 5.6: Segmentation of speed and torque for the whole engine operating range

System identification experiments were conducted at the centres of these nine zones. There are three speed points for the zone centroids: 1050rpm, 1550rpm and 2050rpm. The centroid load at the three zones with a centroid speed value of 1550rpm is slightly higher than the centroid load values of the adjacent regions because the pattern of the segmentation follows the engine maximum power curve. The gain-scheduling MPC control block diagram is shown in Figure 5.7. Setpoints and predictive models were selected according to the location of the measured speed and torque value. Two hysteresis functions were implemented to reduce the system sensitivity to noise in the measured speed and torque signals close to the switch boundary.

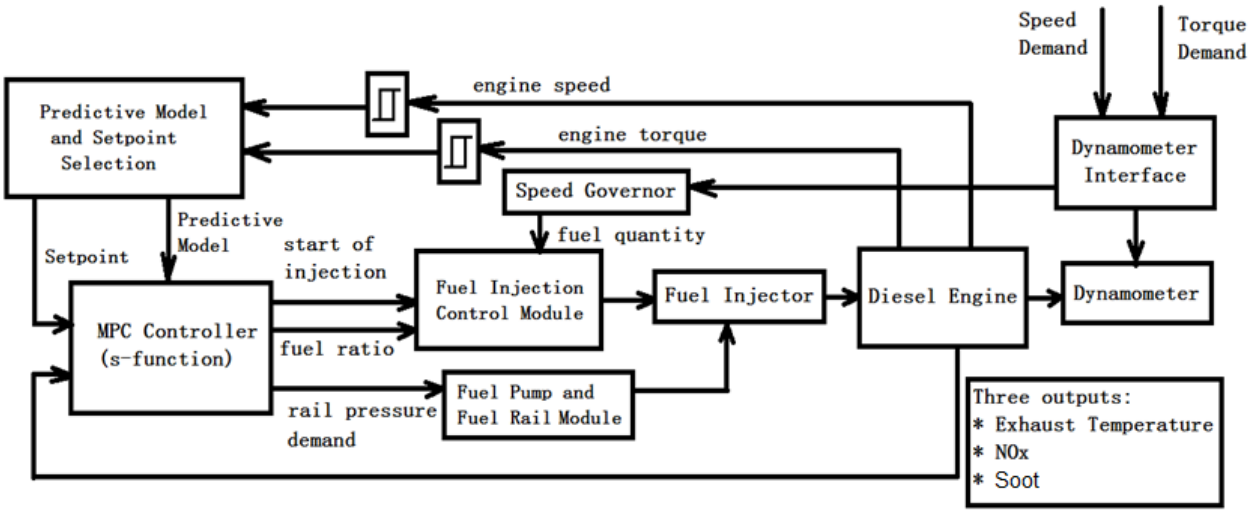

Figure 5.7: Block diagram of gain-scheduling 3I3O MPC diesel engine fuel-path control

Experimental tests with MPC showed that when the speed is varying with the load fixed, the control system is stable. However when the load is varying while speed is fixed, the control system lost stability especially when the load was varying near the zone torque boundary. To overcome this problem, an improved predictive model is introduced. The improved predictive model was obtained by a modified system identification experiment strategy. The number of divided zones is still the same as Figure 5.6. However, the system identification experiment was not conducted at the centroid of each zone but conducted at six points within each zone. These six points are equally spaced according to torque range bounded by each zone, Figure 5.8.

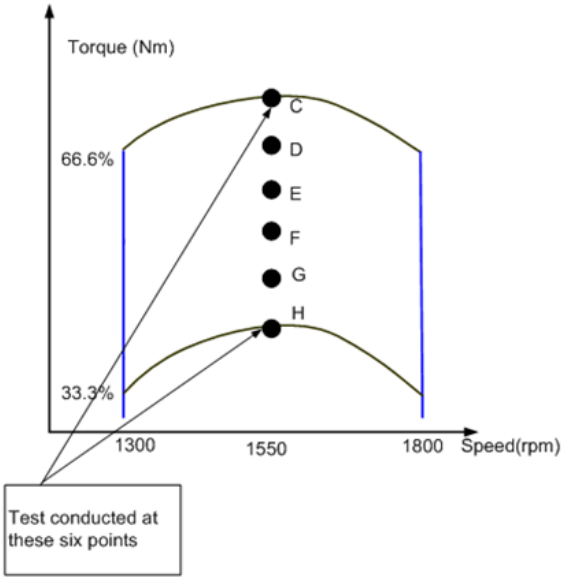

Figure 5.8: Six different points for perturbation test in each region

Within each zone, each of the six perturbation tests lasted for 20 minutes with the result data set divided such that the first 10 minutes was used for model training and the final 10 minutes used for model validation for each operating point. All 60 minutes of the training test data was combined into a single data set and from this was obtained an identified 5th-order state space model which was used as the predictive control model for this zone.

The control experimental results showed that the performance of this MPC fuel-path control system was improved. This MPC control system was stable over the whole engine operating range using the improved predictive model for each segment. Engine speed and load transient curves and their locations in the gain-scheduling segment map are shown in Figure 5.9. The tracking performance of three controlled outputs during speed and load transient between two engine operating points are shown in Figure 5.10 (a).

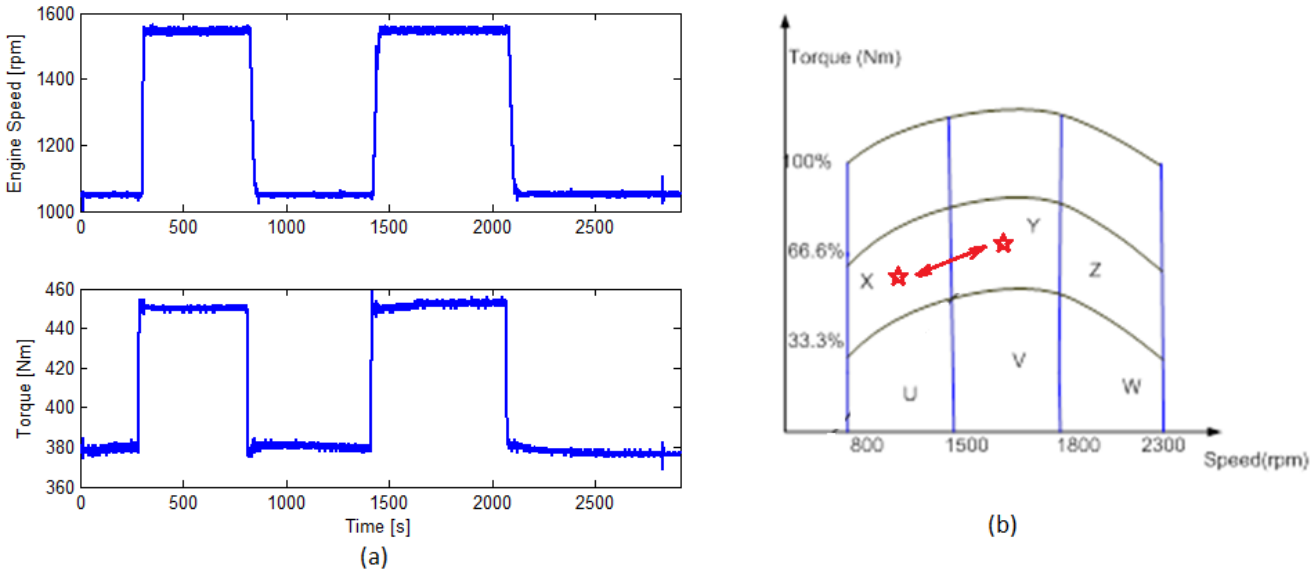

Figure 5.9: Engine speed and torque transient for two point gain-scheduling MPC control: (a) engine speed and torque curves against time; (b) locations of the two steady operating points in gain-scheduling segment map

The two engine operating points are (1050rpm, 380Nm) and (1550rpm, 450Nm). They are located in the centres of zones X and Y respectively, Figure 5.9 (b). There are four occasions of switch action of setpoints and the predictive model during this transient test. The response time of this control system is long at approximately 250 seconds.

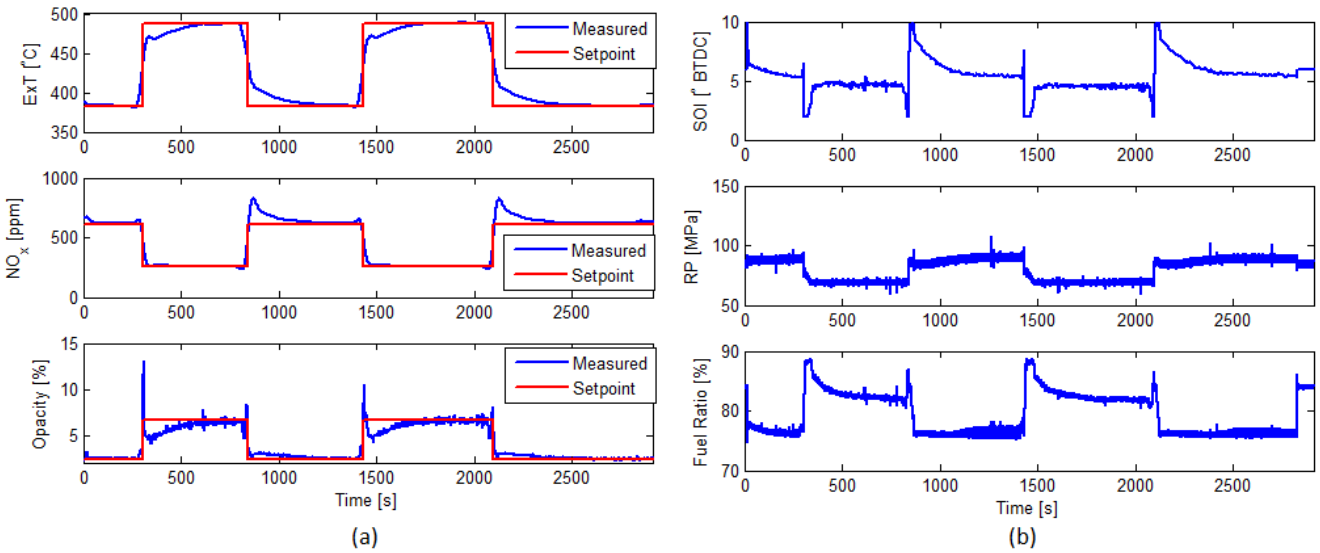

Figure 5.10: Gain-scheduling 3I3O MPC engine test results during engine transient: (a) three outputs and their setpoints; (b) three inputs

The substantial overshoot of NO_x occurs when the engine transits from high to low speed and it can take as long as 250 seconds before it settles at the setpoint, see the central plot in Figure 5.10 (a). A substantial overshoot of soot occurs as the engine transits from low load to high load; see the lower plot in Figure 5.10 (a). However, the time duration of the soot overshoot is relatively small. After the overshoot, soot drops lower than the set point demand value and then steadily increases to the setpoint in parallel to the ExT. This is the best control performance obtained after tuning the MPC control parameters that included the weighting values in the cost function.

The corresponding values of the three control inputs which are SOI, rail pressure and fuel ratio, are plotted in Figure 5.10 (b). It can be seen that the control solutions to the setpoints of two steady-state engine operating points are all within the control constraints i.e. there was no saturation. This means at the two steady-state engine operating points, this 3I3O MPC controller always works in closed loop control mode. The overshoot of soot is caused by the sharp SOI reduction as the engine transits from low load to high load. The slow response of the exhaust temperature and the soot as the engine transits from low load to high load is because of the slow convergence of fuel ratio. The substantial overshoot of NO_x as the engine transits from high speed to low speed is caused by the sharp and significant increase in SOI and its slow convergence to a steady value. This is the best tracking performance that was obtained following online tuning which determined optimum settings for the prediction horizon and control horizon

as 60 and 4 respectively. The improved predictive models obtained through sub-segment of each zone into 6 discrete load points (Figure 5.8) were also used.

The steady-state values of the results in Figure 5.10 are shown in Table 5.2.

Table 5.2: Control solutions of two steady-state engine operating points from 3I3O MPC fuel-path control engine transient test

No.	Engine Operating Points		Setpoints for Controlled Variables			Control Inputs		
	Speed [rpm]	Torque [Nm]	ExT [°C]	NO_x [ppm]	Opacity [%]	SOI [°BTDC]	RP [MPa]	FR [%]
1	1050	380	382	615	2.4	5.4	88	76
2	1550	450	488	255	6.6	4.4	71	82

NB: ExT refers to exhaust temperature; SOI refers to start of injection; RP refers to rail pressure; FR refers to fuel ratio.

The setpoints for exhaust temperature and soot (opacity) were selected such that they were lower in value at low engine speed and low load, while the setpoint for NO_x was selected such that it had a higher value at low engine speed and low load. The setpoints of these three controlled variables should be set within feasible range formed by all possible combination of the three control inputs and this can be determined either from the perturbation test and/or a methodical procedure of finding the extremes of the operating space using a Design of Experiments (DOE) approach with the full range of control inputs with the engine running steady-state at each DOE point.

The combination of setpoints of both lower exhaust temperature and soot at low speed and low load engine operating point resulted in the control solution settling at higher rail pressure and earlier combustion phasing at this engine operating point. This test result shows that this 3I3O MPC fuel-path control system can control the three engine output variables, exhaust temperature, NO_x emission and soot emission around properly designed setpoint values. Zero steady-state errors are achieved for all three controlled variables. However, the response time or settling time is slow and does not suit an engine running highly transient cycles. This slow convergence may be caused by a long prediction horizon, however from tuning it was observed that a shorter prediction horizon, although giving a faster response, resulted in increased steady-state error.

The MPC controller was implemented within the MATLAB® Simulink® environment and communicated with the LabVIEW real-time PXI engine control

system via local Ethernet bus [171]. In principle, the response time could be improved if the MPC controller is embedded directly in the LabVIEW real-time PXI control system. However, this was not investigated due to time constraints.

It is appropriate to provide an indication of the effort required to implement this form of control solution. To obtain the predictive models to cover the whole engine operating range using the methodology discussed, a total of (9×6×20 = 1080 minutes = 18 hours) 18 hours of perturbation testing is required and this process could be automated but in this work it was done manually (i.e. the Simulink PRBS perturbation demands were initiated and sent to the real-time system and a data recorder then started and the test then timed). It is also necessary to include an additional hour for model identification together with controller tuning for each segment zone.

5.3 SOI and RP Online Adjustment

After a careful study of the combustion process dynamics, a reliable and simple 2I2O feedback control structure using combustion process parameters as setpoints was developed to replace the lookup table based SOI and fuel rail pressure control system normally used for engines of this type. This control system has a faster response time than the MPC control system discussed in the forgoing section. The parameters controlled were combustion phasing and a variable consisting of a combination of information about ignition delay and combustion duration. The control strategy was a decentralized control which could also be termed a two single loop control system. The references for these two combustion parameters were calculated from two linear algebra equations with just two engine variables: speed and load.

The control results from speed and load transient tests show that this controller works not only smoothly but reliably and gives the engine improved fuel consumption and exhaust gas emissions performance compared to a traditional lookup table control system. By applying this control strategy with closed-loop control of combustion, the calibration work normally associated with the fuel-path would be substantially reduced.

5.3.1 Effects of SOI and RP on Engine Performance

In the two-pulse injection mode, each of the five injection variables identified in Figure 3.6 has an effect on the engine NO_x and soot emissions and fuel consumption performance. A measure of total fuel mass is used as a feedback

variable by the engine speed governor to control engine speed in the face of load variations. Even though FR (ratio of fuel volume between injections) was used in the 3I3O MPC fuel-path control system discussed above, the available calibration range of fuel ratio and dwell time is relatively small due to combustion stability and combustion noise issues. In comparison, SOI and fuel RP have a relatively wide calibration range. The range for SOI and RP could be from 12°BTDC to 6°ATDC and 45MPa to 120MPa respectively for the C6.6 test engine used in this study. However, in reality both SOI and RP need to be varied with engine operating point to meet constraints on emissions, combustion noise and stability; therefore leading to the practical range for each control input being smaller at any given engine operating point.

In order to have a picture of the effect of SOI and RP on engine fuel consumption and emissions performance, SOI and RP sweep tests were carried out at several engine operating points. The results of 1400rpm and 400Nm are presented in Figure 5.11 and Figure 5.12.

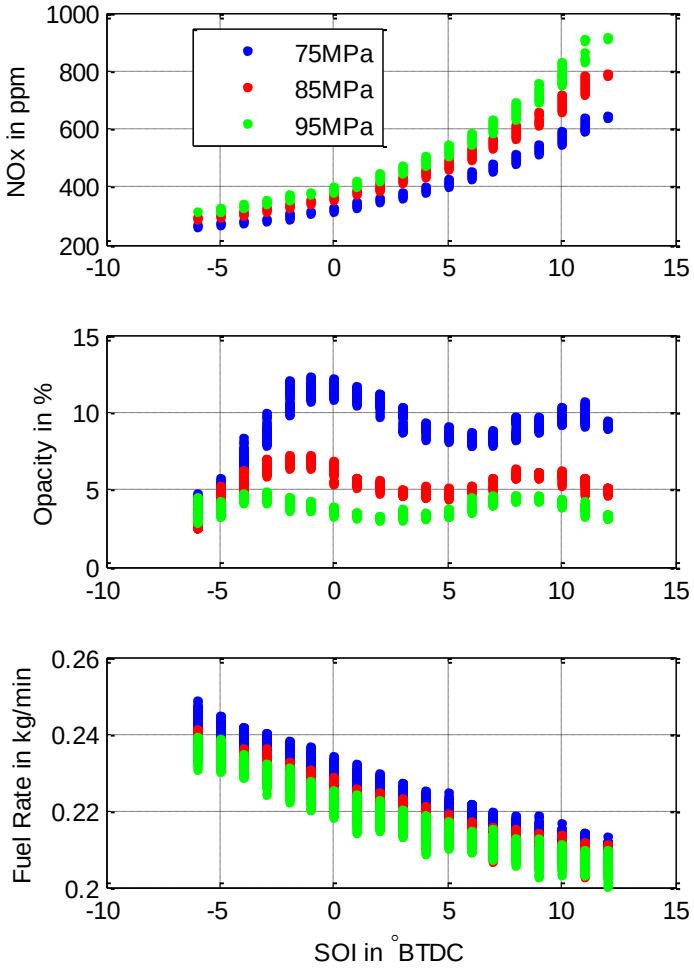

Figure 5.11: NO_x and soot emissions and fuel rate from SOI sweep tests at different RP when the engine was running at: 1400rpm, 400Nm

To study the coupling effects between SOI and RP, for each SOI and RP sweep test, results of three different cases with the other input variables fixed at respectively three constant values were plotted together. The sweep range of SOI was from 12°BTDC to 6°ATDC (-6°BTDC). Considering the emission performance, the sweep range of RP was from 75MPa to 96MPa when SOI was fixed at 3°BTDC and 0°BTDC, while 70MPa to 95MPa when SOI was fixed at -3°BTDC. The NO_x and soot emissions and fuel consumption during the SOI and RP sweep are plotted in Figure 5.11 and Figure 5.12 respectively.

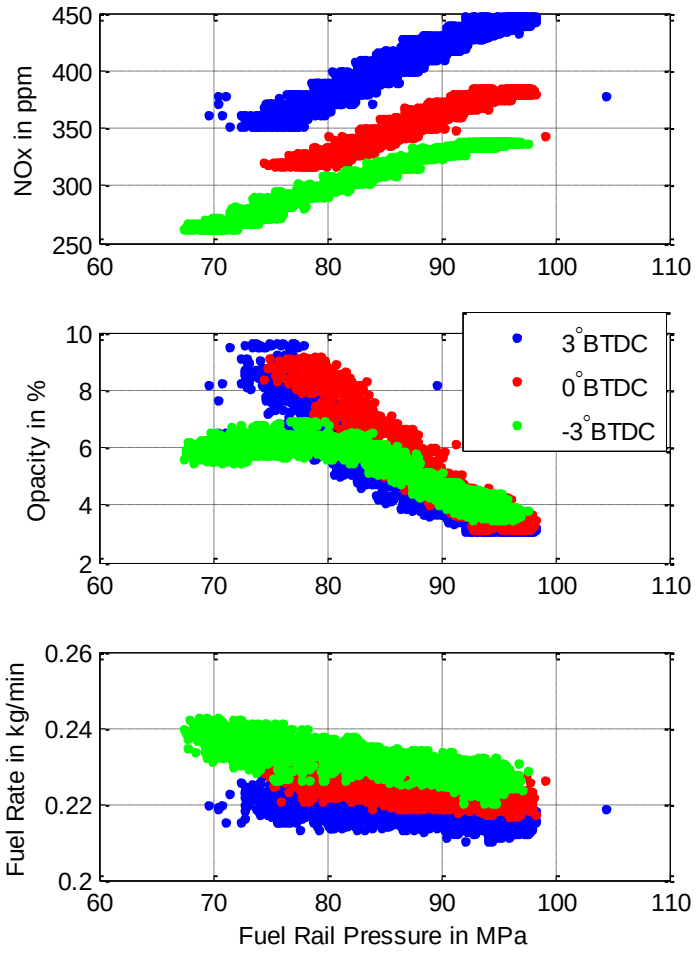

Figure 5.12: NO_x and soot emissions and fuel rate from RP sweep tests at different SOI when engine was running at: 1400rpm, 400Nm

It can be seen from the first and the third plot in Figure 5.11 that when RP is fixed, an early SOI results in higher NO_x emissions and lower fuel consumption. The second plot in Figure 5.11 shows that when RP is fixed, soot emissions have a nonlinear 'wave pattern' relationship with SOI. This is possibly caused by a pressure wave in the common fuel rail. More discussion about this phenomenon can be found later in Section 5.4 on the topic of "P_{max} and IMEP control". The soot emissions decrease very quickly when SOI is retarded to be later than TDC

(i.e. negative). This may due to the fuel injection taking place during the early part of the expansion process when air motion assists combustion resulting in less soot emissions. The third plot in Figure 5.11 shows that fuel consumption deteriorates when SOI is retarded due to a poor alignment of phasing between heat release and piston motion.

The first plot in Figure 5.12 indicates that when SOI is fixed, higher fuel RP results in higher NO_x emissions. The second plot in Figure 5.12 shows that when SOI is at 3°BTDC and 0°BTDC, higher rail pressure results in lower soot emissions. When SOI is at -3°BTDC, the soot emissions starts to drop when RP is lower than 78MPa; a similar phenomenon was also seen at other engine operating points. It is likely the timing of fuel injection relative to the piston position during downwards movement is the cause of these observations. For example; at a fixed engine speed and load operating point, lower rail pressure requires a longer fuel injection duration time. When SOI is -3°BTDC, lower rail pressure causes fuel injection at a progressively lower point in the piston motion possibly allowing oxidation of the soot when temperatures remain high late in the cycle. It can be seen from the third plot in Figure 5.12 that for different fixed SOI, higher rail pressure leads to lower fuel consumption. This is because of better fuel atomization at higher rail pressure and hence better combustion efficiency. Figure 5.12 also reaffirms that that more advanced SOI timing also results in reduced fuel consumption.

5.3.2 Trade-off Potential in Engine Performance

When NO_x, soot and fuel rate from the sweep tests are plotted together in pairs, the trade-offs among engine performance of fuel consumption and emissions can be seen. The first plot in Figure 5.13 shows the obvious trade-off between fuel rate and NO_x when the SOI is swept. If fuel consumption and NO_x emission are both needed to be kept as small as possible, SOI should be at a position near TDC. It can be seen from Figure 5.14 that when SOI is fixed and RP is varied, both fuel rate and NO_x, and NO_x and soot have trade-off relationships. There is no trade-off relationship between fuel rate and soot emission. Higher soot emission is accompanied by higher fuel consumption which is the result of lower fuel rail pressure. In this way, RP can be seen to select the trade-off point between NO_x and soot emissions.

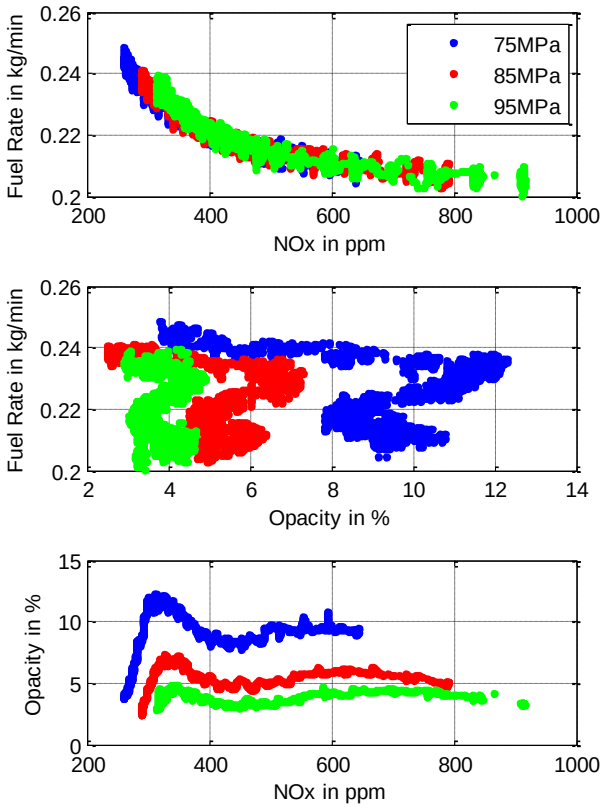

Figure 5.13: Scatter plots of NO_x, soot versus fuel rate for SOI sweep tests at different RP when engine was running at: 1400rpm, 400Nm

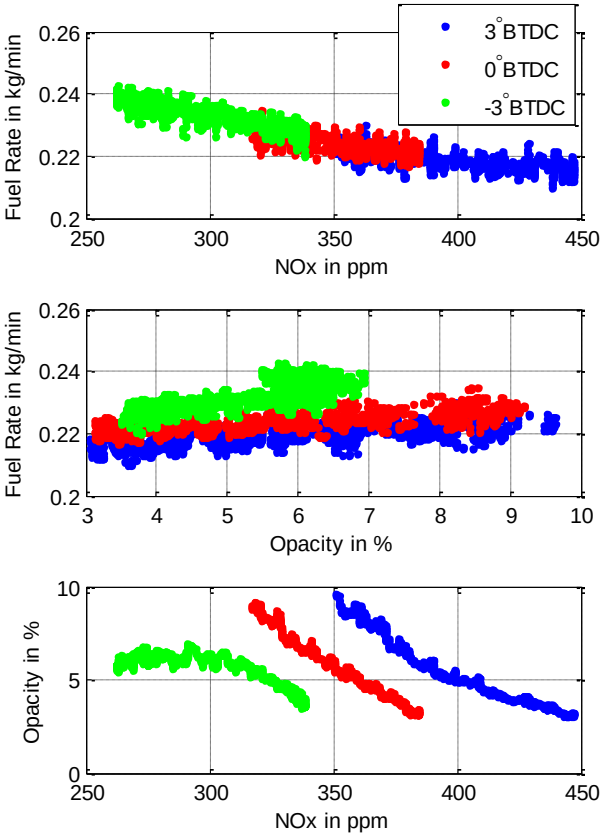

Figure 5.14: Scatter plots of NO_x, soot versus fuel rate and soot versus NO_x for RP sweep tests at different SOI when engine was running at: 1400rpm, 400Nm

5.3.3 Static Control Input-Output Relationships

From cylinder combustion pressure data, several combustion parameters such as ignition delay, combustion width, peak pressure, CA50 etc. can be estimated. Two parameters were selected as combustion performance feedback variables: CA50 and Alpha. CA50 is the crank angle degree of 50% mass burned and Alpha is the crank angle interval between SOI and CA50. Alpha represents the quasi first half of the combustion process since SOI rather than SOC was used as a reference point since the real time estimation of SOC is not very reliable in transients. Consequently the key estimated variable in this control system is CA50. CA50 can be computed reliably at the end of a combustion cycle from the cylinder pressure trace across a wide range of engine operating conditions.

The 2I2O closed-loop controller proposed here employs SOI and RP to control CA50 and Alpha. In other words, it is an online adjustment system of SOI and RP based on the setpoint demand of CA50 and Alpha. Therefore knowledge of the static relationships from SOI, RP to CA50 and Alpha would help in understanding the strategy required for this control system.

Static relationships between SOI and CA50, and between SOI and Alpha at an engine operating point of 1400rpm, 400Nm are shown in Figure 5.15. These results derive from SOI sweep tests. It can be seen that CA50 linearly varies with SOI, with more advanced SOI resulting in smaller CA50. The second plot in Figure 5.15 shows that there is little variation in Alpha during the SOI sweep. The transfer function model from SOI to CA50 obtained via system identification process is discussed in Section 3.4.4.

Figure 5.16 is a scatter plot of Alpha versus CA50 from the SOI sweep test results. It can be seen that as SOI is retarded, both CA50 and Alpha increase. But compared to the total CA50 variation which is more than 15 crank angle degrees, total variation of Alpha caused by the SOI sweep from -6° BTDC to 12° BTDC is only one crank angle degree. It is therefore appropriate to use CA50 as a control feedback variable for the online adjustment of SOI. With this feedback control configuration, the variation of injector performance and the effect of other disturbances to the fuel injection system can be compensated or rejected online.

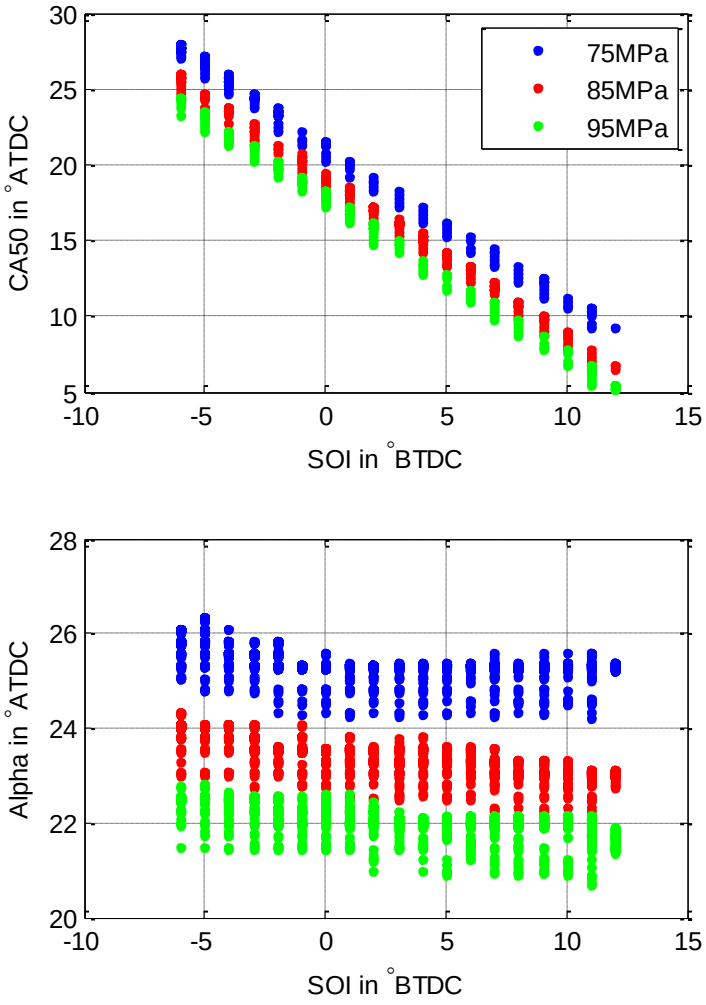

Figure 5.15: CA50 and Alpha in SOI sweep tests at three different RP when engine was running at: 1400rpm, 400Nm

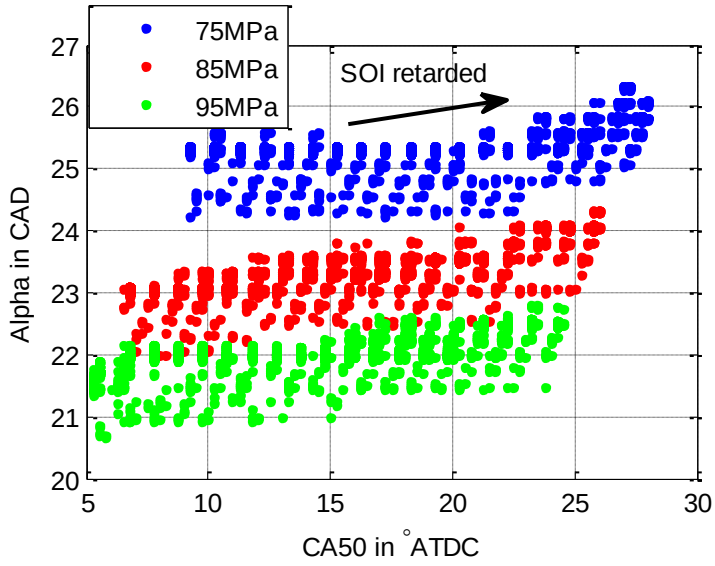

Figure 5.16: Scatter plot of Alpha versus CA50 from SOI sweep tests at three different RP when engine was running at: 1400rpm, 400Nm

From the RP sweep tests data, the relationships between RP and CA50 and between RP and Alpha are shown in Figure 5.17. It can be seen that when RP increases, both CA50 and Alpha decrease. Similar to Figure 5.16, Figure 5.18 is the scatter plot of Alpha and CA50 and this figure illustrates these trends more clearly.

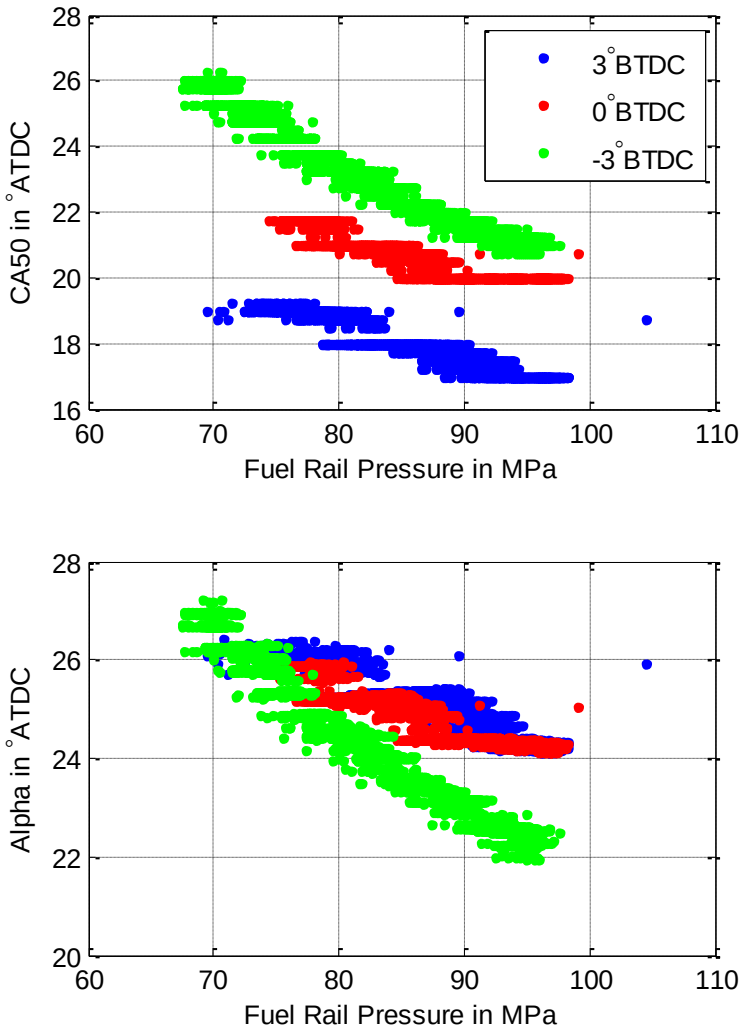

Figure 5.17: CA50 and Alpha in RP sweep tests at three different SOI when engine was running at: 1400rpm, 400Nm

This trend implies that RP influences both CA50 and Alpha. As SOI is only suitable for use in controlling CA50, RP was selected as the control input for Alpha feedback control. The closed-loop control structure of CA50 and Alpha enables the values of SOI and RP to be found on-line and then continuously adjusted.

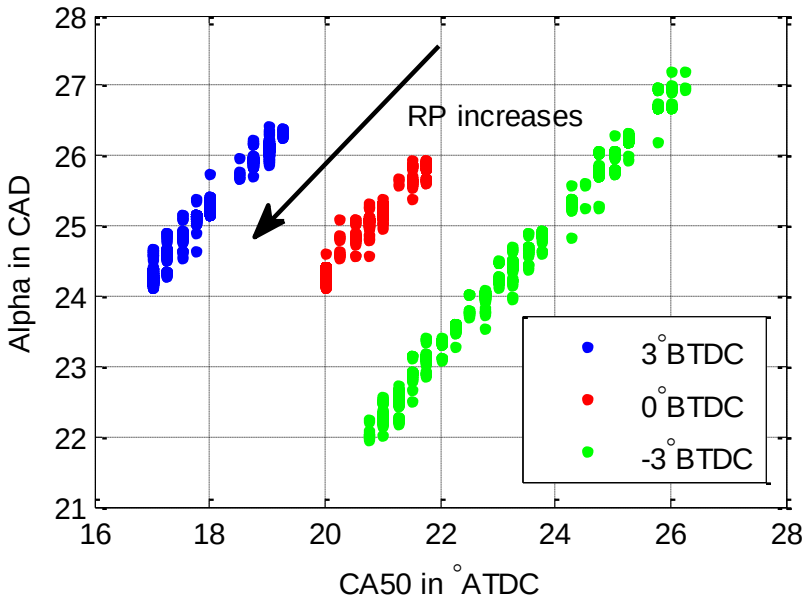

Figure 5.18: Scatter plot of Alpha and CA50 from RP sweep tests at three different SOI when engine was running at: 1400rpm, 400Nm

5.3.4 Effects of Engine Speed and Torque

In order to know in what way CA50 and Alpha vary with engine operating point, a speed sweep test from 1000rpm to 1600rpm was conducted whilst the engine torque was kept at 400Nm, the SOI at 3°BTDC and the RP at 86MPa. The pattern of variation of CA50, Alpha and NO_x emissions with speed can be seen in Figure 5.19.

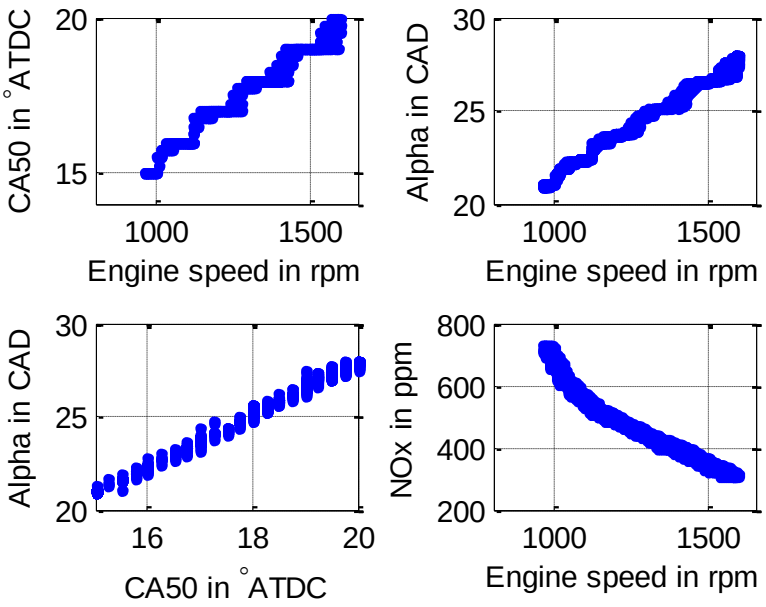

Figure 5.19: CA50, Alpha and NO_x when engine speed vary and engine torque is kept constant at 400Nm

Figure 5.19 illustrates that both CA50 and Alpha increase when engine speed increases and NO_x emissions decrease. CA50 and Alpha increase with engine speed because the diffusion dominated combustion process requires more crank angle degrees at constant load and RP conditions. The reason that NO_x emissions fall with an increase in engine speed is that the time available for the combustion process decreases as engine speed increases, giving a lower formation time for NO_x even though the time for the diffusion dominated combustion process remains the same.

The relationships of fuel rate and soot emissions with engine speed are shown in Figure 5.20. As engine speed increases, higher mechanical friction and less combustion efficiency result in higher fuel consumption. Below 1300rpm, soot emissions fall slightly as speed increases. However, above 1300rpm, soot emissions increase rapidly with the increase of engine speed. This may be due to the relative motion of fuel spray and the piston crown which changes with engine speed. A more precise understanding of this nonlinear feature requires further exploration work which lies outside the scope of this study. The obvious increase of soot with engine speed increase after 1300rpm can be explained as the shorter time after diffusion combustion, giving less time for soot oxidation.

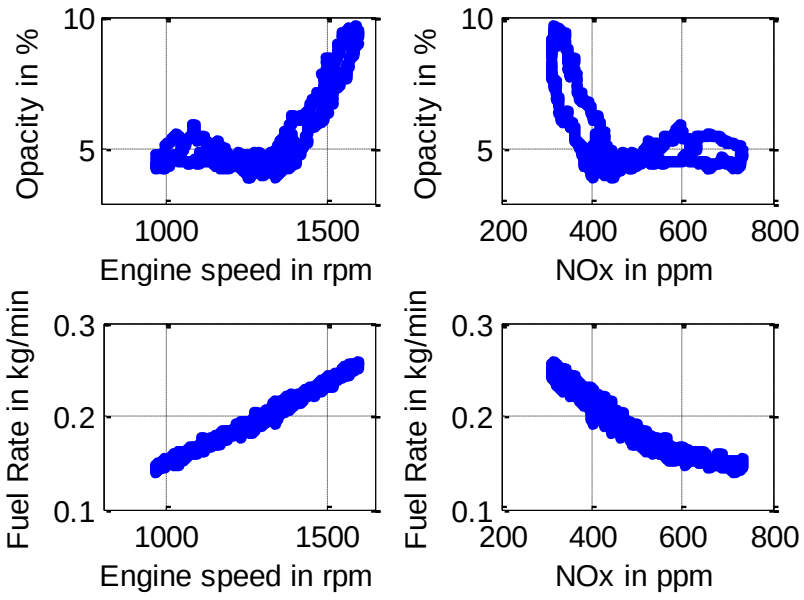

Figure 5.20: Soot, Fuel rate and NO_x as engine speed varies and engine torque is kept constant at 400Nm

When trying to experimentally explore the effect of load on engine emissions and fuel economy, it was found to be practically impossible to fix RP for a wide load sweep because of the very poor soot and or NO_x emissions that would occur

at some load condition. Consequently, two engine load points were compared to show the effect of torque on CA50, Alpha and emissions. Figure 5.21 shows CA50, Alpha, soot and NO_x emissions and fuel rate from the SOI sweep test with two different load points with RP fixed at 76MPa.

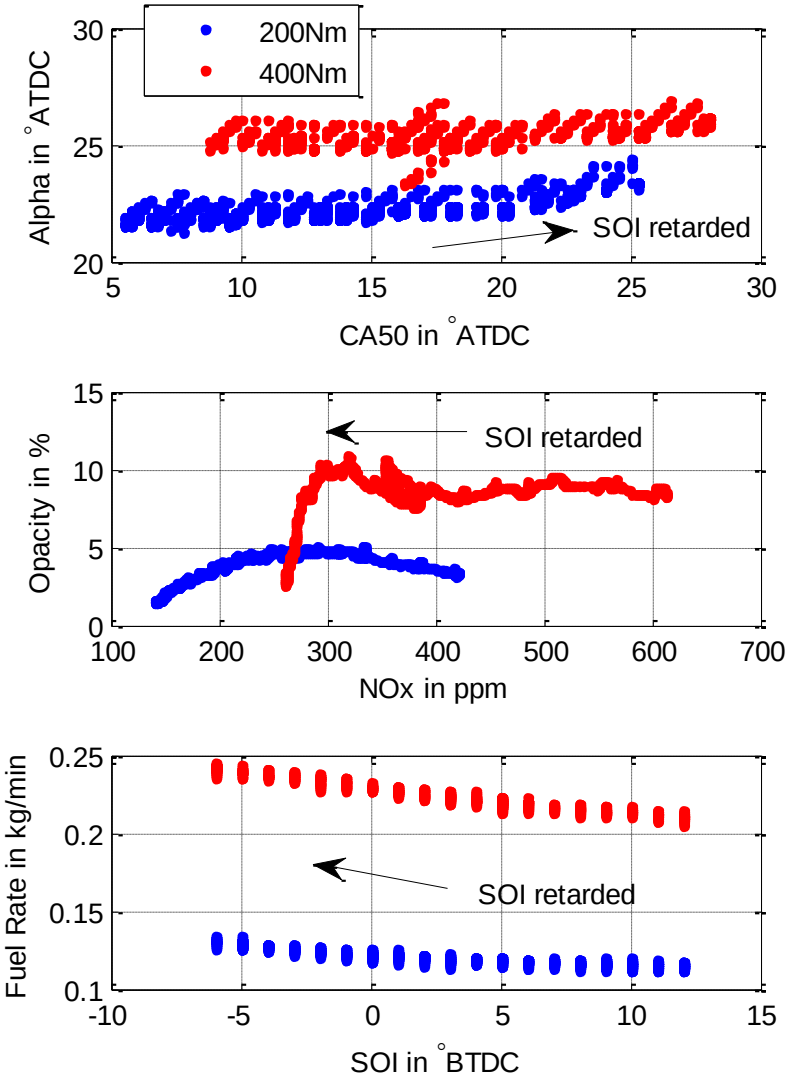

Figure 5.21: Alpha versus CA50, Opacity versus NO_x and Fuel Rate versus SOI from SOI sweep tests at 1400rpm, two load cases: 200Nm and 400Nm

It can be seen that both CA50 and Alpha at 400Nm load are greater than those observed at 200Nm. This is simply due to the injection duration time at higher engine loads being greater than that at lower engine loads when RP is kept constant. Since more fuel is injected at higher engine loads, NO_x and soot emissions are also higher in value at higher engine loads when other engine control variables are kept the same. The best way of evaluating and comparing emissions is using the emission values normalized to engine power output. However, in this study, only absolute values of emissions were compared

because the comparison was carried out between two control systems of the same engine running at the same transient.

Meanwhile, at higher engine load, the longer the combustion process, the longer the period of high combustion temperature resulting in higher NO_x emissions. However, the second plot in Figure 5.21 indicates that both NO_x and soot emissions at the 400Nm load condition were even lower than those at 200Nm load when SOI was significantly retarded. This appears to indicate that the effect of very late combustion on emissions surpasses the effect of increased fuel mass on emissions. At this very late combustion, there is heavy penalty on fuel consumption; see the third plot in Figure 5.21.

This experimental study of the relationships for the two fuel-path inputs (SOI and RP) to the two engine combustion variables (CA50 and Alpha) reveals that it is feasible to develop a 2I2O feedback control system that uses the measured CA50 and Alpha to make automatic, online adjustments to both SOI and RP. The nature of the increases in CA50 and Alpha with both speed and load indicates that the control setpoints of CA50 and Alpha should be designed to change according to both engine speed and load.

5.3.5 Control System Design

The block diagram of this 2I2O closed-loop control system for online adjustment of SOI and RP is shown in Figure 5.22.

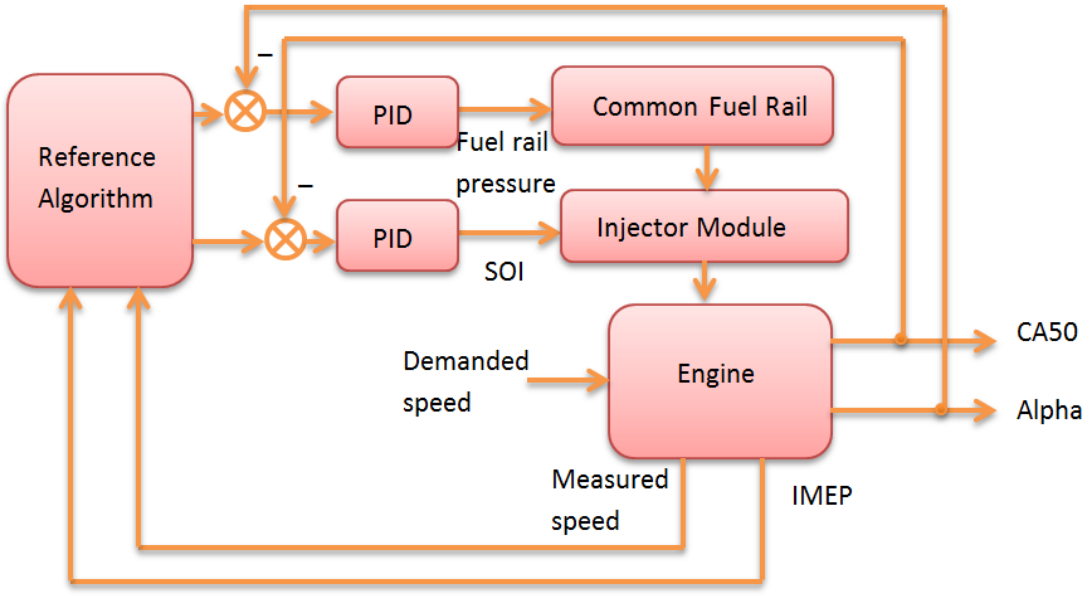

Figure 5.22: Block diagram of online start of injection and fuel rail pressure adjustment system

This system is a decentralized PID control system but it can also be designed as a multi-variable control system to further improve transient control performance. There are three key parts in this control system. The first is the estimation of three combustion parameters based on combustion cylinder pressure trace. The three combustion parameters are CA50, Alpha and IMEP. CA50 and Alpha are used as feedback variables to adjust SOI and RP. IMEP is used as a variable representing the engine load that is one of the inputs to the reference generating algorithm. They are all estimated from real-time measured cylinder pressure data. The computation algorithms involved are shown in the following equations:

$$\frac{dQ}{d\theta} = \frac{\gamma}{\gamma-1} p_c(\theta) dV(\theta) + \frac{1}{\gamma-1} dp_c(\theta) V(\theta) \quad (\mathbf{5.5})$$

$$\int_{SOC}^{CA50} dQ = 0.5 \times \int_{SOC}^{EOC} dQ \quad (\mathbf{5.6})$$

$$IMEP = \frac{\int p_c(\theta) dV(\theta)}{V_d} \quad (\mathbf{5.7})$$

$$\text{Alpha} = CA50 - SOI \quad (\mathbf{5.8})$$

Where, dQ is heat release rate. $\mathrm{V}(\theta)$ is cylinder volume at θ crank angle degree. γ is the ratio of specific heats. $\mathrm{V_d}$ is cylinder displacement volume. SOC is the crank angle degree of start of combustion. EOC is the crank angle degree of end of combustion. SOC and EOC were both estimated from heat release curve which is the integral of heat release rate $\frac{dQ}{d\theta}$.

The second key part of the control system is represented by the two single loop PID controllers. From the experimental study of dynamics from SOI, RP to CA50 and Alpha using system identification technique, the dynamic models for controller design can be as simple as first order transfer functions. The gain and time constant of the transfer function are taken as the average value from the identified model of different engine operating points since they differ little between the different engine operating points. The average transfer function from SOI to CA50 and RP to Alpha are shown in Equation (5.9) and Equation (5.10) respectively.

$$\frac{CA50}{SOI} = \frac{-1}{s+1} \quad (\mathbf{5.9})$$

$$\frac{Alpha}{RP} = \frac{-0.2}{s+1} \quad (\mathbf{5.10})$$

The parameters of the two PID controllers were designed based on the above two dynamic models and were then tuned online to give the control system optimal performance in a step response.

Another key part in this control system is the algorithm which is used to generate reference setpoints for CA50 and Alpha using measured engine speed and IMEP as inputs. This reference algorithm is directly related to engine emissions and fuel consumption performance. A linear algorithm was used in this study. It can also be nonlinear algorithm or a look-up table. Equation (5.11) and Equation (5.12) are the equations for computing the reference for CA50 and Alpha respectively:

$$r_{CA50} = a_0 \times N + a_1 \times IMEP \tag{5.11}$$

$$r_{Alpha} = b_0 \times N + b_1 \times IMEP \tag{5.12}$$

Where, a_0, a_1, b_0, b_1 are constants, N is measured engine speed, IMEP is indicated mean effective pressure, which is estimated from measured cylinder pressure using Equation (5.7). The choice of constants a_0, a_1, b_0, b_1 is based on the choice of a point on two trade-off relationships, (i) between fuel consumption and total NO_x emissions and (ii) between NO_x emissions and soot emissions. For example, bigger $\mathrm{r}_{\mathrm{CA50}}$ will result in later combustion with which the engine would have better NO_x emissions but worse fuel consumption while bigger $\mathrm{r}_{\mathrm{Alpha}}$ will result in lower fuel rail pressure that in turn will make the engine have less NO_x emissions but higher soot emissions. In this study, these four parameters a_0, a_1, b_0, b_1 were selected empirically. However, they can be optimally selected using optimization technology in the future work.

5.3.6 Engine Test Results

A simple speed and load transient engine test was programmed in the test bed control system (Cadet V12) for evaluation of the engine NO_x and soot emissions and also the fuel consumption. A comparison was performed between look-up table based SOI and RP control system and the closed loop CA50-Alpha based SOI and RP online adjustment control system. The minimum torque was selected above 50Nm to avoid the range in which the estimation of CA50 is less reliable. The maximum torque was in the engine median load range.

Measured speed and load traces during the transient test for both look-up table control system and feedback control system are plotted together in Figure 5.23. NO_x and soot emissions and also fuel flow rate for these two different

control systems are plotted together for comparison in Figure 5.24. In these figures, *LT* refers to engine lookup table control system and *CL* refers to the 2I2O, CA50-Alpha feedback control system. Look-up tables for SOI and RP were copied from the production engine ECM control software implemented in the LabVIEW real-time PXI control system [171]. In both control systems during the transient test, the VGT vane position was fixed at 50% and the EGR valve was closed. The constants in reference algorithm were: $a_0 = 0.0144$, $a_1 = 0.25$, $b_0 = 0.0102$, $b_1 = 0.2$. Only pressure data from cylinder No. 2 was used to estimate CA50 and Alpha. The SOI controller output was applied to all cylinders and the fuel injection mode was two-pulse.

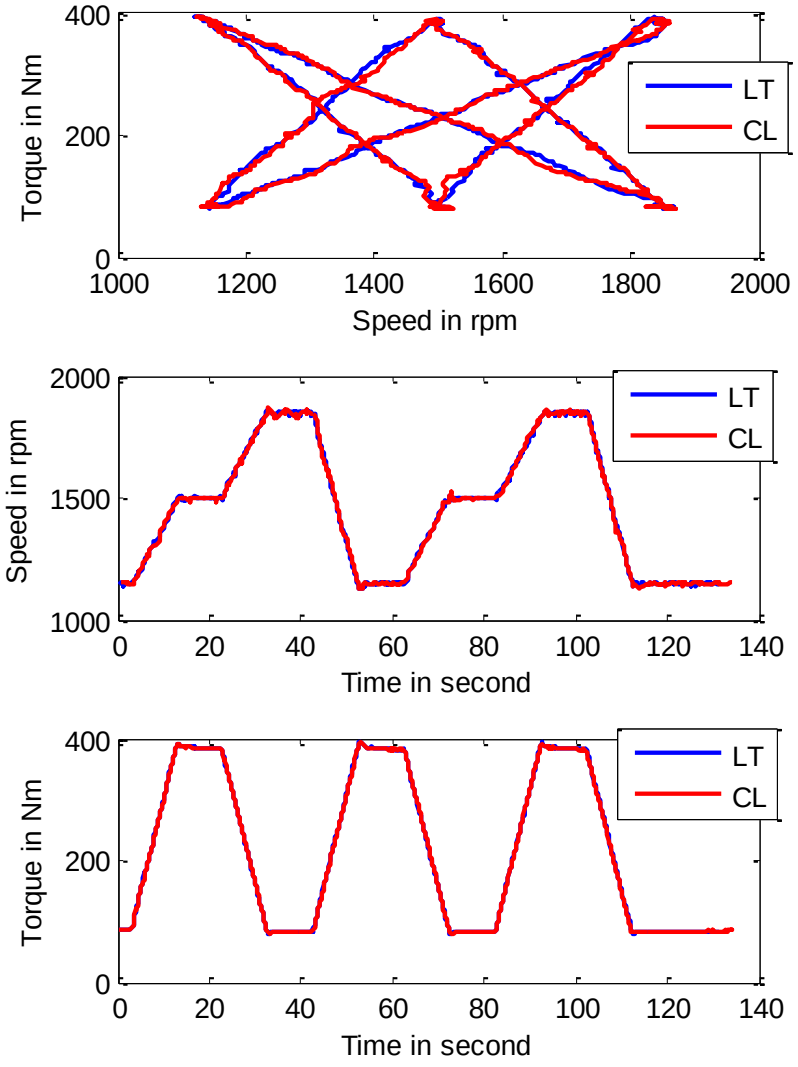

Figure 5.23: Engine speed and torque of engine transient test

From Figure 5.24, it can be seen that total NO_x and soot emissions are both reduced by closed-loop control. Fuel consumption is nearly the same except at

around 100 seconds at which engine is at a high-speed and high-load operating condition where the closed-loop control system offers a small improvement.

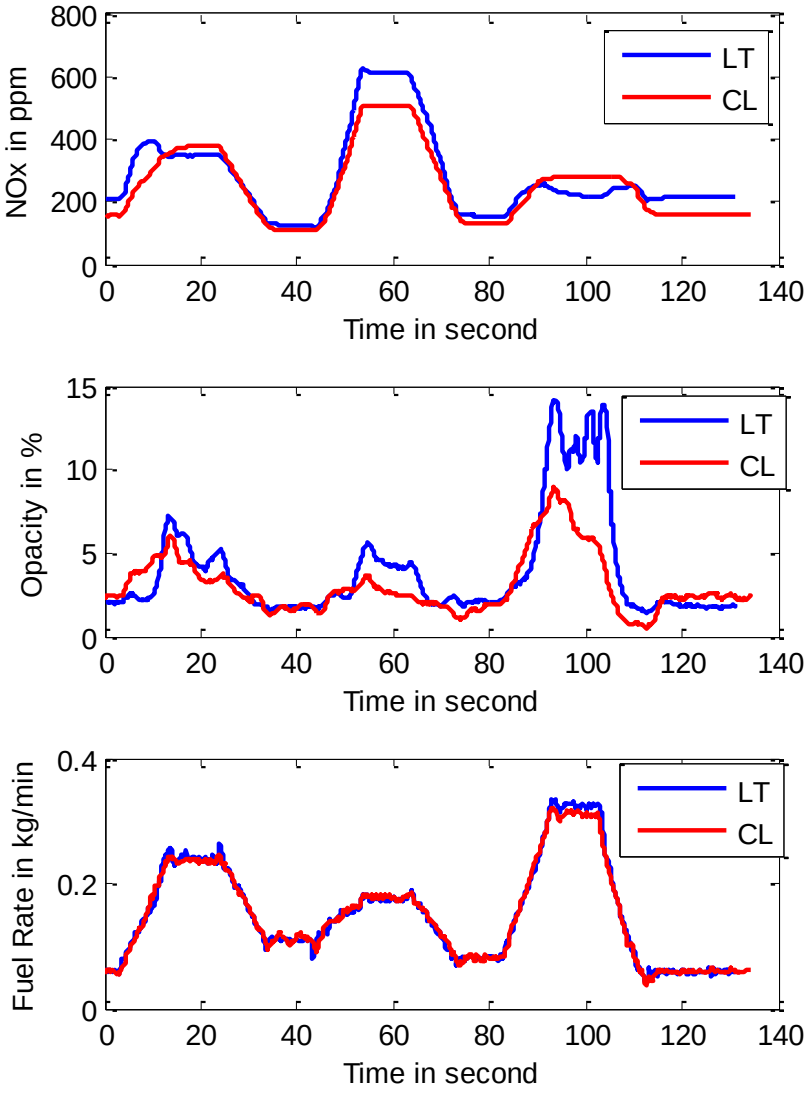

Figure 5.24: NO_x and smoke emission and also fuel consumption during engine transient test (LT=Real Time system lookup table control system; CL=Closed Loop SOI and RP online adjustment system)

However, at this same operating point the NO_x emissions of the closed-loop control system are worse than those of the look-up table control system. The differences may be explained by the use of later combustion phasing for these operating points in the look-up table. As both CA50 and Alpha reference algorithms of the proposed closed-loop control system are linear, it cannot be guaranteed that at any operating point, engine emissions and engine fuel consumptions are always less than the look-up table control within which the calibration would normally be related to operating conditions through a non-linear relationship.

However, the advantage of this closed-loop control system to be able to maintain the desired trade-off in total emissions and fuel consumption is very obvious, even without highly optimised CA50 and Alpha setpoints. Figure 5.25 is the scatter plot of NO_x and soot emissions for both systems. It shows that with the CA50 and Alpha feedback control system, NO_x and soot are controlled to a smaller space relative to the lookup table control system.

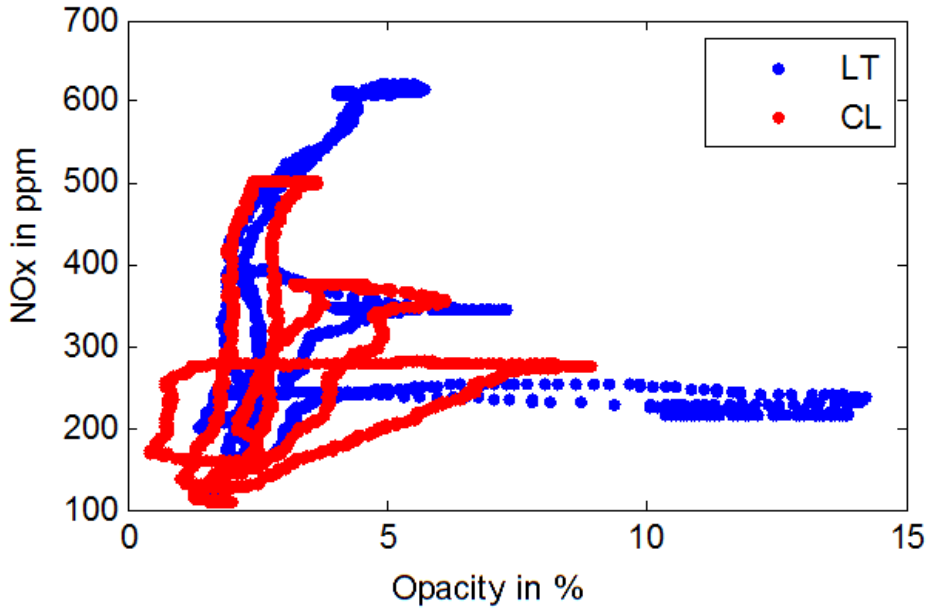

Figure 5.25: NO_x versus soot during engine transient test (RT=Real Time system lookup table control system; CL=SOI and RP online adjustment system)

Figure 5.26 shows that the relationships between CA50 and Alpha of both systems are nearly linear. This is a very revealing result as the slope of CA50 to Alpha of the look-up table control system is steeper than that of the closed-loop control system and results in a bigger Alpha and CA50 range. Those differences imply there is a different balance in engine emissions and fuel consumption achieved for the same engine test cycle between the two control systems. Indeed, the integral of NO_x, soot emissions and also the fuel rate of the closed-loop control system for these experimental engine transient tests are all smaller than those of the open-loop control system.

Even though a linear reference algorithm was used in the design of setpoints for CA50 and Alpha, the engine performance of NO_x, soot emissions and fuel consumption of the SOI and RP online adjustment system are all improved compared with those of the calibrated SOI, RP look-up table control system. There are two significant advantages other than the improved engine performance. One is that within the SOI and RP online adjustment system the

combustion process is monitored and controlled with feedback. The other is that the tedious calibration work of SOI and RP has been reduced to the finding four constant values in the reference algorithm. Since this algorithm is linear, fewer engine tests are therefore required. Consequently, this control method has a highly potential as an alternative to conventional calibrated open-loop look-up table methods.

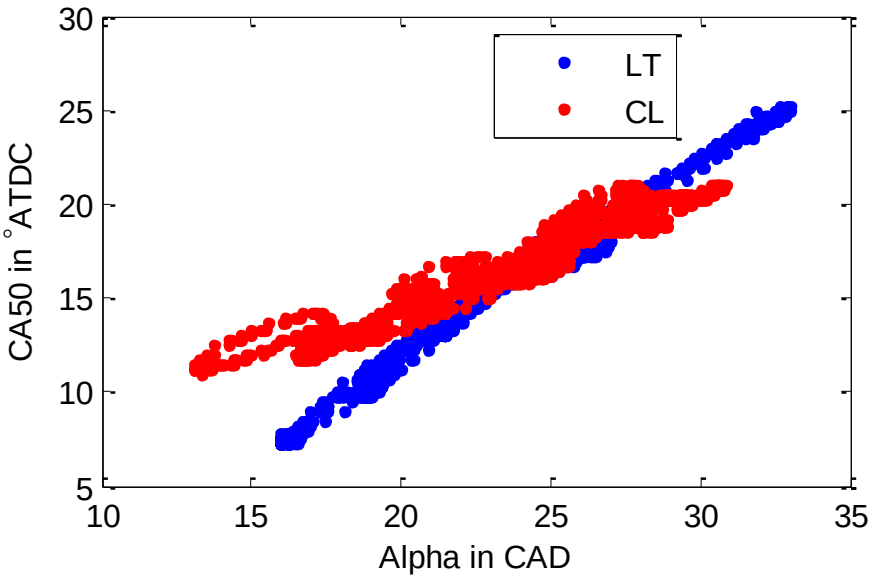

Figure 5.26: CA50 and Alpha during engine transient test (RT=Real Time system lookup table control system; AB=SOI and RP online adjustment system)

5.4 P_{max} and IMEP Control

P_{max} and IMEP represent two other important combustion variables and they are related to the total energy released during combustion. Methods to control P_{max} and IMEP have been explored in this study. In order to have decoupled control inputs for P_{max} and IMEP and also considering the potential of intra-cycle control, a three-pulse fuel injection mode was used. The control input variables were defined previously in Chapter 3, Figure 3.6. An example of measured Injection Current (IC) and cylinder pressure trace for the three-pulse fuel injection mode is shown in Figure 5.27. The three injection pulses are named as *pilot injection*, *main injection* and *post injection* and occur in this order as depicted by the example sequence depicted in Figure 5.27.

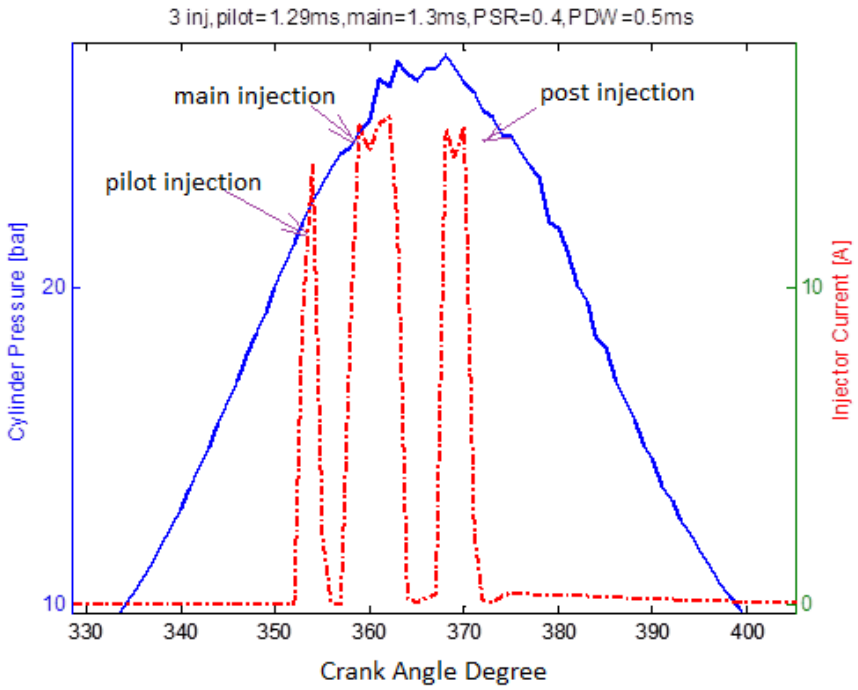

Figure 5.27: Measured injection current and cylinder pressure

5.4.1 Variation with Dwell Time: 'Dragon Pattern'

When the real-time system engine speed governor was disabled and the individual engine cylinder fuel injection quantity was fixed; the engine speed was controlled in closed-loop by the dynamometer (Cadet V12) control system using load i.e. the dynamometer controller was set to *speed control mode* and the engine-dynamometer set speed was fixed; thus for any change in combustion efficiency, shaft torque of the engine would also change but the dynamometer controller would counter this by adjusting the load to maintain the same engine-dynamometer speed. In this way, it was possible to evaluate the effects of changes in the 3-mode injection pattern of Figure 5.27 on combustion efficiency and hence IMEP and also engine shaft torque at constant engine speed. Utilising this control configuration, an interesting pattern of variation in the combustion variables P_{max} and IMEP was observed in response to sweeps in either the dwell time or the Post Dwell Time (PDW). DW is the time interval from the end of pilot injection and the start of the main injection. PDW is the time interval from the end of main injection to the start of post injection.

Figure 5.28 (a) and (b) presents the five cylinders' IMEPs varying with the DW and PDW respectively (the IMEP of cylinder 6 is missing as the cylinder pressure transducer installed in cylinder 6 was not functioning). The engine was running at a constant 1200rpm for these experiments and the other engine

control inputs such as SOI, RP, fuel ratio, EGR valve position and VGT vane position were also kept constant. The cylinder 1 IMEP is lower than for the other cylinders due to the cylinder 1 injector being a special instrumented injector (needle lift and sac volume pressure) supplied by Caterpillar. The fuel injection rate of this injector was lower than that of the other injectors for the same injector current signal as a consequence of the modifications made to this injector to fit the installed sensors.

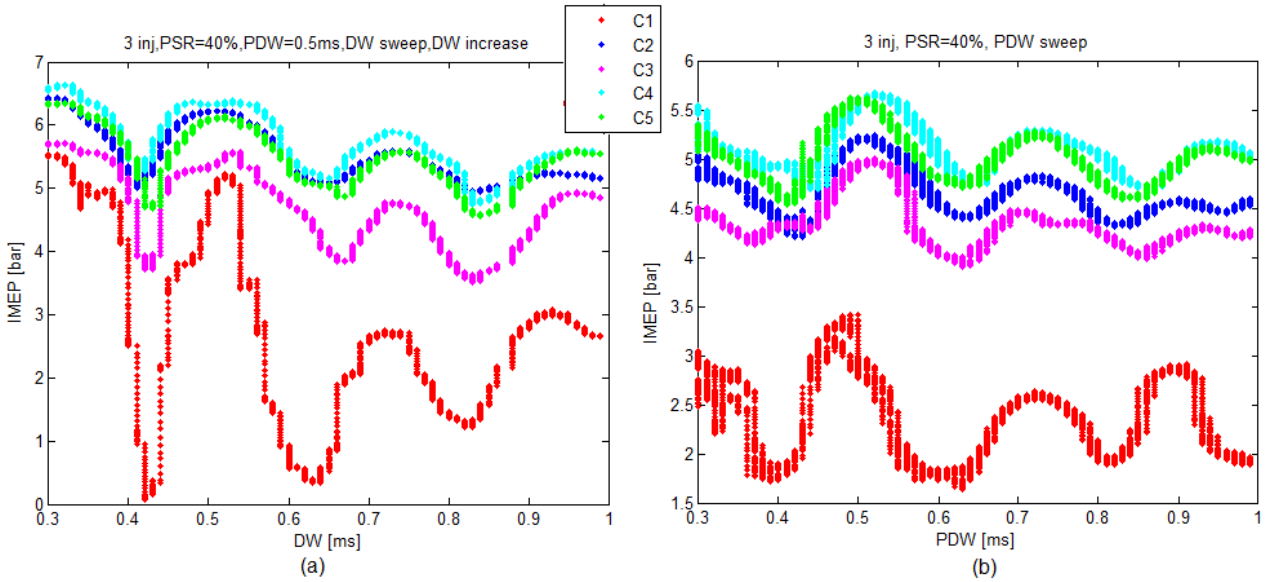

Figure 5.28: Five cylinders' IMEP against DW (a) and PDW (b)

The corresponding measured engine torque is shown in Figure 5.29. The variation patterns of IMEP and torque are the same and are referred to as having a "dragon pattern" because of the resemblance to a Chinese dragon's shape.

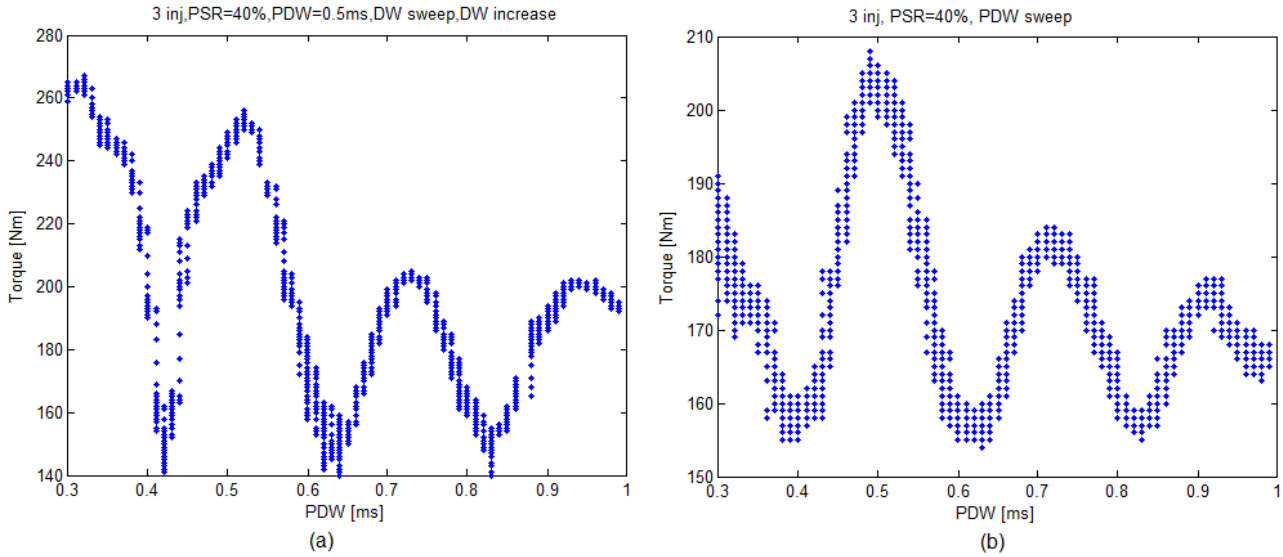

Figure 5.29: Measured engine torque against DW (a) and PDW (b)

Figure 3.30 shows that the variation of P_{max} is similar to that of IMEP during the PDW sweep test.

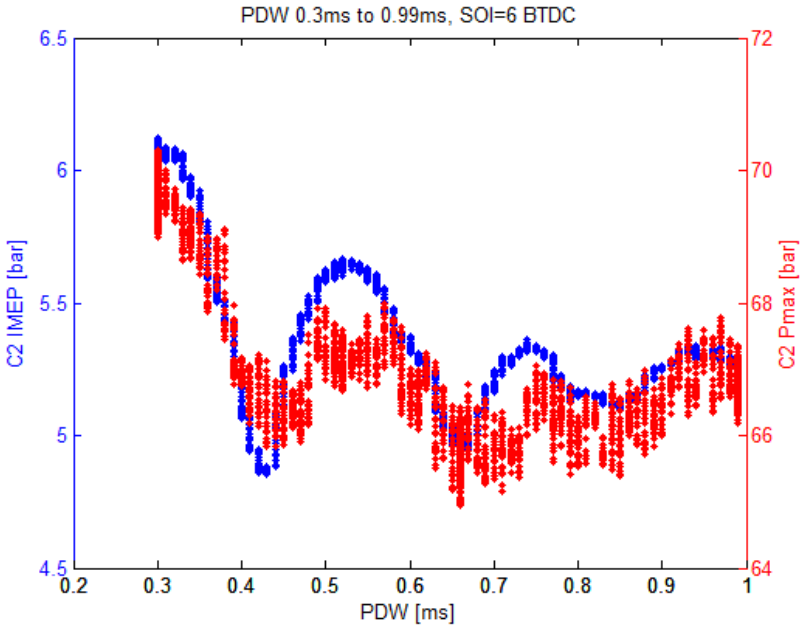

Figure 5.30: P_{max} and IMEP of cylinder 2 against PDW

The cause of the dragon pattern was found to be pressure waves in the fuel rail which represented the combined effect of the rail pressure control action and the fuel injection action. Fuel injection causes the rail pressure to drop while the operation of the fuel pump valve tends to increase rail pressure. Normalized injection current and rail pressure, normalized Needle Lift (NL) and rail pressure for two different PDW values are plotted in Figure 5.31 (a) and (b) respectively.

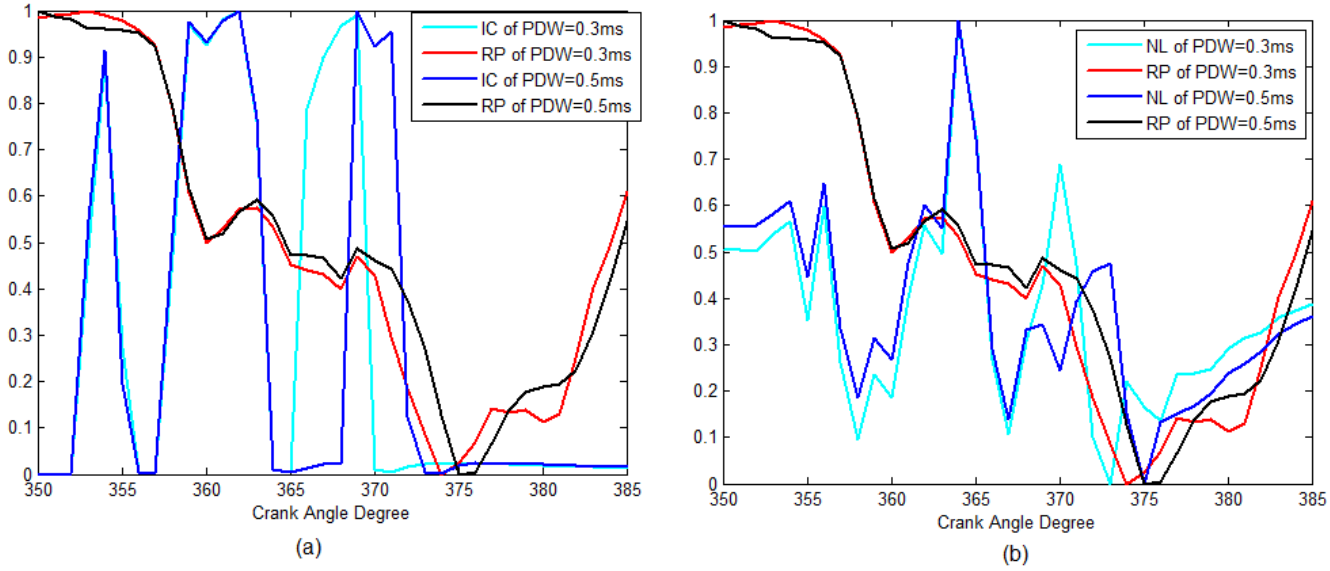

Figure 5.31: (a) Normalized IC and RP; (b) normalized NL and RP of two PDW cases

The needle lift action is observed to be later than injection current as the injector needs time to respond to the injector current and therefore taken together these two signals help to understand what is occurring. In the case where the PDW=0.3ms, the post injection is more advanced compared to that of PDW=0.5ms case. For this retarded post injection case, the need lift is observed to be much smaller and this correlates to the point where the RP suddenly falls between 370 and 375 cycle crank angle degrees. Thus, it would appear that the much smaller needle lift of the retarded post injection case may be caused by the quickly reducing rail pressure.

Figure 5.32 shows the normalized high pressure fuel pump valve drive current and the measured RP of 1000 successive engine steady-state cycles. i_p refers to measured fuel pump valve drive current. p_r refers to measured fuel rail pressure. Note that for the C6.6 engine used in this study, the engine is equipped with a standard C6.6 engine high pressure fuel pump; however the drive signal to the pump is produced by the LabVIEW real-time PXI control system via an adapted DRIVVEN injector driver module [171]. The control of this drive signal replicates as close as possible the original ECM rail pressure control system and also the current profile of the drive signal originally produced by the ECM drive circuitry (i.e. the current amplitude, the peak hold and secondary peak hold periods – the waveform shape illustrated in Figure 5.32) within the capability of the DRIVVEN injector driver module and the FPGA drivers produced by DRIVVEN [171].

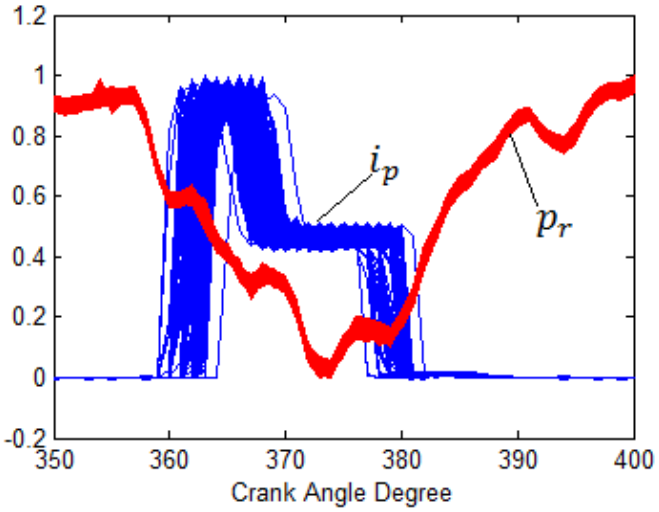

Figure 5.32: Normalized Pump valve drive current and RP of continuous 1000 steady-state engine cycles

The main trend of the rail pressure signal in Figure 5.32 is a repeat of that illustrated in Figure 5.31, in that it shows a decrease during the entirety of the fuel injection period which is approximately from 350 to 375 crank angle degrees. However, there are two small rail pressure peaks near 363 and 370 crank angle degrees. Each of these two small rail pressure peaks represent the combined effect of fuel pump valve opening, which corresponds to high pressure fuel pumped into the fuel rail, followed by a fuel injection: DW for the first peak and PDW for the second peak. Thus, the post injection fuel is under different rail pressure conditions depending upon the PDW value. Although this rail pressure difference is small, Figure 5.29 shows the actual change in measured torque caused by the change in the applied PDW is quite significant. The combustion process therefore acts like an amplifier, accentuating the effect of rail pressure variations.

To aide clarity, the fuel common rail and fuel injection system of the C6.6 test engine is shown in Figure 5.33 and Figure 5.34.

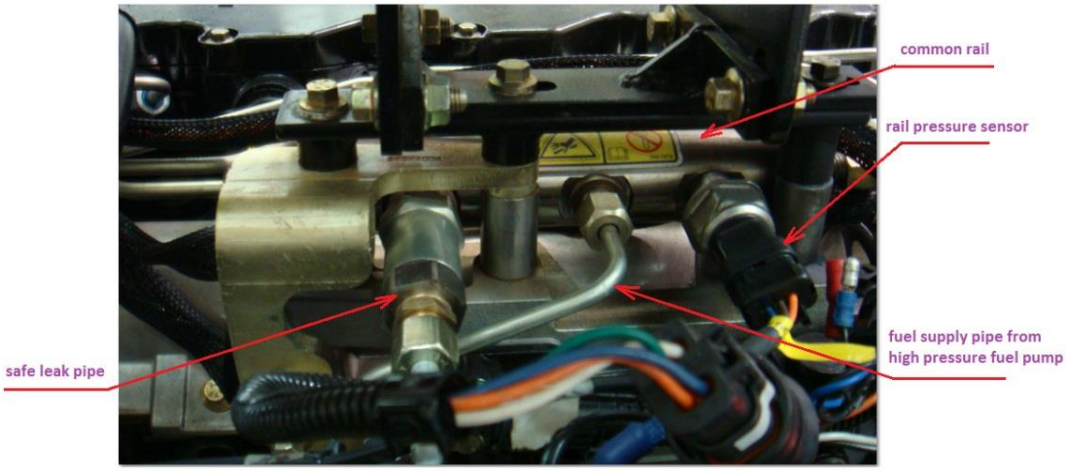

Figure 5.33: C6.6 diesel engine common fuel rail

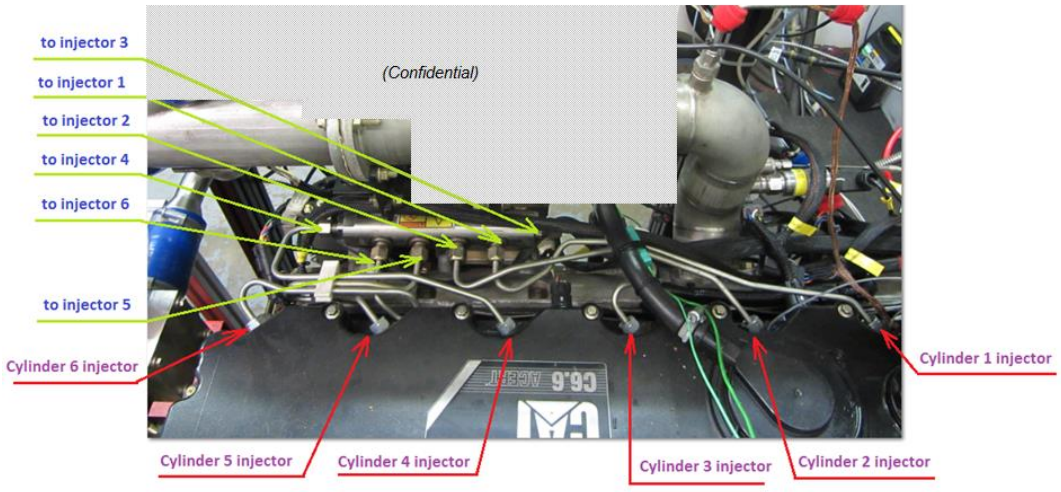

Figure 5.34: C6.6 diesel engine injection system

5.4.2 IMEP Control Using PDW

The phenomenon of the change of IMEP with PDW that was discussed in the previous section can be utilised to develop an IMEP feedback control system that aims to reduce combustion variation. This is a one input one output closed-loop control system. It was implemented for cylinder 1 IMEP control for demonstration. In Figure 5.28 (b), it can be observed that when PDW varies from 0.5ms to 0.6ms, the IMEP of cylinder 1 varies from 1.7bar to 3.2bar. Therefore, the closed-loop control system was designed using PDW in the range from 0.5ms to 0.6ms to control cylinder 1 IMEP range from 1.7 bar to 3.2bar. A simple PI controller was applied. The parameters of the PI controller were tuned online. The result of experimental step change response test of this closed-loop control system is shown in Figure 5.35. Step changes are from 3bar to 2.1bar and then back. The Engine was running at 1200rpm steady-state, the same for the results discussed in Section 5.4.1 previously.

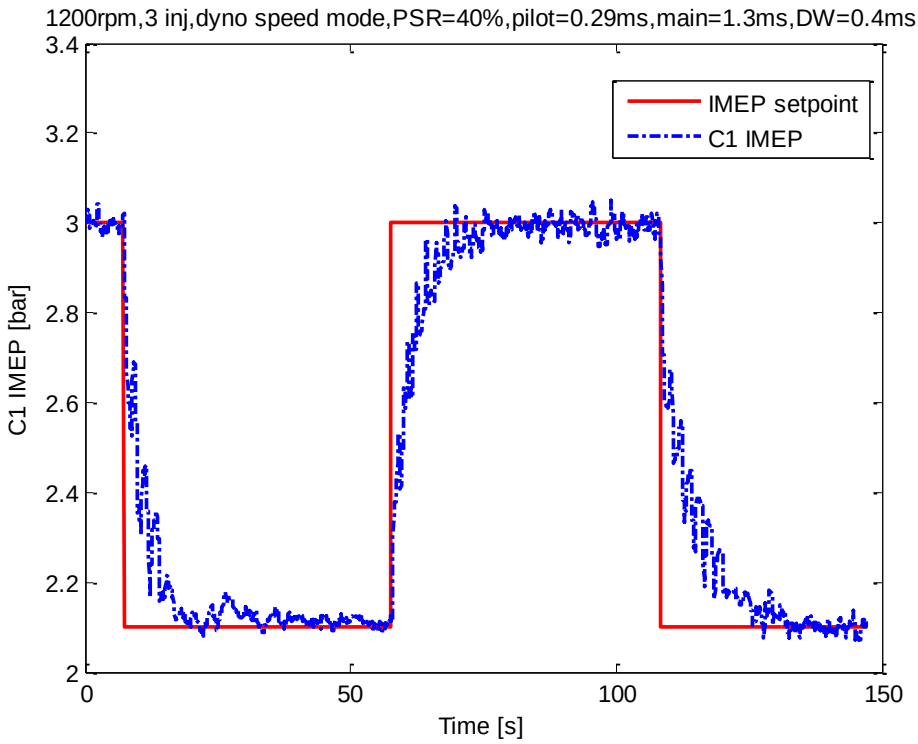

Figure 5.35: Step response of Cylinder 1 IMEP in PDW-to-IMEP control system

Figure 5.35 shows that the step change tracking performance for IMEP is good. This indicates that such a control system has the ability to control IMEP within at least a limited range using the variation in the rail pressure wave caused by different PDW values. Measured IMEP values of cylinder 1 with feedback control and without feedback control under the same engine steady-state

conditions are shown in Figure 5.36 (a). For the feedback control case, the control results of two IMEP setpoint values, 3bar and 2.2bar are shown in Figure 5.36 (a). Obviously, the variation of IMEP without feedback control is much more significant than in the case of IMEP with feedback control. This indicates that the feedback control of IMEP based on the PDW variable can increase combustion stability. The Coefficient of Variation (COV) of IMEP which is a commonly accepted index of combustion stability is defined in Equation (5.12). Computed COV values of 300 continuous IMEP measurements in Figure 5.36 (a) are listed in Table 5.3. COV of IMEP with closed-loop control is much lower than that of IMEP without closed-loop control.

$$COV(IMEP) = \frac{\sigma(IMEP)}{\mu(IMEP)} \times 100\% \qquad (\mathbf{5.12})$$

Where, $\sigma(\mathrm{IMEP})$ is the standard deviation of IMEP and $\mu(\mathrm{IMEP})$ is the mean value of IMEP.

Figure 5.36 (b) shows PDW variables for the corresponding three cases shown in Figure 5.36 (a). PDW is fixed at 0.6ms for IMEP without closed-loop control. This illustrates the range of the control action for PDW as it is automatically adjusted by the IMEP feedback PI controller for IMEP 3bar and 2.2bar feedback control. The proportional and integral terms were fixed at values that were determined from a manual tune of the terms to achieve stable IMEP control for the engine steady-state conditions for the result presented in Figure 5.36.

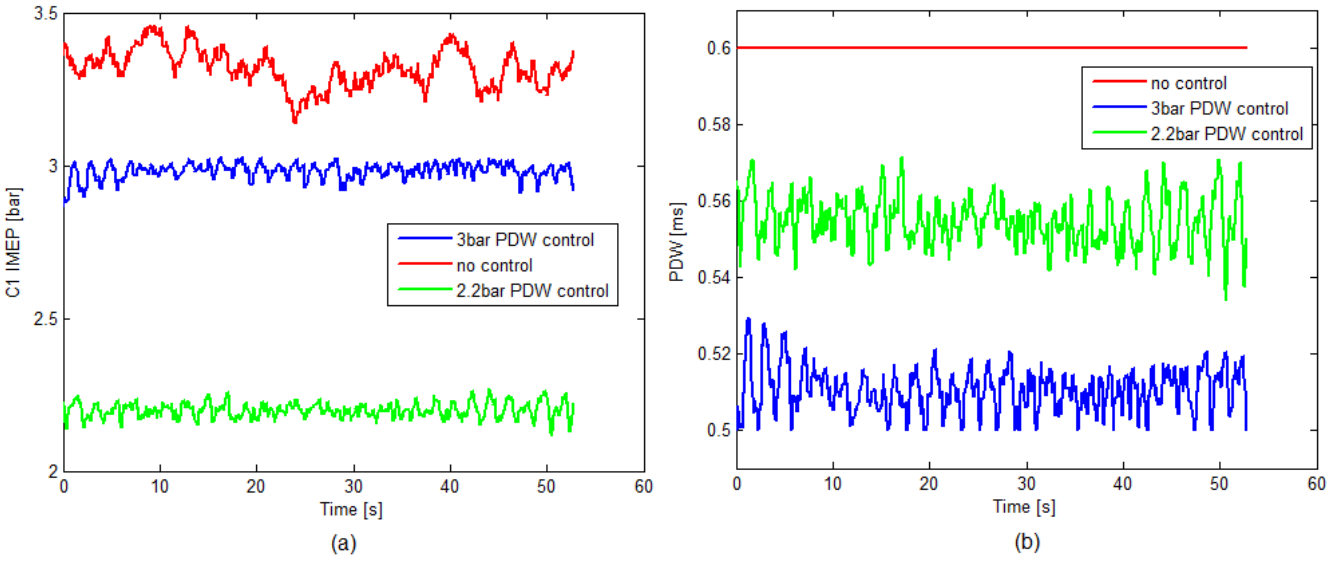

Figure 5.36: (a) IMEP of Cylinder1 with and without closed loop control; (b) PDW with and without IMEP control

Table 5.3: Covariance of IMEP with and without feedback control

	Without IMEP CL control	IMEP CL control 3bar	IMEP CL control 2.2bar
COV	1.85%	0.85%	1.12%

5.4.3 IMEP Control Using Fuel Injection Quantity

IMEP closed-loop control using fuel-path variables not only can improve combustion stability, it can also improve the disturbance rejection ability of combustion process. The most reliable control input for IMEP closed loop control is the fuel injection quantity. Closed loop control of IMEP in Cylinder No 1 using injection duration as the control variable has been developed. The controller is of PID format. Other cylinders have no IMEP closed-loop control and form a useful comparison. Fuel injection quantity is represented by injection total pulse duration in units [ms]. Engine speed was controlled in closed loop at 1200rpm by the dyno control system as described in Section 5.4.1. The disturbance sources are also fuel-path inputs. They are SOI, DW, and RP. The IMEP of five cylinders and the corresponding disturbance and control input signals are shown in Figure 5.37, Figure 5.38 and Figure 5.39.

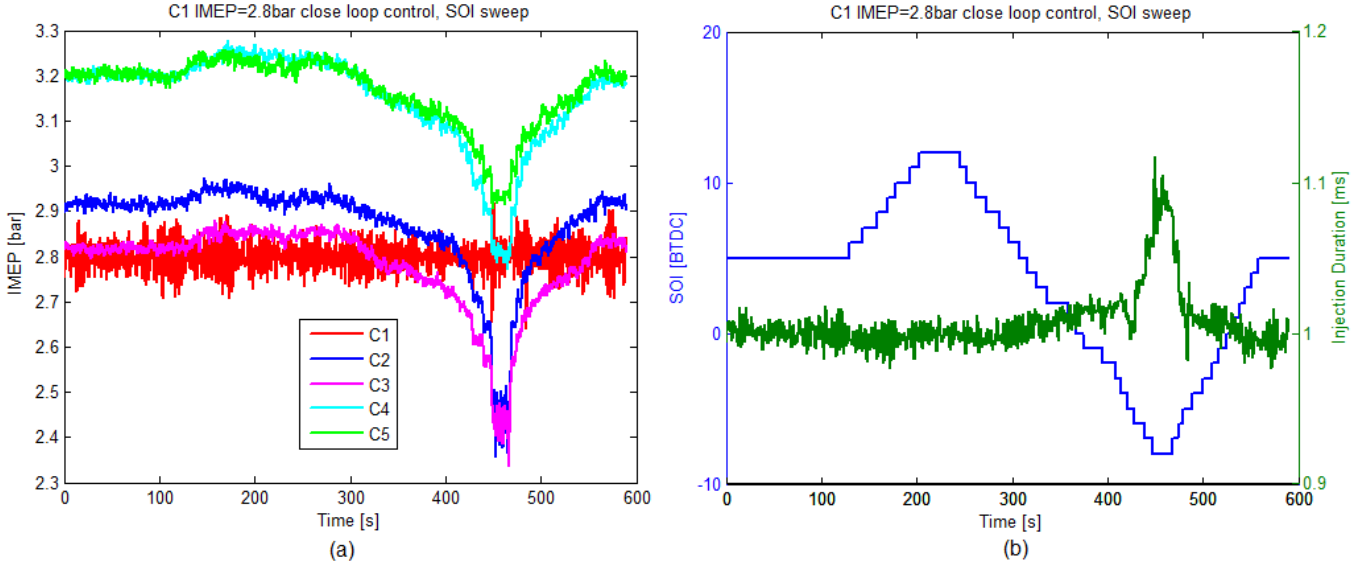

Figure 5.37: (a) Five cylinders' IMEP during SOI disturbance; (b) SOI disturbance signal and injection duration for cylinder 1

It can be seen from IMEP curves of cylinder 2, 3, and 4, that the disturbance inputs SOI, DW and RP all cause large IMEP variations. However, the IMEP of Cylinder 1 is kept constant under all of these three disturbance because the feedback control system adjusts the fuel injection duration (proportional to fuel injection quantity) to automatically keep IMEP to its reference value.

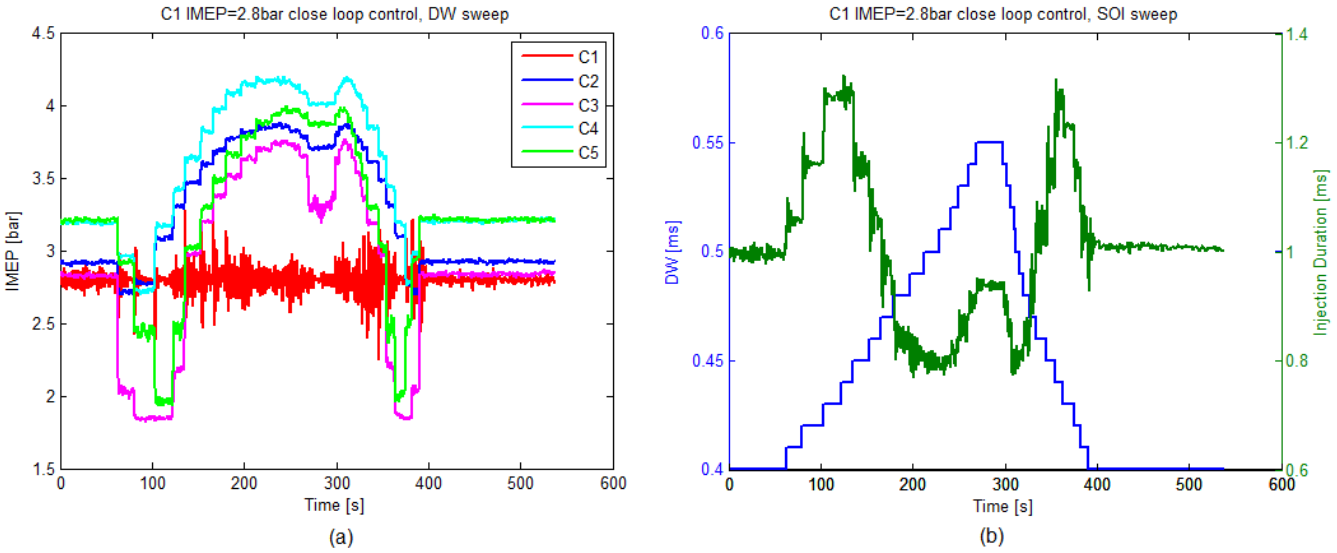

Figure 5.38: (a) Five cylinders' IMEP during DW disturbance; (b) DW disturbance signal and injection duration for cylinder 1

The control response is faster than the conventional speed governor in rejecting disturbance as it measures and feeds back the IMEP of each combustion cycle.

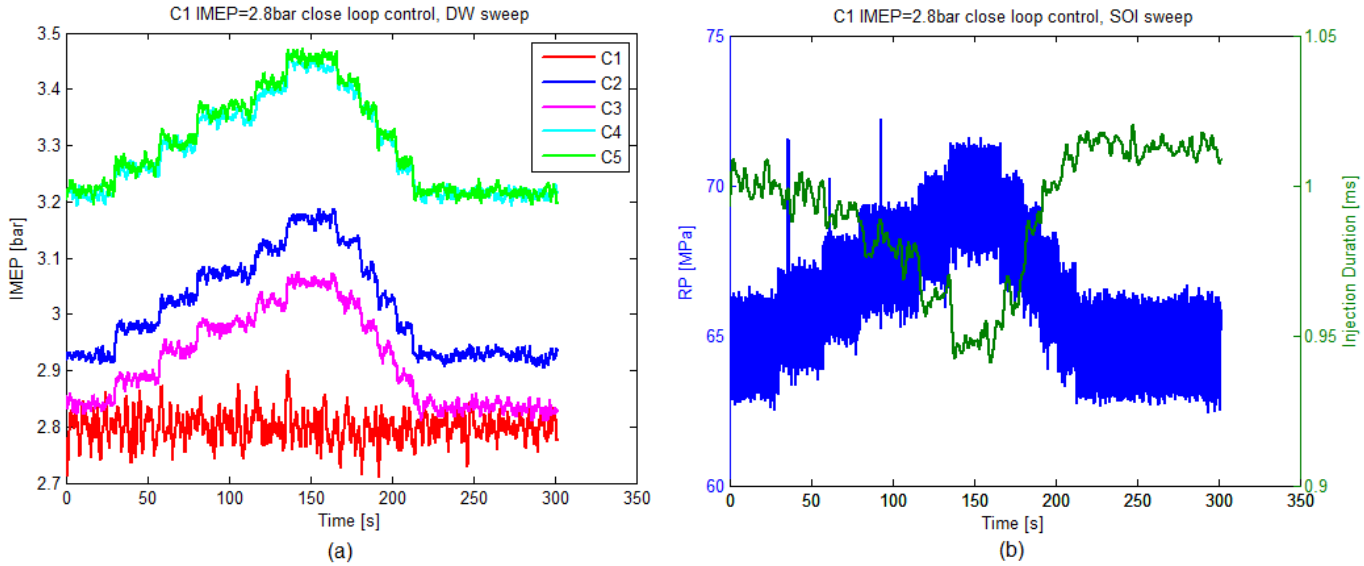

Figure 5.39: (a) Five cylinders' IMEP during RP disturbance; (b) RP disturbance signal and injection duration for cylinder 1

5.4.4 Two Loops Speed Governor

The algorithmic speed governor of the C6.6 test engine implemented in the LabVIEW real-time PXI control system [171] is a one loop feedback control system. The control input is fuel injection quantity. In order to use the advantages of IMEP closed loop control in improving the disturbance rejection capability,

cylinder consistency and combustion stability of the combustion process, a two loops speed governor system has been implemented and evaluated. The block diagram of the control system is shown in Figure 5.40.

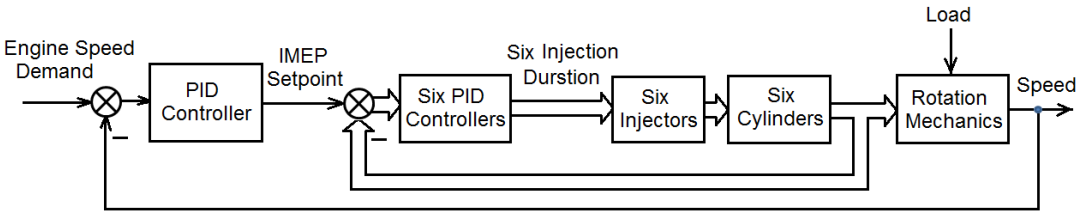

Figure 5.40: Block diagram of two-loop engine speed governor

The two loop governor consists of six inner loops (one for each cylinder IMEP control) and one outer loop which is for engine speed closed-loop control. The controllers used in this control system are all PID controllers. The output of the engine speed feedback PID controller is fed to the six IMEP PID controllers as IMEP setpoint input. The measured feedback variables for the six IMEP PID controllers are the IMEP values estimated from the six measured cylinder pressures respectively. Since the cylinder pressure sensor of cylinder 6 was not available, the IMEP of cylinder 6 was controlled by the IMEP controller of cylinder 5. When this two-loop engine speed governor works together with the 2I2O SOI, RP online adjustment system, its control structure is like that in Figure 5.41.

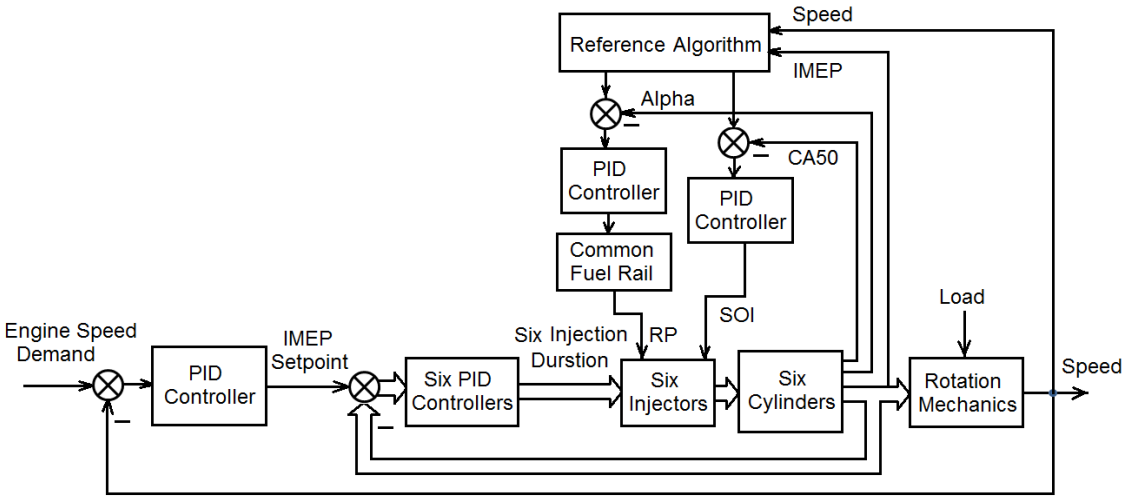

Figure 5.41: Block diagram of two-loop speed governor together with CA50 and Alpha control system

There are total nine PID feedback control loops. Eight of them are based on estimated combustion variables such as CA50, Alpha and IMEP from measured cylinder pressure data. It can be considered as a multi-loop combustion process control system. All six cylinders share one CA50 controller and one Alpha PID

controller, Section 5.3.5. The measured feedback CA50 or Alpha value was the average value of the individual values of the five cylinders. Experimental observations suggested that the deviation of CA50 among the cylinders was not so large. As a consequence, it was not necessary to have six control loops of SOI feedback control. No doubt, if the crank angle degree resolution could be increased, the closed-loop control of CA50 for individual cylinder would be more accurate than single loop of average CA50. When using RP to control Alpha, there is only need for one closed-loop as all six cylinders share a common fuel rail.

A special speed and load transient test was carried out using the multi-loop combustion control system shown in Figure 5.41. The dynamometer was set for torque control mode. Engine speed was programmed to ramp up and down between 1150rpm and 1850rpm with the speed ramp rate set to 30rpm/s. Meanwhile, torque was programed to ramp up and down between 100Nm and 400Nm with a ramp rate of 30Nm/s. During this transient test, the CA50 setpoint was fixed at 15 BTDC and the Alpha set point was generated using the linear algorithm in Equation (5.12) with constant parameters: $b_0 = 0.0156$, $b_1 = 0.15$. For comparison, the same speed and load transient test was conducted using the LabVIEW real-time PXI control system [171] which has only one single loop engine speed closed loop control. The C6.6 test engine was otherwise the same.

Measured speed and load for both control systems are plotted together in Figure 5.42 (a) and (b) respectively.

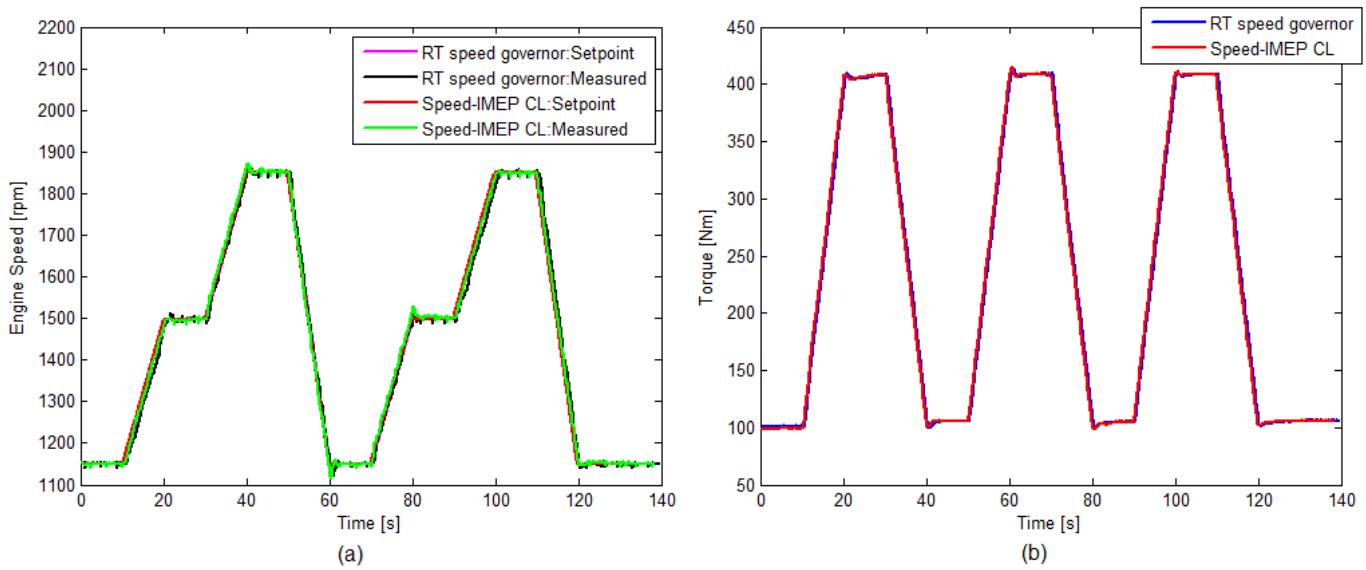

Figure 5.42: (a) Measured engine speed and setpoint for the RT control system and speed-IMEP two loop control system; (b) Measured torque for the RT control system and speed-IMEP two-loop control system

It can be seen that the speed control performance is similar for these two control systems. The IMEP of five cylinders of the RT control system and the speed-IMEP two loop control system are plotted in Figure 5.43 (a) and (b) respectively.

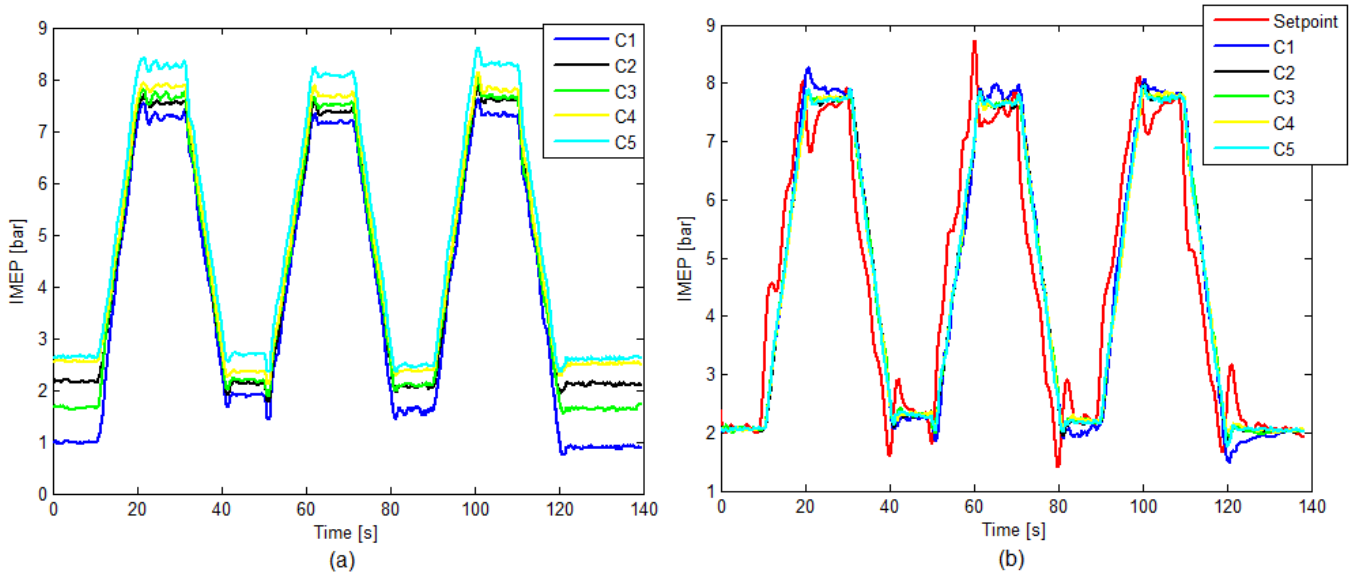

Figure 5.43: (a) Measured IMEP of five cylinders of the RT control system; (b) Measured IMEP of five cylinders and IMEP setpoint of speed-IMEP two-loop control system

In the LabVIEW real-time PXI control system, engine speed is the only feedback to the speed governor and the speed governor computes the injection fuel amount and then converts it to injection duration period that is applied to all six cylinder injectors equally. However, this same injection duration cannot guarantee the same fuel amount injected into each cylinder due to individual injector variation, this is because the LabVIEW real-time PXI control system does not employ any injector compensation or 'trim'. Figure 5.43 (a) therefore shows that the IMEP of all six cylinders are different to each other as a consequence of the individual injector variation.

In the speed-IMEP two loop control system, each cylinder has an individual IMEP closed-loop controller and the output of the speed closed loop controller is the setpoint to all six IMEP closed-loop control systems for the six cylinders. Figure 5.43 (b) shows that in such a control system, the IMEP of the six cylinders are equalised; this means the combustion consistency of mechanical power output among the cylinders was improved. Thus, this form of individual cylinder IMEP feedback closed loop control could replace the need for individual injector

'trim' adjustments to be set in the engine ECM for each injector and additionally would enable the engine to compensate for a developing injector fault and even then trigger a diagnostic fault when the compensation for that injector supersedes a pre-determined threshold. An example of a scenario where this form of closed loop control would be beneficial is the progressive 'coking' that can occur for diesel engine injector nozzles resulting from poor fuel quality combined with prolonged operation of the engine at conditions which exacerbate coking.

The NO_x and soot emissions of these two different engine control systems are plotted together in Figure 5.44 (a). NO_x and soot emissions are quite different between these two systems. This is not because of the different control structure of the speed governor but because of the difference of SOI and RP control strategy. Figure 5.44 (b) shows that fuel consumption of the multi-loop combustion control system is slightly improved over that of LabVIEW real-time PXI control system, particularly at around 3500 seconds where the Speed-IMEP controller uses a far more advanced SOI, Figure 5.45 (a).

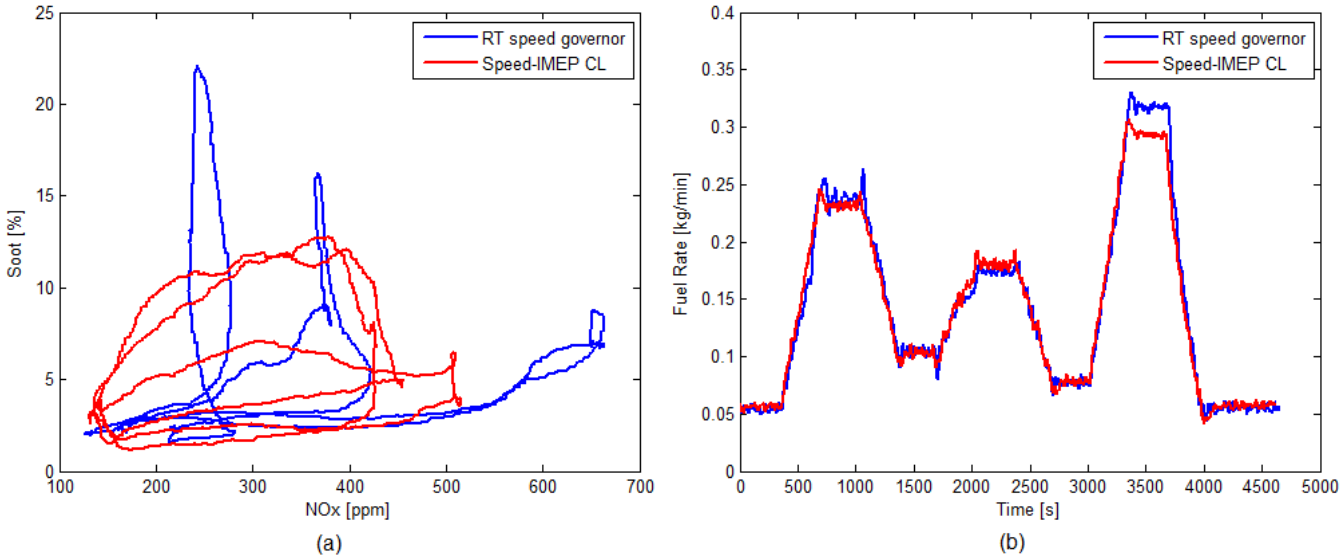

Figure 5.44: (a) Soot and NO_x emission for the RT control system and speed-IMEP two loop control system; (b) Measured fuel rate for the RT control system and speed-IMEP two-loop control system

Figure 5.45 illustrates the difference in SOI and RP between the two engine control systems. The SOI and the RP of the LabVIEW real-time PXI control system were drawn from look-up tables which were copied from the ECM control software of the test engine. SOI and RP of the speed-IMEP closed loop control system were the feedback control solutions from CA50 and Alpha feedback control functions. It is interesting that the SOI control of the two control solutions

typically opposed each other in regard to the change in SOI during the test whereas the RP control generally agreed. Additionally, whereas the RP decreased for both control systems roughly at the same time, the rise in RP for the Speed-IMEP controller was retarded and avoided the overshoots characteristics of the LabVIEW real-time PXI control system. It is these differences which were responsible for the much tighter control of both NOx and soot emissions as illustrated in Figure 5.44 (a).

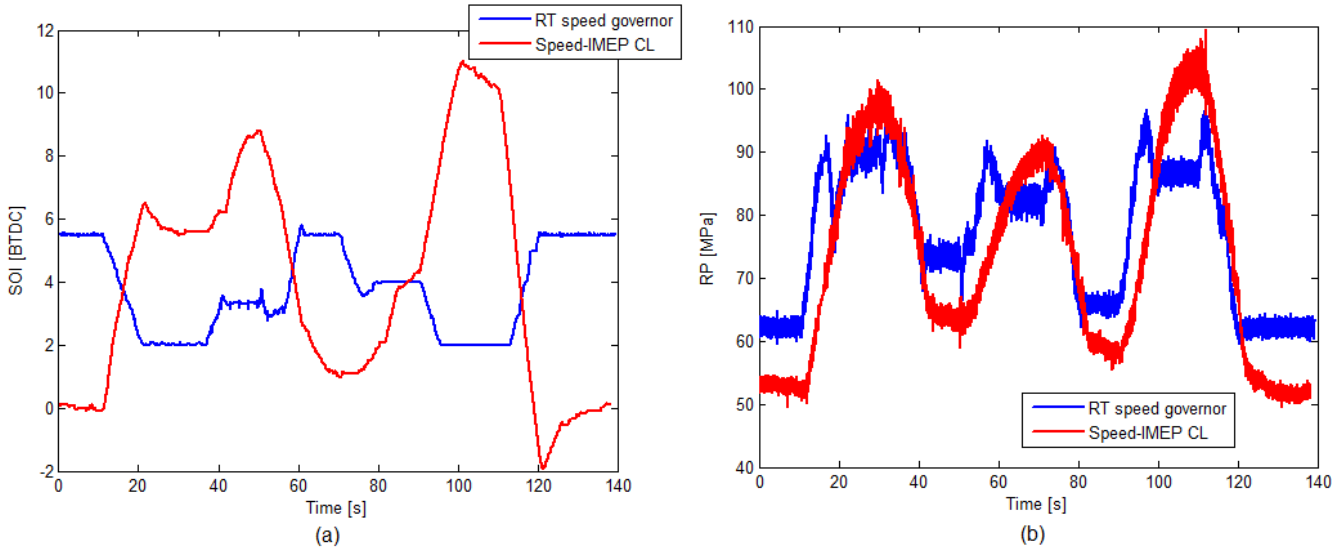

Figure 5.45: (a) SOI from the RT control system and speed-IMEP two loop control system; (b) RP from the RT control system and speed-IMEP two-loop control system

5.4.5 2I2O P_{max} and IMEP Control

When the fuel injection mode is set to three pulses, it was noticed that the effects of main injection quantity and the post injection quantity on P_{max} or IMEP are quite different. This can be viewed from the results of sweep tests of main injection quantity and post main injection quantity. Main injection quantity and post injection quantity were indicated by the corresponding injection duration time m_1 and m_2 in unit [ms]. The engine was running at 1100rpm which was controlled by the dynamometer (Cadet V12) control system using engine load as described previously in Section 5.4.1. The engine speed governor was disabled and there was no IMEP closed loop control.

The main injection duration is defined as m_1 and the post injection duration is defined as m_2 (i.e. treating the main and post injections in combination as a split main injection) and these two durations can be controlled independently in the LabVIEW real-time PXI control system [171]. Figure 5.46 shows P_{max} against

IMEP for cylinder 2 resulting from four different configurations of m_1 and m_2 sweep tests.

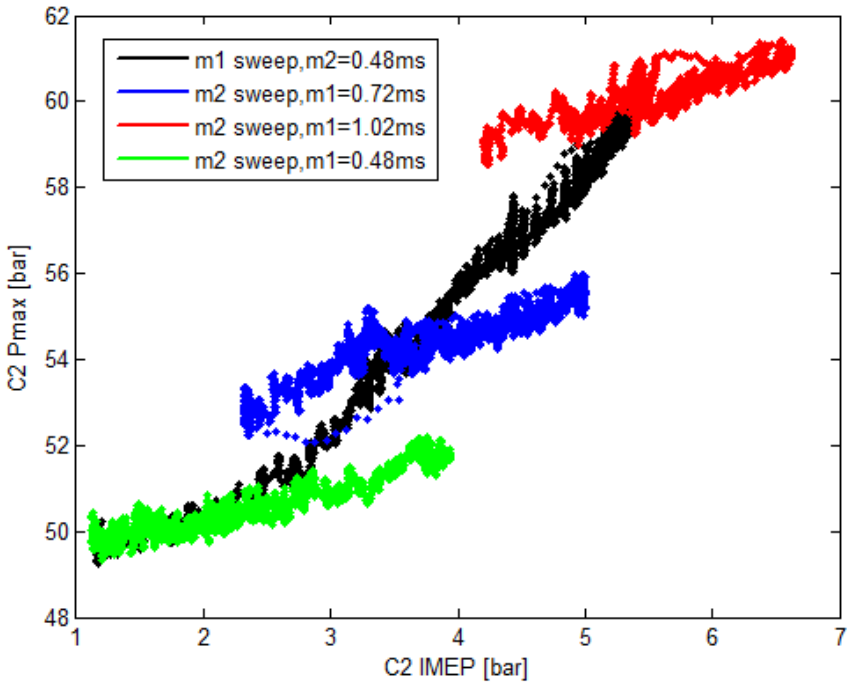

Figure 5.46: P_{max} against IMEP of cylinder 2 from m_1 and m_2 sweep tests of test engine running at 1100rpm

During these four sweep tests both SOI and RP were kept constant. It should also be noted that when m_2 was kept constant and m_1 was increased, the total main injection quantity was also increased (i.e. $m_1 + m_2$). P_{max} was observed to increase faster when m_2 was kept constant and m_1 was increased. IMEP was observed to increase faster when m_1 was kept constant and m_2 was increased. This implies that P_{max} and IMEP can be separately adjusted within a certain range using m_1 and m_2 as control inputs respectively.

The block diagram of this 2I2O P_{max} and IMEP closed-loop control system is shown in Figure 5.47.

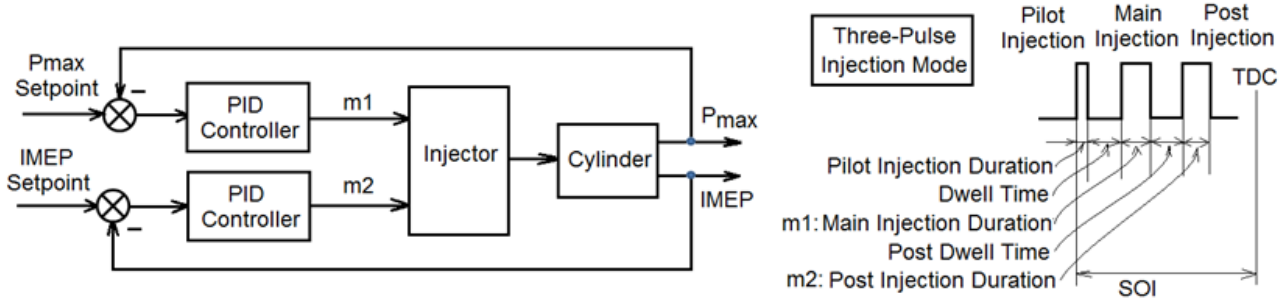

Figure 5.47: Block diagram of 2I2O P_{max} and IMEP closed loop control system

This is a two loop decentralized PID control system and it was tested on cylinder 2 of the C6.6 test engine as was done for the sweep test results summarised in Figure 5.46. During these tests the fuel injection control of the other cylinders was left open loop controlled with fixed m_1 and m_2 values. The engine was running at 1100rpm with the dynamometer controlled in speed mode (the applied load was constantly adjusted to maintain engine speed). The step response of P_{max} and IMEP are plotted in Figure 5.48 (a) and (b) respectively.

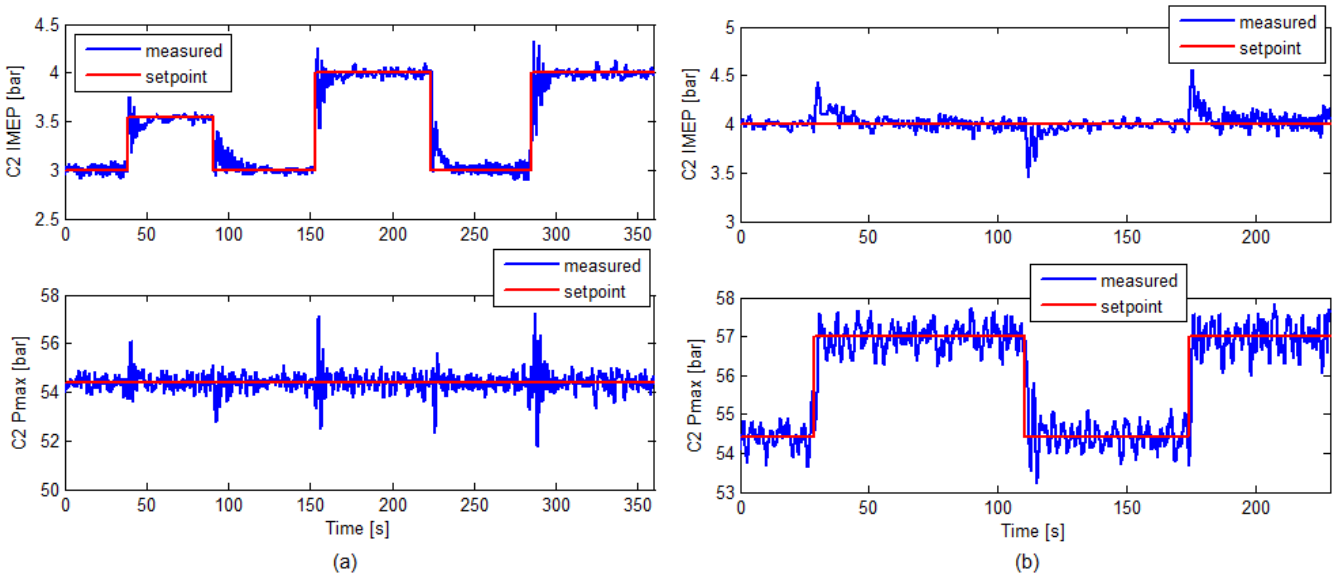

Figure 5.48: (a) Step response of cylinder I IMEP closed loop control; (b) Step response of cylinder 1 P_{max} closed loop control. Engine was running at 1100rpm

From Figure 5.48 it can be seen that P_{max} and IMEP could be separately controlled within a limited area. Therefore this form of diesel engine fuel system controller provides a potential avenue for keeping P_{max} as low as possible whilst maintaining the required IMEP of the combustion process.

The disturbance rejection capability of this control system was tested by a dwell time step test. Figure 5.49 (a) shows the IMEP and P_{max} of Cylinder 2 increase as DW increases when there is no P_{max} and IMEP closed loop control. When this 2I2O P_{max} and IMEP feedback control system is in action, both P_{max} and IMEP of Cylinder 2 were maintained around their setpoint values during the DW step disturbance change, Figure 5.49 (b).

However, for the C6.6 test engine, it was found that the ability to decouple and control P_{max} and IMEP was only valid when the engine speed was lower than 1400rpm. When the speed of C6.6 test engine was greater than 1400rpm, the variation of m_1 and m_2 has the same effect on P_{max} and IMEP and this is illustrated in Figure 5.50.

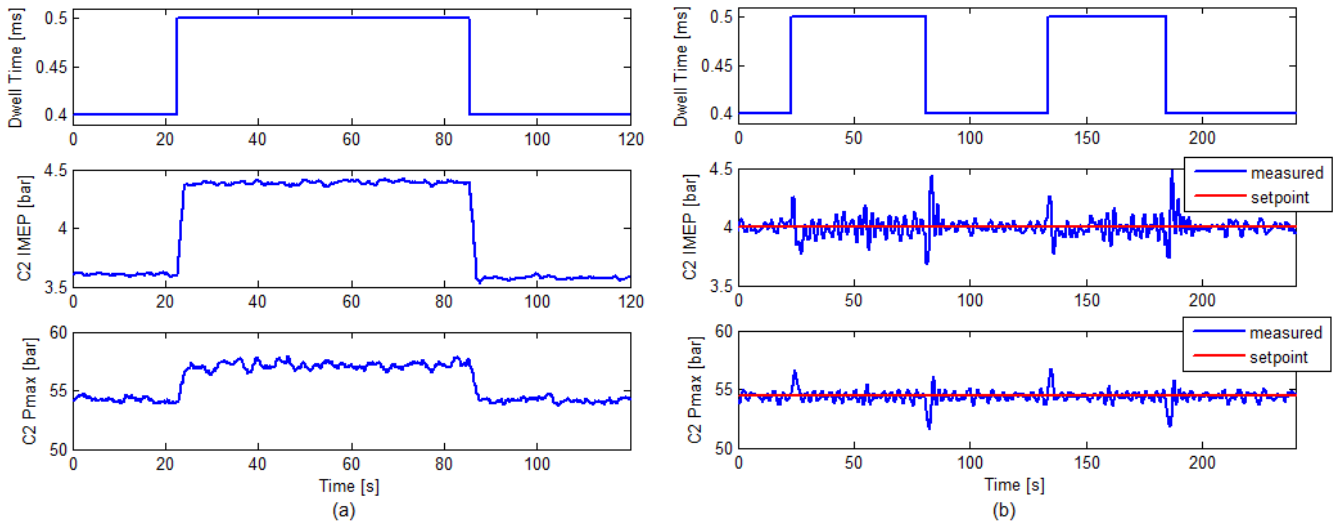

Figure 5.49: (a) Dwell time disturbance and its effect on cylinder1 IMEP and P_{max} when there is no P_{max} and IMEP closed loop control; (b) Dwell time disturbance and its effect on cylinder1 IMEP and Pmax when there is P_{max} and IMEP closed loop control. Engine was running at 1100rpm

Figure 5.50 (b) shows the plot of P_{max} against IMEP of cylinder 2 from the m_1 and m_2 sweep test with the engine at 1400rpm and all four lines are overlapping as one line. The relationship between P_{max} and IMEP was therefore fixed and they were completely coupled. One possible reason for this phenomenon is the dominant effect of feedback air system via VGT path at high engine speed. To understand this in full would require additional investigation of coupling and disturbance effects between the fuel and air systems.

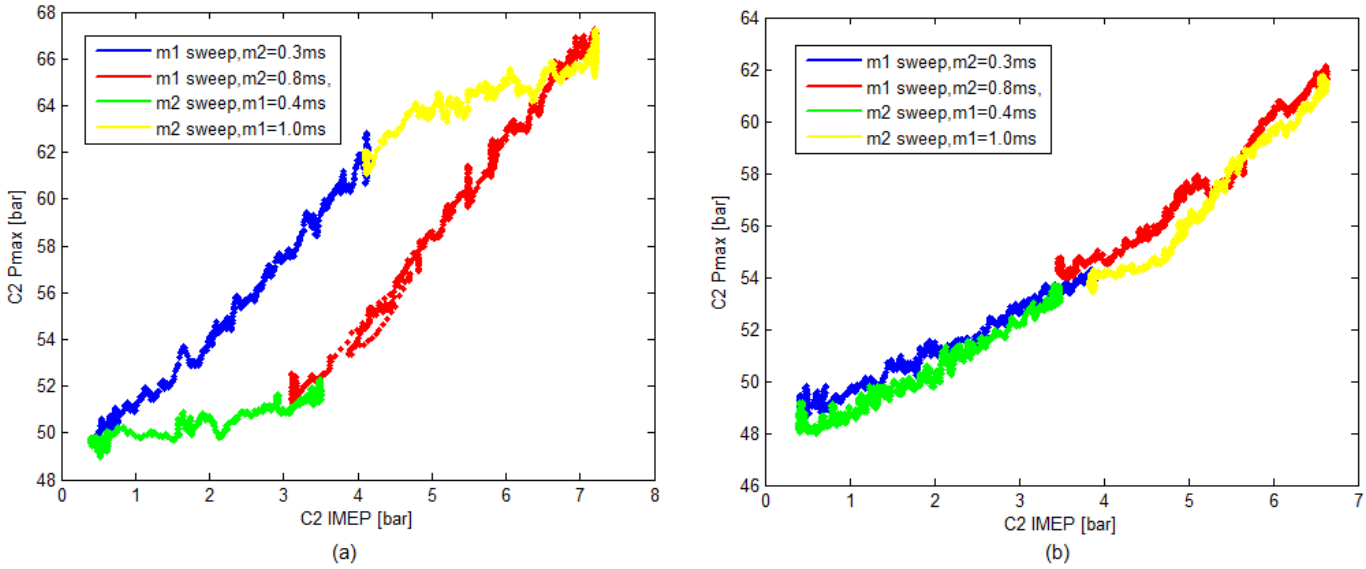

Figure 5.50: (a) P_{max} against IMEP of cylinder 1 from m_1 and m_2 sweep tests of test engine running at 950rpm; (b) P_{max} against IMEP of cylinder 1 from m_1 and m_2 sweep tests of test engine running at 1400rpm

5.5 Conclusions

This study makes several noteworthy contributions to the current literature on diesel engine fuel-path control:

1. A 3I3O gain-scheduling MPC fuel-path control system has been developed and tested on a C6.6 diesel engine. The test results show that each controlled variable has good tracking performance during the change of engine operating point. This is the first study reporting the application of 3I3O square multi-variable MPC in diesel engine fuel-path control.
2. An innovative 2I2O closed loop control system using SOI and RP to control both the CA50 angular position and the difference between CA50 angular position and SOI angular position, has been developed and tested on a C6.6 engine. A setpoint algorithm which is linearly correlated to engine speed and load was first proposed and implemented with this 2I2O control system and provides an example of a fuel-path control system design which can avoid the multiple look-up tables of traditional calibration based open-loop control systems.
3. A 'dragon shape' pattern in the variation of IMEP and P_{max} caused by the sweep of dwell time between the two injections of a split main injection for a three injection mode has been found on the C6.6 diesel engine used in this study. This study is the first practical demonstration that this phenomenon can be used to develop a closed loop control of IMEP with the aim to reduce the cycle-to-cycle variation when the engine is operating at steady-state.
4. The disturbance rejection capability of IMEP closed loop control using injection quantity has also been experimentally explored on a C6.6 diesel engine as a method to reduce cycle-to-cycle variability. It was found that this IMEP closed loop control system has very good disturbance rejection capability. This finding provides additional evidence of the advantages of using IMEP closed loop control within a diesel engine.
5. An innovative diesel engine speed control system which consists of a combination of two types of closed-loop control has been developed which incorporates an inner and an outer loop. The inner control loop achieves closed-loop control of IMEP for each individual cylinder following the same IMEP setpoint, thus balancing individual cylinder work (i.e. adapts to differences in injector fuel delivery rate). The outer loop uses the engine desired speed and speed feedback to set the IMEP demand (in place of the cycle fuel quantity demand of the original speed governor). This work

therefore contributes to the practical method of the reduction of combustion inconsistency among cylinders via closed-loop control and provides a control system solution which removes the need for individual injector calibration or 'trim' adjustment to be programmed into the ECM.

6. An IMEP and P_{max} correlation pattern under a three-pulse injection mode was first reported in this chapter. Based on this finding, an innovative 2I2O IMEP and P_{max} decentralized control system has been developed and tested on a C6.6 diesel engine. This research has demonstrated, for the first time that IMEP and P_{max} can be separately controlled and such a control system has both good tracking and disturbance rejection capability. The correlation pattern of P_{max} and IMEP when boost pressure is isolated from exhaust pressure needs to be further investigated to better understand the phenomenon.

All the different diesel engine fuel-path feedback control practical demonstrations in this chapter have shown that the diesel engine performance, fuel consumption and emissions can be improved through feedback control of combustion variables. Thus, feedback control can be a practical replacement for the more traditional and highly time intensive and costly calibration and open loop look-up table based diesel engine control methods. Indeed, two of the demonstrated closed-loop control systems (items 2 and 5 above) inherently introduce simplification to the management of both setpoints and also cycle-to-cycle and cylinder-to-cylinder variations compared to traditional open-loop techniques.

All of the fuel-path feedback control demonstrations in this study can be classed as *inter-cycle* in which the control action responds on the following combustion cycles. Such were the demonstrated advantages of closed-loop fuel-path diesel engine control that the next logical step for future fuel-path control work beyond this study is to consider *intra-cycle* control in which the control action responds during combustion to hi-speed instantaneous in-cycle measurements. Implementation of appropriate algorithms and controls to investigate this would require considerable upgrades to the LabVIEW real-time PXI control system used in this study. Signal analysis, model and control execution time would need to significantly increase and the 40MHz FPGA of the existing LabVIEW PXI system could facilitate this. However, such work would require new modelling methodologies and control system designs compatible with FPGA programming capabilities and very fast execution times.

Chapter 6

6 Conclusions and Contributions

6.1 Introduction

This study set out to explore potential new ways to either improve diesel engine performance or reduce engine control calibration cost through novel use of electrical control methods. More specifically, this study set out to address the two research questions:

3) How can multivariable control strategy MPC be applied in diesel engine control? What are the challenges and advantages to implement MPC in diesel engine control?
4) Are there new closed loop control structures that can either improve diesel engine performance or reduce engine control calibration effort?

Thus, the overall aim of this study is to improve the knowledge of the application of MPC in diesel engines. This has required improvements in the understanding of the diesel engine dynamics specifically in regard to diesel engine control input and feedback signals. The study has identified clear patterns in both the diesel engine air-path and fuel path dynamics using system identification techniques; patterns that can be utilised for model based control. The air-path and fuel-path control problems have been separately investigated and this study has demonstrated a 2I2O MPC engine air-path control and a 3I3O MPC fuel-path control on a C6.6 diesel engine. Through the improved understanding of diesel engine dynamics, a series of novel diesel engine control systems have been developed and demonstrated for the first time in this study. These include: a two loop diesel engine speed control system, an online SOI and RP adjustment control system and a control system that achieves independent P_{max} and IMEP control. These various diesel engine control system demonstrations provide practical solutions to both research questions.

6.2 Findings

This section summarizes the research findings that directly address the two original research questions of this study:

How can MPC be applied in diesel engine control?

By properly selecting the controlled variables and control manipulated variables, this study has demonstrated practically that square MPC control strategy can be applied in either diesel engine air-path or fuel-path control. Furthermore, system identification together with model gain-scheduling can be used in developing MPC in diesel engine control. By dividing the engine operating range into several segments, perturbation tests plus a system identification modelling method can be used to obtain engine dynamic models which can used in MPC control strategy.

Challenges in implementing MPC in diesel engine control:

a) **Obtaining the dynamic models for MPC algorithm**: There were no examples found in literature of a mature engine dynamic model which is completely based on first principles that can be used in MPC algorithm. Since engine dynamic models vary with engine operating point, it is necessary when using a system identification technique to perform perturbation tests at multiple engine operating points. Models derived through this methodology have been found in this work to be inflexible; only performing satisfactorily in a limited engine speed and load operating area centred on the operating point where the perturbation test was conducted. This required a gain-scheduling procedure to dynamically switch the MPC model in response to engine operating point change. The identified models were also found in this study to only work for a maximum three square MPC control structure. It is believed that the strong and complex coupling effect among different control inputs (both in the air-path and fuel-path) is responsible for the model limitations and the constraints on the MPC controller number of input and outputs.

b) **A complicated optimization algorithm**: The core of the MPC algorithm is an optimization algorithm. The need for MPC model gain-scheduling results in increased difficulty and complexity in respect to implementation of MPC control and tuning, constraining its potential advantages.

c) **The weights in MPC cost function and the limitations of control rate:** For each divided MPC segment in the engine operating range, both time and effort are needed in the calibration of weights and limits which constrain the potential reduction in engine calibration effort compared to conventional PID control plus calibration maps.

Advantages in applying MPC in diesel engine control:

MPC was found in this study to cope well with the strong coupling effects among different control inputs at localised engine operating points. It was also able to achieve good control performance in fast engine transients. Compared to a comparable decentralized PID control system; MPC was found to achieve improved control performance especially when more than two setpoints were changed.

Are there new control structures that can either improve diesel engine performance or reduce engine control calibration effort?

Several novel control system solutions have been demonstrated in this study that can either improve diesel engine performance or reduce engine control calibration effort. These are listed under Contributions, Section 6.4.

6.3 Conclusions

The review of literature identified several key knowledge gaps in respect to diesel engine air-path and fuel-path control which have been directly addressed in this study. A full description of the identified weaknesses in the literature and the specific solutions demonstrated in this study are detailed in the conclusions of Chapter 2. The broader conclusions of this study will now be discussed.

6.3.1 Diesel Engine Dynamics (Chapter 3)

The study of the C6.6 diesel engine air-path and fuel-path dynamics revealed that fuel-path dynamics were less sensitive to the change of engine operating point compared to the air-path dynamics. The results also revealed it is practical to use a form of regression model to predict the gain and system time of the transfer model with greater than 80% accuracy and thus demonstrates the applicability of model based control to both air-path and fuel-path. Critically, a complex coupling between the engine air-path and fuel-path systems was demonstrated and a scheme was proposed to summarise the mechanisms of this coupling.

Observations of cycle-to-cycle combustion variation for the C6.6 engine used in this study was attributed to the LabVIEW real time PXI control system hardware which produced the signals that drove the engine fuel injectors and high pressure pump. Specifically, the DRIVVEN injector driver modules used to drive the six injectors and the high pressure pump solenoid control valve could not reproduce all the fine details of the original drive signals produced by the

ECM. Additionally, the compensation for differences in injector fuel quantity delivery in the original ECM were not implemented in the LabVIEW real time PXI control system and this resulted in cylinder-to-cylinder inconsistency which was exacerbated for the cylinder 1 injector as this injector had undergone remedial work to install a needle lift sensor and a sac volume pressure sensor.

6.3.2 Air-Path Control (Chapter 4)

Investigation of the air-path relationship of MAF and MAP in respect to step changes in VGT and EGR revealed that there exists a series of linear MAF to MAP relationships that scale with engine speed and load when the EGR and VGT respectively are fixed. The details of these relationships demonstrated that MAP is more sensitive to VGT position than MAF (VGT should therefore be used to close-loop control MAP) and that at constant engine speed, closing the VGT vane position is equivalent to increasing the engine load in regard to the effects on MAF and MAP. Conversely, the opening of the EGR valve at fixed engine load has the same effect on the MAF to MAP relationship as decreasing the engine speed. These clear linear relationships demonstrate the feasibly to use an MVEM to model the MAF and MAP for different engine operating conditions. These findings confirm the viability of closed-loop model based control as a replacement for open-loop look-up table air-path control methods.

Evaluation of the NOx emissions in respect to the EGR ratio revealed clear linear relationships and thus EGR ratio was identified as a far better candidate for closed-loop control of engine out NOx emissions than closed-loop control of EGR valve position directly. EGR ratio estimation requires either direct EGR mass flow measurement or alternatively it can be estimated using an EGR mass flow model. Therefore accurate knowledge of the EGR mass flow is very important in the proper control of diesel engine air-path, especially for model based control.

An orifice valve flow rate model is most often used in literature to estimate EGR mass flow but in this study the performance of this form of model was shown to be poor on a practical engine due to sensitivity to pressure sensor noise. An alternative model based on the total flow rate minus the measured air flow rate (MAF) when the EGR valve is open was used. This model fundamentally requires accurate estimation of volumetric efficiency and a nonlinear regression model of the C6.6 engine volumetric efficiency was developed from experimental data. The combination of the total flow rate model

with this nonlinear volumetric efficiency model proved to be far more successful for predicting the EGR mass flow compared to the orifice flow model.

A 2I2O linear air-path MPC control system was developed on a C6.6 diesel engine to control MAP and MAF with VGT and EGR respectively. An accurate air-path dynamic model was found to be crucial in the effective design of this air-path controller and in this study a system identification methodology was employed using the *pem* function in the MATLAB® system identification toolbox. It was found that a fifth order identified state-space model was sufficient for achieving good steady state and transient control performance. This study therefore confirms that system identification derived linear MPC of the diesel engine air-path MAP and MAF is feasible and practical. However, model gain-scheduling is required for this controller to perform over the full engine operating range.

The control performance of this MPC air-path controller was compared to a 2I2O PID decentralized MAF and EGR mas flow rate (model estimated) control system which was based on identified transfer function models. Decentralised PID was found to deliver good steady-state air-path control performance following local tuning but for good control performance at multiple engine operating points, gain scheduling was essential due to the complex air-path dynamics. Consequently, when transiting engine operating points, it was found that MPC control generally performed better in regard to set-point tracking compared to decentralised PID. At the engine operating points examined, the MPC controller was also observed to have improved setpoint tracking compared to the decentralised 2I2O PID control.

More research is required to develop a fast and low cost way of obtaining accurate dynamic models for MPC and to explore the feasible setpoints' space as well as the setpoint determination policy. Furthermore, a combined air-path and fuel-path model based control system, which was not investigated in this study, can be postulated to have increased system disturbance rejection capability and also potentially achieve more precise control the desired engine variables. This is because the system would in principle manage the mutual disturbances of the coupling between the air-path and fuel-path systems where currently in traditional open loop diesel engine control, such mutual disturbances are managed using time consuming and costly engine calibration.

6.3.3 Fuel-Path Control (Chapter 5)

A series of novel fuel-path control system designs were practically demonstrated on a C6.6 diesel engine in this study and these targeted a variety of important fuel-path control tasks, with several noteworthy contributions to literature on diesel engine fuel path control.

A 3I3O gain-scheduling MPC fuel-path control system has been demonstrated. The results show that each controlled variable has good tracking performance during the change of engine operating point. This is the first study reporting the application of 3I3O square multi-variable MPC in diesel engine fuel-path control.

An innovative 2I2O closed loop control system using SOI and RP to control both the CA50 angular position and the difference between CA50 angular position and SOI angular position has been demonstrated. A setpoint algorithm which is linearly correlated to engine speed and load was first proposed and implemented with this 2I2O control system and provides an example of a fuel-path control system design which avoids the multiple look-up tables of traditional calibration based open-loop control systems.

A ‘dragon shape’ pattern in the variation of IMEP and P_{max} caused by the sweep of dwell time between the two injections of a split main injection for a three injection mode was found for the C6.6 diesel engine. This study is the first practical demonstration that this phenomenon can be used to develop a closed loop control of IMEP with the aim to reduce the cycle-to-cycle variation when the engine is operating at steady-state.

The disturbance rejection capability of IMEP closed loop control using injection quantity has also been explored as a method to reduce cycle-to-cycle variability. It was found that this IMEP closed loop control system has very good disturbance rejection capability. This finding provides additional evidence of the advantages of using IMEP closed loop control within a diesel engine.

An innovative diesel engine speed control system which consists of a combination of two types of closed-loop control has been developed which incorporates an inner and an outer loop. The inner control loop achieves closed-loop control of IMEP for each individual cylinder following the same IMEP setpoint, thus balancing individual cylinder work (i.e. adapts to differences in injector fuel delivery rate). The outer loop uses the engine desired speed and speed feedback to set the IMEP demand (in place of the cycle fuel quantity

demand of the original speed governor). This work therefore contributes to the practical method of the reduction of combustion inconsistency among cylinders via closed-loop control and provides a control system solution which removes the need for individual injector calibration or 'trim' adjustment in the ECM.

An IMEP and P_{max} correlation pattern under a three-pulse injection mode was identified for the C6.6 engine. Based on this finding, an innovative 2I2O IMEP and P_{max} decentralized control system has been developed and tested. This research has demonstrated, for the first time that IMEP and P_{max} can be separately controlled and such a control system has both good tracking and disturbance rejection capability. The correlation pattern of P_{max} and IMEP when boost pressure is isolated from exhaust pressure needs to be further investigated to better understand the fundamentals of the observed phenomenon.

Direct combustion process feedback control based on variables such as CA50, P_{max}, IMEP etc. is therefore promising; offering the potential to improve combustion process consistency among different cylinders, to reduce control calibration effort, to reduce cycle-to-cycle variations, to reduce P_{max} etc. Thus, feedback control can be a practical replacement for the more traditional and highly time intensive and costly calibration and open loop look-up table based diesel engine control methods. Indeed, two of the demonstrated closed-loop control systems (1. 2I2O closed loop control system using SOI and RP, 2. inner and outer loop speed governor) inherently introduce simplification to the management of both setpoints and also cycle-to-cycle and cylinder-to-cylinder variations compared to traditional open-loop techniques.

All of the fuel-path feedback control demonstrations in this study can be classed as *inter-cycle* in which the control action responds on the following cycles. Such were the demonstrated advantages of closed-loop fuel-path diesel engine control that the next logical step for future fuel-path control work beyond this study is to consider *intra-cycle* control in which the control action responds during combustion to hi-speed instantaneous in-cycle measurements. Implementation of appropriate algorithms and controls to investigate this would require considerable upgrades to the LabVIEW real-time PXI control system used in this study. Signal analysis, model and control execution time would need to significantly increase and the 40MHz FPGA of the existing LabVIEW PXI system could facilitate this. However, such work would require new modelling methodologies and control system designs compatible with FPGA programming capabilities and very fast execution times.

6.4 Contributions

This study makes several contributions to the body of knowledge in the field of diesel engine control. The major contributions are:

7) Reveals some basic features of the diesel test engine such as how the basic air-path and fuel-path dynamics vary with engine operating points; e.g. MAF-MAP relationships for both steady-state and transient conditions, disturbance sources, a standing wave type relationship between IMEP and injection dwell time attributed to a pressure wave inside the fuel rail and also significant combustion inconsistency among different cylinders.
8) Experimentally proves that MPC can be quickly implemented on a test engine and applied to both air-path (2I2O) and fuel-path (3I3O) and perform well in both steady-state and transient conditions.
9) Demonstration of a 2I2O SOI, RP online regulatory system which uses combustion diagnostics (CA50) and a pair of novel control set-points which relate CA50 to SOI and SOC and which requires minimal set-point calibration to achieve optimised diesel engine performance over a wide operating range.
10) Developed a novel two loop engine speed controller with an outer loop that controls IMEP set-point based on engine speed error and an inner loop which independently controls fuel quantity on each cylinder to match the IMEP demand of the outer control loop.
11) Reveals that for the test engine operating below 1400rpm with a three-pulse injection mode; the control of the split in fuel quantity between the second and third injections enables the separation of P_{max} and IMEP such that the second and the third injection fuel quantity can be used as control inputs respectively for P_{max} and IMEP.
12) Developed a closed-loop fuel-path controller which utilises the fuel rail pressure wave phenomenon to reduce combustion variation by adjustment of the dwell time between a split main injection.

Chapter 7

7 Future Work

7.1 Introduction

This study has focussed on diesel engine air-path and fuel-path control and has also considered the modelling techniques that best support the implementation of model based control. From the research undertaken in these areas and presented herein, several key topics have been identified for future research.

7.2 Diesel Engine Air-Path and Fuel-Path Control

The research into new engine control structures in both the engine air-path and fuel-path in this study has revealed several issues in need of further investigation:

1) A fuel common rail with high pressure pump and control system which minimises the fuel rail pressure fluctuation caused by fuel injection would help to reduce combustion cycle-to-cycle variation. The optimization of both common rail shape and the rail pressure control system are recommended approaches to achieve this. Furthermore, research into the effects of fuel rail pressure fluctuation on fuel injector performance and the combustion process based on the work presented in this study in Section 5.4.1 and Section 5.4.2 would be a potentially rich avenue for future research and exploitation for diesel engine fuel-path control.
2) Intra-cycle combustion process control would help to reduce cycle-to-cycle combustion variation. In the laboratory, the key to such research is the development of an accurate predictive model and the implementation of FPGA techniques to best manage the high algorithmic processing demand required for such a control system. Development of tools in both of these areas would greatly enhance the research capabilities for intra-cycle combustion process control.
3) The development of a low cost, mass produced, high reliability combustion pressure sensor without sacrifice of the sensor's response time, resolution and accuracy is very important. Combustion pressure

sensors are crucial in fast combustion process control demonstrated herein such as: SOI, RP online adjustment system, two loops engine speed control, P_{max} and IMEP separate control demonstrated in this study.

4) The results of the experimental study on the three pulse injection mode showed that P_{max} and IMEP can be separately controlled in a limited operating range i.e. when the engine speed was lower than 1400rpm for the C6.6 engine used in this study. This offers the potential to minimise peak cylinder pressure for the same IMEP with potential benefits in reduced engine weight. Further experimental research should be carried out to investigate this phenomenon with intake manifold pressure isolated from the exhaust system conditions and different fuel system designs and low level controllers (i.e. rail pressure). Theoretical analysis should also be undertaken on this phenomenon based on combustion process modelling to understand better the P_{max} and IMEP relationship and how it may be manipulated.

7.3 MPC Control

MIMO MPC control was demonstrated practically on the C6.6 engine used in this study. Following the findings of this research, several proposals for future research in this area have been developed:

1) Investigation of the implementation of a combined air-path and fuel-path MPC controller in the diesel engine. Such an MPC controller will require more than three control inputs. It was found in this study that for cases of more than three inputs, it was difficult to achieve good control performance using a system identified dynamic model in the MPC controller. Therefore, it is proposed that the model in such a control system should be a physical one.
2) A tuning process methodology should be developed for the tuning of the weights in an MPC cost function and also the change of rate of control inputs. This would significantly help with the reduction in the calibration time and effort required; it would also achieve a more reliable performance level for MPC controllers developed for the diesel engine.
3) The robustness of MPC control of the diesel engine should also be carefully studied both mathematically and experimentally, ideally including both different modelling methodologies for the controller model and also the tuning process methodology mentioned above.

4) Research into the application of adaptive modelling techniques in MPC control strategy would be of great help to improve the robustness and/or maintain good performance of an MPC controller during the full working life cycle of the engine.

7.4 Engine Control Models

The type of model and the model development methodology for a control model was found in this study to be a critical part of the successful achievement of diesel engine MIMO MPC control. Several proposals for the future research that is required for the development of successful diesel engines control models are as follows:

1) Development of a low order physical nonlinear dynamic fuel-path model for application in a fuel-path MPC controller is essential for achieving the full potential of MPC diesel engine fuel-path control.
2) The investigation of the application of nonlinear state space physical air-path dynamic models in air-path MPC controller design is a very important research avenue. Most important is finding a reliable and quick method to develop an accurate nonlinear physical air-path dynamic model which covers all available engine operating point conditions. This will reduce the model uncertainty introduced by the engine perturbation test and system identification process used in this study. This will also save significant time and cost that is needed in developing dynamic models covering all the engine operating range using system identification techniques. Such models can also be validated in simulation prior to practical engine testing. There are two paths for investigating the nonlinear physical air-path dynamic model in air-path MPC control. One is to directly embed it in an NMPC control strategy. The other is to linearize this nonlinear dynamic model according to different engine speed and load conditions to form an LPV model and then use it to construct a linear MPC controller.
3) A low order semi-empirical combustion process model, an emission model and also an air-path physical model need to be combined together for the study of the feasible engine performance space and fast setpoints selection for engine closed loop control systems. These models should be able to be developed quickly by using minimal engine test data and avoiding the necessity to input detailed information regarding engine mechanical dimensions.

References

1. Khair, M. K. and Majewski, W. A., Diesel Emissions and Their Control, SAE international, ISBN: 978-0-7680-4974-9.
2. Magner, S., Cooper, S. and Jankovic, M., Engine Control for Multiple Combustion Optimization Devices, SAE paper 2006-21-0003.
3. Guzzella, L. and Amstutz, A., Control of diesel engines, Control Systems, IEEE, Volume: 18 , Issue: 5 , 1998 (53-71), doi: 10.1109/37.722253.
4. Badami, M., Millo, F. and D'Amato, D.D., Experimental Investigation on Soot and NOx Formation in a DI Common Rail Diesel Engine with Pilot Injection, SAE paper 2001-01-0657.
5. Heywood J.B., Internal Combustion Engine Fundamentals. McGraw-Hill International Editions. 1988 ISBN 0-07-100499-8.
6. Hiroyasu H., Kadota, T. and Arai, M., Development and use of a spray combustion modeling to predict Diesel engine efficiency and pollutant emissions, Bulletin of the JSME 26 (214) (1983).
7. http://www.gtisoft.com/img/broch/broch_gtpower.pdf, last accessed 2013-07-31.
8. Henein, N. A., Lai, M-C., Singh, I. P., Zhong, L. and Han, J., Characteristics of a Common Rail Diesel Injection System under Pilot and Post Injection Modes, SAE paper 2002-01-0218.
9. Park, C., Kook, S. and Bae, C., Effects of Multiple Injections in a HSDI Diesel Engine Equipped With Common Rail Injection System, SAE paper 2004-01-0127.
10. Alfieri,E., Amstutz, A. and Guzzella, L., Gain-scheduled model-based feedback control of the air/fuel ratio in diesel engines, Control Engineering Practice, Volume 17, Issue 12, December 2009, Pages 1417-1425.
11. Ortner, P. and Re, L., Predictive control of a diesel engine air path, IEEE Transactions on Control Systems Technology, 15(3):449–456, 2007.
12. Wei, X. and del Re, L., Gain Scheduled Hinf Control for Air Path Systems of Diesel Engines Using LPV Techniques, IEEE Transactions on Control Systems Technology, Vol. 15, No. 3, May 2007.
13. Mohammadpour, J., Grigoriadis, K., Franchek, M., Wang, Y. and Haskara, I., LPV Decoupling and Input Shaping for Control of Diesel Engines, American Control Conference, Marriott Waterfront, Baltimore, MD, USA, June 30-July 02, 2010.

14. Wang, Y., Haskara, I. and Yaniv, O., Model-Based Quantitative Feedback Control of EGR Rate and Boost Pressure for Turbocharged Diesel Engines, American Control Conference Westin Seattle Hotel, Seattle, Washington, USA, June 11-13, 2008.
15. Liu, L., Wei, X. and Zhu, T., Quasi-LPV gain scheduling control for the air path system of diesel engines, Control and Decision Conference, Page(s): 4893 – 4898, CCDC 2008. Chinese, doi: 10.1109/CCDC.2008.4598258.
16. Stefanopoulou, A.G., Kolmanovsky, I., and Freudenberg, J.S., Control of variable geometry turbocharged diesel engines for reduced emissions, IEEE Transactions on Control Systems Technology, Volume: 8 , Issue: 4, 2000 , Page(s): 733 – 745.
17. Jankovic, M. and Kolmanovsky, I., Constructive Lyapunov control design for turbocharged diesel engines, IEEE Transactions on Control Systems Technology, Volume: 8 , Issue: 2, 2000, Page(s): 288 – 299.
18. Deng, C., Colin, G., Chamaillard, Y. and Gruel, D.N., Sequential robust control design methodology application to the MIMO air path of a diesel engine, IECON 2012 - 38th Annual Conference on IEEE Industrial Electronics Society, Page(s): 2138 – 2143.
19. Sassano, M., Passenbrunner, T.E., Hirsch, M., del Re, L. and Astolfi, A., Approximate optimal control of the air path of a diesel engine, American Control Conference (ACC), 2012 , Page(s): 4204 – 4209.
20. Ammann, M., Fekete, N. P., Guzzella, L., and Glattfelder, A. H., Model-Based Control of the VGT and EGR in a Turbocharged Common-Rail Diesel Engine: Theory and Passenger Car Implementation, SAE paper 2003-01-0357.
21. van Nieuwstadt, M., Kolmanovsky, I. and Moraal, P., Coordinated EGR-VGT Control for Diesel Engines: an Experimental Comparison, SAE paper 2000-01-0266.
22. Wang, J., Hybrid Robust Air-Path Control for Diesel Engines Operating Conventional and Low Temperature Combustion Modes, IEEE Transactions on Control Systems Technology, Vol. 16, No.6, November 2008.
23. Langthaler, P. and del Re, L., Robust Model Predictive Control of a Diesel Engine Airpath, Proceedings of the 17th World Congress, The International Federation of Automatic Control, Seoul, Korea, July 6-11, 2008.
24. Ahmed Ali, .S., N'doye, B., Nicolas, L., Sliding mode control for Turbocharged Diesel Engine, Control & Automation (MED), 2012 20th Mediterranean Conference on, 2012 , Page(s): 996 – 1001, doi: 10.1109/MED.2012.6265768.
25. Plianos, A., Achir, A., Stobart, R., Langlois, N. and Chafouk, H., Dynamic feedback linearization based control synthesis of the turbocharged Diesel engine, American Control Conference, ACC '07, 2007 , Page(s): 4407 – 4412, doi: 10.1109/ACC.2007.4282344.

26. Mendoza-Soto, J.L. and Alvarez-Icaza, L., Generalized predictive control of a turbocharged diesel engine, American Control Conference (ACC), 2012, Page(s): 5725 – 5730.
27. Maruyama, T. , Shimura, T. , Ejiri, A. , Ikai, Y. and Shimotani, K., Model predictive control applied to a diesel engine air-path system with dead time, Proceedings of SICE Annual Conference (SICE), 2011 , Page(s): 2628 – 2633.
28. Ortner, P. , Langthaler, P. , Garcia O., Jose V. and del Re, L., MPC for a diesel engine air path using an explicit approach for constraint systems, Computer Aided Control System Design, IEEE International Conference on Control Applications, 2006 , Page(s): 2760 – 2765.
29. Djemili, I. , Wang, H.P. , Aitouche, A., Cocquempot, V., Bosche, J. and El Hajjaji, A., Control strategy for the air path dynamic system, Control & Automation (MED), 2012 20th Mediterranean Conference on, 2012 , Page(s): 990 – 995, doi: 10.1109/MED.2012.6265767.
30. Liu, L., Wei, X. and Liu, Z., Switching LPV control for the air path system of diesel engines, Control and Decision Conference, 2008. CCDC 2008. Chinese, Page(s): 4167 – 4172, doi: 10.1109/CCDC.2008.4598114.
31. Liu, L., Wei, X. and Liu, X., Low order H∞ controller design for the air path system of diesel engines, 4th IEEE Conference on Industrial Electronics and Applications, ICIEA 2009, Page(s): 3470 – 3475.
32. García-Nieto, S., Martínez, M., Blasco, X. and Sanchis, J., Nonlinear predictive control based on local model networks for air management in diesel engines ,Control Engineering Practice, Volume 16, Issue 12, December 2008, Pages 1399-1413.
33. Bhushan Das, H. and Dhinagar, S.J., Airpath Modeling and Control for a Turbocharged Diesel Engine, SAE paper 2008-01-0999.
34. Lee, T. K. and Filipi, Z., Nonlinear Model Predictive Control of Advanced Engines Using Discretized Nonlinear Control Oriented Models, SAE Paper 2010-01-2216
35. Plianos, A., Stobart, R. and Achir, A., Real-time Adaptive Predictive Control of the Diesel Engine Air-path Based on Fuzzy Parameters Estimation, SAE Paper 2007-01-0971.
36. Amstutz, A. and Del Re, L. R., EGO Sensor Based Robust Output Control of EGR in Diesel Engines, IEEE Transaction on Control System Technology, Vol. 3, No. 1, March, 1995.
37. Iwadare, M., Ueno, M., Adachi, S., Multi-Variable Air-Path Management for a Clean Diesel Engine Using Model Predictive Control, SAE Paper 2009-01-0733.
38. Yokomura, H., Kouketsu, S., Kotooka, S. and Akao, Y., Transient EGR Control for a Turbocharged Heavy Duty Diesel Engine, SAE Paper 2004-01-0120.

39. Shutty, J., Control Strategy Optimization for Hybrid EGR Engines, SAE Paper 2009-01-1451.
40. Shutty, J., Benali, H., Daeubler, L., and Traver, M., Air System Control for Advanced Diesel Engines, SAE Paper 2007-01-0970.
41. Malkhede, D. N., Seth, B., and Dhariwal, H. C., Mean Value Model and Control of a Marine Turbocharged Diesel Engine, SAE Paper 2005-01-3889.
42. George, S., Morris, G., Dixon, J., Pearce, D. and Heslo, G., Optimal Boost Control for an Electrical Supercharging Application, SAE Paper 2004-01-0523.
43. Wahistrom, J., Eriksson, L., Nielsen, L. and Pettersson, M., PID Controllers and Their Tuning for EGR and VGT Control in Diesel Engines, Proceedings of the 16th World Congress, 2005.
44. Herceg, M., Raff, T., Findeisen, R. and Allgowe, F., Nonlinear model predictive control of a turbocharged diesel engine, IEEE International Conference on Control Applications Computer Aided Control System Design, 2006, Page(s): 2766 – 2771, doi: 10.1109/CACSD-CCA-ISIC.2006.4777076.
45. Wang, Y., Haskara, I., Yaniv, O., Quantitative Feedback Design of Air and Boost Pressure Control System for Turbocharged Diesel Engines, Control Engineering Practice 19 (2011) 626–637.
46. Ahmed, F.S., Laghrouche, S. and El Bagdouri, M.,Second-order sliding mode based output-feedback control of an engine air path actuator in presence of uncertainties, Control and Fault-Tolerant Systems (SysTol), 2010 Conference on, 2010 , Page(s): 50 – 56, doi: 10.1109/SYSTOL.2010.5675973.
47. Deng, J., Xue, Y., Stobart, R., and Maass, B., Fuel path control of a diesel engine at the operating point of the low load and medium speed, Control and Decision Conference (CCDC), 2011 China.
48. Nakayama, S., Ibuki, T. Hosaki, H. and Tominaga, H., An Application of Model Based Combustion Control to Transient Cycle-by-Cycle Diesel Combustion, SAE paper 2008-01-1311.
49. Karlsson, M., Ekholm, K., Strandh, P., Johansson, R. and Tunestål, P., Multiple-Input Multiple-Output Model Predictive Control of a Diesel Engine, the 6th IFAC Symposium on Advances in Automotive Control, Germany, July 12-14, 2010.
50. Tschanz, F., Amstutz, A., Onder, C. H. and Guzzella, L., Feedback control of particulate matter and nitrogen oxide emissions in diesel engines, Original Research Article Control Engineering Practice, In Press, Corrected Proof, Available online 17 October 2012.

51. Alberer, D., Hirsch, M. and del Re, L., A virtual references design approach for diesel engine control optimization, Original Research Article, Control Engineering Practice, Volume 18, Issue 11, November 2010, Pages 1263-1271.
52. Jiang, J., Generalized Gain Scheduling Control of a Diesel Engine based on H2 Optimization, American Control Conference, San Francisco, USA , 2nd -4th June 1993.
53. Reddy, B. B., Ramesh, A., Manivannan, P. V. and Vasudevan, K., Studies on an Electronic Governor with a Stepper Motor Actuator for a Diesel Engine, SAE Paper 2004-28-0059.
54. Mruthunjaya, U. and Dhariwal, H. C., Investigation of Control of Speed of Diesel Engines Using PID Governor, SAE Paper 2000-01-0264.
55. Willems, F., Doosje, E., Engels, F. and Seykens, X., Cylinder Pressure-Based Control in Heavy-Duty EGR Diesel Engines Using a Virtual Heat Release and Emission Sensor, SAE paper 2010-01-0564.
56. Husted, H., Kruger, D., Fattic, G., Ripley, G. and Kelly, E., Cylinder Pressure-Based Control of Pre-Mixed Diesel Combustion, SAE paper 2007-01-0773.
57. Yoon, M., Lee, K., Sunwoo, M., and Oh, B., Cylinder Pressure Based Combustion Phasing Control of a CRDI Diesel Engine, SAE Technical Paper 2007-01-0772.
58. Schnorbus, T., Pischinger, S., Korfer, T., Lamping, M., Tomazic, D., and Tatur, M., "Diesel Combustion Control with Closed-loop Control of the Injection Strategy," SAE Technical Paper 2008-01-0651, 2008, doi:10.4271/2008-01-0651.
59. Payri, F., Broatch, A., Salavert, J.M., and Martin, J., "Investigation of Diesel Combustion Using Multiple Injection Strategies for Idling after Cold Start of Passenger-Car Engines," Experimental Thermal and Fluid Sciende 34 (2010) 857-865.
60. Yan, F. and Wang, J., Air- and fuel-path coordinated control for advanced combustion mode transitions in Diesel engines, American Control Conference (ACC), 2012, Page(s): 2890 – 2895.
61. Satkoski, C. A., Ruikar, N. S., Biggs, S. D. and Shaver, G. M., Cycle-to-cycle Estimation and Control of Multiple Pulse Profiles for a Piezoelectric Fuel Injector, 2011 American Control Conference on O'Farrell Street, San Francisco, CA, USA June 29 - July 01, 2011.
62. Zander, C.-G., Tunestal, P., Stenlåås, O., Johansson, B., "In-Cycle Closed Loop Control of the Fuel Injection on a 1-Cylinder Heavy Duty CI-Engine", Proceedings of the ASME Internal Combustion Engine Division ICED 2010 Fall Technical Conference, pp. 405-414, ICEF2010-35100, 2010,doi:10.1115/ICEF2010-35100.

63. Mayne, et al, Constrained model predictive control. stability and optimality, Automatica, 2000.
64. Cutler, C. R., and Ramaker, B. L., Dynamic Matrix Control-A Computer Control Algorithm, AIChE Meeting, Houston, 1979.
65. Richaler, J., Rault, A., Testud, J. L. and Papon, J., Model Predictive Heuristic Control: Application to Industrial Processes, Automatica, 14, 413, 1978.
66. Soeterboek, R., Predictive Control, Prentice Hall, 1992, ISBN 0-13-678350-3.
67. Macjiejowski, J.M., Predictive Control: with Constraints, Pearson Education Limited, 2002, ISBN 0 201 39823 0 PPR.
68. del Re, L., Allgower, F., Glielmo, L., Guardiola, C. and Kolmanovsky, I., Automotive Model Predictive Control,-Models, Methods and Applications, Springer-Verlag Berlin Heidelberg, 2010 ISBN 978-1-84996-070-0.
69. Huang, S., Tan, K. K., Lee, T. H., Applied Predictive Control Advanced in Industrial Control, Springer, 2001, ISBN 1852333383.
70. Bemporad, A., Morari, M., Dua, V., Pistikopoulos, E. N., The Explicit Linear Quadratic Regulator for Constrained Systems, Automatica, 38, 3-20, 2002.
71. Bengtsson, J., Strandh , P., Johansson , R., Tunest°al, P. and Johansson , B., Model Predictive Control of Homogeneous Charge Compression Ignition (HCCI) Engine Dynamics, Proceedings of the 2006 IEEE International Conference on Control Applications.
72. http://large.stanford.edu/courses/2010/ph240/veltman1/, last accessed 2013-07-31.
73. Wei, X., del Re., L., Lihua, L., Air Path identification of diesel engines by LPV techniques for gain scheduled control, Mathematical and Computer Modelling of Dynamical Systems, 14(6), 495-513 (2008).
74. Wang, J., Air Fraction Estimation for Multiple Combustion Mode Diesel Engines with Dual-Loop EGR Systems, Control Engineering Practice 16 (2008) 1479– 1486.
75. Catania, A., Finesso, R., Spessa, E., di Torino, P., Real-Time Calculation of EGR Rate and Intake Charge Oxygen Concentration for Misfire Detection in Diesel Engines, SAE Paper 2011-24-0149.
76. Livengood, J. C., Rogowski, A. R., and Taylor, C. F., The Volumetric Efficiency of Four-Stroke Engines, SAE Paper 520259.
77. Ahmad, N., Babu, M. K. G., Simulation and Experimental Studies on Combustion and Performance Characteristics for a Turbocharged and Naturally Aspirated Multi– Cylinder Compression Ignition Engine, SAE Paper 2006-01-3487.
78. Zhang, L., A Study of Pilot Injection in a DI Diesel Engine, SAE paper 1999-01-3493.
79. Olsson, J., Tunestål, P. and Johansson, B., Closed-Loop Control of an HCCI Engine, SAE paper 2001-01-1031.

80. Bengtsson, J. , Strandh, P. , Johansson, R., Tunesta˚ l , P. and Johansson, B., Closed-loop combustion control of homogeneous charge compression ignition (HCCI) engines dynamics, Int. J. Adaptive Control and Signal Processing, 18, pp. 167–179, 2004b.
81. Chmela, F.G. and Orthaber, G.C., Rate of heat release prediction for direct injection Diesel engines based on purely mixing controlled combustion, SAE Paper 1999-01-0186.
82. Naber, J. D., and Siebers, D. L., Effects of Gas Density and Vaporization on Penetration and Dispersion of Diesel Sprays, SAE Paper 960034.
83. Siebers, D. L., Scaling Liquid-Phase Fuel Penetration in Diesel Sprays Based on Mixing-Limited Vaporization, SAE Paper 1999-01-0528.
84. Higgins, B. S., Mueller, C. J., and Siebers, D. L., Measurements of Fuel Effects On Liquid-Phase Penetration in DI Sprays, SAE Paper 1999-01-0519.
85. Asay, R. J., A Five-Zone Model for Direct Injection Diesel Combustion, M.S. Thesis, Brigham Young University, 2003.
86. Oppenheim, A. K., Kuhl, A. L., Packard, K. A., Hedrick, J. K. and Johnson, W. P., Model and Control of Heat Release in Engines, SAE paper 960601.
87. Arrègle, J., López, J. J., Martín, J. and Mocholí, E. M., Development of a Mixing and Combustion Zero - Dimensional Model for Diesel Engines, SAE paper 2006-01-1382.
88. Kong, S. and D. Reitz R., Modeling the Effects of Injector Nozzle Geometry on Diesel Sprays, SAE paper 1999-01-0912.
89. Tanner, F. X., Liquid Jet Atomization an Droplet Breakup Modeling of Non-Evaporating Diesel Fuel Sprays, SAE Paper 970050.
90. Patterson, M., Reitz, R. D., Modeling the Effects of Fuel Spray Characteristics on Diesel Engine Combustion and Emission, SAE Paper 980131.
91. Arai, M., Tabata, M., Hiroyasu, H. and Shimizu, M., Desintegrating Process and Spray Characterization of Fuel Jet Injected by a Diesel Nozzle, SAE paper 840275.
92. Elkotb, M. M., Fuel Atomization for Spray Modeling, Prog. Energy Combust. Sci., Vol. 8, pp. 61-91, 1982.
93. Kuleshov, A.S., Use of Multi-Zone DI Diesel Spray Combustion Model for Simulation and Optimization of Performance and Emissions of Engines with Multiple Injection, SAE 2006-01-1385.
94. Poetsch, C., Ofner, H. and Cartellieri, W., Analysis of Thermodynamic Characteristics of Diesel Engine Emission Control Strategies Using a Multi-Zone Combustion Model , SAE paper 2012-01-1340.

95. Cho, H. and Kim, W., Numerical Simulation of Diesel Spray Combustion in a Constant Volume Chamber by Eulerian and Lagrangian Conditional Moment Closure Models , SAE paper 2013-01-1600.
96. Tanner, F. X., Zhu, G. and Reitz, R. D., Non-Equilibrium Turbulence Considerations for Combustion Processes in the Simulation of DI Diesel Engines, SAE paper 2000-01-0586.
97. Kudo, Y. and Yokota, H., Computational Study of a Pre-Mixed Diesel Combustion by Means of Shell Model, SAE paper 2003-08-0291.
98. Shioji, M., Nakatani, K., Ihara, T. and Ikegami, M., Stochastic approach for describing mixture formation and initial combustion in diesel sprays, SAE paper 1999-08-0372.
99. Gupta, A. K., Mehta, P. S. and Gupta, C. P., Model for Predicting Air-Fuel Mixing and Combustion for Direct Injection Diesel Engine, SAE paper 860331.
100. Schihl, P., Tasdemir, J., Schwarz, E. and Bryzik, W., Development of a Zero - Dimensional Heat Release Model for Application to Small Bore Diesel Engines, SAE paper 2002-01-0073, doi: 10.4271/2002-01-0073.
101. Hountalas, D. T. , Kouremenos, D. A., Mavropoulos, G. C., Binder, K. B. and Schwarz V., Multi-Zone Combustion Modeling as a Tool for DI Diesel Engine Development – Application for the Effect of Injection Pressure , SAE paper 2004-01-0115.
102. Rezaei, R., Eckert, P., Seebode, J. and Behnk, K., Zero-Dimensional Modeling of Combustion and Heat Release Rate in DI Diesel Engines, SAE paper 2012-01-1065.
103. Morel, T., Wahiduzzaman, S., Modeling of Diesel Combustion and Emissions, FISITA, 1996.
104. Stiesch, G. and Merker, G., A Phenomenological Model for Accurate and Time Efficient Prediction of Heat Release and Exhaust Emissions in Direct-Injection Diesel Engines, SAE Paper 1999-01-1535.
105. Thoma, M., Stiesch, G., Merker, G.P., A Phenomenological Spray and Combustion Model for Diesel Engines with Pre-Injection, 5th Int Symp Internal Combustion Diagnostics, Baden-Baden, 2002.
106. Rether, D., Grill, M., Schmid, A., and Bargende, M., Quasi-Dimensional Modeling of CI-Combustion with Multiple Pilot- and Post Injections, SAE Paper 2010-01-0150, doi:10.4271/2010-01-0150.
107. Chmela, F., Pirker, G., Wimmer, A., Zero-dimensional ROHR simulation for DI diesel engines - A generic approach, Journal of energy conversion and Management, Vol. 48 pages: 2942-2950, 2007.

108. Arsie, I., Di Genova, F., Mogavero, A., Pianese, C., Rizzo, G., Caraceni, A., Cioffi, P. and Flauti, G., Multi-Zone Predictive Modeling of Common Rail Multi-Injection Diesel Engines, SAE Paper 2006-01-1384.

109. Arsie, I., Di Genova, F., Pianese, C., Sorrentino, M., Rizzo, G., Caraceni, A., Cioffi, P. and Flauti, G., Development and Identification of Phenomenological Models for Combustion and Emissions of Common-Rail Multi-Jet Diesel Engines, SAE Paper 2005-01-1877.

110. Arsie, I., Di Genova, F., Pianese, C., Rizzo, G., Caraceni, A., Cioffi, P. and Flauti, Thermodynamic Modeling of Jet Formation and Combustion in Common Rail Multi-Jet Diesel Engines, SAE Paper 2005-01-1121.

111. Saad, C., maroteaux, F., Millet, J. and Aubertin, F., Combustion Modeling of a Direct Injection Diesel Engine Using Double Wiebe Functions: Application to HiL Real-Time Simulations, SAE Paper 2011-24-0143.

112. Dulbecco, A., Lafossas, F.A. and Poinsot, T. J., A 0D Phenomenological Approach to Model Diesel HCCI Combustion with Multi-Injection Strategies Using Probability Density Functions and Detailed Tabulated Chemistry, SAE paper 2009-01-0678.

113. Loganathan,S., Manohar, R. M., Thamaraikannan, R., Dhanasekaran, R., Rameshbabu, A. and Krishnamoorthy, V., Direct Injection Diesel Engine Rate of Heat Release Prediction using Universal Load Correction Factor in Double Wiebe Function for Performance Simulation, SAE paper 2011-01-2456.

114. Bordet, N., Caillol, C., Higelin, P. and Talon, V., A Physical 0D Combustion Model Using Tabulated Chemistry with Presumed Probability Density Function Approach for Multi-Injection Diesel Engines, SAE paper 2010-01-1493.

115. Westlund , A., Ångström, H., Lindström, M., Validation of a Simplified Model for Combustion and Emission Formation in Diesel Engines Based on Correlations for Spray Penetration and Dispersion, Gas Entrainment into Sprays and Flame Lift-off, SAE paper 2010-01-1494.

116. Barba, C., Burkhardt, C., Boulouchos, K. and Bargende, M., A Phenomenological Combustion Model for Heat Release Rate Prediction in High-Speed DI Diesel Engines with Common Rail Injection, SAE paper 2000-01-2933.

117. Subramanian, G., Pires Da Cruz, A., Colin, O. and Vervisch, L., Modeling Engine Turbulent Auto-Ignition Using Tabulated Detailed Chemistry, SAE paper 2007-01-0150.

118. Mauviot , G., Albrecht, A. and Poinsot, T. J., A New 0D Approach for Diesel Combustion Modeling Coupling Probability Density Function with Complex Chemistry, SAE paper 2006-01-3332.

119. Catania, A., Finesso, R., Spessa, E., Catanese, A. and Landsmann, G., Combustion Prediction by a Low-Throughput Model in Modern Diesel Engines, SAE paper 2011-01-1410.

120. Catania, A. E., Finesso, R. and Spessa, E., Predictive zero-dimensional combustion model for DI diesel engine feed-forward control, Energy Conversion and Management, Vol. 52 (2011) 3159–3175.

121. Grill, M., Bargende, M., Rether, D. and Schmid, A., Quasi-dimensional and Empirical Modeling of Compression-Ignition Engine Combustion and Emissions, SAE paper SAE 2010-01-0151.

122. Skogestad, S. and Postlethwaite, I., Multivariable Feedback Control Analysis and Design, John Wiley & Sons Ltd, 2005 ISBN-13978-0-470-01167-6 (HB).

123. Wei, X., del Re, L., Langthaler, P., LPV dynamical models of diesel engine NOx emission, First IFAC Symposium on Advances in Automotive Control, University of Salerno, Salerno, Italy, April 2004, pp. 262-267 (2004).

124. Kolmanovsky, I., Morall, P., van Nieuwstadt, M. and Stefanopoulou, A., Issues in modelling and control of intake flow in variable geometry turbocharged engines. Proceedings of the 18th IFIP TC7 Conference on Systems Modelling and Optimization, pp. 436-445.

125. Yilmaz, H. and Stefanopoulou, Control of Charge Dilution in Turbocharged Diesel Engines via Exhaust Valve Timing. IEEE Proceedings of the American Control Conference, 2003 Pages pp. 761-766.

126. Darlington, A., Glover, K. and Collings, N., A Simple Diesel Engine Air-Path Model to Predict the Cylinder Charge During Transients: Strategies for Reducing Transient Emissions Spikes, University of Cambridge, SAE technical paper 2006.

127. Desantes, J.M., Galindo, J., Guardiola, C. and Dolz, V., Air mass flow estimation in turbocharged diesel engines from in-cylinder pressure measurement, Experimental Thermal and Fluid Science, Vol. 34(1) 1 (January, 2010), p. 37-47, doi: 10.1016/j.expthermflusci.2009.08.009.

128. Storset, O.F., Stefanopoulou, A. G., and Smith, R., Adaptive air charge estimation for turbocharged diesel engines without exhaust gas recirculation, http://www-personal.umich.edu/~annastef/papers_TC_diesel/M02_074.pdf, last accessed 2013-07-31.

129. Wahlström, J. and Eriksson, L., Modelling diesel engines with a variable-geometry turbocharger and exhaust gas recirculation by optimization of model parameters for capturing non-linear system dynamics, 2011, Proceedings of the Institution of mechanical engineers. Part D, journal of automobile engineering, (225), 7, 960-986, doi: 10.1177/0954407011398177.

130. Scappin, F., Stefansson, S.H., Haglind, F., Andreasen, A. and Larsen, U., Validation of a zero-dimensional model for prediction of NOx and engine performance for electronically controlled marine two-stroke diesel engines, Appl Therm Eng 2012;37:344–52.

131. Bayer, J. and Foster, D. E., Zero-Dimensional Soot Modeling, SAE Paper 2003-01-1070.

132. Hegarty, K., Favrot, R., Rollett D. and Rindone, G., Semi-Empiric Model Based Approach for Dynamic Prediction of NOx Engine Out Emissions on Diesel Engines, SAE paper 2010-01-0155.

133. Quérel, C., Grondin, O. and Letellier, C., State of the Art and Analysis of Control Oriented NOx Models, SAE paper 2012-01-0723.

134. Asprion, J., Chinellato, O., Guzzella, L., Optimisation-oriented modelling of the NOx emissions of a Diesel engine, Energy Conversion and Management, Volume 75, November 2013, Pages 61-73.

135. Rao, V. and Honnery, D., A comparison of two NOx prediction schemes for use in diesel engine thermodynamic modelling, Fuel 107 (2013) 662–670.

136. Mellor, A., Mello, J., Duffy, K., Easley, W. and Faulkner, J., Skeletal mechanism for NOx chemistry in Diesel Engines, SAE paper 981450.

137. Aithal, S., Modeling of NOx formation in diesel engines using finite-rate chemical kinetics. Appl Energy 2010;87(7):2256–65.

138. Goldsworthy, L., Reduced kinetics schemes for oxides of nitrogen emissions from a slow-speed marine diesel engine. Energy Fuels 2003;17(2):450–6.

139. Easley, W. L., Mellor, A.M. and Plee, S. L., NO formation and decomposition models for DI Diesel Engines. SAE paper 2000-01-0582.

140. Polifke, W., Dobbeling, K., Sattlemayer, T., Nicol, D.G. and Malte, P.C., A NOx Prediction scheme for lean premixed gas turbine combustion based on detailed chemical kinetics. J Eng Gas Turbines Power 1996;118(4):765–72.

141. Hernandez, J.J. and Lapuerta, M., Perez-Collado J. A combustion kinetic model for estimating diesel engine NOx emissions. Combust Theory Model 2006;10(4):639–57.

142. Psota, M.and Mellor, A., Dynamic application of a skeletal mechanism for DI Diesel NOx emissions, SAE paper 2001-01-1984.

143. Oppenauer, K. S. and del Re, L., Hybrid 2-Zone Diesel Combustion Model for NO Formation, SAE paper 2009-24-0135.

144. Tan , P.Q., Hu a, Z.Y., Deng , K.Y., Lu, J.X., Lou, D.M. and Wan , G., Particulate matter emission modelling based on soot and SOF from direct injection diesel engines, Energy Conversion and Management, 48 (2007) 510‑518.

145. Micklow G, Gong W. A multistage combustion model and soot formation model for direct-injection diesel engines. Proceedings of the Institution of Mechanical Engineers – Part D, Journal of Automobile Engineering 2002;216(6):495–504.

146. Seykens, X. L. J., Baert, R. S. G., Somers, L. M. T. and Willems, F. P. T., Experimental Validation of Extended NO and Soot Model for Advanced HD Diesel Engine Combustion, SAE paper 2009-01-0683.

147. Oppenauer, K. S., Alberer, D. and del Re, L., Control Oriented Crank Angle Based Analysis of Soot Dynamics During Diesel Combustion, SAE paper 2010-01-2105.

148. Gao, Z. and Schreiber, W., A phenomenologically based computer model to predict soot and NOx emission in a direct injection diesel engine, Int J Engine Res, 2001;2(3):177–88.

149. Guo, H. and Smallwood, G.J., The interaction between soot and NO formation in a laminar axisymmetric coflow ethylene/air diffusion flame, Combust Flame 2007;149(1-2):225–33.

150. Kong, S., Sun, Y. and Rietz, R. D., Modeling diesel spray flame liftoff, sooting tendency, and NOx emissions using detailed chemistry with phenomenological soot model, J Eng Gas Turbines Power 2007;129(1): 245–51.

151. Tao, F., Reitz, R. D., Foster, D. E. and Liu, Y., Nine-step phenomenological diesel soot model validated over a wide range of engine conditions, International Journal of Thermal Sciences, Volume 48, Issue 6, June 2009, Pages 1223-1234.

152. Adlouni,M., Modeling of soot emission for heavy-duty diesel engines in transient operation, http://www3.control.lth.se/documents/2011/5870.pdf

153. Ljung, L., System Identification, Wiley Encyclopedia of Electrical and Electronics Engineering, 1999.

154. Deng, J., Maass, B. and Stobart,R., Using Artificial Neural Networks for Representing the Brake Specific-Fuel Consumption and Intake Manifold pressure of a Diesel Engine, Power and Energy Engineering Conference, APPEEC 2009, Asia-Pacific.

155. Deng, J., Stobart, R. and Plianos, A., Combined hybrid clustering techniques and neural fuzzy networks to predict diesel engine emissions, IEEE International Conference on Systems, Man and Cybernetics, 2007, ISIC.

156. Maass, B., Stobart, R., and Deng, J., Prediction of NOx Emissions of a Heavy Duty Diesel Engine with a NLARX Model, SAE paper 2009-01-2796.

157. Maass, B., Deng, J. and Stobart, R., In-Cylinder Pressure Modelling with Artificial Neural Networks, SAE paper 2011-01-1417.

158. Deng, J., Maass, B., Stobart, R., Winward E. and Yang, Z., Accurate and Continuous Fuel Flow Rate Measurement Prediction for Real Time Application, SAE paper 2011-01-1303.

159. Maass, B., Stobart, R., Deng, J., Diesel engine emissions prediction using parallel neural networks , American Control Conference, 2009, Page(s): 1122 – 1127, doi: 10.1109/ACC.2009.5160119.

160. Hu, M. and Kai, Z., On-line predicting diesel engine EGR rate based on Chaos-Neural Networks, Natural Computation (ICNC), 2010 Sixth International Conference on, Vol. 3, doi: 10.1109/ICNC.2010.5583612.

161. Cui, Y., Feng, X., Liu, L., Hou, T. and Liu, C., Research on active control of diesel engine based on wavelet neural network, Industrial Mechatronics and Automation, ICIMA 2009, International Conference on, doi: 10.1109/ICIMA.2009.5156651.

162. Omran, R., Younes, R. and Champoussin, J.C., Optimal Control of a Variable Geometry Turbocharged Diesel Engine Using Neural Networks: Applications on the ETC Test Cycle, IEEE Transactions on Control Systems Technology, 2009, Vol. 17, Issue 2, Page (s): 380-393, doi: 10.1109/TCST.2008.2001049.

163. Wang, J., Zhang, Y., Xiong, Q. and Ding, X., NOx Prediction by Cylinder Pressure Based on RBF Neural Network in Diesel Engine, Measuring Technology and Mechatronics Automation (ICMTMA), 2010 International Conference on, Vol. 2, doi: 10.1109/ICMTMA.2010.621.

164. Li, J., He, C. and Jia, D., Emission modeling of diesel engine fueled with biodiesel based on back propagation neural network, IEEE International Conference on Computer Science and Information Technology (ICCSIT), 2010 3rd, Vol. 4, Page(s): 379 – 381, doi: 10.1109/ICCSIT.2010.5564152.

165. Brzozowska, L., Brzozowski, K. and Nowakowski, J., An Application of Artificial Neural Network to Diesel Engine Modelling, Intelligent Data Acquisition and Advanced Computing Systems: Technology and Applications, IDAACS 2005. IEEE, Page(s): 142 – 146, doi: 10.1109/IDAACS.2005.282958.

166. Moon, G., Lee, Y., Choi, K. and Jeong, D., Experimental study on characteristics of diesel particulate emissions with diesel, GTL, and blended fuels, SAE paper 2009-24-0098.

167. Aatola, H., Larmi, M., Sarjovaara, T. and Mikkonen, S., Hydrotreated Vegetable Oil (HVO) as a Renewable Diesel Fuel: Trade-off between NOx, Particulate Emission, and Fuel Consumption of a Heavy Duty Engine, SAE paper 2008-01-2500.

168. Kawamoto,K., Araki,T., Shinzawa, M. and Kimura, S., Combination of Combustion Concept and Fuel Property for Ultra-Clean DI Diesel (MK combustion), SAE paper 2004-01-1868.

169. Catania, A. E., d'Ambrosio, S., Finesso, R. and Spessa, E., Effects of Rail Pressure, Pilot Scheduling and EGR Rate on Combustion and Emissions in Conventional and PCCI Diesel Engines, SAE paper 2010-01-1109.

170. Gao, Z., Schreiber, W., The Effects of EGR and Split Fuel Injections on Diesel Engine Emissions, Int. J. Automotive Technol., Vol. 2, No. 4, 2001.

171. Winward, E., Deng, J., and Stobart, R.K., "Innovations In Experimental Techniques for the Development of Fuel Path Control in Diesel Engines," SAE Technical Paper 2010-01-1132, 2010, doi:10.4271/2010-01-1132.

172. C6.6 Engine User Manual: System Operation Testing and Adjusting, Perkins, 2005.

173. Zheng, M., Reader, G. T. and Hawley, J. G., Diesel Engine Exhaust Gas Recirculation-A Review on Advanced and Novel Concepts, Energy Conversion and Management 45, 883-900, 2004.

174. Acheson, D. J., Elementary Fluid Dynamics, Clarendon Press, 1990.

175. Shariff, H. M., Hezri, M., Rahiman, F and Tajjudin, M., Nonlinear System Identification: Comparison between PRBS and Random Gaussian Perturbation on Steam Distillation Pilot Plant, 2013 IEEE 3rd International Conference on System Engineering and Technology, 19-20 Aug 2013, Shah Alam, Malaysia.

176. . Alessio, A. and Bemporad, A., A Survey on Explicit Model Predictive Control, Nonlinear Model Predictive Control, Lecture Notes in Control and Information Sciences Volume 384, 2009, pp 345-369.

177. Kouramas, K. I., Faisca, N. P., Panos, C. and Pistikopoulos, E. N., Explicit/Multi-Parametric Model Predictive Control (MPC) of Linear Discrete-Time Systems by Dynamic and Multi-Parametric Programming, Automatica 47, 1638-1645, 2011.

178. Besselmann, T., Lofberg, J. and Morari, M., Explicit Model Predictive Control for Systems with Linear Parameter-Varying State Transition Matrix, Proceedings of the 17th World Congress, The International Federation of Automatic Control, Seoul, Korea, July 6-11, 2008.

"Never give up on something that you can't go a day without thinking about."

Winston Churchill